Photostimulated catalytic reduction of CO2 with iron porphyrins

Heng Rao

Thèse de doctorat

de l'Université Sorbonne Paris Cité

Préparée à l'Université Paris Diderot

Ecole doctorale 388

Chimie Physique et Chimie Analytique de Paris Centre

Laboratoire d'Electrochimie Moléculaire

Photostimulated Catalytic Reduction of CO_2 with Iron Porphyrins

Heng RAO

Dirigée par

Julien BONIN et Marc ROBERT

Présentée et soutenue publiquement à Paris le 25 Septembre 2018 devant le jury composé de :

Presidente	Marie-Noëlle Collomb	Dr, Université Grenoble Alpes
Rapporteurs	Jérôme Chauvin	MCF,Université Grenoble Alpes
	Ally Aukauloo	Pr, Université Paris Saclay
Examinateurs	Caroline Mellot-Draznieks	Dr, Collège de France
	Sophia Haussener	Pr, École Polytechnique Fédérale de Lausanne
Directeur de thèse	Julien Bonin	MCF, Université Paris Diderot
Co-directeur de thèse	Marc Robert	Pr, Université Paris Diderot

Abstract

Photocatalytic reduction of CO_2 into value-added chemicals and fuels could not only contributes to mitigating CO_2 emissions, but also provides valuable fuels and thus enhances energy security in light of the depletion of fossil resources and the strong fluctuation of oil prices. At the same time, it will provide a new approach for the storage of renewable energy. It is like killing three birds with one stone.

Iron porphyrins have been shown to be the most efficient electrochemical CO_2-to-CO conversion molecular catalysts in our lab. We introduced four trimethylammonio groups on the para position of the phenyl rings of an iron porphyrin which makes the complex active under visible light for the photochemical reduction of CO_2 to CO, without additional photosensitizer. When combining with a simple organic dye (namely purpurin) as the photosensitizer, CO is produced with a catalytic selectivity of 95% and turnover number up to 120 in aqueous solutions under visible light irradiation. The catalysis is ultimately limited by progressive sensitizer degradation but it could be restarted by adding fresh sensitizer. This work opens new perspectives for developing efficient CO_2 reduction photocatalysis in water. On the other hand, if the same catalyst is sensitized by a much stronger sensitizer, such as $Ir(ppy)_3$ (ppy = 2-phenylpyridine), not only the absolute amount of CO increases, but CO_2 can also can be converted into CH_4. This complex complicated eight-electron and eight-proton catalytic process is efficiently driven by visible light irradiation at ambient temperature and pressure. CO_2 could be selectively reduced into CO and the later gas is transformed to CH_4 with an overall 82% selectivity, the production of which was sustained over several days. As far as we know, it's the first efficient homogenous photochemical CO_2-to-CH_4 catalytic system. When $Ir(ppy)_3$ was replaced by $Ir(ppy)_2(bpy)PF_3$ in a aqueous solution, the process of CO_2-to-CH_4 conversion continued, while the process of CO-to-CH_4 conversion was inhibited thanks to the deactivation of the photosensitizer. Finally, a phenoxazine-based organic photosensitizer was found to drive the whole catalysis. Above all, the absolute mol number of methane produced in this non-noble-element system is even 2 times higher than the Ir sensitized system.

Keywords: iron porphyrin; CO_2 reduction; photochemistry; homogeneous catalysis; molecular catalyst; solar fuels.

Résumé

La réduction photocatalytique du CO_2 en composés à haute valeur ajoutée ou en carburants pourrait non seulement contribuer à la limitation des émissions de CO_2 mais également sécurises une ressource énergétique et pallier la baisse des ressources naturelles et les fluctuations de prix. Dans le même temps, cela ouvrirait une nouvelle voie pour le stockage des énergies renouvelables. En résumé, cela reviendrait à faire d'une pierre *trois* coups. Il a été montré au sein du laboratoire que les porphyrines de fer étaient les catalyseurs moléculaires les plus efficaces pour la conversion électrochimique de CO_2 en CO. Nous avons introduit quatre groupements triméthylammonium dans les positions *para* des cycles phényles d'une porphyrine ce qui permet de la rendre activable par la lumière visible et donc pour la réduction photostimulée de CO_2 en CO, sans l'aide d'un sensibilisateur externe. Associée à un colorant organique simple (la purpurine) en guise de sensibilisateur, CO est obtenu avec une sélectivité catalytique de 95% et un nombre de cycles catalytique de 120 en solution aqueuse sous lumière visible. La catalyse est cependant limitée par la dégradation progressive du sensibilisateur mais elle peut être restaurée par un ajout de sensibilisateur frais. Ce travail ouvre de nouvelles perspectives pour le développement de la réduction catalytique photochimique de CO_2 dans l'eau. Par ailleurs, nous avons montré que ce même catalyseur, associé à un sensibilisateur plus réducteur, à savoir un complexe d'iridium ($Ir(ppy)_3$), permettait d'obtenir un nombre de cycles catalytiques en CO plus élevé, mais également de parvenir à la réduction de CO_2 en CH_4. Ce processus complexe, impliquant le transfert de 8 électrons et 8 protons, a été conduit de manière efficace sous lumière visible et à pression et température ambiantes. CO est d'abord obtenu sélectivement puis transformé en CH4, de manière durable sur plusieurs jours, avec une sélectivité globale de 82%. A ce jour, ceci constitue la première démonstration de faisabilité de cette transformation en catalyse photochimique homogène. Lorsque le complexe d'iridium est remplacé par un complexe analogue soluble en solution aqueuse, la conversion de CO_2 en CH_4 est également observé mais pas celle de CO en CH_4 par dégradation du sensibilisateur. Enfin, de nouveaux sensibilisateur organiques de type phénoxazine ont été utilisés avec succès pour ce processus, permettant d'obtenir des quantités absolues de méthane 2 fois plus élevées tout en n'employant plus d'élément rare et cher.

Mots-clés: porphyrine de fer; réduction du CO_2; photochimie; catalyse homogène; catalyseur moléculaire; carburants solaires.

“Reducing greenhouse gases requires honesty, courage and responsibility, above all on the part of those countries which are more powerful and pollute the most.”

—Pope Francis

Table of Contents

Chapter 1 Introduction

1.1 Background

1.1.1 Traditional fossil fuels and the increasing atmospheric carbon dioxide concentration

Fossil fuels, as one of the most important primary energy resources, make great contribution to the development of human beings since Industrial Revolution. However, due to the worldwide increasing demand and the accompanying excessive emissions of carbon dioxide (one of the main greenhouse gases), energy shortage and global warming present to be two main crises for the sustainable development of human society in the 21st century.

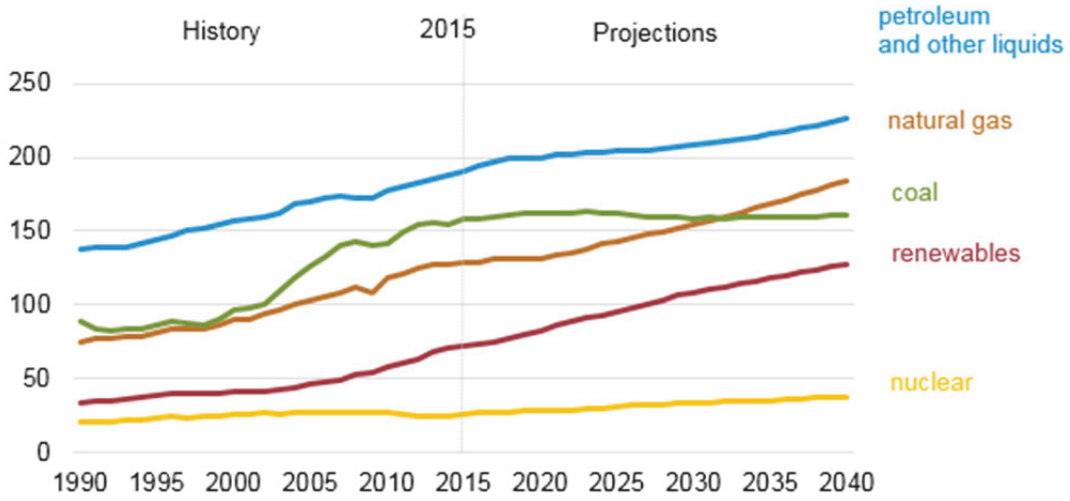

Figure 1.1 World energy consumption by energy source over time, in quadrillion Btu. Data obtained from International Energy Outlook Executive Summary 2017[1].

The consumption of abundant fossil fuels, particularly coal and oil, becomes more accessible with the developing technology. Two hundred years ago, global energy consumption was almost exclusively in the form of biofuels such as crop straw and wood; however, the use of coal first and then oil and natural gas has skyrocketed, particularly in the past century. Fossil fuel usage accounts for the vast majority due to several factors, including abundance, availability, energy density, storability and transportability. In the International Energy Outlook 2017 (IEO2017) Reference case, world consumption of marketed energy from all fuel sources increased, except coal, for which demand is essentially flat through 2040 (Figure 1.1).[1] Renewable energies are the

world's fastest-growing sources, with consumption increasing by an average 2.3%/year between 2015 and 2040. The world's second fastest-growing source of energy is nuclear power, with consumption increasing by 1.5%/year over that period. Although consumption of non-fossil fuels is expected to grow faster than fossil fuels, the latter still account for 77% of energy use in 2040. In other words, fossil fuels will still be the main energy sources for quite some time.

At the very beginning, the natural carbon cycle driven by sunlight, together with the water and nitrogen cycles, is one of the main processes allowing life to take place. On earth, carbon exists in various reservoirs. The main atmospheric reservoir is in the form of gaseous CO_2. But carbon is also bound on land in living vegetation, in soils and in carbon containing minerals, whereas in the oceans, carbon exists in equilibrium between dissolved CO_2, bicarbonates and carbonates. The carbon cycle links these reservoirs by various fluxes, as shown in Figure 1.2.[2] However, the red numbers greatly impacted the fluxes in the earth's carbon cycle and have thereby significantly disturbed its equilibrium. In particular, the widespread utilization of fossil fuels has led to a drastic increase in carbon dioxide emissions.

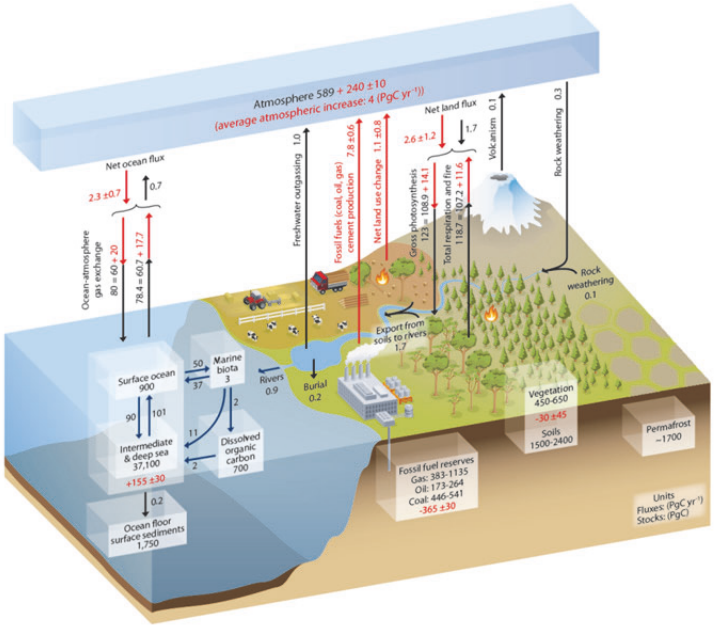

Figure 1.2 Schematic of the global carbon cycle. Numbers represent reservoir masses (or 'carbon stocks' in PgC (= 10^{15} gC) and annual carbon exchange fluxes (in PgC yr^{-1}). Source: IPCC.

CO_2 concentration in the atmosphere has lately risen far beyond the amplitude of typical historic oscillations due to ice ages at the geologic time scale and to seasonal variations on a yearly basis. As shown in Figure 1.3, the current atmospheric CO_2 concentration has risen up to

408 ppm (part per million) from 280 ppm at the beginning of the industrial age (ca. 1750) giving a drastic increase of ~45.7%.[3] In the past 60 years, it increased about 25% and it is currently rising by about 2 ppm/year. What is worse, this growth trends will keep going even faster if we do nothing. The massive quantities of carbon dioxide, about a quarter of the total emitted since the start of the Industrial Revolution, have entered the oceans. While this dissolution of CO_2 has mitigated the change in atmospheric carbon, it has led to detectable acidification of the oceans because it forms carbonic acid, threatening the vast biodiversity of that ecosystem.

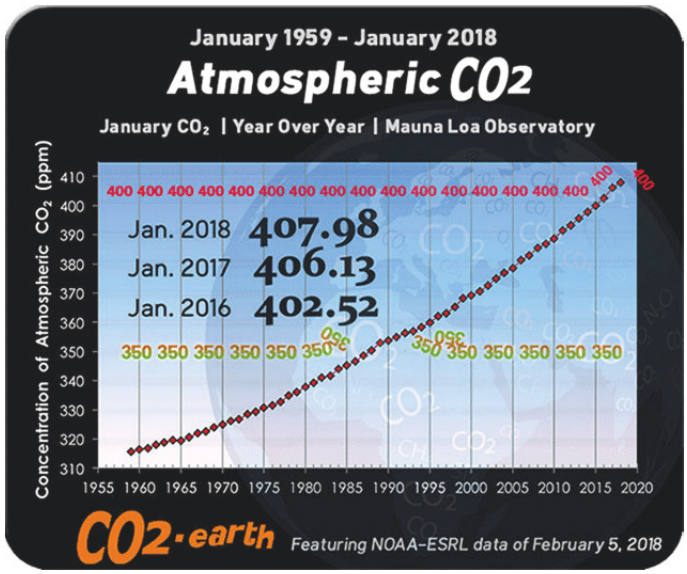

Figure 1.3 Variation of atmospheric CO_2 concentration over the past 58 years.[3]

In addition to ocean acidification, the rising of atmospheric CO_2 levels have been associated with the strengthening of the greenhouse effect and have been implicated greatly in climate change.[4] The increase of carbon dioxide, which will absorb and re-emit infrared radiation strongly, leads to a huge decrease in the net amount of energy radiated out of the atmosphere by the Earth. As a consequence, the global temperature has been trending upward relative to long-term patterns, particularly in the past several decades, with a surface temperature deviation of 1.3 °C from the pre-industrial levels already.[5] The most optimistic of predicted scenarios, in which CO_2 emissions peak immediately and subsequently decline, anticipates a total temperature change of about 1.0 °C by the end of the twenty-first century.[6] According to the International Panel on Climate Change (IPCC), a CO_2 level above 450 ppm carries a high risk of causing global warming by more than 2 °C. If the temperature change can be limited to less than 2 °C, there is a good chance that human society can adapt.[7] Unless we are able to radically reduce CO_2

emissions within the next 20 years, exceeding the 450 ppm level seems unavoidable. The most pessimistic projection, but unfortunately the most politically and economically likely at present, in which CO_2 emissions continue to rise throughout the century as energy demands increase, predicts a mean temperature change of over 4 °C by 2100. Such drastic global temperature shifts would cause massive changes in climate, ice coverage, sea levels, and plant and animal diversity. A lot of low elevation countries and regions will disappear permanently from the earth. Human society, faced with the numerous agricultural, economic crises and geopolitical that would unfold because of these transformations, would be forced to adapt quickly to the rapidly changing world.

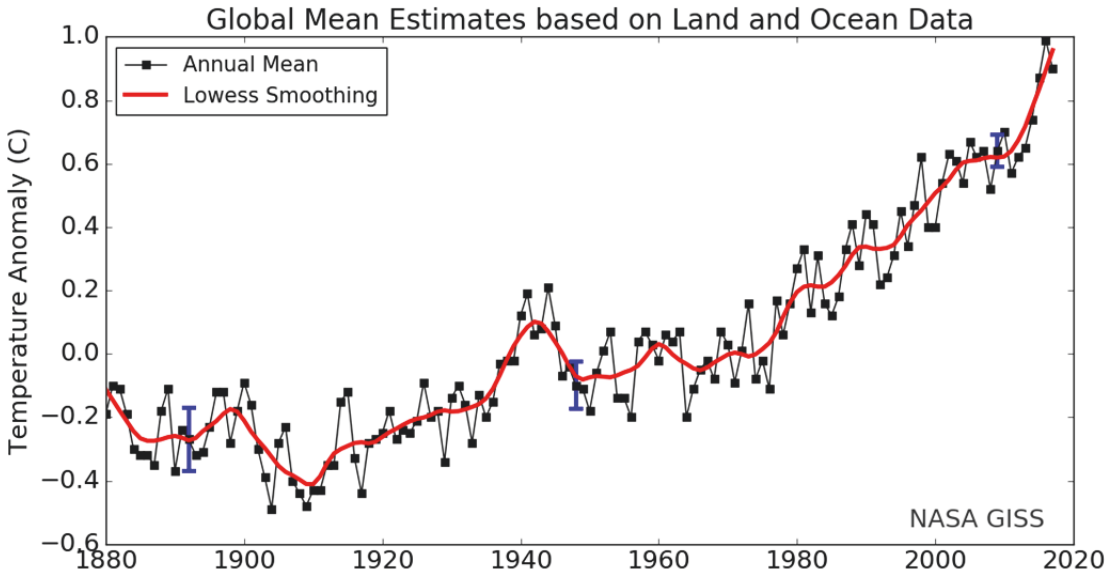

Figure 1.4 Land-ocean temperature indexes, 1880 to present, with base period 1951-1980. The solid black line is the global annual mean and the solid red line is the five-year lowest smooth. The blue uncertainty bars (95% confidence limit) account only for incomplete spatial sampling.[5]

Human being's production and living cause these issues because it does not form a closed cycle but instead simply consists in the rapid depletion of fossil carbon reservoirs. If the same fuels, however, had been generated by fixing carbon from the atmosphere, namely no net increase of atmospheric carbon dioxide concentration would occur, bringing about the system entirely carbon neutral. The production of fuels from CO_2 and water is practically feasible but requires energy. If the invested energy derives from renewable resources, *e.g.* solar energy, the production of fuels from CO_2 opens the door to a closed and sustainable anthropogenic carbon cycle, the Holy Grail to solving the issues of global warming and energy crisis. The conversion of carbon

dioxide into small molecules using solar energy would thus be like killing two birds with one stone.

1.1.2 Solar energy and artificial photosynthesis

The generalized solar energy is the source of much energy on earth, such as wind energy, chemical energy, water potential energy and so on. Fossil fuels can be called ancient solar energy. Solar energy is extremely rich, environmentally friendly and omnipresent. Solar irradiation gives rise to biological processes taking place on Earth all the time. Through a complex cyclic process, solar energy is absorbed by chlorophyll molecules in green plants and then used to drive the transformation of water and carbon dioxide into carbohydrates, which serve as the source of energy for all life. This process is called photosynthesis, in which molecular oxygen is released as a byproduct, allowing for aerobic life forms to exist. Inspired by this, many research efforts have contributed to replicating the efficient natural process of photosynthesis by using mimetic or bio-inspired model systems under ambient conditions.

Figure 1.5 Area of land that needs to be covered with 10% efficient solar cells in order to generate 20 TW of electrical power.

Solar energy is of great potential and it is considered to be the only source that can meet all of our energy needs. Total solar power reaching earth's surface is estimated to be 120, 000 TW.[8] To generate 20 TW of power from the Sun, the area to be covered by 10% efficient solar cells is about 816, 000 km^2, which corresponds to an area of about 900 × 900 km^2 and accounts for 0.16% of earth's surface. While this appears relatively small when projected onto Africa (Figure 1.5), it

actually is equal to the total area of France and Germany combined. If these solar cells work 4 h every day for 365 days per year, they will produce 2.9×10^{13} kW·h/yr electricity, which is much more than the whole world electricity consumption in 2014 (2.2×10^{13} kW·h/yr).[9]

As the contribution of solar energy to the total energy mix increases, it will become difficult for electricity network operators to cope with the intermittent nature of solar power (day/night cycle, clouds, and seasons). At a certain point, grid-based storage capacities will be exceeded and large-scale energy storage solutions will need to be implemented. One of the more attractive possibilities is to store solar energy in chemical bonds, such as in molecular hydrogen, methane and so on. The energy of a visible-light photon range between 1.5 and 3.1 eV, or 150-310 kJ/mol, which is more than sufficient for many chemical synthesis routes. Compared to, *i.e.*, batteries and mechanical or gravity-based storage systems such as flywheels and pumped water reservoirs, chemical fuels combine the advantages of high energy storage densities and ease of transportation. Inspired by green plants, artificial CO_2 chemical recycling, as a hot research topic at the turn of the century, plays an essential role in preventing CO_2 release in the atmosphere and provides a novel energy source simultaneously through efficient CO_2 reduction.

However, the solar spectrum spreads from photons in the UV range where the wavelengths start at ~250 nm (equals to photon energy of 4.96 eV) to photons in the IR range where the wavelengths can be 2500 nm (equals to photon energy of 0.496 eV). Photon wavelengths, their frequencies and their energies relationship follow Max Planck's equation[10]:

$$E_p = h\nu = \frac{hc}{\lambda} \quad (1)$$

where E_p is the energy of photon, h is Planck's constant and equals to 6.63×10^{-34} J·s, ν is photon frequency, λ is photon wavelength and c is the speed of light which approximately equals to 3.00×10^8 m/s.

UV light is strong enough to activate the photocatalyst (A substance is able to achieve chemical catalysis under illumination.) while it only accounts for about 5% of the total solar irradiance (Figure 1.6).[11] IR light accounts for about 50%, but its energy does not suffice to activate photocatalysts. Visible light, which accounts for about 45%, will be an eclectic choice to be used for artificial photosynthesis. Its photon energy ranging from 1.63 eV to 3.26 eV is strong enough and the energy intensity is also appropriate. In a typical solar simulated system, a Xenon

lamp, with a cut-off filter to shield UV light and a water filter to shield IR light, is usually employed as the light source.

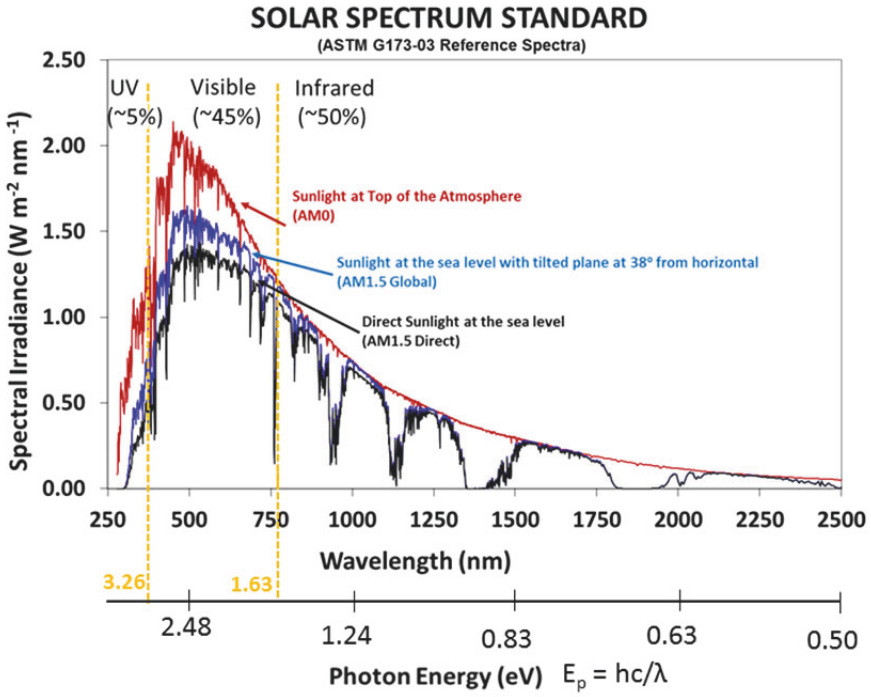

Figure 1.6 Solar spectrum with the x-axis in wavelength (nm) unit and in energy (eV) unit. Data was obtained from National Renewable Energy Laboratory (NREL) at link http://rredc.nrel.gov/solar/spectra/am1.5/astmg173/astmg173.html.[11]

Thomas Edison once said, "I'd put my money on the sun and solar energy. What a source of power! I hope we don't have to wait until oil and coal run out before we tackle that." In the past decades, a range of ever-evolving technologies such as solar heating, photovoltaics, solar thermal energy, solar architecture, molten salt power plants and artificial photosynthesis have been developed. Artificial photosynthesis is commonly used to refer to any scheme for capturing and storing the energy from sunlight in the chemical bonds of a fuel, mainly including photocatalytic water splitting and light-driven carbon dioxide reduction. Solar energy capture and storage in chemical bonds are the key process in artificial photosynthesis. The first investigations towards the development of artificial photosynthesis aimed at directly mimicking the natural system by using components from biology within synthetic structures to effectively produce fuels. A significant development in achieving an artificial photosynthetic system based on a copy of the natural machinery was developed in the late 90s by Thomas A. Moore at Arizona State University.[12] The conception was directly inspired by Nature through photo-induced adenosine

triphosphate (ATP) synthesis, using a triad consisting in a central porphyrin photosensitizer (PS) positioned between an electron donor (ED), a carotenoid, and an electron acceptor (EA), a quinone. It was the first example in which the sunlight capturing strategy was a direct mimic of the natural system, but the energy conversion step to create a useful fuel, *i.e.* sugar in natural photosynthesis, was not developed.

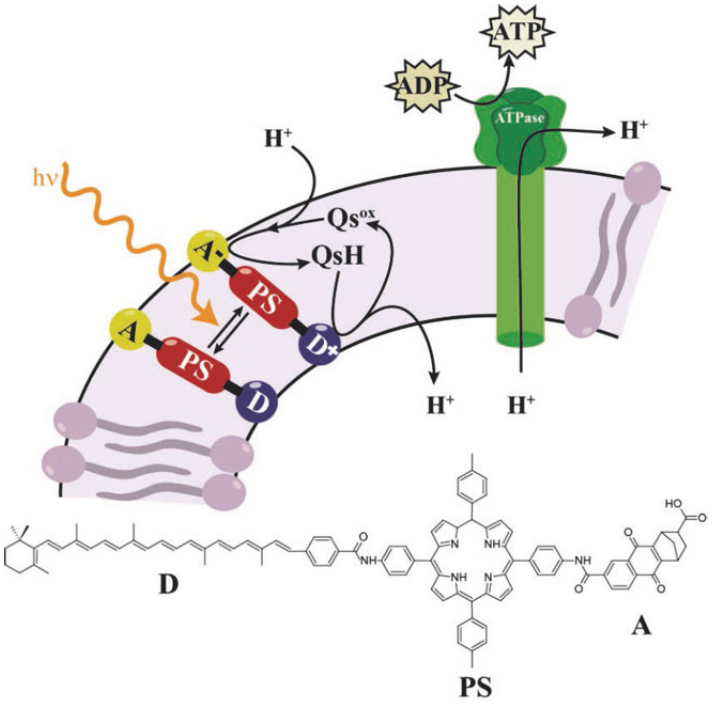

Figure 1.7 Artificial photo-induced ATP-synthesis system developed at Arizona State University.[12]

1.1.3 Routes for carbon dioxide reduction

CO_2 is the most oxidized state of carbon, and therefore the only chemical conversion with extrinsic energy is chemical reduction. A wide range of CO_2 conversion techniques have been attempted as listed below:

(1) Chemical reduction by metals which occurs at relatively high temperatures[13]

$$2Mg + CO_2 \rightarrow 2MgO + C$$

$$Sn + 2CO_2 \rightarrow SnO_2 + 2CO$$

（2）Thermochemical chemical conversion[14]

$$2CO_2 \xrightarrow{Ce,\ T>900\,^{\circ}C} CO + O_2$$

(3) Radiochemical method[15]

$$CO_2 \xrightarrow{\gamma-Radiation} HCOOH, HCHO$$

(4) Biochemical conversion[16]

$$CO_2 + 4H_2 \xrightarrow{Bacteria} CH_4 + 2H_2O$$

(5) Electrochemical conversion[17]

$$CO_2 + xe^- + yH^+ \xrightarrow{eV} CO, HCOOH$$

(6) Photochemical conversion[18]

$$CO_2 \xrightarrow{hv} CO, HCOOH$$

The last approach is very attractive because the breaking of C=O bonds in the very stable CO_2 molecule needs a very high supply of energy that can be easily obtained with the light quanta of UV and visible spectral range. The reduction of CO_2, which is one the most stable forms of C (IV) requires also the presence of electron-supplying agents, typically water or other sacrificial and abundant electron donors, such as ascorbic acid, oxalate, thiols, amines and so on. Among the advantages of the photocatalytic CO_2 conversion are the relatively mild conditions, the simultaneous mitigation of climatic changes caused by ever-increasing anthropogenic CO_2 emission, the possibility of formation of C-C bonds in the form of hydrocarbons, ethers and carbonic acids and others.

1.2 Theoretical concepts

1.2.1 Thermodynamics and kinetics of carbon dioxide reduction

Carbon dioxide molecule contains two C=O bonds with a linear configuration, in which oxygen atoms show a weak Lewis basicity, while the carbon atom is electrophilic. Because it is

centrosymmetric, the molecule has no electrical dipole, and only two vibrational bands are observed in the IR spectrum: an antisymmetric stretching mode at 2349 cm^{-1} and a bending mode near 666 cm^{-1}. There is also a symmetric stretching mode at 1388 cm^{-1} in its Raman spectrum. The orbitals of C atom are *sp*-hybridized, forming two σ bonds with O atoms, while the other two non-hybridized p orbits in C atom form two π_3^4 bonds with the p orbits in O atoms. As a result, C=O bonds are extremely stable in the atmosphere and have a dissociation energy as high as ~750 $kJ \cdot mol^{-1}$, which indicates that a high activation barrier must be overcome for CO_2 activation and C=O bond cleavage. The generation of useful fuels from their highly thermodynamically stable combustion products, CO_2 and H_2O, is necessarily endergonic. Moreover, given the highest chemical state (+4) of C atom in CO_2, the reduction of CO_2 can result in various and complex products including carbon monoxide (CO), formic acid (HCOOH) ($HCOO^-$, basic medium), oxalic acid ($H_2C_2O_4$) ($C_2O_4^{2-}$, basic medium), formaldehyde (HCHO), methanol (CH_3OH), methane (CH_4), carbon (C), ethylene (C_2H_4), ethanol (C_2H_5OH), ethane (C_2H_6), n-propanol (C_3H_7OH), *etc.*[19] Standard enthalpy (ΔH^0), Gibbs free energy (ΔG^0) and redox potential (E^0) of CO_2 reduction are summarized in Table 1.1.[20] All the CO_2 reduction processes are more endothermic than those of water splitting owing to the positive ΔG^0 values, especially for hydrocarbon fuels such as CH_3OH and CH_4, indicating that CO_2 reduction is a much more thermodynamically unfavorable process in ambient conditions.

Table 1.1. Thermodynamic reactions of CO_2 reduction[20]

Equation	Reaction	ΔH^0(kJ mol^{-1})	ΔG^0(kJ mol^{-1})	ΔE^0(V)
1	$CO_2(g) \rightarrow CO(g) + 1/2O_2(g)$	283	257	-1.33
2	$CO_2(g) + H_2O(l) \rightarrow HCOOH(l) + 1/2O_2(g)$	270	286	-1.48
3	$CO_2(g) + H_2O(l) \rightarrow HCHO(l) + O_2(g)$	563	522	-1.35
4	$CO_2(g) + 2H_2O(l) \rightarrow CH_3OH(l) + 3/2O_2(g)$	727	703	-1.21
5	$CO_2(g) + 2H_2O(l) \rightarrow CH_4(g) + 2O_2(g)$	890	818	-1.06
6	$H_2O \rightarrow H_2(g) + 1/2O_2(g)$	286	237	-1.23

The single electron reduction of CO_2 to $CO_2^{\cdot-}$, which has been well recognized as the first step to activate CO_2 for subsequent reduction steps, occurs at -1.90 V versus the normal hydrogen electrode (NHE) at pH 7, due to a large reorganizational energy between linear molecule and bent radical anion. This step has also been determined as the rate determining step (RDS) for CO_2 reduction.

The thermodynamic redox potentials for water splitting and various CO_2 reduction products are listed below.[21] The first step of CO_2 reduction may undergo the one-electron reduction to $CO_2^{\cdot-}$ intermediate, however, this reaction is extremely thermodynamically unfavorable due to the highly negative redox potential of -1.90 V as mentioned above and is generally regarded as the RDS. In contrast, redox potentials of proton-assisted multiple electron reduction processes are very close to the one of H_2 formation. These processes, involving the participation of protons, are called proton-coupled electron transfer (PCET) processes.[22] PCET processes can bypass the formation of thermodynamically unfavorable $CO_2^{\cdot-}$ intermediate and own a much lower energy barrier to break. However, except the thermodynamic barrier, multiple electron transfer reactions usually suffer from kinetic limitations depending on the concentration of available protons in the reaction solution.[23] For instance, although CH_4 formation has a more positive redox potential (E^0 = -0.24 V) than H_2 production (E^0 = -0.41 V), implying that the formation of CH_4 is more thermodynamically favorable, eight electrons and eight protons are needed to participate in this reaction, which is actually much more difficult than the two-electron process of H_2 production. This implies that a preferred catalyst probably entails catalytic sites transferring electrons which are close from sites providing protons. Furthermore, PCET processes always include multistep reactions.[24] Despite the yet ambiguous mechanism, two plausible pathways for CO_2 reduction to CH_4 are extensively studied and partially verified: formaldehyde pathway[25] and carbene pathway[26] (Scheme 1.1). The intermediates could desorb into solvent to form the side products during the reaction processes. For instance, HCOOH and HCHO could be generated in the formaldehyde pathway (Scheme 1.1), while CO is the main side-product in the carbene pathway. In addition, some other pathways involving C-C coupling (*e.g.* glyoxal pathway) were also reported and investigated, which might induce more complex products.[27] The hydrogenation of adsorbed C_1 intermediates is kinetically easier than the formation of C-C bonds, which limits the rate and selectivity of C_2 or higher hydrocarbon production. The maximum faradic efficiency for C_2H_2, namely the simplest C_2 product, was reported to be 60%,[28] whereas that of C_3 product

(C_3H_7OH) is no higher than 30%.[29] The products are sensitively influenced by catalysts and external environments during the processes of reduction, forming a grand challenge for optimizing the selectivity of CO_2 reduction.

Possible CO_2 photoreduction reaction pathways with reduction potentials:

Photooxidation reactions

Water oxidation/decomposition	E^0_{redox}/V *vs.* NHE
$H_2O + 2h^+ \rightarrow 1/2O_2 + 2H^+$	-0.82
Hydrogen peroxide formation	
$2H_2O + 2h^+ \rightarrow H_2O_2 + 2H^+$	-0.695

Photoreduction reaction

Hydrogen formation	E^0_{redox}/V *vs.* NHE
$2H^+ + 2e^- \rightarrow H_2$	-0.41
CO_2 radical formation	
$CO_2 + e^- \rightarrow CO_2^{\cdot -}$	-1.90
Formic acid formation	
$CO_2 + 2H^+ + 2e^- \rightarrow HCOOH$	-0.61
Carbon monoxide formation	
$CO_2 + 2H^+ + 2e^- \rightarrow CO + H_2O$	-0.53
Formaldehyde formation	
$CO_2 + 4H^+ + 4e^- \rightarrow HCHO + H_2O$	-0.48
Methanol formation	
$CO_2 + 6H^+ + 6e^- \rightarrow CH_3OH + H_2O$	-0.38
Methane formation	
$CO_2 + 8H^+ + 8e^- \rightarrow CH_4 + 2H_2O$	-0.24

Ethanol formation

$$CO_2 + 12H^+ + 12e^- \rightarrow CH_3CH_2OH + 3H_2O \qquad -0.16$$

Ethane formation

$$2CO_2 + 14H^+ + 14e^- \rightarrow C_2H_6 + 4H_2O \qquad -0.27$$

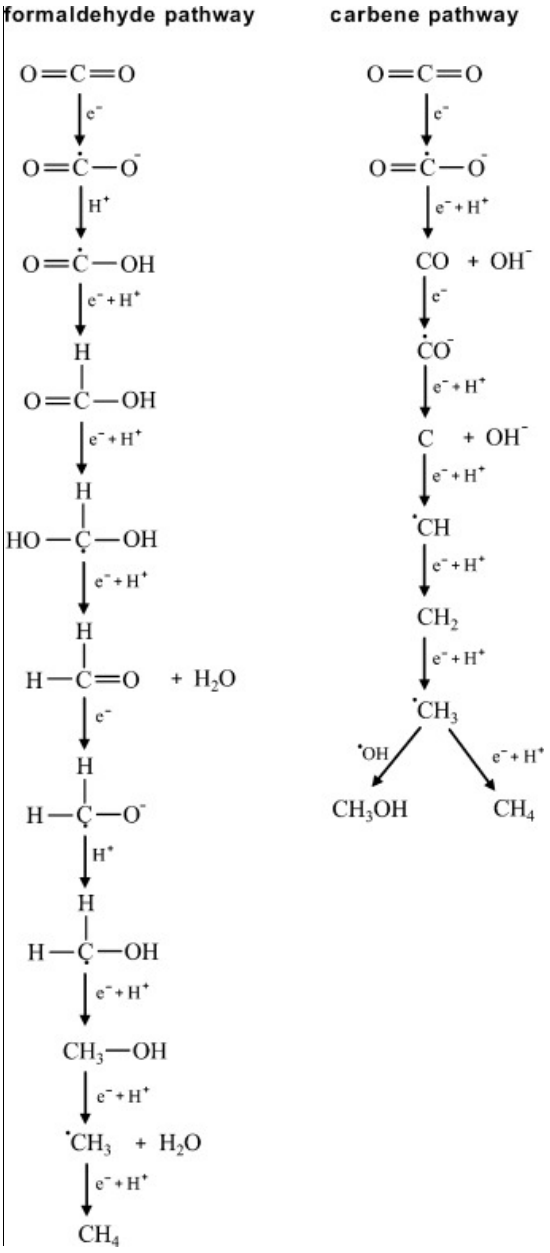

Scheme1.1 Two possible mechanisms for the reduction of CO_2 to methane: formaldehyde and carbine pathways.[24]

1.2.2 Common terms about photochemical reduction of carbon dioxide

The turnover number (TON) is defined as the number of catalytic cycles (*i.e.* number of CO_2 reduction into one of its product) that occur per catalyst unit over the catalyst's lifetime. The turnover frequency (TOF) is a measure of the instantaneous efficiency of a catalyst, calculated as the ratio of the TON over time per active site.[30] TON and TOF are pieces of evaluation for the activity of catalytic active centers, and they have been extensively applied to metal nanoparticles and homogeneous metal complex catalysts. The larger the TON and TOF, indicates the greater the catalytic activity. These definitions for photocatalytic CO_2 reduction are listed below:[31]

$$\text{TON} = \frac{\text{Total moles product}}{Total\ moles\ catalyst} \tag{2}$$

$$\text{TOF (in } t^{-1}) = \frac{\text{Total moles product}}{Total\ moles\ catalyst \times t} \tag{3}$$

where t is the reaction time. Ideally, a catalyst would have infinite TON, and in practical industrial applications, TONs of 1 million are common. It is important to note that TON reported for photochemical reductions are not always measured by Equation (2). A common alternative is to illuminate for a dedicated time interval rather than continuous illumination until catalysis ceases. As such, one needs to carefully examine the definition of TON used by different authors.

Catalytic selectivity (CS) is defined as the molar ratio of one of the CO_2 reduction products to that of total amount of products as follows:

$$\text{CS (\%)} = \frac{Moles\ of\ one\ reduction\ product}{Total\ moles\ products} \times 100\%. \tag{4}$$

Any catalyst that reduces CO_2 to carbon monoxide, formate or other products is also thermodynamically capable of proton reduction to hydrogen. In fact, depending on the number of electrons and protons transferred, CO_2 can be reduced to at least 16 different kinds of products mentioned previously.[32] The competition with protons reduction is always present. CS values provide quantitative data on the efficiency of CO_2 reduction relative to all products in specific experimental conditions (*i.e.* pH, solvent, temperature, pressure). Synthetic modification of the transition-metal catalysts provides the opportunity to tune relative reactivity through inductive and steric effects. The ability to control reactivity at the molecular level represents a significant advantage of homogeneous complexes over heterogeneous materials.

On account of various products, the selectivity is an indispensable parameter for the evaluation of CO_2 reduction. In terms of photoelectrocatalysis, the Faradaic Efficiency (FE) is typically used to assess the efficiency of producing selective products and is calculated by Equation (5).[33]

$$\text{FE (\%)} = \frac{n \times F \times Total\ moles\ products}{Q} \times 100\% \quad (5)$$

where n is the number of needed electrons for product evolution (*e.g.*, 2 for CO and 8 for CH_4), F is the Faraday constant, and Q is the total passed charge.

Quantum yield (QY) is a crucial parameter for assessing the performance of a photocatalyst or photocatalytic system. The internal and apparent quantum yields are defined by Equations 6 and 7, respectively.[34]

$$\text{Internal quantum yield (\%)} = \frac{n \times Total\ moles\ products}{moles\ absorbed\ protons} \times 100\% \quad (6)$$

$$\text{Apparent quantum yield (\%)} = \frac{n \times Total\ moles\ products}{moles\ incident\ protons} \times 100\% \quad (7)$$

where n is the number of needed electrons for product evolution. The apparent quantum yield is estimated to be smaller than the internal quantum yield because the number of absorbed photons is usually smaller than that of incident light. In addition to the quantum yield, the solar energy conversion efficiency that is usually used for evaluation of solar cells is also sometimes reported in the literature. It is defined by Equation 8.

$$\text{Solar energy conversion (\%)} = \frac{\text{Output energy of carbon dioxide reduction evolved}}{\text{Energy of incident solar light}} \times 100\% \quad (8)$$

1.3 Photocatalytic reduction of carbon dioxide

Photocatalysis is a reaction which uses light to activate a substance which modifies the rate of a chemical reaction without being involved itself. A photocatalyst is a substance which can modify the rate of chemical reaction using light irradiation. In Nature, chlorophyll of plants is a typical photocatalyst: it captures sunlight to turn water and carbon dioxide into oxygen and glucose. As inspired by the natural photosynthesis,[35] the nature has been evolved in catalyzing CO_2 reduction with perfect activity and selectivity, and the research area of artificial

photosynthesis has grown exponentially over the past decades.[36] Furthermore, compared with other methods for CO_2 reduction, photocatalytic conversion of CO_2 has a unique advantage of direct using solar energy. Since solar energy is completely inexhaustible and has zero carbon emission, photocatalytic reduction of CO_2 for the formation of synthetic fuels and fine chemicals has a great potential to cut CO_2 emissions and to alleviate our dependence on fossil fuels. Photochemical CO_2 reduction can be catalyzed heterogeneously or homogeneously. In the heterogeneous approach, molecules of the gaseous or liquid reactants are adsorbed on the surface of a solid catalyst. In the homogeneous one, a molecular catalyst is uniformly dispersed in a liquid phase. In most of the existing industrial chemical transformations, catalysts are insoluble solids. Homogeneous catalysts are also feasible because their reduction potentials can be controlled through structural modification to match the potential required for CO_2 reduction and provide selectivity toward specific target products from CO_2 molecules. Moreover, catalysts are well characterized in terms of their chemical composition, structure, optical and redox properties at a molecular level. Since all molecules of a given homogeneous catalyst have the same structure, they facilitate breaking, forming, and reorganization of chemical bonds of the reactants in an identical manner. Both heterogeneous and homogeneous catalysts operate by reducing the energy required to achieve the reorganization of molecular structures of the reactants.

1.3.1 Semiconductor-based carbon dioxide reduction

Since the seminal investigation by Halmann in 1978, the photocatalytic CO_2 reduction into fuels with H_2O, using solar energy as the driving force has drawn much attention.[37] The first studies of the photocatalytic CO2 reduction were performed on GaP, ZnO, ZnS, then a variety of semiconductor (SC) photocatalysts was extended to TiO_2, CdS, SiC, as well as various niobates, tungstates and germinates. It is generally accepted that SC-based photocatalysis for CO_2 reduction with H_2O involves three main steps[19] (Figure 1.8 A). In the first step, activated electron-hole pairs are generated when a SC photocatalyst is illuminated by an appropriate light source with its energy equal or greater than the bandgap energy (E_g) of the semiconductor. Then, the generated electrons and holes migrate to the surface of the SC or a co-catalyst in contact with the SC, with only a fraction of carriers actually reaching the surface. A larger fraction of electron-hole pairs recombine again, with energy released in the form of heat or photons. In the third step, photogenerated electrons can reduce CO_2 which is adsorbed on catalyst surface into CO, CH_4,

CH_3OH or another product, whereas photogenerated holes can oxidize H_2O into O_2. Figure 1.8 B shows the band-gap positions of some typical SCs and the standard reduction potentials for CO_2 reduction reactions. To be thermodynamically feasible, , the conduction band (CB) edge of SCs is required to be above the standard potential of the targeted reduction reaction, whereas photo-oxidation reactions can occur only when the valence band (VB) edge of semiconductors is below the standard potential of the targeted oxidation reaction. It can be seen that photogenerated electrons in the CB of all the SCs do not have enough driving force to carry out the one-electron reduction of CO_2 to $CO_2^{\cdot-}$. In addition, because redox potentials for CO_2 reduction are close to the one of reduction of H_2O into H_2, CO_2 reduction systems always have to compete with H_2 evolution.

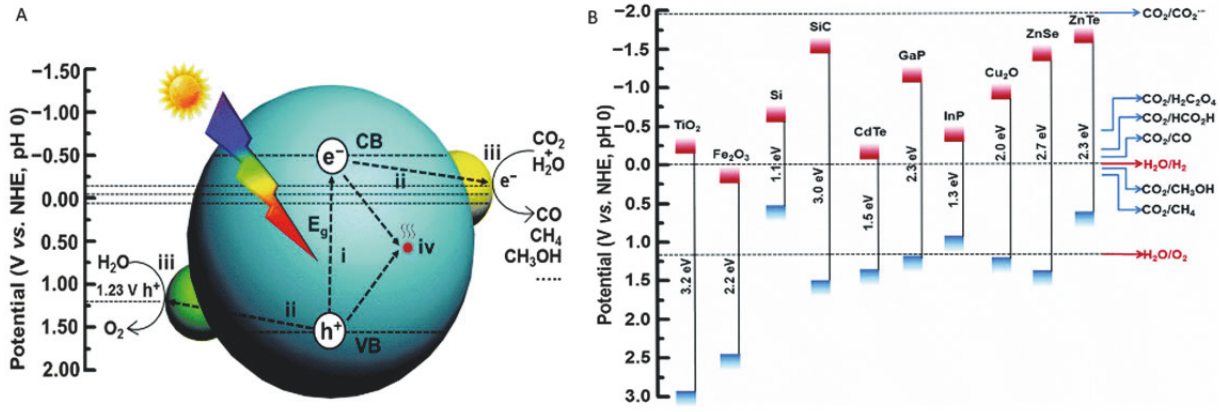

Figure 1.8 (A) Photocatalytic CO_2 reduction with H_2O over a heterogeneous photocatalyst; (B) Conduction band (red) and valence band (blue) positions of some SC photocatalysts and redox potentials versus NHE of CO_2 reduction and water splitting at pH 0.[19]

The photocatalytic conversion of CO_2 with the participation of SC materials is a multi-faced phenomenon that can be analyzed and systematized from various aspects. Therefore, the classification of SC-based systems for CO_2 reduction can be established on the composition and the structure of the photoactive SC phase. It allows grasping the versatility of photocatalytic systems and a scope of materials which can be used in the design of solar-light-driven systems for CO_2 fixation.

Nanocrystalline semiconductors as photocatalysts of CO_2 conversion. Zinc sulfide has relatively negative CB potential (around -1.8 V *vs.* NHE)[38] and therefore this SC is one of the most viable photocatalyst candidates for CO_2 reduction. Nanocrystalline ZnS-based photocatalysts can be produced by a variety of methods, including controlled precipitation[39]

(Figure 1.9), ion-exchange and hydrothermal synthesis, the latter producing the most photo-active materials.[40] Zinc sulfide NPs attached to the surface of montmorillonite were used as a working photosensitive body in reactors of various geometry for CO_2 conversion to methanol, methane, and CO.[41]

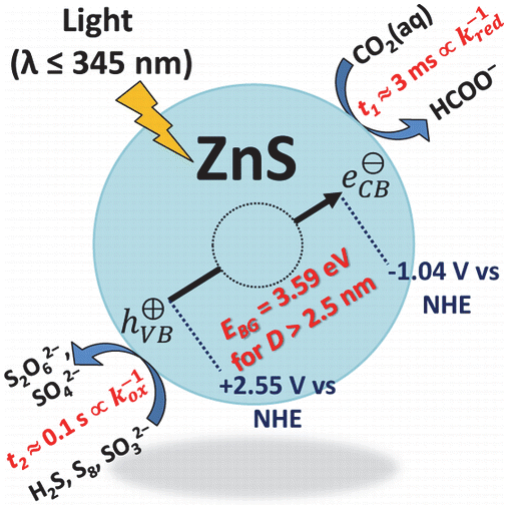

Figure 1.9 Photocatalytic CO_2 reduction with ZnS NPs.[39b]

Cadmium sulfide NPs with a more positive CB potential (E_{CB} = -0.8 V *vs.* NHE) can also be used for CO_2 reduction provided a suitable cocatalyst is introduced into the photocatalytic system. In particular, the efficient visible-light induced conversion of CO_2 into CO was observed for CdS NP assemblies with carbon monoxide dehydrogenase[42] (Figure 1.10). Hexagonal colloidal CdS NPs in N, N'-dimethylformamide (DMF) were found to be visible-light-sensitive photocatalysts for CO_2 reduction with CO as a main product.[43]

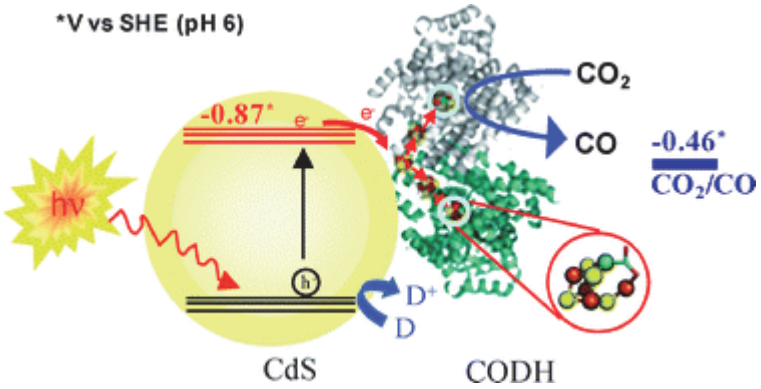

Figure 1.10 Photocatalytic reduction of CO_2 with CdS nanoparticle assemblies.[42]

Recently, open-framework zeolite-like structures consisting of nanosized metal-chalcogenide nanoclusters were tested as visible-light-sensitive photocatalysts of the CO_2 reduction (Figure 1.11). The mixed zinc-germanium-sulfide-based frameworks were found to photocatalyze the carbon dioxide reduction with water to methane and the conversion efficiency is affected by the incorporation of third metal cations (Au^{3+}, Pd^{2+}) into the framework.[44]

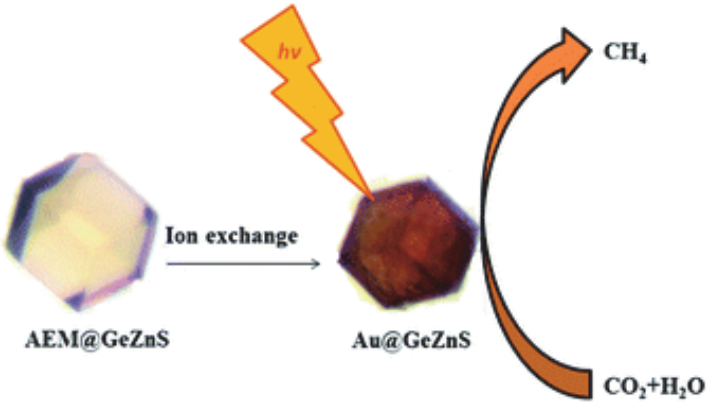

Figure 1.11 Photocatalytic reduction of CO_2 with open framework metal chalcogenides.[44]

Photocatalytic CO_2 reduction was extensively studied in Ti-based systems. In particular, three nanocrystalline TiO_2 polymorphs anatase, rutile, and brookite were compared both in the pristine form and after a treatment with ionized helium flow creating oxygen vacancies on the NP surface (Figure 1.12 (A)).[45] Such treatment resulted in a remarkable (up to 10 times) increase of the rate of photocatalytic CO_2 reduction to CO and CH_4 on anatase and brookite, while rutile retained a low activity in these processes even after the treatment. In situ diffuse reflectance infrared Fourier transform spectroscopy (DRIFTS) revealed that the enhancement effect originates from a higher efficiency of $CO_2^{\cdot-}$ anion radical formation on oxygen vacancies and from the formation of Ti_3^+ sites of the plasma-treated titania NPs. The photoactivity of titania in CO_2 conversion can be increased by introducing co-catalysts, such as metallic NPs which can collect photogenerated electrons and favor multi-electron processes. As shown in Figure 1.12 (B),[46] the rate of photocatalytic CO_2 reduction into methane with water vapor increases from Ag to Rh, Au, Pd and Pt in line with an increase of the electron-accepting capability of the metal NPs. For a given metal, CO_2 conversion increases with a decrease of the NP size and typically shows a dome-shaped dependence on the metal content. CO_2 reduction efficiency is limited by the competing water reduction to H_2 reaction of which can be suppressed by the deposition of an additional protective MgO layer on the photocatalyst surface.

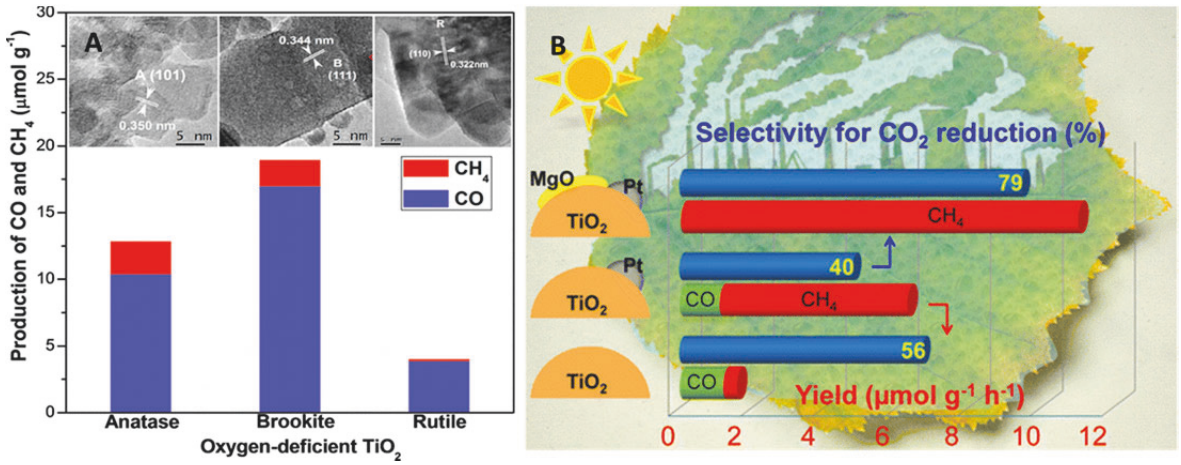

Figure 1.12 (A) Photocatalytic CO_2 reduction with different TiO_2 nanocrystal polymorphs; (B) Schematic illustration of photocatalytic CO_2 reduction with TiO_2/co-catalyst systems.[45-46]

Doped semiconductor as photocatalysts of CO_2 conversion. Doping the wide-bandgap SCs, such as TiO_2, with metal ions or non-metal atoms is one of the most frequent and productive strategies. Through this method, photoreaction efficiency could be increased thanks to recombination inhibition and extension of the spectral sensitivity range of the photocatalysts as a result of the participation of localized or delocalized dopant levels in the light absorption.

The incorporation of Pd, Cu, and Mn ions into the TiO_2 lattice allows the access to the visible range (Figure 1.13).[47] Dopants are present in the titania lattice as -O-M-O- fragments and can actively participate in the trapping of photo-generated charge carriers, *i.e.* VB holes in the case of Pd and Cu and CB electrons in the case of Mn. As a result, doping increases the efficiency of the photocatalytic CO_2 reduction to methane.

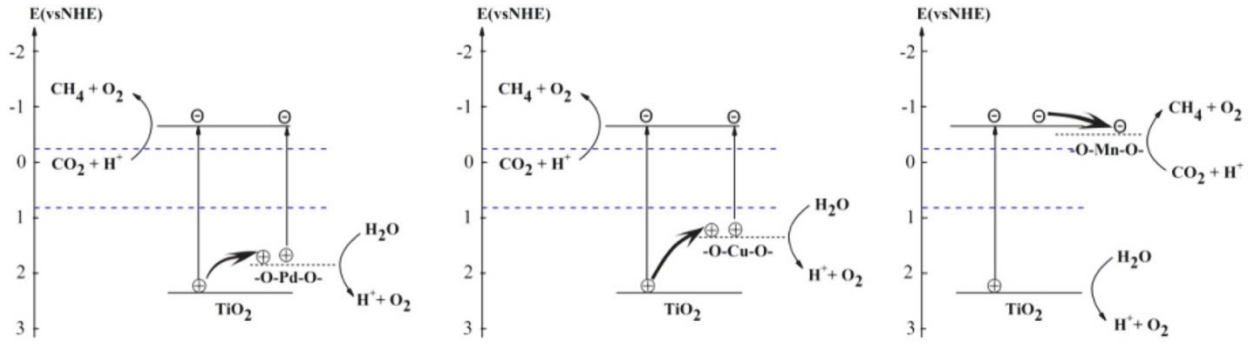

Figure 1.13 Photocatalytic reduction of CO_2 with Pd-, Cu- or Mn-doped TiO_2.[47]

In-doped nanocrystalline TiO_2 was applied as a photo-active phase for the photocatalytic CO_2 conversion in microchannel monolith photoreactors.[48] These systems generate a broad range of

reduction products with a population decreasing in the following sequence: CO > CH_4 > C_2H_6 > C_2H_4 > C_3H_6. After a multi-parameter optimization of the photoreactor performance, quantum yields of CO and CH_4 reached 0.1 and 0.022%, respectively. Doping of the mesoporous titania with In was also reported to change the CO_2 reduction product from CO to CH_4 increasing the light harvesting efficiency by a factor of *ca.* 8.[49]

Nanocrystalline ZnS doped with Ni(II) showed a high selectivity toward the formation of methyl formate as a result of the photocatalytic CO_2 reduction in methanol.[40] The highest yields were observed at ~0.3 mol% dopant content.

Sensitized systems for CO_2 photoreduction. Nanocrystalline titania sensitized with a typical Ru(II)-bipyridyl dye (N719) coupled with a Pt counter electrode was used for the visible-light-driven photoreduction of CO_2 to HCOOH, HCHO and CH_3OH in a two-vessel geometry (Figure 1.14 (A)).[50] The functionalization of TiO_2 NPs with various aminosalicylic acids (ASA) results in the formation of surface charge transfer complexes that extend the absorption range of titania far into the visible range (Figure 1.14 (B)).[51] The photoinduced charge transfer in such complexes occurs directly from the highest occupied molecular orbital (HOMO) of ASA molecules into the CB of TiO_2 NPs and then to adsorbed CO_2 molecules. As a result, the absorption band edge of a ternary TiO_2-ASA-CO_2 system shifts even further into the visible range as compared to the binary TiO_2-ASA charge transfer complex.

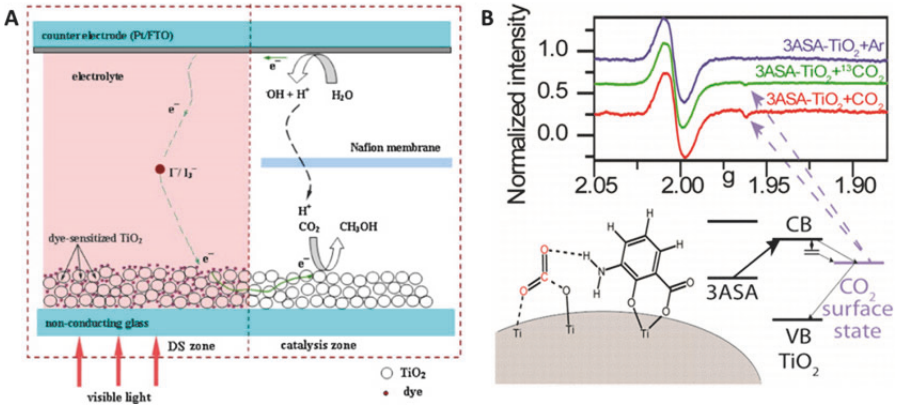

Figure 1.14 (A) Photocatalytic reduction of CO_2 with dye-sensitized TiO_2 film; (B) Photocatalytic reduction of CO_2 with aminosalicylic acids modified TiO_2.[50-51]

A tandem principle was realized for a Nickel (II) oxide photocathode sensitized with a supramolecular Ru(II)-Re(I) complex assembly and coupled to a tantalum oxynitride photoanode

modified with a cobalt oxide co-catalyst (Figure 1.15 (A)).[52] The nickel oxide-based photocathode showed selectivity toward the formation of CO. The system also used water as an electron donor and a low external bias of ~0.3 eV. The p-type $CuGaO_2$ photocathode sensitized by a very similar supramolecular assembly of Ru(II)-Re(I) complexes also revealed a photoelectrochemical activity in the CO_2 reduction by water even without an additional external bias (Figure 1.15 (B)). It is the first self-driven photoelectrochemical cell constructed with a molecular photocatalyst to achieve the reduction of CO_2 by only using visible light as the energy source and water as the reductant.[53]

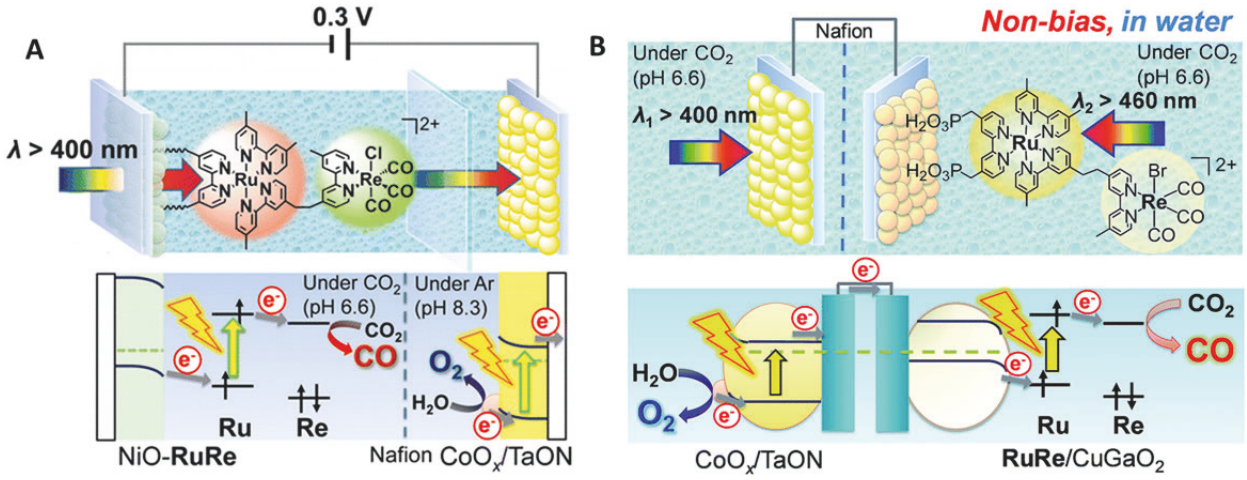

Figure 1.15 (A) Photoelectrochemical reduction of CO_2 with Ru(II)-Re(I) immobilized on a NiO photocathode; (B) Photoelectrochemical reduction of CO_2 with Ru(II)-Re(I) immobilized on a $CuGaO_2$ photocathode.[52-53]

In tandem systems comprising graphitic carbon nitride (g-C_3N_4) and Ru(II)-bipyridyl complexes, the rate and pathway of CO_2 reduction depend on the bipyridyl substituent X in the 4-position.[54] In particular, for tandems based on X = -COOH and X = -PO_3H_2, the main product was HCOOH, while for X = -$CH_2PO_3H_2$ the photoprocess yielded CO and HCOOH with a relatively high selectivity toward the former (40-70%). The difference arises from a photoinduced transformation of the -$CH_2PO_3H_2$-substituted Ru-bipyridyl complex into a polymeric species specifically active toward CO formation. Polymeric Ru-bipyridyl complexes were also used as sensitizers/electrocatalysts to increase the rate of photocatalytic CO_2 reduction to formate over indium phosphide.[55]

Binary semiconductor nanoheterostructures for CO_2 photoreduction. The photocatalytic conversion of CO_2 in the presence of methanol over a CuO/TiO_2 heterostructures results in the

preferential formation of methyl formate.[56] In this case, methanol serves both as reactant and as VB hole scavenger, while CO_2 is reduced by the photogenerated CB electrons. Deposition of Cu_2O NPs onto titania was reported to result in enhanced adsorption of CO_2 and simultaneous inhibition of water adsorption.[57] Simultaneously, Pt NPs deposited onto TiO_2 acts as electron "pools" promoting multi-electron photoinduced reactions. The summary effect of Cu_2O and Pt NPs results in complete suppression of the water reduction pathway on titania surface and in the selective reduction of CO_2 with CH_4 as a sole product. Titania and Cu_2O can also be separated in space and used as photoanode and cathode, respectively, in a photoelectrochemical system for the CO_2 reduction. In this way, Cu_2O can be protected against oxidative photocorrosion by photogenerated VB holes.[58]

Titania coupling with g-C_3N_4 allows the spatial charge carriers separation since photo-generated electrons are collected in the lower-positioned titania CB and VB holes (photogenerated in both SCs) are supplied to the reactants through the VB of carbon nitride. As a result, titania/ g-C_3N_4 composites displayed an enhanced photocatalytic activity.[59] A similar enhancement effect in the CO_2 reduction to methane was also observed for *g*-C_3N_4/$KNbO_3$[60] and *g*-C_3N_4/$NaNbO_3$[61].

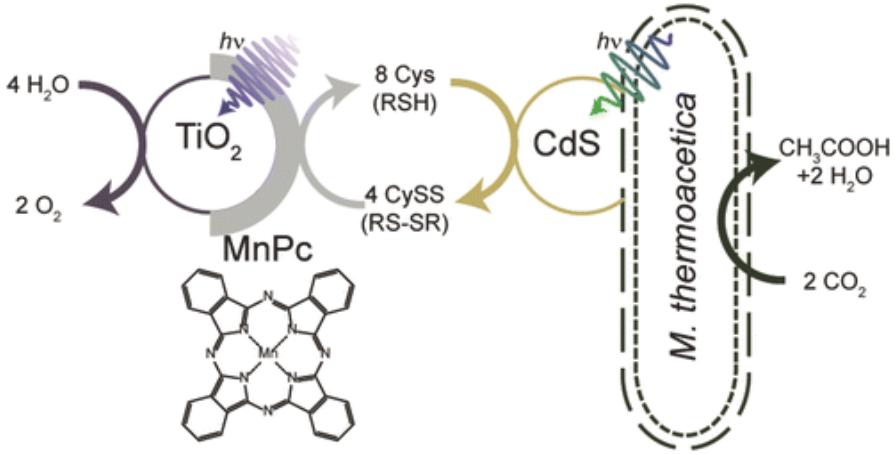

Figure 1.16 Scheme of a "Moorella thermoacetica-CdS/TiO_2-Mn phthalocyanine" tandem system for the CO_2 conversion.[62]

In metal chalcogenide/titania composites with proper CB and VB level positions, CO_2 reduction and donor (for example, water) oxidation occur on the surface of titania and metal chalcogenide NPs, respectively. Both branches of the photoprocess can be additionally separated in space to avoid the re-oxidation of CO_2 reduction products and to promote the formation of C-C

bonds. For example, by combining two subsystems - the *Moorella Thermoacetica* bacteria decorated with CdS NPs and TiO_2 NPs loaded with Mn(III) phthalocyanine into a Z-system - CO_2 reduction to acetic acid can be achieved (Figure 1.16).[62] Both subsystems are connected by a donor/acceptor cysteine/cystine couple. The cysteine gets oxidized on the surface of CdS NPs to cystine and then cystine is regenerated to cysteine on the surface of the phthalocyanine-functionalized titania.

The efficiency of photocatalytic reduction of CO_2 with water vapor over CdSe/Pt/TiO_2 nanoheterostructures was found to depend on the CdSe NP size as a result of a size-dependence of the CdSe CB position (Figure 1.17).[63] The main reduction product was methane with CH_3OH, CO and H_2 present as secondary admixtures.

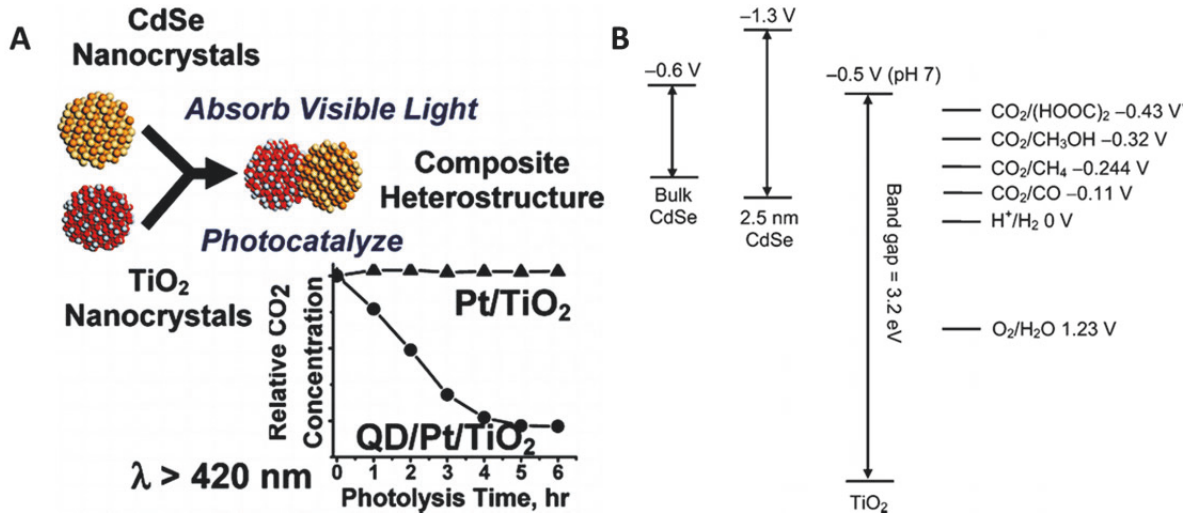

Figure 1.17 (A) Schematic illustration of photoelectrochemical reduction of CO_2 with CdSe/Pt/TiO_2 heterostructured catalysts; (B) Energy diagram of TiO_2/CdSe heterostructures with bulk and nanocrystalline cadmium selenide.[63]

To sum up, in recent years, lots of working groups put intensive efforts in the development of SC photocatalysts for CO_2 reduction. In these simple systems, namely powder in water, SC photocatalysis has a big potential for the wide use in CO_2 reduction. Not only were these materials able to achieve superior efficiency, but their activity was also demonstrated as being amenable to fine-tuning through the control of size and morphology.[64] In this way, materials increase their surface area, thus effectively improving their activity, while at the same time widening their photoelectronic properties. It would be preferable to control each of these independently. Another aspect of heterogeneous catalysis that must be put forth is the fact that

these materials are difficult to rationally control on the molecular level and the most active systems rely mainly on the use of precious and/or rare metals. Thus, tuning the selectivity at the molecular level remains difficult. Its application in commercial use has still far to go.

1.3.2 Molecular metal-based complex for carbon dioxide reduction

Compared to semiconductor-based CO_2 reduction catalysts, transition metal complexes are also at the forefront of potential catalysts. Such compounds can have multiple and accessible redox states which have been shown to promote multiple electron transfer reactivity. Furthermore, the formal reduction potentials can be systematically tuned through ligand modification to better match the redox potential required for CO_2 reduction. A large number of transition metal complexes have been studied for potential CO_2 reduction applications. Some of the typical examples are reviewed below.

Molecular photocatalytic systems for CO_2 reduction typically comprise a catalyst (CAT), a redox photosensitizer (PS) which can harvest light energy and then mediate the transfer of photoelectrons, and a sacrificial donor (SD) which offer electrons and/or protons. Generally, this type of catalytic system is called a three component homogenous photochemical system. First, upon light excitation, the molecular light absorber, such as the typical ruthenium (II) trisbipyridine ($[Ru(bpy)_3]^{2+}$) is promoted to an excited state PS* (Equation 9). Thanks to its strong absorption in the visible range and to internal heavy atom effect (triplet metal-to-ligand-charge-transfer (MLCT)), high quantum efficiency in photocatalysis can be achieved.[65] The excited state PS^* is then reductively quenched by a SD, typically triethylamine (TEA) or triethanolamine (TEOA), to yield the reduced form of the sensitizer, PS^-, and the oxidized form of the donor, $SD^{\cdot+}$ as shown in Equation 10. It is important to note that the oxidized amines are quite reactive and are known to undergo hydrogen atom abstraction and radical rearrangements which result in the formation of highly reduced carbon-centered radical species, $Et_2NC^{\cdot}HCH_3$ or $(HOC_2H_4)_2N(C^{\cdot}HCH_2OH)$, which can, under certain conditions, reduce a second PS (Equation 13 and 14).[66] We denote this carbon-centered radical as $SD^{\cdot}$. The reduced sensitizer, PS^-, is responsible for the electron transfer to a molecular CAT and generates the reduced active state of CAT able to reduce CO_2 (Equations 11 and 12).[67]

$$PS + h\nu \rightarrow PS^* \quad (9)$$

$$PS^{*} + Et_3N \rightarrow PS^{-} + Et_3N^{\cdot+} \quad (10)$$

$$PS^{-} + CAT \rightarrow PS + CAT^{-} \quad (11)$$

$$CAT^{-} + CO_2 \rightarrow\rightarrow CAT + Products \quad (12)$$

$$Et_3N^{\cdot+} + Et_3N \rightarrow Et_3NH^{+} + Et_2NC^{\cdot}HCH_3 \quad (13)$$

$$Et_2NC^{\cdot}HCH_3 + PS \text{ (or CAT)} \rightarrow Et_2N^{+}{=}CHCH_3 + PS^{-} \text{ (or } CAT^{-}) \quad (14)$$

Cobalt and nickel cyclams complexes. In 1984, Tinnemans *et al.* were the first to investigate cobalt and nickel cyclams as CO_2 photoreduction CATs, with $[Ru(bpy)_3]^{2+}$ as PS and ascorbic acid (AA) as SD in water solution.[67-68] Reduction products were identified as carbon monoxide and formate. Scheme 1.2 displays the proposed formation pathways of each product using M^{II}(cyclam) as a representative macrocycle. They originally proposed insertion of CO_2 into a metal-hydride bond to yield a metal-formato complex, $[LM^{III}\text{-}OC(H)O]^{2+}$ (red pathway). The resultant $M^{III}L$ can be subsequently reduced by two electrons to regenerate the catalytically active state. The source of the reducing equivalents may be PS^{-}, $SD\cdot$ or $[M^{I}L]^{+}$, but it is unknown for all mechanistic pathways independent of products formed, which is H_2, CO or $HCOO^{-}$. The insertion of CO_2 into a metal-hydride bond cannot easily account for the formation of carbon monoxide, which is proposed to proceed through a metal-CO_2 intermediate (brown pathway, Scheme 1.2).

In order to avoid the use of precious metal, such as Ru complex as PS, organic dyes have been employed. In 1991, Yanadida *et al.* reported photocatalytic systems using *p*-terphenyl as PS, cobalt cyclams complexes as CAT, and TEA or TEOA as SD in mixed ACN/CH_3OH solutions.[69] Irradiation with UV light ($\lambda > 290$ nm) of these solutions produced CO and $HCOO^{-}$ ($CO/HCOO^{-}$ = 1.5) along with H_2 evolution. These systems showed good selectivity (CS (CO + $HCOO^{-}$) = 86%~99%) and high QY (Φ(CO + $HCOO^{-}$) = 25 % with λ_{ex} = 313 nm). When using $CoCl_2$ instead of Co cyclams as CAT, CO_2 was not transformed. However, these systems can only use UV light because of the limited visible light absorption of *p*-terphenyl. Interestingly, if phenazine was used as the PS, a CS of 93% for the formation of $HCOO^{-}$ was observed ($\Phi(HCOO^{-})$ = 7 %

with λ_{ex} = 313 nm),[69b] which indicates that PS can not only affect the photocatalytic efficiency of the system but also its catalytic selectivity. The PS was able to supply efficiently not only an electron but also a proton at the N atom of the CAT. The formation of the corresponding hydride complex (Co-H) was thus enhanced and followed by CO_2 insertion, resulting in the $HCOO^-$ acting as a ligand in the Co complex.

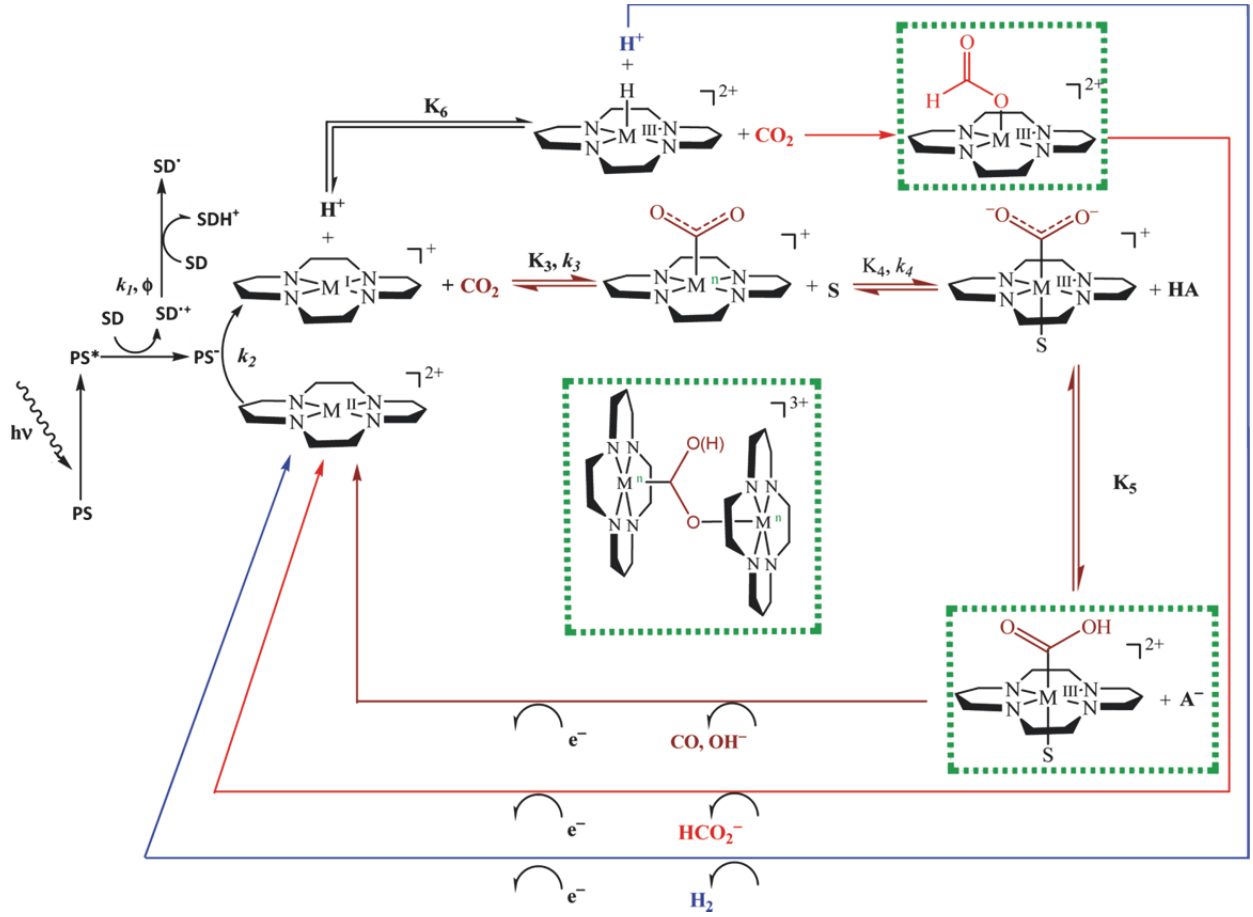

Scheme 1.2. Proposed mechanistic steps in the reduction of CO_2 by Co/Ni Cyclams. Hydrogen (blue), formate (red) and CO (brown), as well as putative intermediates (green) when M = Co or Ni. $SD^{\cdot}$ is a highly reduced carbon-centered radical species.[67-68]

Recently, Reisner *et al.* reported a hybrid assembly consisting in ligand-free ZnSe quantum dots (QDs) as visible-light PS combined with a phosphonic acid-functionalised Ni(cyclam) CAT, NiCycP (Figure 1.18).[69b] This precious metal-free photocatalytic system shows a high activity for aqueous CO_2 reduction to CO (Ni-based TON_{CO} > 120), whereas an anchor-free catalyst, Ni(cyclam)Cl_2, produced three times less CO. Additional ZnSe surface modification with 2-

(dimethylamino)ethanethiol (MEDA) partially suppresses H_2 generation and enhances CO production allowing for a Ni-based TON_{CO} of > 280 and more than 33% selectivity for CO_2 reduction over H_2 evolution, after 20 h visible light irradiation (λ > 400 nm, AM 1.5G, 1 sun). The external quantum yield of 3.4 ± 0.3% at 400 nm is comparable to state-of-the-art precious metal photocatalysts. Transient absorption spectroscopy showed that band-gap excitation of ZnSe QDs is followed by rapid hole scavenging and very fast electron trapping in ZnSe. The trapped electrons transfer to NiCycP on the ps timescale, explaining the high performance for photocatalytic CO_2 reduction.

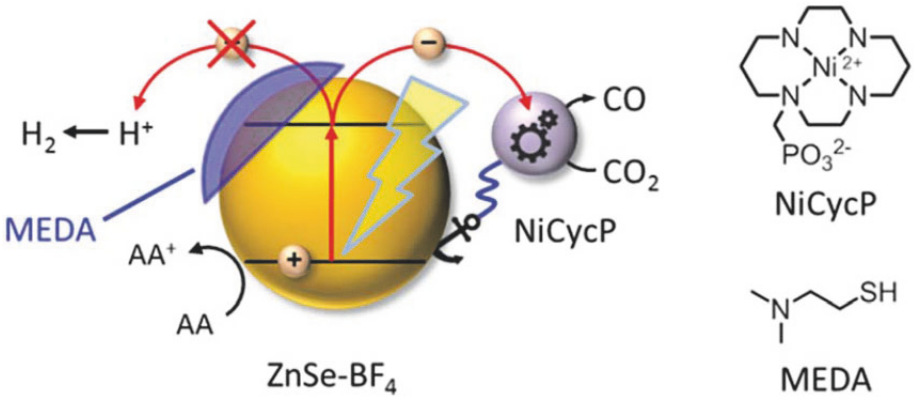

Figure 1.18 Photocatalytic system with ligand-free ZnSe QDs ($ZnSe-BF_4$) combined with a molecular catalyst, NiCycP, for aqueous CO_2 reduction to CO. H_2 evolution can be partially suppressed by a surface inhibitor (MEDA).[69b]

Transition metal polypyridine complexes. Metal polypyridine complexes are often used as a main component, *i.e.,* as redox PS and/or as CAT, in various photocatalytic systems for CO_2 reduction.[70] In particular, the design of highly efficient and selective photocatalytic systems which are based on non-expensive materials is a great challenge for chemists. Lau *et al.* reported the photocatalytic reduction of CO_2 by $[Co(qpy)(OH_2)_2]_2^{+}$ (qpy = 2,2′:6′,2″:6″,2‴-quaterpyridine) and $[Fe(qpy)(OH_2)_2]_2^{+}$ (Figure 1.19).[71] With $Ru(bpy)_3^{2+}$ as PS and 1,3-dimethyl-2-phenyl-2,3-dihydro-1H-benzo[d]imidazole (BIH) as the SD reductant in ACN/TEOA solution under visible-light excitation (blue light-emitting diode), a TON_{CO} as high as 2660 with 98% selectivity can be achieved for the Co catalyst. In the case of the Fe catalyst, the TON was > 3000 with up to 95% selectivity. More significantly, when $Ru(bpy)_3^{2+}$ was replaced by the organic dye sensitizer purpurin, TONs of 790 and 1365 were achieved in N, N-dimethylformamide for the cobalt and iron catalysts, respectively.

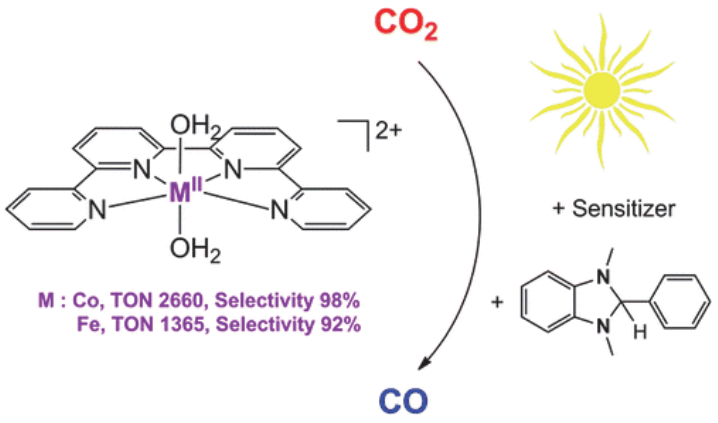

Figure 1.19 Photocatalytic system with Fe/Co quaterpyridine complexes for CO_2 reduction.[71]

Chan, Che and co-workers reported a similar type of photocatalytic system using a Co^{II} complex containing a pyridine based tetradentate tripodal ligand as CAT and Ir^{III} based complexes as PS (Figure 1.20). When $Ir(ppy)_3$ as PS, a selectivity for CO formation of 85% was obtained, with a TON_{CO} of 953 based on the CAT over 70 h.[72] In addition, by employing $[Ir(ppy)_2(bis\text{-}NHC)]^+$ (bis-NHC = cis-chelating bis(N-heterocyclic carbene)), a new PS owing better emissivity and photostability, the selectivity and the TON_{CO} for CO formation in this system were successfully improved to > 95% and > 2400 based on CAT in similar reaction conditions.[73]

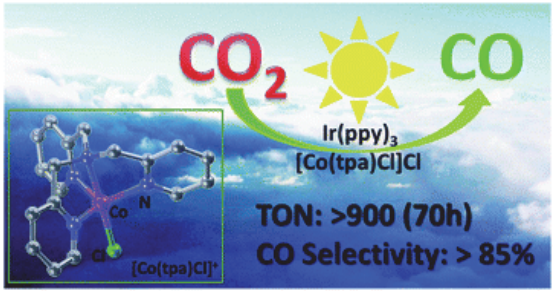

Figure 1.20 Photocatalytic system with a cobalt complex supported by a pyridine-based tetradentate tripodal ligand for CO_2 reduction.[72]

A large number of non-noble metal complexes as CAT have been reported, but stable and efficient PS containing non-precious metals are still rare, since it is very difficult to compete with the high efficiency of triplet harvesting complexes Ru or Ir. Heteroleptic emissive Cu^I PS developed by the Beller group for photocatalytic proton reduction are also suitable for CO_2 reduction in the visible light range. Ishitani *et al.* reported the first Fe/Cu system for the effective reduction of CO_2 by employing a dimeric macromolecular heteroleptic CuPS with one diamine

and one diphosphine ligand, together with an iron diamine complex as CAT (Figure 1.21).[74] Visible light irradiation of an ACN/TEOA solution containing PS, CAT and BIH as SD produced a TON_{CO} of 270, with a selectivity of 78% with respect to CO. Quantum yields of 6.7% (mononuclear) and 2.6% with a $TON_{CO} > 54$ (dimeric) were reached. The catalytic process was initiated by reductive quenching of the exited state of the Cu complex by BIH.

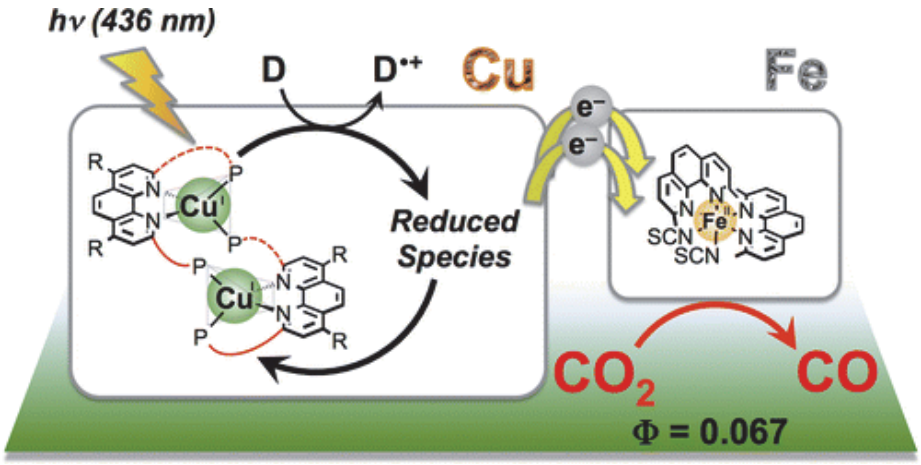

Figure 1.21. Photocatalytic system with Fe polypyridine CAT and Cu PS for CO_2 reduction.[74]

Another type of catalysis consists in one compound both acting as the light absorber and the catalyst. The "all in one" molecular photocatalysis lowers the number of required components and intermolecular electron transfer events, which may be more efficient for catalytic CO_2 reduction. The photocatalyst, PCAT, is reduced by excited state reductive quenching as described in the first type catalysis (Equations 15 and 16). Similarly, the oxidized amine donors undergo subsequent reactivity to produce $SD^{\cdot}$ radical, which can continue reducing the PCAT (Equations 18 and 19). The reduced $PCAT^{-}$ is a catalyst active state and can directly interact with CO_2 and then form products (Equation 17). Very few catalysts are capable of both absorbing solar spectrum irradiation and reducing CO_2. It should be noted that all these type of catalysts could also be used as CATs for the first type approaches with an appropriate PS.

$$PCAT + h\nu \rightarrow PCAT^{*} \quad (15)$$

$$PCAT^{*} + Et_3N \rightarrow PCAT^{-} + Et_3N^{\cdot+} \quad (16)$$

$$PCAT^{-} + CO_2 \rightarrow PCAT + \text{products} \quad (17)$$

$$Et_3N^{\cdot+} + Et_3N \rightarrow Et_3NH^{+} + Et_2NC^{\cdot}HCH_3 \quad (18)$$

$$Et_2NC^{\cdot}HCH_3 + PCAT \rightarrow Et_2N^{+}{=}CHCH_3 + PCAT^{-} \quad (19)$$

$Re(CO)_3(bpy)X$-based Complexes. Hawecker *et al.* were the first to investigate $Re^I(L)(CO)_3X$, where X = Cl^- or Br^- and L = 4,4'-R2-2,2'-bipyridine (R = H or CH_3) or 1,10-phenanthroline, for photocatalytic CO_2 reduction.[68, 75] Upon light excitation, $Re^I(L)(CO)_3X$ is promoted to a MLCT excited state with a Re^{II} metal center and an electron located on the L ligand. In the presence of a SD, the excited state catalyst is reductively quenched to form $[ReI(L^-)(CO)_3X]^-$ species (where L^- is an anion radical in Scheme 1.3). Solvent (S) is proposed to replace the halide ligand to yield the putative catalytically active state, $[ReI(L^-)(CO)_3S]$.[76] Halide ligand exchange, Cl^- for Br^-, was also observed for $[ReI(L^-)(CO)_3X]^-$. Reactions of $[ReI(L^-)(CO)_3S]$ with a proton are proposed to result in the formation of a rhenium-hydride bond. Formate production is thought to occur through CO_2 insertion into the Re-hydride intermediate (red in Scheme 1.3), whose behavior is consistent with other catalysts. Sullivan *et al.* prepared the analogous $[Re^I(bpy)(CO)_3H]$ and tested it with CO_2.[77] The rate constant of this dark reaction indicated a remarkable solvent dependency which increased with the dielectric constant of the medium.[78] $[Re^I(bpy)(CO)_3(OC(H)O)]$ was formed with a 81% yield in CO_2 saturated THF solution. Addition of excess halide to the solvent would prevent $[Re^I(bpy)(CO)_3(OC(H)O)]$ formation and increased the yield of CO production.

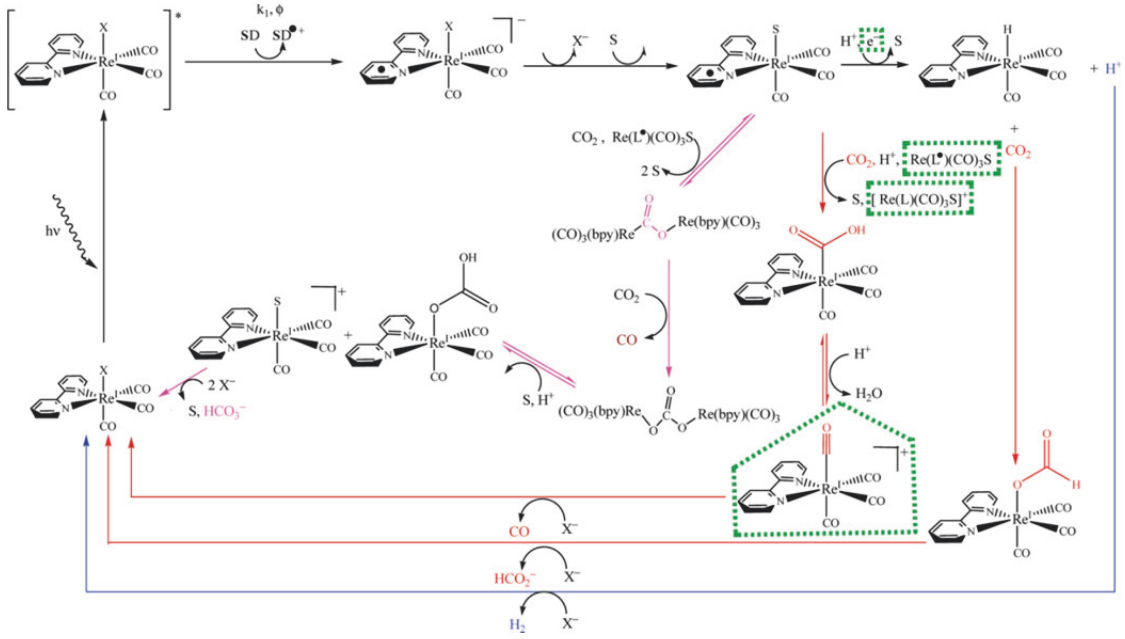

Scheme 1.3. Proposed mechanistic steps in the reduction of CO_2 by $Re(CO)_3(bpy)X$. Hydrogen (blue), formate (red), CO (brown and pink) and bicarbonate formation (pink), as well as putative intermediates and electron sources (green).[68]

While formate production is reasonably understood, the mechanism of CO formation is still an area of active investigation and debate. Upon protonation of a putative Re-CO_2 adduct, a metal carboxylate intermediate was observed that undergoes acid-promoted hydrolysis to yield H_2O and CO. Gibson *et al.* characterized $Re(L)(CO)_3(COOH)$ and proposed that proton-promoted dehydroxylation of $Re(L)(CO)_3(COOH)$ could yield $Re(L)(CO)_4^+$ which would release CO under irradiation (or when it reacts with X^-) and then regenerate the initial compound.[79] As all CO in $Re(L)(CO)_4^+$ may exchange with X^-, this pathway explains prior results which demonstrated that the use of $^{13}CO_2$ resulted in the formation of the fully labeled fac-$Re^I(L)(^{13}CO)_3X$.

Recently, Grätzel *et al.* were the first to report a molecular $Re(CO)_3(bpy)X$-based complex coupled to protected Cu_2O photocathodes for CO_2-to-CO conversion (Figure 1.22 (A)).[80] The device produced a high photovoltage of 560 mV and a photocurrent density of 2.1 mA cm^{-2}, corresponding to the highest photocurrent observed towards CO_2 reduction on an oxide material. The protection of the Cu_2O photocathode by TiO_2 enabled stable and selective reduction of CO_2 over several hours, and they found that the protic electrolyte additives were needed to overcome the unexpected charge transfer limitations on the protected photocathode surface. The discovery of charge transfer limitations from the surface of TiO_2 to the $Re(CO)_3(bpy)X$-based molecular catalyst and its elimination by the use of protic additives is highly relevant to the field of photoelectrochemistry where there is a general trend towards the use of protective overlayers. More recently, they reported a similar system with the $Re(CO)_3(bpy)X$-based complex was covalently immobilized on the photocathode with phosphonate linking groups (Figure 1.22 (B)).[81] The direct link between the CAT and the SC is not a strict requirement for high electron injection efficiency and as a positive side effect, the utilization of a spacing group between the phosphonic acid and the bipyridine ligand allows for positioning the catalytic redox center at a considerable distance away from the SC surface, making it more accessible for the reaction. This led to a 40-fold enhancement of the catalytic photocurrent as compared to planar devices, resulting in the sunlight-driven evolution of CO at large current densities and with high selectivity.

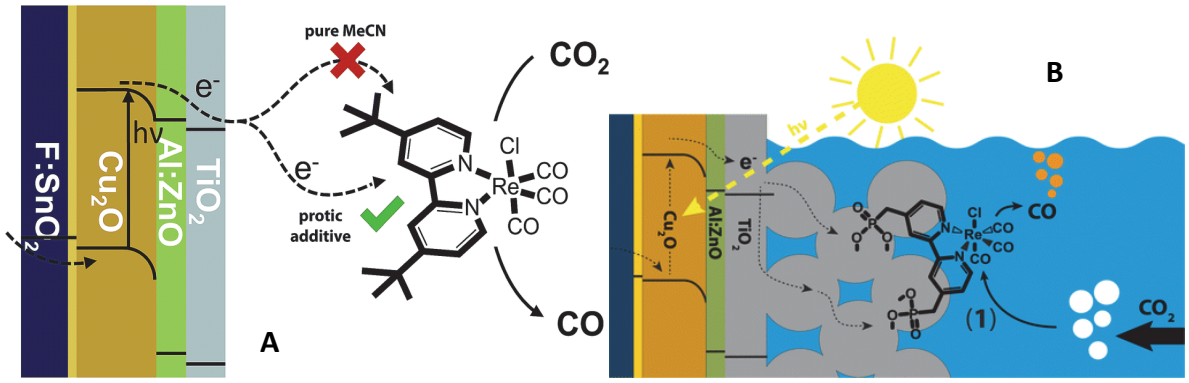

Figure 1.22 Schematic diagram of a non-covalent (A) and covalent (B) immobilization of a molecular $Re(CO)_3(bpy)X$-based complex on Cu_2O photocathodes for CO_2 reduction.[80-81]

However, it should be noted that Re is a precious and rare metal. A recent development in this field has been the successful application of analogous $Mn(CO)_3(bpy)X$-based complexes as CO_2 reduction catalysts, taking advantage of the much more abundant and economical first row transition metal, manganese. These series of catalysts covert CO_2 into both CO and $HCOO^-$ and their catalytic selectivity is flexible. For example, Ishitani *et al.* recently reported *fac*-$Mn(CO)_3(bpy)Br$ as a CAT for photocatalytic CO_2 reduction.[81] A DMF/TEOA (4:1 v/v) solution containing the Mn complex (0.05 mM), $Ru(dmb)_3^{2+}$ (0.05 mM, bmb = 4,4'-dimethyl-2,2'-bipyridine) as PS, and 1-benzyl-1,4-dihydronicotinamide (BNAH) as SD was irradiated at λ_{ex} = 480 nm under a CO_2 atmosphere, producing HCOOH after a short induction period with a Φ_{HCOOH} of 5.3%. A TON_{HCOOH} of 149 was obtained after 12 h irradiation. Such performance is comparable to the photocatalytic system using *fac*-$Re(dmb)(CO)_3Cl$, under similar reaction conditions (Φ_{CO} = 6.2%).[82] Note that the reaction product was HCOOH and not CO, although CO was the main product in the electrochemical CO_2 reduction using the same Mn catalyst.[83] During the induction period of HCOOH formation, a Mn dimer ($[Mn(bpy)(CO)_3]_2$) with a Mn-Mn bond was formed *via* a one-electron reduction of the original Mn complex. During this period, CO was the main product. Reduction of the Mn dimer by the reductive PS might proceed giving $[Mn(bpy)(CO)_3]^-$, along a slow process. After the Mn dimer was no longer detected in the reaction solution, the production of HCOOH proceeded more rapidly, and formation of CO just stopped. This suggests that the Mn dimer does not lead to HCOOH formation but might produce CO.

Metal porphyrins and their derivates. Metalloporphyrins are well known for their electron transfer roles in a myriad of redox systems in Nature (chlorophyll, heme, vitamin B_{12},

cytochrome P450, etc.) as well as highly effective photocatalysts thanks to their strong absorption in the 400-450 nm region (Soret band) and weak absorption in the 500-700 nm region (Q-bands). Metalloporphyrins (MP) and related derivatives studied for CO_2 reduction reactivity include metallocorrins (MN), metallophthalocyanines (MPc) and metallocorroles (MC) (Figure 1.23, where M = Fe or Co).[84] Scheme 1.4 illustrates the mechanism with a MP, as representative compound. The catalytic active states as identified by cyclic voltammetry show the metal center is in the formal oxidation state of zero for porphyrins $[M^0P]^{2-}$ and corrins $[M^0N]^{2-}$, +1 for corroles $[M^IC]^{2-}$ and +1 with a reduced phthalocyanine ring $[M^IPc^{\cdot-}]^{2-}$. Some MPs previously investigated bear functional groups with negative or positive charges at the *meso* substituents, which will greatly affect the efficiency of their catalytic properties.

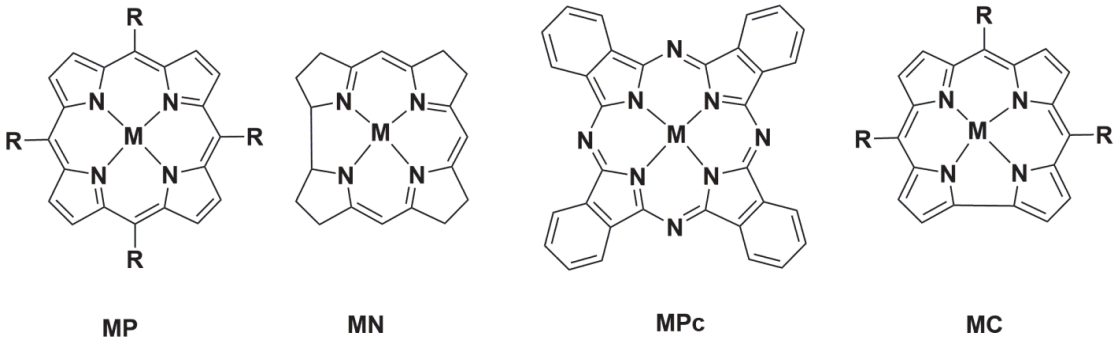

Figure 1.23. Metalloporphyrin and derivatives investigated for CO_2 reduction: (left to right) metalloporphyrin (MP), metallocorrin (MN), metallophthalocyanine (MPc) and metallocorrole (MC).

Prolonged illumination of MPs in the presence of TEA as SD results in the formation of $[M^IP]^-$, $[M^IN]^-$, $[M^IPc]^-$ and $[M^{II}C]^-$ through stepwise reductive quenching with quantum yields for the sequential steps, ϕ_1 and ϕ_2 (Scheme 1.4).[68, 85] More specifically, a donor molecule (here TEA) binds axially to $[M^{III}P]^+$ to form an adduct (Equation 20) which could yield $[M^{II}P]$ under light excitation, through an intramolecular reductive quenching step (Equation 21). While TEA binds to $[M^{III}P]^+$, the UV-Vis spectrum of the resultant $[M^{II}P]$ is not dependent on the TEA concentration, indicating that TEA does not bind to it. However, given the extremely short lifetime of exited state of MPs, like hemes, a weak TEA adduct must form prior to absorption of the second photon to account for the observed formation of $[M^IP]^-$.[85] The quantum yield for the second quenching step is typically an order of magnitude lower than for the first quenching step due to the weaker ground state adduct formed. It should be noted that for each of these catalysts, further reduction is needed to generate the catalytically active state.

$$M^{III}P\text{-}Cl + Et_3N \rightarrow Et_3NM^{III}P\text{-}Cl \quad (20)$$

$$Et_3NM^{III}P\text{-}Cl + h\nu \rightarrow [Et_3NM^{III}P\text{-}Cl]^{\cdot} \rightarrow Et_3N^{\cdot+} + Cl^{-} + M^{II}P \quad (21)$$

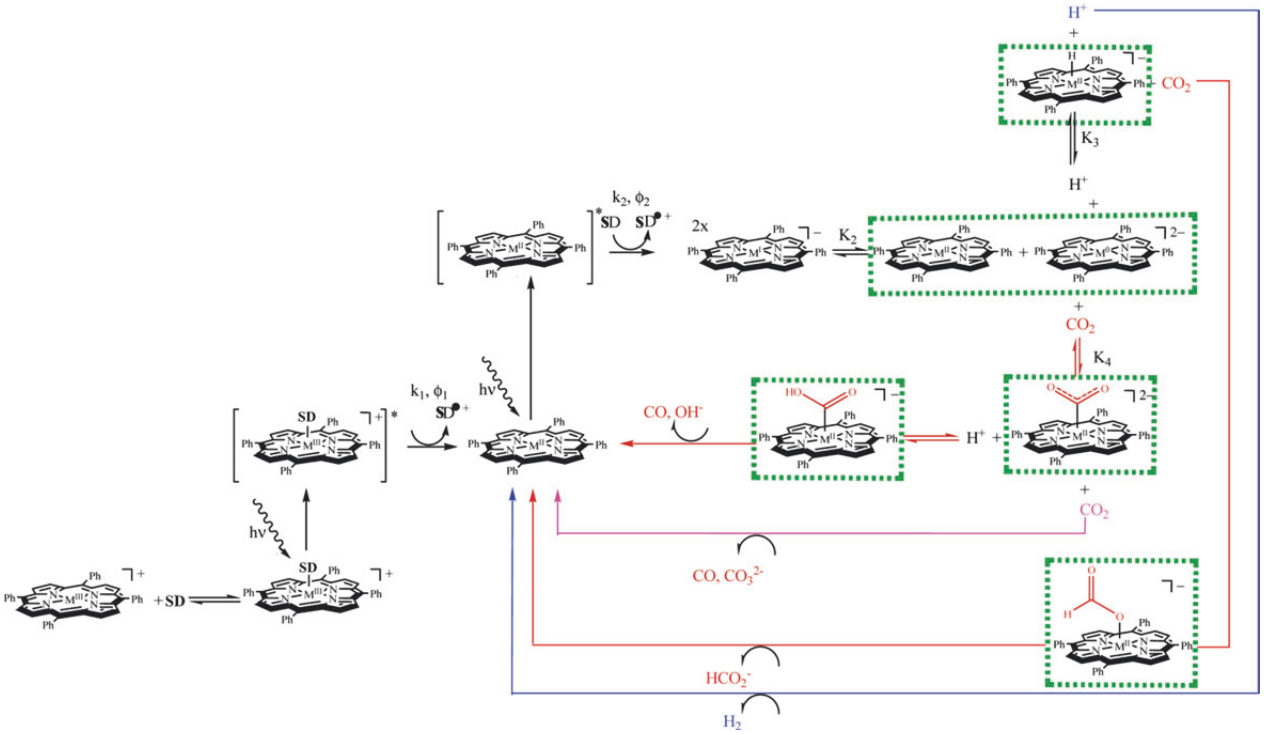

Scheme 1.4. Proposed mechanism in the reduction of CO_2 by metalloporphyrin (M = Fe or Co). Hydrogen (blue), formate (red) and CO formation (brown and pink), as well as putative intermediates (green).[68, 85]

The formation of the catalytically active state $[M^0P]^{2-}$ by direct light excitation has not been observed. Alternatively, it is proposed that this state is formed *via* disproportionation (Equation 22).

$$2[M^IP] \leftrightarrow [M^0P]^{2-} + [M^{II}P] \quad (22)$$

Kinetic evidence for a disproportionation reaction of $[Fe^IP]^-$, where P = tetrakis(N-methyl-2-pyridyl)porphyrin, was indeed reported.[84a] While the kinetic data was complicated by the presence of different porphyrin isomers, the rate law was clearly second-order in $[Fe^IP]^-$, consistent with Equation 22.

Disproportionation is highly unfavorable for all the metallomacrocyles discussed, and therefore the concentration of the active state, $[M^0P]^{2-}$, must be small. The observed reactivity has been rationalized by a favorable interaction between the active state and H^+ or CO_2 (K_3 and K_4 in

Scheme 1.4). However, increasing electron density on the cobalt(I) in tetraaza-macrocycles favored the binging of CO_2; therefore, it is likely that the active $[M^0P]^{2-}$ favors adduct formation relative to more oxidized forms.[86] Protonation of the putative $[M^0P\text{-}CO_2]^{2-}$ to form a metal carboxylic acid intermediate that subsequently decomposes to $M^{II}P$, CO, and HO^- has been proposed. Alternatively, under high CO_2 concentrations, $[M^0P{-}CO_2]^{2-}$ may react with CO_2 to yield $M^{II}P$, CO, and CO_3^{2-} (cyan in Scheme 1.4). Experimental proof of $[M^0P{-}CO_2]^{2-}$ species is lacking due to the reactive nature of these highly reduced compounds; indeed, $[M^0P\text{-}CO_2]^{2-}$ has neither been observed nor isolated. However, electrochemical reduction of CO_2 reported by Hammouche *et al.*[87] indicates that $[Fe^0P]^{2-}$ is the catalytically active species, consistent with photochemical data. Therefore the reaction mechanisms proposed for formate and carbon monoxide production are based on presumed similarities to other catalysts discussed.

MPs and related derivatives are strong light absorbers with extremely large extinction coefficients in the visible spectral region. However, yields of active catalysts formed after light absorption are very low, mainly due to the short (picosecond) lifetimes of their excited states. In addition, MPs and derivatives undergo unwanted photo-Birch reduction of the porphyrin ring, converting it to the corresponding chlorin structure, followed by further photochemical rapid decomposition, and these degradation products seem to catalyze the reduction of protons over CO_2.

Addition of *p*-terphenyl as a PS to photocatalytic CO_2 reduction with FeTPP, which made up a sensitized system, was investigated in order to overcome the above-mentioned problems.[85] The standard reduction potential of reduced *p*-terphenyl was negative enough (-2.45 V *vs.* SCE in dimethylamine) to reduce the Fe^{II}TPP (-1.05 V *vs.* SCE) and Fe^{I}TPP species (-1.66 V *vs.* SCE) so as to form the corresponding Fe^0TPP active state. This system exhibited 10 times higher photocatalytic efficiency than in the absence of PS. Moreover, Co porphyrin analogue can also be used to produce CO, and its photocatalytic efficiency was about 1.5 times higher compared to the Fe porphyrin.

Recently, Weiss *et al.* reported a colloidal $CuInS_2$/ZnS QDs sensitized FeTPP to reduce CO_2 to CO by using 450 nm light (Figure 1.24).[88] They underlined the crucial role of the sensitization process which has to be highly efficient in the transfer of redox equivalents from the PS to the CAT; in systems with molecular PSs, this transfer is often slow because it depends on diffusion-

limited collisions between PS and CAT. The colloidal sensitization efficiency (turnover number per absorbed unit of photon energy) of the QD system is a factor of 18 greater than analogous systems with molecular PS. The selectivity for CO is 84% (16% H_2). The QD/FeTPP mixture is stable after 40 h of illumination at 4.5 mW. The sensitization efficiency of the system originates from the ultrafast electron transfer between the QD and FeTPP: the time constants for the dominant electron-transfer processes responsible for the first two sensitization steps ($Fe^{III}TPP \rightarrow Fe^{IIT}TPP$, and $Fe^{II}TPP \rightarrow Fe^{I}TPP$) are both < 200 fs. This ultrafast photoreduction is enabled by formation of a quasi-static QD/FeTPP complex, probably driven by the interaction between Fe and sulfur on the surface of the QD. The ability of QDs to self-assemble with a co-catalyst is a crucial advantage of the QD-sensitized system over molecular systems, where the rate of charge transfer is limited by occasional collisions between freely diffusing species.

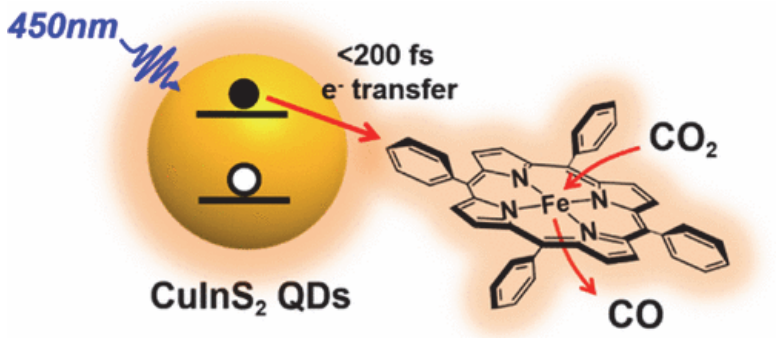

Figure 1.24 $CuInS_2$ QDs sensitized FeTPP system for CO_2 reduction.[88]

The redox property of porphyrin complexes, which are closely related to CO_2 reduction efficiency, could be easily tuned through substituents modification on the four benzene rings. The photocatalytic reaction using iron porphyrin with two -OH groups on the *o*-positions of the four phenyl groups was investigated in a ACN solution containing the CAT and TEA as tSD. Irradiation (λ_{ex} > 280 nm) of the solution gave CO with higher selectivity (ca. 85%) compared to unmodified FeTPP.[89] The introduction of -OH groups stabilizes the CO_2 adduct owing to the internal hydrogen bonding between -OH groups and the CO_2 bound to the metal center. It was also shown that -OH groups accelerate the cleavage of the C-O bond. In the photocatalytic CO_2 reduction, the TON_{CO} was ca. 30 (with the production of a small amount of H_2), although in electrochemical conditions, the selective CO_2 reduction continued with little degradation, exhibiting a high faradaic yield of CO (> 95%). Robert *et al.* further improved this photocatalytic CO_2 reduction by adding *fac*-Ir(ppy)$_3$ (ppy = 2-phenylpyridine) as PS. Visible-light irradiation

with λ > 420 nm light in the presence of TEA as SD led to CO evolution with a higher efficiency and selectivity (ca. 93%).[90] The TON was also improved to 140, which was significantly higher than in the absence of PS. An organic dye, 9-cyanoanthracene (9CNA), was also used as PS instead of the Ir complex and the new system exhibited visible-light-driven CO_2 reduction, with a high selectivity of nearly 100% for CO formation. The reduced 9CNA exhibits strong reducing power (E^0 = -1.58 V vs SCE), high enough to reduce the Fe porphyrins to Fe^0 active species. However, the durability still needs to be improved (TON_{CO} = ca. 60). PS fulfills its function as light collector and thanks to its reductive quenching with SD, it generates a highly reducing species able to increase the Fe^0 formation rate and to efficiently assist the C-O bond breaking in the CO_2-CAT adduct and thus to favor the CO generation at the detriment of the H_2 evolution. Lowering the excitation energy and separating the light absorption from catalysis roles also prevented catalyst degradation.

Photoreduction of CO_2 can be also realized over inorganic catalytic materials. Whereas molecular catalysts usually exhibit high activity but low stability and often become inactive under long term irradiation, materials has low activity but very good stability. He *et al.* reported the use of graphitic carbon nitride (*g*-C_3N_4) nanosheets as PS to integrate with Fe tetra(4-carboxylphenyl)porphyrin chloride (FeTCPP) molecular catalyst (Figure 1.25).[91] Besides π-π stacking between the tris-triazine unit and the porphyrin, carboxyl group modified Fe-porphyrin is used for CO_2 photoreduction so as to form hydrogen bonding with the rich amino groups in g-C_3N_4 nanosheets. *g*-C_3N_4/FeTCPP heterogeneous catalysts are prepared *via* a facile self-assembly approach, in which light harvesting is spatially and temporally separated from catalysis. The obtained *g*-C_3N_4/FeTCPP heterogeneous catalysts exhibit high activity for CO_2 reduction under visible-light irradiation, with a CO yield of 6.52 mmol g^{-1} in 6 h and selectivity up to 98%. The authors proposed a mechanism which is slightly different from the Fe^0 mechanism in the purely homogenous system. The formation of Fe^0 species being much slower under heterogeneous photochemical conditions, Fe^{II}TCPP-CO_2 intermediates will be directly formed after the one-electron reduction of the CAT. Since Fe^{II} and Fe^{I} species do accumulate in the solution for several minutes, as evidenced by quasi in-situ electron spin resonance (ESR) and UV-vis measurements, the formation of Fe^{II}TCPP-CO_2 intermediates may be crucial and take precedence for the CO_2 photoreduction in the reported system. Moreover, carboxyl substituents on the phenyl ring can enhance the interaction between *g*-C_3N_4 nanosheets and FeTCPP and stabilize CO_2

adduct formed with FeTCPP *via* intramolecular hydrogen bonding thus improving photocatalytic activity of the *g*-C_3N_4/FeTCPP heterogeneous assembly.

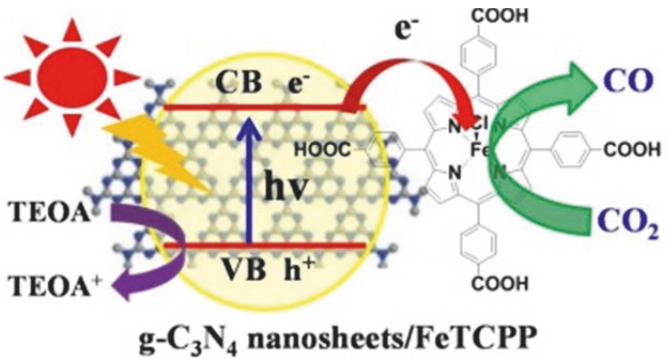

Figure 1.25 *g*-C_3N_4 nanosheets/FeTCPP system for CO_2 reduction.[91]

Apart from self-assembly approach of g-C_3N_4 nanosheets/FeTCPP heterogeneous catalyst, Ye *et al.* reported a covalently linked Co-porphyrin/low-molecular-weight C_3N_4 hybrids for photochemical CO_2 reduction (Figure 1.26).[92] Covalent hybrid Co-porphyrin-oligomers (Co-POM) was obtained through the condensation between amino-group from oligomer and ketonic-group from porphyrin. The hybrids possessed 13-fold higher photocatalytic activity (17 μmol/g/h) compared to bulk C_3N_4, and more than twice compared to the Co-porphyrin loaded C_3N_4 heterojunction system. The efficient electron transfer and trapping by the Co active sites as well as the affinity of Co-porphyrin for CO_2 are considered to account for the enhanced activity. This work may open a promising route to modify carbon nitride and provide a feasible approach to immobilize the active site into the light-harvest antenna for efficient electron-hole separation, electron transfer and the following redox reactions in photocatalytic process, which reforms the conventional semiconductor-cocatalyst heterojunction system.

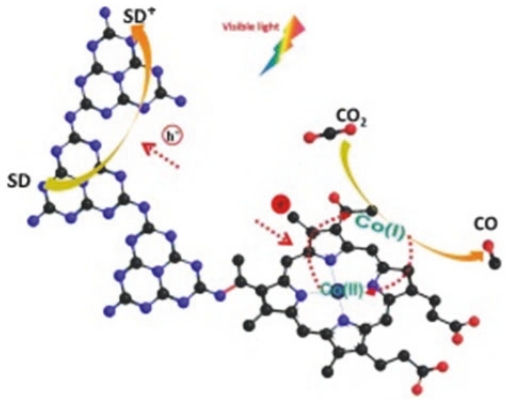

Figure 1.26 Co-porphyrin-oligomers of melems (Co-POM) for CO_2 reduction.[92]

Fe and Co MPcs and MCs also exhibit photocatalytic activity for CO_2 reduction. In the case of MPs, TONs (50-90) were not higher than for porphyrin analogues even in the presence of *p*-terphenyl as PS.[84c] In the case of MCs, photocatalytic activities (TONs = 40-100) were comparable to those using FeTPP and CoTPP under the same conditions, with *p*-terphenyl as PS.[84d]

As discussed above, tremendous advances have been achieved in the photochemical reduction of carbon dioxide using either SC or molecular catalysts, in terms of both activity and selectivity. With the proper structure design of a redox-active catalyst, it will be possible to selectively reduce CO_2 to CO or HCOOH as main products. However, the drawbacks of these catalytic systems such as poor efficiency and low stability under operating conditions, greatly limit the real application of this technology. Most of the reported catalysts will be decomposed after a few hours of reaction, which is a severe impediment to their implementation on a large scale. Hence, the future research efforts in this field should focus on developing strategies to extend the lifetime of such catalysts. In addition, initial steps should be taken towards the integration of these catalysts in tandem cells, where electrons and protons for the reduction of carbon dioxide are provided by the oxidation of H_2O instead of an external SD, to demonstrate the sustainability of this promising technology.

1.4 Motivation and outline of this thesis

Developing photocatalytic systems for CO_2 reduction will provide useful and energy-rich compounds, which will be one of the most important focuses in the field of "artificial photosynthesis" and "solar fuels". In the past few decades, such studies have been conducted from the perspective of basic science and for solving the shortage of fossil resource. However, it is still substantially lagging behind the astonishing progress that has been achieved for the production of hydrogen from solar energy. It is still a big challenge to develop more efficient, more stable, more selective CO_2 reduction photocatalytic systems.

This thesis discusses serval Fe-porphyrin based homogenous systems for visible light driven photochemical carbon dioxide reduction under ambient conditions. Both spectroscopic and electrochemical methods are used to elucidate the mechanism. The goal of this thesis to develop

highly efficient and stable molecular photochemical CO_2 reduction systems which may be industrialized for generating carbon-based solar fuels from solar energy.

Chapter 2 describes a non-sensitized iron porphyrin-based molecular photochemical system for efficient CO_2-to-CO conversion. Similar catalysis will be enhanced with the addition of an organic dye (purpurin) as the photosensitizer even in aqueous solutions.

Chapter 3 discusses with the introducing of a much stronger Ir-based photosensitizer, the efficiency of CO_2-to-CO conversion is greatly increased and more marvelously, CH_4 is formed in this system. Actually, this system can also drive CO-to-CH_4 conversion directly, which is very similar to a molecular Fischer-Tropsch synthesis. And then this catalysis is transformed into a aqueous system with a water soluble Ir-based photosensitizer. Finally, we also develop a pure non-noble-element system for both CO_2-to-CH_4 conversion and CO-to-CH_4 conversion with a phenoxazine-based organic photosensitizer.

Chapter 4 gives a short summary of the work completed during this thesis, with an overview of ongoing projects and possible future developments.

Chapter 2 Photochemical Reduction of CO_2 to CO under Visible Light with Iron(0) Porphyrins

2.1 Introduction

The efficient photochemical reduction of carbon dioxide into useful high-energy density fuel will be an important step in the concept of a CO_2 neutral cycle, as it will allow for the direct conversion of solar energy into stored chemical energy, in a very similar way than Nature does. Green plants fix CO_2 from the atmosphere by photosynthesis with porphyrin-based enzymes which selectively binds CO_2 and inserts it into existing carbon chains by reductive carboxylation, the high energy electrons needed in this process being photogenerated through Photosystem II.

Synthetic catalysts for the photocatalytic reduction of CO_2, which can facilitate an "artificial photosynthetic" CO_2 neutral cycle, have been investigated for several decades.[67, 75] The use of light energy for breaking and/or making chemical bonds can decrease the temperature and pressure needed to drive the reaction. Although great progress have been made in the past few years, a lot of huge challenges still need our concern.[93] For example, low efficiency and yield are the major shortcomings of photocatalytic CO_2 reduction. This process indeed involves multi-electron steps which produce various products, including carbon monoxide, methanol, methane, formaldehyde, formic acid and higher hydrocarbons, which makes it way more complicated to conduct than proton reduction in photocatalytic water splitting. Except CO_2 reduction itself, there always accompanies with several intermediate processes, such as proton transfer, hydroxylation and so on. Since a wide range of products can be formed, controlling the selectivity for a desired product is a main issue. Additional challenges include the low solubility of CO_2 in water (if the reaction is performed in aqueous solution) as well as the competition of hydrogen evolution in aqueous media. A relatively poor understanding of the process and the difficulty in elucidating mechanisms at the molecular scale still prevent the design of optimal catalysts.

Recent fundamental and theoretical works have reconsidered porphyrin-based molecular catalysts for CO_2 reduction. Tripkovic *et al.* have performed extensive density functional theory (DFT) calculations of metal-functionalized porphyrin-like graphene surfaces and predicted the potential formation of methane and methanol from CO_2.[94] Similar results reported by Shen *et al.*

showed that cobalt porphyrins could efficiently electrochemically reduce CO_2 into renewable energy fuels, and formic acid can be produced as minor product through a [Co(P)-(OCHO)] intermediate, while CO is the main product through a decoupled proton-electron transfer.[95] CH_4 is produced as minor product from subsequent CO reduction by concerted proton-coupled electron transfers (PCET) assumed for each electrochemical step. Previous works in our team considered ligand modifications of iron-based porphyrins and found that local proton sources built into the porphyrin ring give rise to high activity and good Faradaic efficiency for the electrocatalytic reduction of CO_2 to CO in a mixed DMF-water solvent.[96] With the same catalyst, it could directly photochemically convert CO_2 into CO, with H_2 as a minor product under irradiation.[89] Moreover, when combined with a PS, the catalytic CO_2 reduction efficiency can be greatly enhanced.[90] In fact, it has been known since the early 1980s that porphyrin based complexes, through either electrochemical or photochemical methods, act as effective catalysts for CO_2 reduction.[97]

In this chapter, we will report on a Fe-porphyrin complex which is able both to collect visible light and to selectively catalyze the reduction of CO_2 into CO. This single-molecule approach is rare, especially considering the high stability of the process and the fact that the catalyst is based on earth abundant metal. We will also discuss the possible mechanism based on electrochemical and spectroscopic measurements. Remarkably, this catalyst can also work in an aqueous solution system with the addition of a proper PS. Therefore, we believe that these insights have significant implications for the design of new and improved molecular catalyst for the design of optimized process conditions for efficient photochemical CO_2 reduction in both organic and water solution.

2.2 Non-sensitized system in acetonitrile solution for CO_2-to-CO conversion

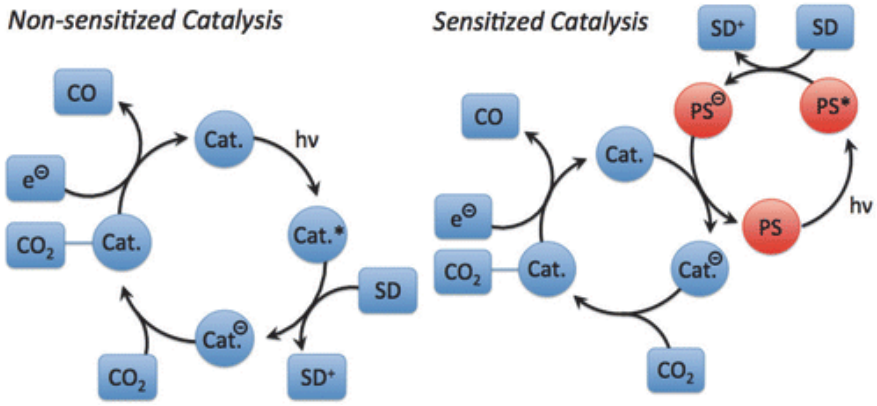

Figure 2.1 Illustration of non-sensitized (left) and sensitized (right) photochemical catalytic CO_2 reduction processes.[98]

In ideal conditions, the energy to drive the catalytic reduction of CO_2 would be derived directly (photocatalysis) or indirectly (solar-driven electrocatalysis) from the Sun. Numerous reports on electrocatalysis since the 1970s have emerged using a host of transition metals including Re, Ru, Co, Fe, Ni and others.[99] Some of these electrocatalysts have been demonstrated as capable of reducing CO_2 when combined with a visible-light photosensitizer (Figure 2.1).[98] In the past several years, we were particularly interested in using metal complexes as homogeneous catalyst based on earth abundant elements such as cobalt or iron, both as electro- and photocatalysts.[90, 100] In the latter approach, the goal is to use visible light as the only incoming energy, since almost 50% of the solar light flux is located in the visible range. We have previously showed that iron porphyrins could be used as photocatalysts for the reduction of CO_2 into CO, but they suffered from photodegradation under near-UV irradiation[89] and were inactive under visible light if not associated with a photosensitizer.[90] Actually, very few catalysts capable of both absorbing solar spectrum irradiation and reducing CO_2 were reported to date. Sensitization (Figure 2.1) is a common solution to shift and/or extend light absorption of a catalytic system, but it implies the use of an additional molecular partner which is frequently based on noble metal (*e.g.* Ru, Ir) complexes, even if some examples of cheaper organic sensitizers have been identified.[74, 90, 100a] Luminescent tricarbonyl Re(I) diimines complexes have been used as selective catalysts for the CO_2-to-CO conversion in aprotic solvent without sensitizer, but the solar light utilization is

limited in these cases by the weak visible absorption due to the weak tailing in this range.[101] Replacing a CO ligand with an N,O or N,S-NHC containing ligand (weaker π-accepting ligand) led to shifting the MLCT transitions to lower energy and makes the complex able to harvest visible light (λ > 480 nm).[102] Recently Re(I) pyridyl N-heterocyclic carbene (NHC) complexes have also been used to directly absorb visible light and catalyze CO_2 reduction.[98] Another series of non-sensitized CO_2 reduction catalysts involving an iridium center, a noble metal, were also reported to have moderate activity under visible light.[74, 89, 98, 100c, 100d, 101-103] Such examples of non-sensitized molecular photochemical conversion of CO_2 however remain scarce. And as alluded above rare examples using an earth abundant metal based complex have been identified so far (Co tetraphenyl porphyrin[85], Fe phatlocyanine[84c] and substituted Fe tetraphenyl porphyrins[89] and they all led to low TONs and poor stability over time, while employing UV light as an excitation source. In this part, a modified tetraphenyl iron porphyrin (Fe-*p*-TMA, Figure 2.2) which operates under visible light irradiation without the assistance of another light collector was used for directly reduce CO_2.

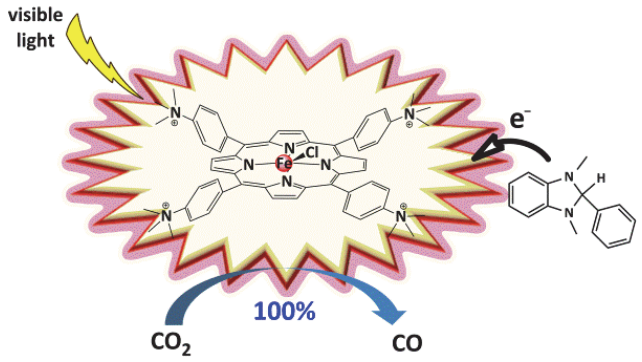

Figure 2.2 Non-sensitized Fe-*p*-TMA system for photochemical CO_2 reduction.[104]

In a typical photochemical CO_2 reduction reaction, irradiations of acetonitrile (ACN) solutions containing 2 μM Fe-*p*-TMA is as the catalyst, 0.05 M triethylamine (TEA) or 0.02 M 1,3-dimethyl-2-phenyl-2,3-dihydro-1H-benzo[d]imidazole (BIH) as the sacrificial electron donor (SD), and 0.1 M TFE or phenol as weak acid if necessary.

Two different sacrificial electron donors were used in ACN solutions. First, a typical tertiary amine (TEA) was employed and the results were compared to our previous studies. Upon visible light irradiation (λ > 420 nm), formation of CO was observed to follow a linear evolution with time, reaching a number of catalytic cycles in CO of 33 after 47 hours (Figure 2.3, black dots),

with no trace of H_2 being detected. This performance was already significantly better than what we observed with hydroxyl-functionalized porphyrins in the absence of PS.[89] The selectivity towards CO formation reaches 100% with Fe-*p*-TMA, whereas some H_2 formation was systematically noticed in the case of hydroxyl-functionalized porphyrin, along with rapid degradation of the catalyst through photo-Birch reduction of the porphyrin ring, converting it to chlorin-type compounds which were ultimately photodecomposed.[89] We then used another SD, namely BIH (Figure 2.2), since this compound was recently reported[105] to enhance the photocatalytic formation of CO from CO_2, thanks to its high reductive ability ($E_{1/2}^{ox}$ = +0.33 V *vs.* SCE),[106] its fast deprotonation to $BI^{\cdot}$ once oxidized and its overall two-electron donation capacity ($BI^{\cdot}$ could be in turn easily oxidized to BI^{+}). With BIH as SD, the selectivity and robustness were maintained, and the efficiency was increased by a factor of ca. 2, with the number of catalytic cycles in CO reaching 63 after 47 hours of irradiation (Figure 2.3, blue squares and diamonds). Blank experiments performed in the absence of the catalyst, light or CO_2 all led to the absence of CO production. As can been seen in Figure 2.4, both electron donors used had no absorption in the irradiation domain, which also indicated that CO_2 reduction needed a photocatalyst to respond light absorption. The effect of an added external weak acid was explored through the addition of 0.1 M trifluoroethanol (TFE) or phenol (PhOH), respectively, as illustrated in Figure 2.3 (red and green triangles).

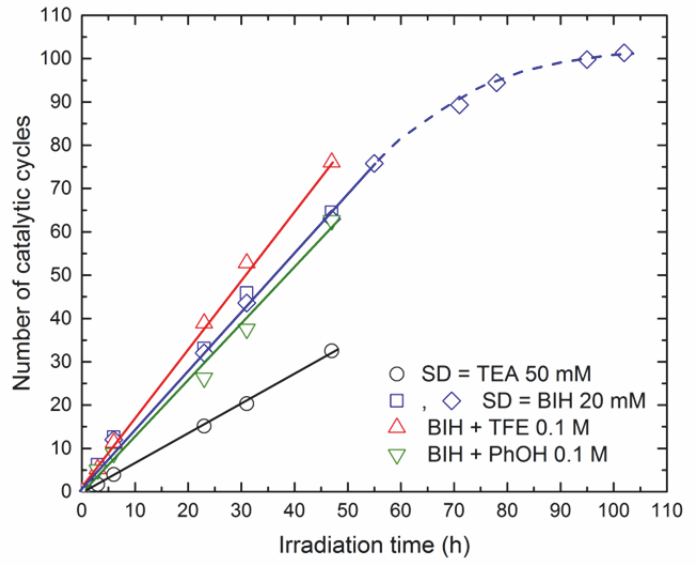

Figure 2.3 CO formation upon visible irradiation (λ > 420 nm) of a CO_2-saturated ACN solution containing 2 µM Fe-*p*-TMA and 0.05 M TEA (○), 0.02 M BIH (□, ◊), 0.02 M BIH + 0.1 M trifluoroethanol (TFE, △), 0.02 M BIH + 0.1 M phenol (PhOH, ▽).[104]

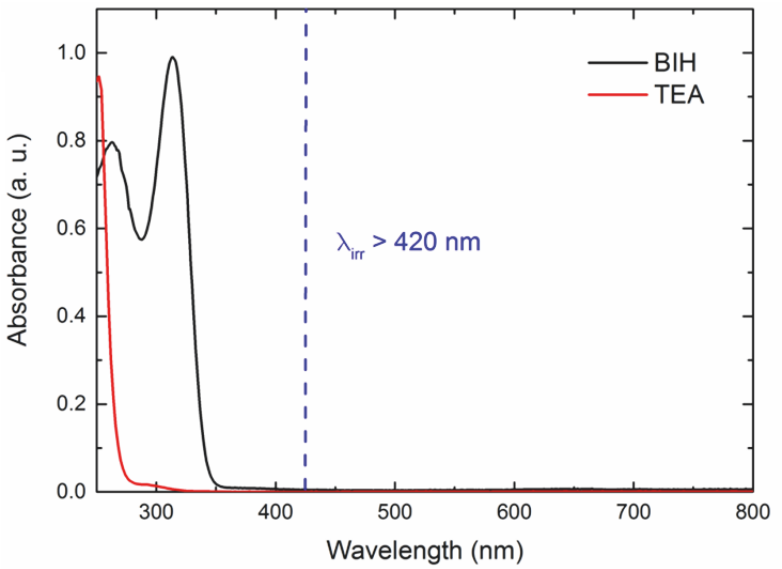

Figure 2.4 UV-Visible absorption spectra of TEA and BIH in ACN.[104]

Remarkably, the selectivity for CO formation remained equal to 100% and the acid does not lead to any degradation of the catalyst as shown by the linear evolution of the product formation with irradiation time. It indicates that no hydride intermediate is formed from the Fe^0 active species with the competing reaction with CO_2 being much faster. It also shows that the porphyrin ring is not reduced and/or hydrogenated since it would have led to the rapid degradation of the catalyst, as previously observed with other analogs.[89] We think the substituted tertraphenyls may help stabilizing the CAT-CO_2 intermediate and it will be discussed in more details in the next chapter. However, the catalytic reaction rate was only weakly enhanced by the acid addition and the number of catalytic cycles was similar with and without acid, reaching 78 *vs.* 63, respectively, after 2 days of irradiation. One explanation may be that the catalysis is limited by the reduction of the porphyrin to its active state (from the Fe^{III} starting reactant to the Fe^0 catalytic species) with essentially no influence of the acid content on these charge transfer reactions. Another possibility is that the reaction is limited by the release of CO from the Fe-CO adduct obtained after one C-O bond cleavage occurs.

This point is discussed below based on absorption spectroscopy data. The photocatalytic reaction was pursued until the CO production levels off (Figure 2.3), reaching a plateau after 100 hours. A turnover number (TON) value of 101 was obtained after 102 hours of continuous irradiation, again illustrating the robustness of the porphyrin under these conditions. The spectral evolution upon visible irradiation of a CO_2-saturated solution containing the porphyrin catalyst

and a sacrificial electron donor (TEA or BIH) is sketched in Figure 2.5 and confirms catalyst stability. The exact attribution of the absorption bands of porphyrins is difficult owing to the overlapping between the bands related to the different states of the iron center.

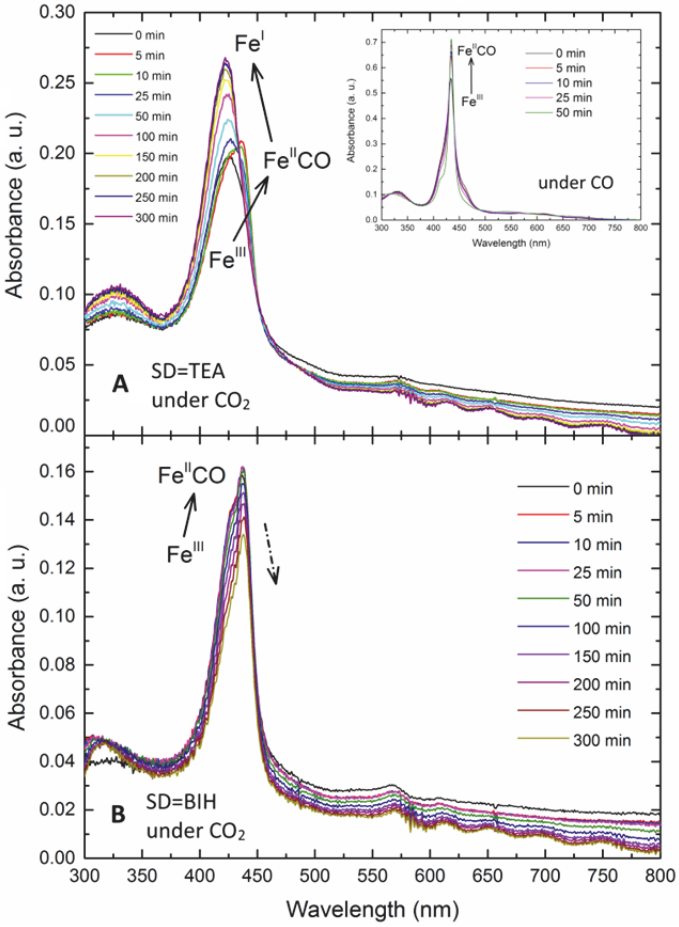

Figure 2.5 Spectral evolution upon visible irradiation (λ > 420 nm) for a CO_2-saturated ACN solution containing 5 μM Fe-*p*-TMA and 0.05 M TEA (A) or 0.02 M BIH (B). Inset (A): Spectral evolution upon visible irradiation (λ > 420 nm) for a CO-saturated ACN solution containing 5 μM Fe-*p*-TMA and 0.05 M TEA.[104]

Still, the porphyrin characteristic LMCT band with a peak at 325 nm could be observed at all irradiation times, while the Fe^{III} Soret band at 427 nm rapidly evolves with the formation of the Fe^{II}-CO state, whose stationary concentration is large enough to be the dominant contribution to the spectra with BIH as the SD (Figure 2.5B). In that case, a slight decrease (15%) of the absorption band occurs after 300 min of irradiation, being either due to the slow degradation of the porphyrin or to a non-stationary concentration of Fe^{II}-CO species because of a faster light induced cleavage of the adduct as compared to its formation rate. When using TEA as SD, the typical Soret band of an Fe^{I} porphyrin peaking at 423 nm became the dominant contribution after

30 min of irradiation (Figure 2.5A). In that case, and because TEA is a less efficient electron donor as compared to BIH, the Fe^{I} species are slowly reduced to Fe^{0} which then accumulate. In addition, the absorbance of Soret band in BIH containing system is always much lower than that in TEA containing system, which indicates a lower concentration of $Fe^{II}CO$ intermediate leads to the faster reaction in the former conditions. This spectral evolution stands in line with the slower formation of CO observed with TEA as compared to BIH (Figure 2.3). When the system is irradiated under CO atmosphere, the absorbance of Soret band at 430 nm keeps increasing in 50 min (Figure 2.5A inset), which is the formation of $Fe^{II}CO$ intermediate and can also be found after 10 min in the CO_2 atmosphere system.

As shown in Figure 2.6, the cyclic voltammogram of 0.5 M Fe-*p*-TMA in 0.1 M $TBAPF_6$ of Ar-saturated DMF solutions features three reversible monoelectronic waves at -0.1 V, -0.95 V and -1.47 V *vs.* SCE. They are attributed to the Fe^{III}/Fe^{II}, Fe^{II}/Fe^{I} and $Fe^{I}Fe^{0}$ couples, respectively, similarly to FeTPP.[107]

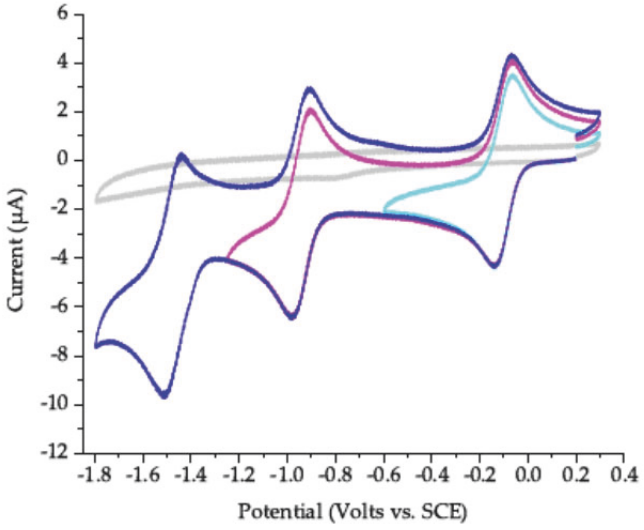

Figure 2.6 Cyclic voltammetry of 0.5 mM Fe-*p*-TMA in DMF + 0.1 M $TBAPF_6$ under inert argon atmosphere. Gray trace is the blank experiment with no catalyst. T = 21°C, scan rate = 100 mV s^{-1}, work electrode (WE) = 3 mm diameter glassy carbon.

When the system is saturated with CO_2, the two first redox waves remain unchanged while the third increases and the corresponding oxidation wave on the reverse sweep disappear. This irreversibility is fully consistent with an electrocatalytic process, whereby the Fe^{0} species formed during the forward sweep is transformed back to Fe^{I} upon reduction of CO_2 (Figure 2.7, red). Irreversibility and somewhat increased current compared with the blank experiment may reflect

some catalysis of H_2 evolution from water reduction (Figure 2.6, blue). Trimethylammonio groups are strong electron-withdrawing substituents which will decrease the electron density of the central Fe atom and thus will make it easier to reduce (and harder to oxidize, conversely). When the Fe porphyrin catalyst is well stabilized, the second electron transfer becomes more difficult than the electro-generation of the Fe^0 and the mechanism is a electrochemical chemical chemical electrochemical (ECCE) process, which is different from that of FeTPP with a electrochemical chemical electrochemical chemical (ECEC) process.[108] However, through a systematic analysis of the wave obtained under 1 atm CO_2 and in the presence of 3 M phenol according to the foot-of-the wave approach, which aims at minimizing the effects of side phenomena which interfere at large catalytic currents. It assumes that the electrochemical reaction mechanism is of the same type as for FeTPP.[109] Introducing the four trimethylammonio groups leads to a positive shift of the Fe^I/Fe^0 potential, *i.e.* a favorable factor in terms of overpotencial, *ca.* 200 mV less negative than for FeTPP. More surprising is that this effect, which tends to decrease the electron density on the iron and porphyrin ring at the oxidation state 0, does not slow down the catalytic reaction to a significant extent. It has been described to through-space electrostatic interactions between the trimethylamonio groups (positively charged) and the oxygen atom (negatively charged) of the CO_2 bound to the Fe center, leaving to a very efficient binding step of CO_2 to the Fe^0 catalytic active species.

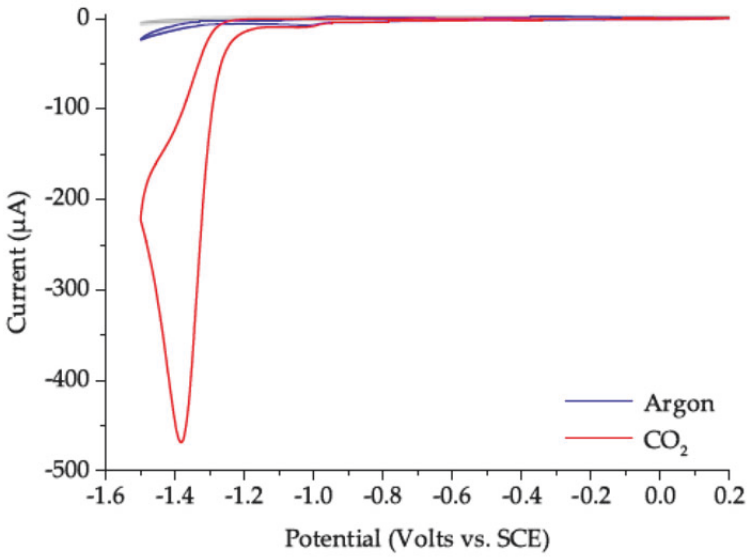

Figure 2.7 Cyclic voltammetry of 0.5 mM FeTNT + 0.1 M KCl in H_2O. Gray trace is the blank experiment with no catalyst. T = 21 °C, scan rate = 100 mVs^{-1}, WE = ϕ 3 mm glassy carbon, pH = 5.8 (Argon, unbuffered) and 6.7 (CO_2, 0.1 M $KHCO_3$ buffer).

Deciphering the detailed mechanism for the CO_2-to-CO conversion will require further spectroscopic investigations; however, based on previous in-depth studies related to variously substituted tetraphenyl Fe-porphyrins[75, 96] and the electrocatalytic mechanism, we suggest that the generation of the Fe^0 catalytically active species likely occurs upon a series of electron transfer steps (the total porphyrin charge is also indicated for all species):

$$\left[\mathrm{Fe^{III}\text{-}p\text{-}TMA-Cl}\right]^{4+} \xrightarrow{h\nu} \left[\mathrm{Fe^{II}\text{-}p\text{-}TMA}\right]^{4+} + \mathrm{Cl^{\bullet}} \quad (23)$$

$$\left[\mathrm{Fe^{III}\text{-}p\text{-}TMA-Cl}\right]^{4+} + \mathrm{SD} \xrightarrow{h\nu} \left[\mathrm{Fe^{II}\text{-}p\text{-}TMA}\right]^{4+} + \mathrm{Cl^{-}} + \mathrm{SD^{\bullet+}} \quad (23')$$

$$\left[\mathrm{Fe^{II}\text{-}p\text{-}TMA}\right]^{4+} + \mathrm{SD} \xrightarrow{h\nu} \left[\mathrm{Fe^{I}\text{-}p\text{-}TMA}\right]^{3+} + \mathrm{SD^{\bullet+}} \quad (24)$$

$$\left[\mathrm{Fe^{I}\text{-}p\text{-}TMA}\right]^{3+} + \mathrm{SD} \xrightarrow{h\nu} \left[\mathrm{Fe^{0}\text{-}p\text{-}TMA}\right]^{2+} + \mathrm{SD^{\bullet+}} \quad (25)$$

First, the catalyst obtains three electrons from the SD to form the Fe^0 active state with the help of light. The Fe^0 porphyrin then efficiently binds to CO_2 and the Fe-CO_2 adduct (that could be described both as $Fe^{I}CO_2^{\cdot-}$ or $Fe^{II}CO_2^{2-}$) is stabilized by through-space coulombic interaction between the positive charge of the Me_3N^+ substituents on the porphyrin ring and the partial negative charge borne by the oxygen atoms of the gas molecule (see the proposed mechanism in Scheme 2.1).[109-110] The Fe^I/Fe^0 standard redox potential (-1.47 V *vs.* SCE) measured by cyclic voltammetry in DMF is less negative than the value obtained with the non-substituted tetraphenyl Fe porphyrin (-1.67 V *vs.* SCE). It is ascribed to the strong electron withdrawing effect of the trimethylammonio groups. As a consequence, the Fe^0 species is less prone to give a hydride by reaction with acids present in the solution in the case of Fe-*p*-TMA and H_2 evolution is not observed. Moreover, degradation of the catalyst through reductive hydrogenation of the porphyrin ring is also minimized with Fe-*p*-TMA. C-O bond cleavage may then occur by protonation of the Fe-CO_2 adduct and would lead to the release of a water molecule and an Fe-CO adduct. The latter species further releases CO either upon photo-irradiation and/or by a one-electron homogeneous reduction by the Fe^0 species.

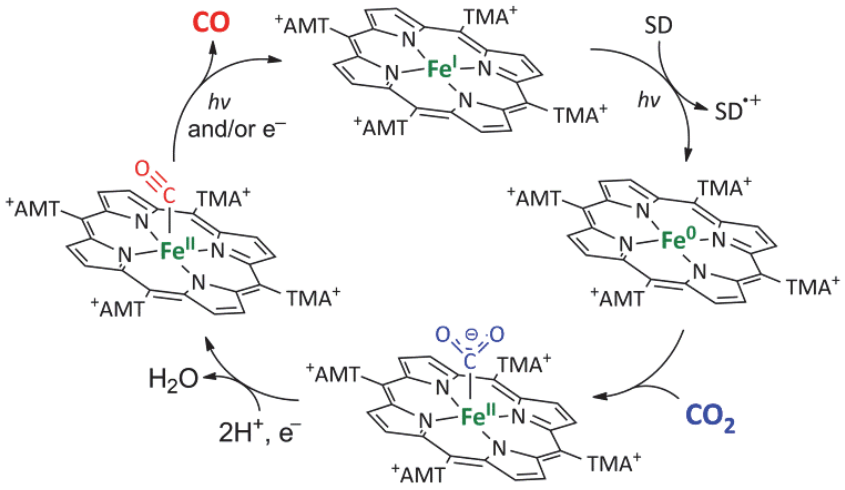

Scheme 2.1 Catalyst cycle for CO formation showing the stabilization of the Fe-CO_2 adduct and the C-O bond cleavage steps.[89]

As already observed during electrochemical studies, CO formation from the Fe-CO_2 adduct is efficient and fast,[110] so that the catalytic rate under photochemical conditions may be limited by the generation of the active Fe^0 species along the (1)-(3) reactions, even if these reactions are more thermodynamically favorable than in the case of the unsubstituted porphyrin. It is probably the case when TEA is used as SD since the Fe^I state gives a major contribution to the absorption spectra upon irradiation (Figure 2.5 A). In the case of BIH as SD, the driving forces for the electron transfer reactions are larger because BIH is more easily oxidized. In that case, the major contribution to the absorption spectra upon irradiation comes from the Fe-CO adduct (Figure 2.5 B), while Fe^I species do not accumulate, suggesting that the adduct photo-cleavage or homogeneous reduction by an Fe^0 species is rate determining. Further mechanistic investigation will shed more light on these aspects.

In conclusion, the introduction of four trimethylammonio groups onto the para position of the phenyl rings of an iron porphyrin makes the complex active under visible light for the photochemical reduction of CO_2 to CO, without an additional photosensitizer. Irradiation does not lead to catalyst photodegradation and the competitive hydride formation pathway previously observed with other porphyrins is avoided. Thanks to the stabilizing role of the four positively charged groups, the catalyst is highly selective and robust, generating pure CO from CO_2 with no loss of activity over 2.5 days, albeit at a moderate rate.

2.3 Purpurin-sensitized system in aqueous solution for CO_2-to-CO conversion

As mentioned before, most of the reported molecular catalysts are employed in organic solvent such as in ACN, DMF or THF. Aqueous CO_2 reduction systems are quite rare but certainly more interesting in terms of large scale applications. We already recalled that the direct reduction of CO_2 is a highly unfavored and that a coupled proton transfer reaction is always necessary for facilitating the reduction process above one electron. If water can be used as both the proton source and the reaction solvent, in a similar way that in natural photosynthesis, the whole process will be much more sustainable, scalable and environmentally friendly. However, proton reduction in water-containing systems proton reduction is inevitably competitive with CO_2 reduction due to the thermodynamic stability of CO_2, leading to a decrease in both efficiency and selectivity for CO_2-to-CO conversion.[18] Moreover, CO_2 solubility in water is much lower than that in organic solvent as shown in Table 2.1.[111]

Table 2.1 Solubility of CO_2 in common solvents at 298 K and low pressure.

Solvent	Solvent solubility parameter ($atm^{1/2}$)	Gas solubility*
ACN	24.1	7.1
acetone	19.8	6.6
THF	19.1	6.2
MeAc	19.4	6.0
DMF	24.0	4.1
PC	26.0	3.9
MeOH	29.5	3.6
$CHCl_3$	19.0	3.6
DMSO	26.3	2.9
n-hexane	15.0	2.1
Water	48.0	0.76

* Gas solubility in units of cm^3 (STP)/(cm^3 atm), where STP is standard temperature and pressure.[111]

Photocatalytic CO_2-to-CO in water with inexpensive molecular catalysts has thus been reported only in a few cases and confronted with dire challenges. Previous examples include the use of [Co(cyclam)] at pH 4 with a maximum TON of 22,[67] and the use of [Ni(cyclam)] at pH 4-6 with a maximum TON of 4.4,[84c, 85, 103c, 105] with $[Ru(bpy)_3]^{2+}$ as PS. Recently, a Ni complex bearing a 2,2':6',2"-terpyridine ligand and anchored at the surface of CdS quantum dots was reported to reach a maximum TON of 20 at pH 6.5, with a catalytic selectivity of 90 % after few hours irradiation, progressively decreasing to produce mainly H_2 after 24 h.[106] As a consequence, for a scalable water-containing system for artificial photosynthesis combining CO_2 reduction with water oxidation, it is of great importance to develop catalysts which can exhibit high activity and selectivity for a desired product even in water solutions.

With the introduction of four trimethylammonio groups at the para position of the phenyl ring on the Fe-porphyrin, not only the electron density of the catalyst center and the redox potential were changed, but also the polarity of this molecular was greatly changed. In fact, the solubility of Fe-*p*-TMA in water is even greater than in ACN. It is also one of our final targets that to do the catalysis of CO_2 reduction in pure water. As a consequence, this section is dedicated to the use of Fe-*p*-TMA as a selective and stable catalyst for the photochemical conversion of CO_2-to-CO in association with a cheap organic PS, namely purpurin (PP) under visible light irradiation ($\lambda >$ 420 nm) and aqueous conditions (Figure 2.8).

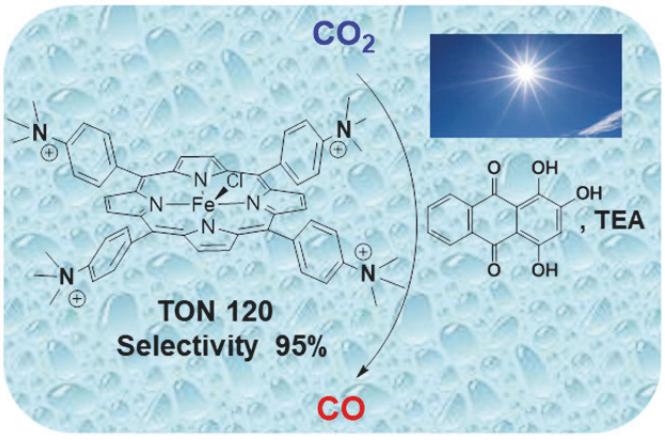

Figure 2.8 Purpurin-sensitized Fe-*p*-TMA system for CO_2 reduction in aqueous conditions.[112]

Photocatalytic CO_2 reduction by Fe-*p*-TMA was studied in pH 6.7 aqueous solutions containing 0.1 M $NaHCO_3$ to control the pH value of the reaction mixture and 10% ACN added (but kept miminum) to ensure a sufficient solubility of PP. 0.1 M $NaHCO_3$ was also added to

buffer the pH value of the reaction mixture. As can be seen from Scheme 2.2, PP exists in three different species, neutral, mono-anion and di-anion depending on the pH value.[113] As a consequence, both absorption and fluorescence spectra of PP changes with pH, which are also accompanied by color changes. By increasing the pH, the spectra shift to the red and the fluorescence quantum yield increases. The use of a buffer is thus necessary and the pH of the whole reaction was maintained at 6.7. PP is in its monoanionic form (pK_a= 4.7, 9.5) and thus will be noted as PP^- in the following.

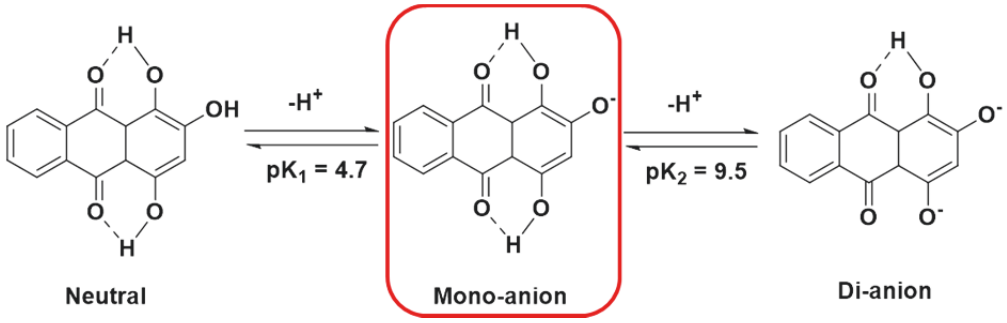

Scheme 2.2 Neutral, mono-anion and di-anion form of the purpurin dye.

Tertiary amines are widely used as sacrificial electron donors (SDs) in photocatalytic systems. Several amines were used as SDs in this system. The best results were obtained with triethylamine (TEA). As shown in Figure 2.9 and in Table 2.2 (entry 1), CO is produced upon visible light irradiation ($\lambda > 420$ nm). The amount of CO keeps increasing for about two days and then levels off, with a TON of 60. A small amount of H_2 is also produced with a TON of 5. Hence the selectivity for CO production is 95 %.

Interestingly, in the absence of PP^-, a TON of 6 was obtained for CO after 47 h irradiation, showing that the Fe catalyst is also able to slowly convert CO_2 into CO without any sensitizer. When the amine was omitted, TONs of 8.4 for CO and 1.6 for H_2 were measured, indicating that water itself could act as a sacrificial electron donor. Figure 2.9 shows the effect of the nature of the amine used. TEA gave slightly better results than triethanolamine (TEOA) and ethylenediamine tetraacetic acid (EDTA), although the TONs are not very different (Table 2.2, entries 2-4), reflecting the fact all three donors have similar redox potentials.[114] It is remarkable that the selectivity for CO formation remained very high even under these aqueous conditions. As already discussed in this thesis, the active species reacting with CO_2 is the reduced Fe^0 porphyrin, implying that the latter compound does not lead to hydride formation followed by hydrogen

evolution. It also indicates that the porphyrin ring itself is not reductively hydrogenated, since that would have

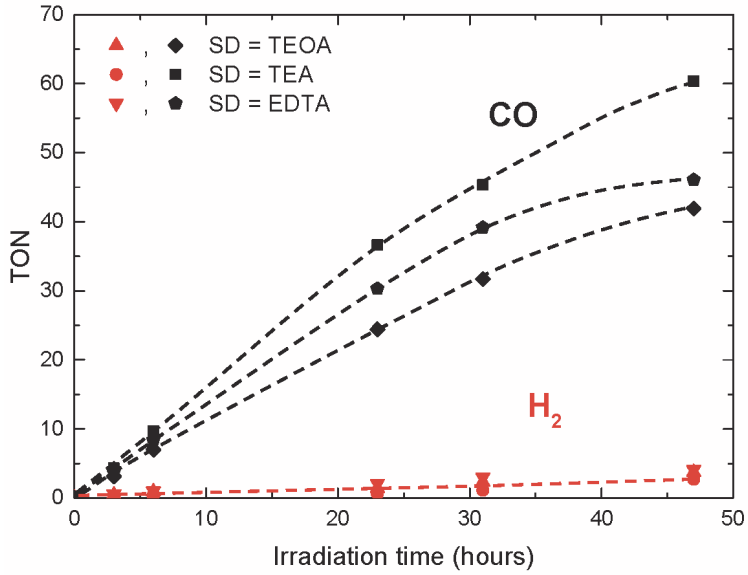

Figure 2.9 CO (black symbols) and H_2 (red symbols) production upon visible light irradiation (> 420 nm) of a CO_2-saturated ACN:H_2O (1:9, v:v) solution containing 2 µM Fe-*p*-TMA, 0.2 mM PP, 0.1 M $NaHCO_3$ and 0.05 M SD: TEA (●, ■), TEOA (▲, ◆) or EDTA (▼, ⬟).[112]

led to rapid degradation of the catalyst, as previously reported for similar derivatives.[89] These results are also in accordance with recent electrochemical studies, which showed that Fe-*p*-TMA is one of the few molecular catalysts to keep its high activity towards CO_2 in aqueous solutions.[109] One major reason for the catalytic activity levelling off is photosensitizer instability, as shown in Figure 2.10, where the main absorption peak of PP^- (at 510 nm) starts decreasing after a couple of hours, reaching a 60 % lessening after 47 h. PP^- photobleaching has otherwise been described.[115] Adding more PP^- to the solution mixture after two days of irradiation almost fully restored the catalytic activity (Figure 2.11), with a TON of 120 for CO and retention of 95 % catalytic selectivity at the end of a four-day experiment (Table 2.2, entry 6). When a more concentrated solution of the photosensitizer (0.4 mM PP^-) was initially used, more CO was also produced (TON = 71; Table 2.2, entry 2) while the same excellent catalytic selectivity towards carbon dioxide reduction was maintained. Upon adding more catalyst to the solution after 47 h of irradiation, only a slight increase of the TON for CO was observed (Figure 2.11, left, and Table 2.2, entry 3), confirming that sensitizer stability over time is the main factor explaining the levelling off of formation of the reduction product. This observation is also in accordance with

recent studies that showed that Fe-*p*-TMA remains stable even after extensive visible-light irradiation.[104, 116]

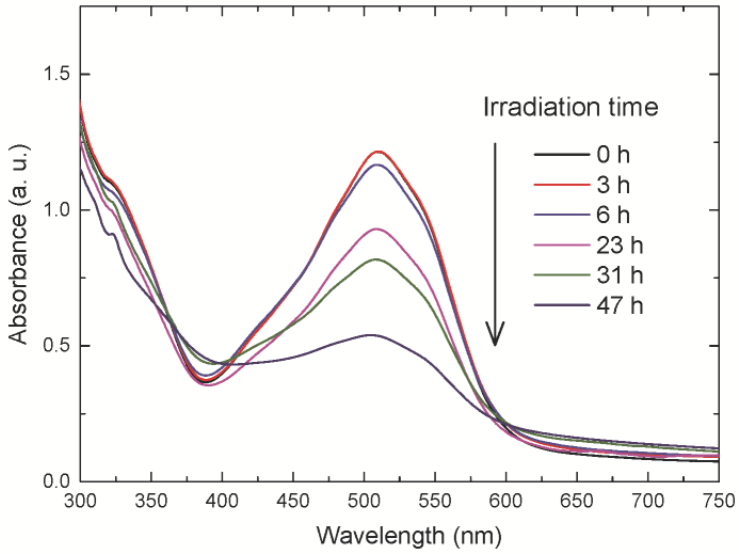

Figure 2.10 Spectral evolution with time upon visible irradiation (> 420 nm) of a CO_2-saturated ACN:H_2O (1:9, v:v) solution containing 2 µM Fe-*p*-TMA, 0.2 mM PP, 0.1 M $NaHCO_3$ and 0.05 M TEA.[112]

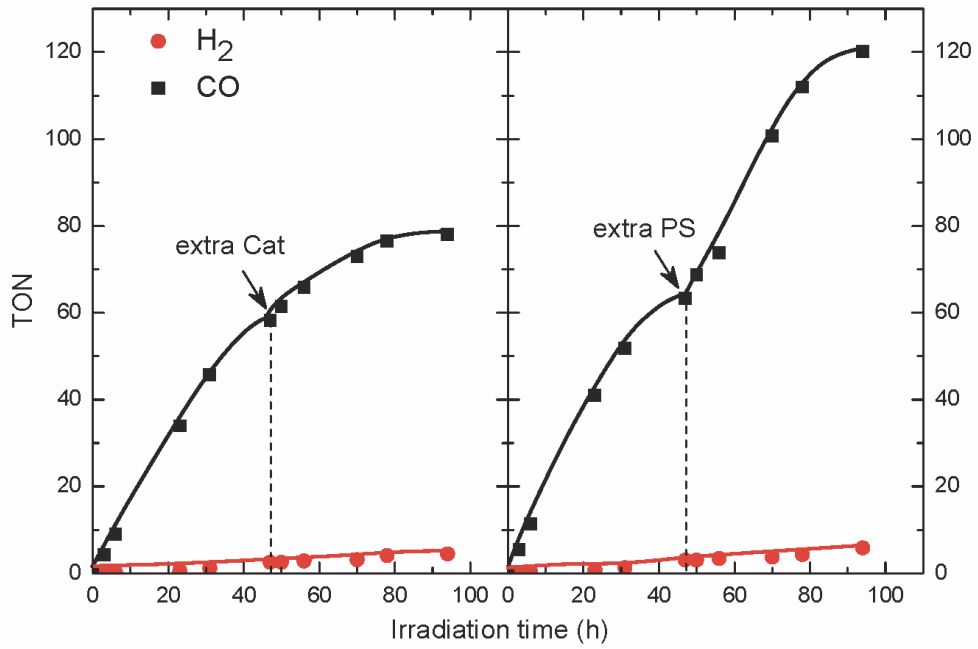

Figure 2.11 CO (black squares) and H_2 (red circles) production upon visible light irradiation (> 420 nm) of a CO_2-saturated ACN:H_2O (1:9, v:v) solution containing 2 µM Fe-*p*-TMA, 0.2 mM PP, 0.1 M $NaHCO_3$ and 0.05 M TEA. After 47 hours irradiation, 1 equivalent of Fe-*p*-TMA catalyst (left) or of PP photosensitizer (right) was added to the solution.[112]

Table 2.2. Catalytic performance (TON) and selectivity (CS) of a 2 μM Fe-*p*-TMA CO_2-saturated ACN:H_2O (1:9, v:v) solution after 47 h of visible-light (> 420 nm) irradiation in the presence of 0.1 M $NaHCO_3$, 50 mM of different SDs and 0.2 mM PP.

entry	SD	TON		CS (%)	
		H_2	CO	H_2	CO
1	TEA	3	60	5	95
2[a]	TEA	4	71	5	95
3	TEOA	4	42	9	91
4	EDTA	4	46	8	92
5[b]	TEA	3 / 5	58 / 78	5 / 6	95 / 94
6[c]	TEA	3 / 6	63 / 120	5 / 5	95 / 95

[a] 0.4 mM PP. [b] After 47h / 47h irradiation and addition of one equivalent of Fe-*p*-TMA after the first 47h. [c] After 47h / 47h irradiation and addition of one equivalent of PP after the first 47h.[112]

In the absence of catalyst no product was detected, while photocatalysis using ^{13}C-labeled CO_2 led to ^{13}CO production as detected by GC-MS, confirming that carbon monoxide was issued from CO_2 reduction (Figure 2.12).

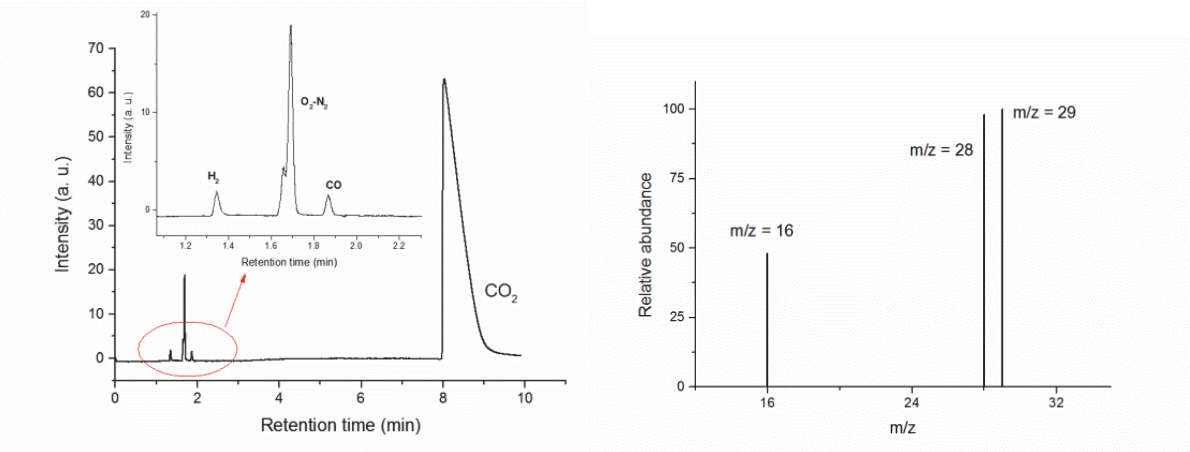

Figure 2.12 Gas chromatogram (a) and mass spectrum (b) analysis of the generated gas from the photocatalytic reduction of $^{13}CO_2$ upon visible light irradiation (> 420 nm) of a $^{13}CO_2$-saturated ACN:H_2O (1:9, v:v) solution containing 2 μM Fe-*p*-TMA, 0.2 mM PP, 0.1 M $NaHCO_3$ and 0.05 M TEA. Since the sodium hydrogenocarbonate contains ^{12}C, the mass spectrum both includes peaks at m/z 29 and 28.[112]

In experiments done without a PS, the catalyst was directly exited by visible light and then reduced to its active state Fe^0 by three oxidative quenching reactions with TEA. The oxidation pathway of TEA has been investigated previously.[117] Oxidation and degradation of TEA may be represented as follows (Scheme 2.3). In these processes, different radical and cationic species are involved, and they, together with products from their decomposition, can potentially influence the structures and reactivities of photosensitizers and catalysts.

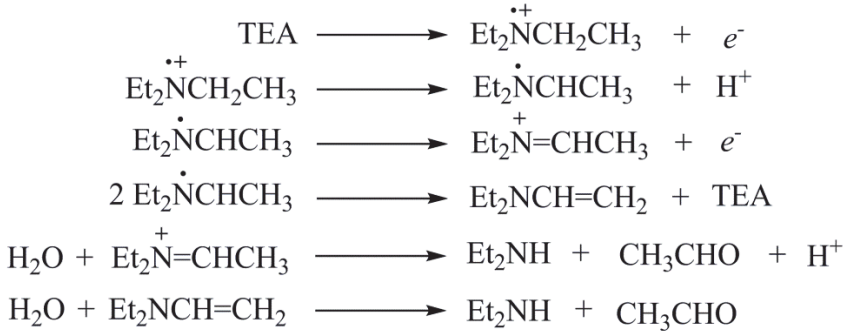

Scheme 2.3 Proposed reactions of TEA as a SD in photocatalytic systems.

The interaction of CO_2 with amines can be governed by several different mechanisms. Instead of directly reacting with CO_2, tertiary amines catalyze the formation of bicarbonate. The mechanism involving the base-catalyzed hydration of CO_2 for the reaction of CO_2 with tertiary amines as first reported by Donaldson[118] and later reviewed by Kenig[119] is detailed in Scheme 2.4. In the first step, the tertiary amine reacts with H_2O to form a quaternary cationic species and HO^-. Hydroxide ion then attacks CO_2 to form the bicarbonate anion. Then the last step is the ionic association of the protonated amine and bicarbonate. Liu *et al.* also shed light on the chemical interactions between CO_2 and N-containing organic bases through density functional theory (DFT).[120] The CO_2 molecule can be directly activated by organic bases in polar solvent to give a carbamate zwitterion intermediate. The distance between the CO_2 molecule and the Lewis base center in this intermediate being short (1.61-1.67 Å), it results in an increase in the C=O bond length from 1.16 to 1.22 Å and in a distortion of the linear O=C=O bond angle to ~137°. This suggests that although the chemical interactions between CO_2 and organic bases are relatively weak, the CO_2 molecule can still be well activated through a non-bicarbonate route in a polar solvent environment.

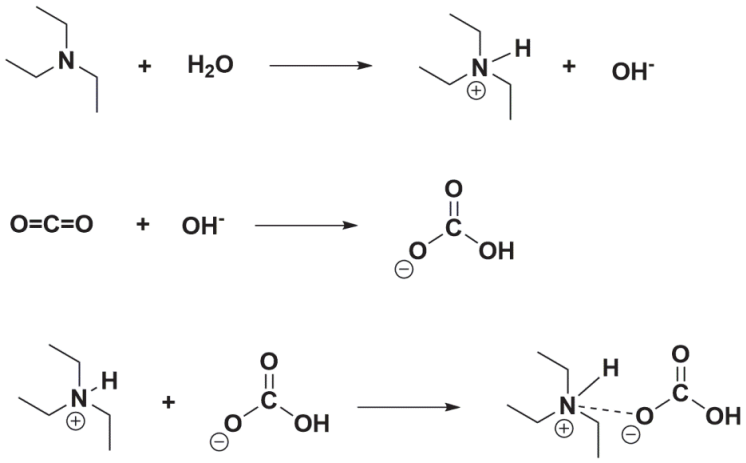

Scheme 2.4 Proposed mechanisms for the reaction of CO_2 with tertiary amines (TEA as an example).

In the presence of PP as PS, we need to determine whether the exited state PS^* is quenched by the CAT and/or by the SD in order to draw the mechanistic scheme. Emission quenching measurements in 0.1 M $NaHCO_3$ ACN/H_2O (1/9, v/v) solutions containing 0.2 mM PP with increasing concentration of either TEA or CAT (using concentration ratios similar to those used under photocatalytic conditions) were conducted and then analyzed according to the Stern-Volmer equation:

$$\frac{I_0}{I} = 1 + k_q \tau_0 [Q]$$

where I_0 and I are the emission intensities without and with quencher, respectively, k_q is the apparent quenching rate constant, τ_0 is the exited-state lifetime without quencher, and [Q] is the quencher concentration. Based on literature data,[113] the excited-state lifetime of PP is in its monoanionic species was taken as 2600 ps. Quenching experiments of a PP^- solution excited at 420 nm showed that PP^{*-} reacts with TEA extremely fast, close to the diffusion limit, the quenching rate constant being estimated at 1.2×10^{10} L mol^{-1} s^{-1} (Figure 2.13).

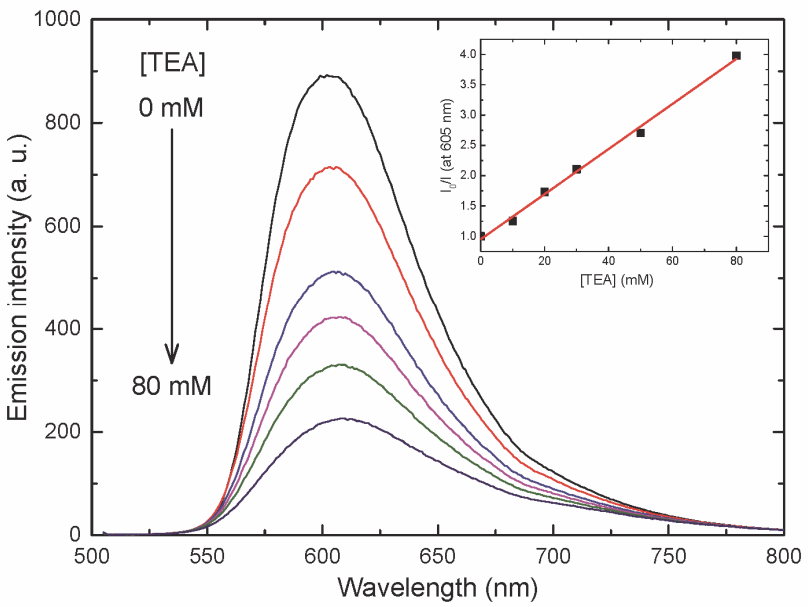

Figure 2.13 Emission spectra of a 0.2 mM PP in ACN:H_2O (1:9, v:v) solution with increasing concentration of TEA. Inset: linear plot (R^2 = 0.996) of the PP normalized emission ratio at 605 nm versus TEA concentration according to the Stern-Volmer equation.[112]

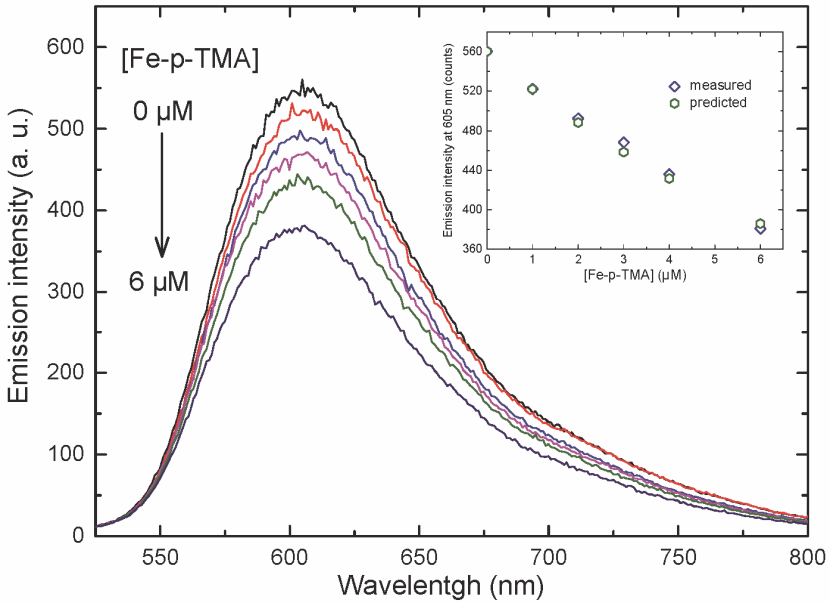

Figure 2.14 Emission spectra of a 0.2 mM PP in ACN:H_2O (1:9, v:v) solution with increasing concentration of Fe-*p*-TMA. Inset: measured (blue diamonds) and predicted (green hexagons) emission intensity at 605 nm of an ACN:H_2O (1:9, v:v) solution containing 0.2 mM PP as a function of the concentration in Fe-*p*-TMA catalyst.[112]

The result for the quenching between PP^{*} and Fe-*p*-TMA is different. Since Fe-*p*-TMA has a non-negligible absorbance at both λ_{ex} = 420 nm and λ_{em} = 605 nm (Figure 2.14), two attenuation factors have to be considered during emission quenching measurements (Figure 2.15): one corresponds to the excitation attenuation due to the absorption of Fe-*p*-TMA at the irradiation wavelength, leading to a lower excitation of PP; the other corresponds to the attenuation of the measured emission intensity due to *in situ* absorption of Fe-*p*-TMA molecules, leading to a measured intensity lower than the real emission.

Considering, for both attenuation factors, a mean solution thickness of 5 mm, and taking into account absorbance values at each Fe-*p*-TMA concentration, the predicted emission intensity as a function of [Fe-*p*-TMA] (Figure 2.14, Inset) perfectly matches the experimentally measured emission intensity. The emission decrease is thus not due to a quenching reaction between PP^{*} and Fe-*p*-TMA but is due to optical attenuation. In conclusion, PP^{*-} is only poorly quenched by Fe-*p*-TMA.

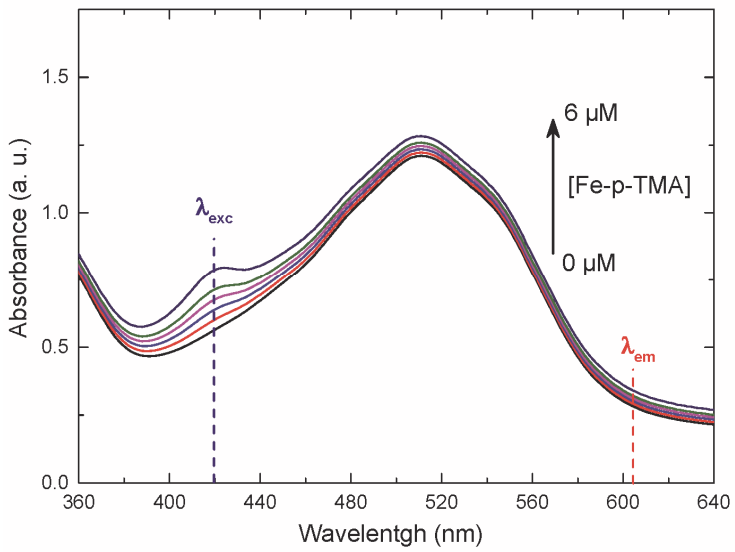

Figure 2.15 Absorption spectrum of a ACN:H_2O (1:9, v:v) solution containing 0.2 mM PP and increasing concentration of Fe-*p*-TMA catalyst showing the typical growing of the porphyrin Soret band around 420 nm.[112]

The redox potential of PP was obtained through cyclic voltammetry under argon atmosphere (Figure 2.16). The reduced PP^{2-} species has a standard redox potential (E^0 = -0.66 V *vs.* SCE) negative enough to reduce the Fe^{III} porphyrin to Fe^{II}, since the onset $E^0(Fe^{III}/Fe^{II})\approx$-0.3 V *vs.* SCE.[109] It can, however, not reduce Fe^{II} [$E^0(Fe^{II}/Fe^{I}) \approx$ -1 V *vs.* SCE] or Fe^{I} [$E^0(Fe^{I}/Fe^{0}) \approx$ -1.3

V *vs.* SCE] species, the corresponding driving forces being largely negative. As PP^{2-} is a stable species, it may be excited to PP^{*2-} and further quenched by TEA to the doubly reduced species PP^{3-}. The standard redox potential of the former species was determined by CV to be -0.83 V *vs.* SCE (Figure 2.16). PP^{3-} could then both react by electron transfer with Fe^{II} porphyrin and further reduce Fe^{I} to the catalytically active Fe^{0} species. The following series of electron transfer steps (the global charge is also indicated for all porphyrins) could thus be proposed:

$$\left[\mathrm{Fe^{III}\text{-}p\text{-}TMA-Cl}\right]^{4+} + \mathrm{PP^{2-}} \longrightarrow \left[\mathrm{Fe^{II}\text{-}p\text{-}TMA}\right]^{4+} + \mathrm{PP^{-}} + \mathrm{Cl^{-}} \quad (26)$$

$$\left[\mathrm{Fe^{II}\text{-}p\text{-}TMA}\right]^{4+} + \mathrm{PP^{3-}} \longrightarrow \left[\mathrm{Fe^{I}\text{-}p\text{-}TMA}\right]^{3+} + \mathrm{PP^{2-}} \quad (27)$$

$$\left[\mathrm{Fe^{I}\text{-}p\text{-}TMA}\right]^{3+} + \mathrm{PP^{3-}} \longrightarrow \left[\mathrm{Fe^{0}\text{-}p\text{-}TMA}\right]^{2+} + \mathrm{PP^{2-}} \quad (28)$$

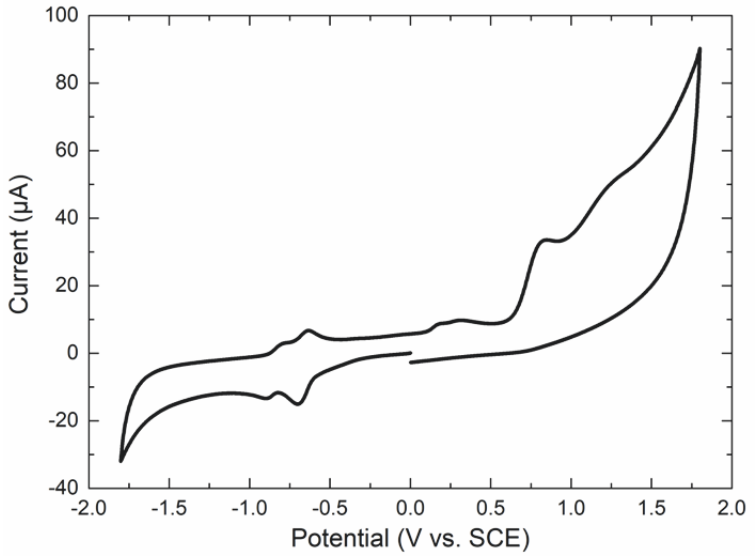

Figure 2.16 Cyclic voltammogram of an argon-saturated ACN:H_2O (1:9, v:v) solution containing 0.5 mM PP and 0.1 M $NaHCO_3$ as supporting electrolyte. Scan rate was 0.1 V s^{-1}.[112]

The thermodynamics for reactions (27) and (28) are still uphill by +0.17 eV and +0.47 eV respectively. However, when taking into account the work terms, these reactions are favorable in the case of Fe^{II} reduction and only slightly endergonic for Fe^{I} reduction. The driving force for electron transfer is given by Equation 29:

$$\Delta G^0 = E^0_{PP^{3-}/PP^{2-}} - E^0_{Fe^{n+}/Fe^{(n-1)+}} + w_R + w_P \quad (29)$$

where w_R and w_P are the work terms required to bring the reactants and products, respectively, from infinity to reacting distance. These terms are assumed to be purely electrostatic in origin and are significant, since both reactants and products are charged. They can be estimated as follows: $w_R + w_P = (-3 \times 4 - 2 \times 3) \times w_0 = -18 \times w_0 = -0.47$ eV for reaction (27) and $w_R + w_P = (-3 \times 3 - 2 \times 2) \times w_0 = -13 \times w_0 = -0.338$ eV for reaction (6); $w_0 = e_0^2 / (4\pi \times \varepsilon_0 \times \varepsilon_S \times d) = 0.026$ eV, where d is the distance between the two reactants (it has been estimated in similar cases to be 7 Å)[121] and ε_S is the solvent dielectric constant (78.8 for water). By using Equation (29), $\Delta G^0 = -0.3$ eV for (27) and 0.13 eV for (28), showing that the two electron transfer reactions are indeed feasible. In the case of reaction (28), the reaction is still slightly unfavorable but it is followed by the fast, favorable binding to CO_2.

After reduction to the Fe^0 catalytically active species, the porphyrin binds to CO_2. The Fe-CO_2 adduct [Fe-$CO_2^{\cdot -}$ ↔ $Fe^{II}CO_2^{2-}$] is likely stabilized by a through-space coulombic interaction between the positive charges borne by the phenyl rings and the partial negative charges of the oxygen atoms of the carbon dioxide, as already suggested.[110] C-O bond cleavage may then occur from protonation of the Fe-CO_2 adduct, leading to the release of a water molecule and a Fe-CO adduct. The latter species furnishes CO either upon photoirradiation or by a one-electron homogeneous reduction by the Fe^0 species.[104]

In conclusion, introducing trimethylammonio groups on the para position of the phenyl rings of an iron porphyrin provides a water soluble molecular catalyst able to perform photochemical conversion of CO_2 into CO in aqueous solutions, at close to neutral pH. By using visible light and a cheap organic sensitizer, selective production of CO was maintained over two days of irradiation. Catalysis is ultimately limited by progressive sensitizer degradation but it could be started again by adding fresh sensitizer. This work opens new perspectives for developing efficient CO_2 photocatalysis in water. Further studies aiming at this goal will include the development of new sensitizers combining efficient light absorption properties with increased stability over long-term irradiation.

Chapter 3 Photochemical Reduction of CO_2 to CH_4 under Visible Light with porphyrin Molecular Catalysts

3.1 Introduction

The production of carbon-based fuels or chemicals using the most abundant carbon source (CO_2) requires designing efficient, cheap, selective and sustainable processes able to convert CO_2 into target products.[122] Such processes could be achieved using electrolyzers, the electricity being issued from renewable sources.[21b, 123] Photochemical processes in which visible light would be directly harvested by an appropriate sensitizer which could furnish electrons to a competent catalyst for the CO_2 reduction are also conceivable.[124] In these photoinduced approaches, metal complexes have been used in conjunction with a photosensitizer (being itself a metal complex or a solid material as *e.g.* a large band gap semi-conductor) and a sacrificial electron donor. The use of earth abundant metal (Fe, Mn or Cu) based catalysts remains a challenge, and the design of selective and stable photo- or electro-catalyst has been only achieved in few cases.[100d] Most of them are related to the two electrons and two protons reduction of CO_2 into CO or HCOOH. Rare electrochemical examples have been identified where highly reduced compounds like hydrocarbons are produced. One example concerns a cobalt proto-porphyrin adsorbed onto a graphite electrode and led to a 2.5% faradaic yield of methane under 10 atm CO_2 at pH 1.[125] Another one deals with a Cu porphyrin also absorbed onto a carbon electrode and led to 30% faradaic yield in methane upon electrolysis at -1.63 V *vs.* SCE in water at pH ~7,[126] although in that case demetalation of the catalyst and further formation of Cu particles, which are highly active towards CO_2 reduction,[127] should not be ruled out. More recently, Wang *et al.* reported the copper(II) phthalocyanine based material that exhibited by far the highest activity for yielding methane with a Faradaic efficiency of 66% and a partial current density of 13 mA cm^{-2} at the potential of -1.06 V versus the reversible hydrogen electrode.[128] The highest activity and selectivity of CuPc for catalyzing CO_2-to-CH_4 conversion among the three structures has been explained by its reversible restructuring to form ~2 nm metallic Cu nanoclusters, which are identified as the active sites for the electrocatalysis. In photochemistry, one recent example involves the catalytic production of CH_4 and C_2H_4 with a cobalt porphyrin adsorbed onto

graphene, although no labelling experiment under $^{13}CO_2$ was performed to assess the origin of the hydrocarbons while their production rate was modest (1.7×10^{-2} µmol per hour and per cm^2 of catalytic material).[129] An alternative approach involves the chemical reduction of CO_2, with the noticeable tandem hydrosilylation of $HCOOSiEt_3$ with mixed organo-Lewis acid catalysts, $Al(C_6F_5)_3$ and $B(C_6F_5)_3$,[130] leading to high yield of methane at moderate temperature (80°C) with a catalytic turnover frequency of a few per hour for more than a day. Finally, semi-conductive solid materials possibly doped with co-catalysts have also been recently developed for the CO_2-to-CH_4 reduction, with hydrocarbon production rate not exceeding a few µmol per hour and per gram of catalyst.[131]

To sum up, most reports on CO_2 reduction to methane have involved copper-based electrodes or semiconductor materials in a heterogonous photocatalytic system. The development of molecular catalysts for homogeneous photocatalytic CO_2-to-CH_4 conversion is of far-reaching significance for fundamental understanding of the process. In this chapter, we will discuss the possibility for Fe-porphyrin complexes to achieve the photochemical CO_2-to-CH_4 conversion.

3.2 $Ir(ppy)_3$ sensitized Fe-porphyrin system for CO_2 reduction in ACN solution

3.2.1. Choice of the sensitizer and components of the system

As already discussed in Chapter 1, most of the transition metal complex catalysts show poor absorption in the visible region, a photosensitizer is thus very necessary for the utilization of solar light. Systems applied for light-driven CO_2 reduction usually include a catalyst, responsible for the capture of CO_2 molecules and their subsequent reduction; a sacrificial electron donor (SD), which is consumed stoichiometrically; and a photosensitizer (PS) for harvesting light energy and mediating the electron transfer from the sacrificial electron donor to the catalyst. Two well-known mechanisms by which the excited PS is quenched are illustrated in Figure 3.1. In the oxidative quenching process, a first step consists in an electron transfer from the PS^* to the catalyst, whereby the PS is oxidized, and the active, reduced form of the catalyst is generated. In the second step, the original PS is regenerated by donation of an electron from SD to PS^+. Whereas it is different from the reductive quenching mechanism, the excited PS is first reduced

by an SD to form PS^- and SD^+. This electron is then transported to the neutral catalyst to generate the active CAT^-. The preference for one mechanism over the other is strongly dependent on the respective redox potentials of the particular species of the CAT, PS and SD. And most of the time, both these two mechanism can happen at the same time. Their relationship is competitive with each other.

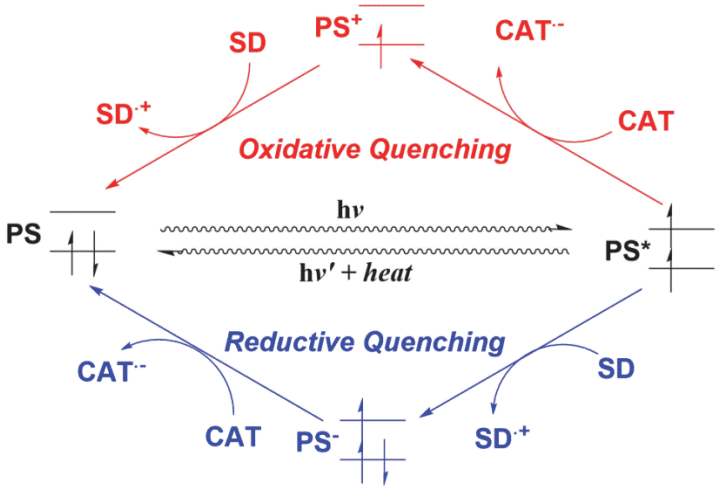

Figure 3.1 Oxidative and reductive quenching mechanisms in photochemical catalyst activation.

Several typical organic dyes, p-terphenyl, phenazine and their derivatives (Figure 3.2, PS-1 to -4) are the representatives used as PS in photochemical CO_2 reduction. Generally, they are very cheap and of easy access. However, they also suffer from relatively low quantum yield and easy decomposition after prolonged irradiation. Ruthenium complexes ($Ru(N\hat{}N)_3$) bearing diimine ligands such as 2, 2'-bipyridine (bpy) or phenanthroline (Figure 3.2, PS-5 to -7), along with cyclometalated iridium complexes ($Ir(C\hat{}N)_3$) such as $Ir(ppy)_3$ (ppy = 2-phenylpyridine) and their derivatives, are widely used as light-harvesting components (Figure 3.2, PS-8 to -10). Thanks to their absorption in the visible range and their strong internal heavy atom effect (triplet MLCT), high quantum efficiency in photochemical catalysis could be achieved.[132]

In homogeneous processes, *i.e.* without electrode to furnish electrons, the use of a SD, as illustrated in Figure 3.3, is imperative. Few examples reporting water as SD were reported to date. The role of the SD is to provide electron(s) either to the PS (reductive quenching) or the catalyst (oxidative quenching). Organic amines, ascorbic acid or EDTA are widely used in homogeneous processes as already illustrated in the previous chapter. BNAH and BIH were also reported as efficient SDs due to their two-electron and one-proton releasing property as well as their much

stronger reducing capacity. Researchers are also facing challenges in employing water as a simple and green electron donor and combining CO_2 reduction with water oxidation in an effort to mimic photosynthesis.[114]

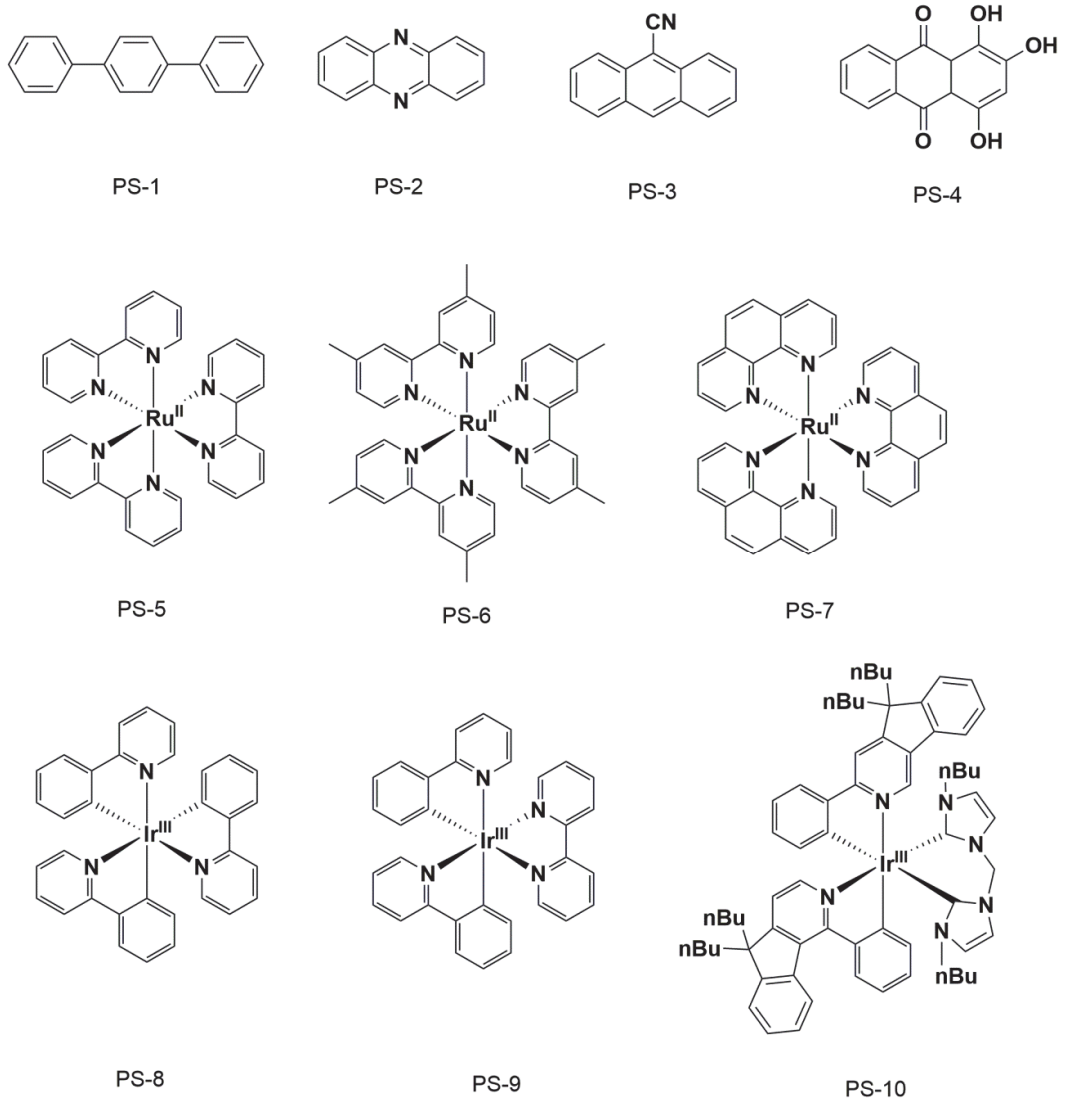

Figure 3.2 Molecular structures of typical organic dyes and transition metal complexes used as photosensitizer in photochemical catalysis.

Among the CO_2-to-CO conversion molecular catalysts, iron tetraphenylporphyrins electrochemically reduced to the Fe^0 species have been shown to be the most efficient ones.[100c, 110] The nucleophilic Fe center binds to CO_2 and the Fe-CO_2 adduct is further protonated and reduced to afford CO upon cleavage of one C-O bond. Substitution of the phenyl rings allowed tuning the reactivity of the catalyst and led to remarkable selective and efficient reaction, combined with high durability.

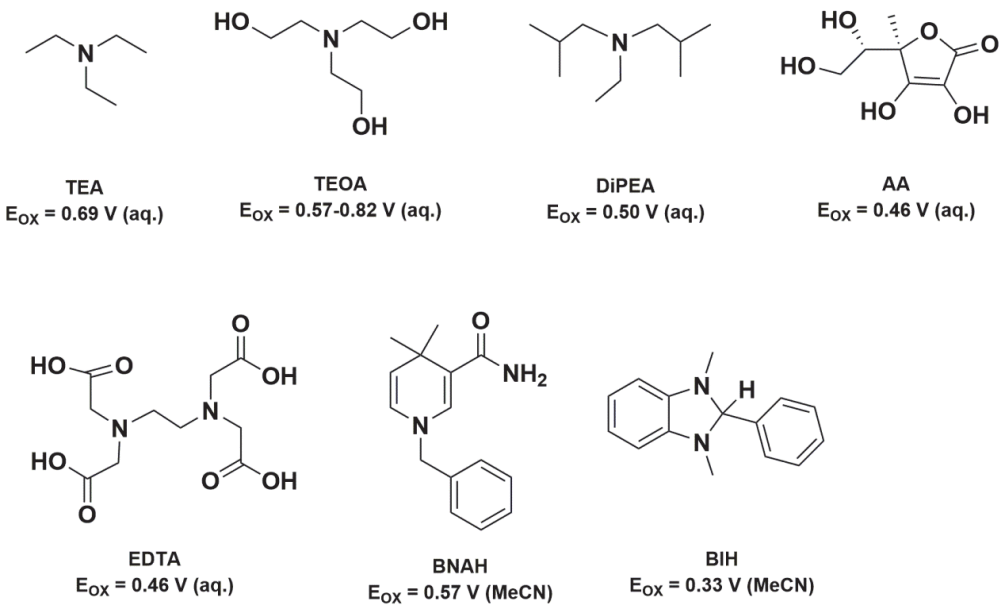

Figure 3.3 Chemical structures of typical sacrificial electron donors used in photochemical catalysis (Redox potential given in V *vs.* SCE).

In particular, substitution of the four para-phenyl hydrogens by trimethylammonio groups[109] led to CO formation with selectivity close to 95% in water at pH 7 as well as in aprotic solvent such as N, N-dimethylformamide (DMF), at low overpotentials and with catalytic activity that could be maintained over several days. The fact that the standard redox potential of the Fe^{I}/Fe^{0} is not very negative (E^{0} = -1.50 V *vs.* SCE) combined to the remarkable high intrinsic activity towards CO_2 reduction makes these catalysts good candidates for photochemical reduction of the gas. In the last chapter, we have showed that Fe-*p*-TMA can photochemically converts CO_2 into CO without any PS or with an organic dye as PS. In this part, we will choose $Ir(ppy)_3$ (PS-8) as the PS owing to its much stronger redox ability, which may sharply promote the catalytic efficiency.

3.2.2 Experiments under CO_2 atmosphere

In Chapter 2, Fe-*p*-TMA was used as a photocatalyst without a photosensitizer under visible light irradiation (> 420nm) with triethylamine (TEA, 50 mM) as SD. Illumination of a 1 atm CO_2-saturated solution of acetonitrile containing 2 μM of Fe-*p*-TMA at room temperature for 47 h selectively produced CO, with a turnover number in CO relative to catalyst concentration of 33. No side products were observed, and the linear production of CO with time indicates good

stability of the catalytic system. When purpurin was added as PS, the TON of the system increased. Nevertheless, it suffered from the instability of PP under a long-run irradiation.

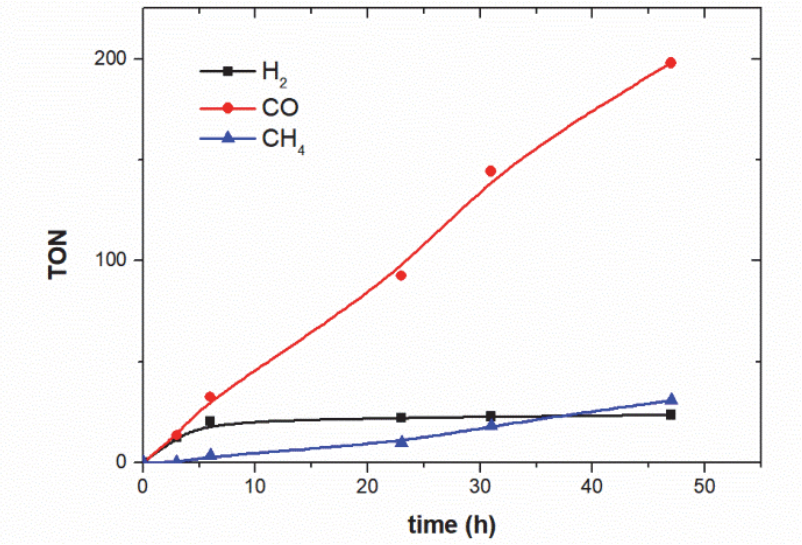

Figure 3.4 H_2 (black), CO (red) and CH_4 (blue) formation with irradiation (> 420 nm) time of a CO_2-saturated ACN solution containing 2 µM Fe-*p*-TMA, 0.05 M TEA, and 0.2 mM PS-8.

A factor that can potentially limit the catalytic rate of this system[90, 104] is the three-electron reduction of the initial Fe^{III} porphyrin species to generate the active Fe^0 state. Using electron donors with high reducing ability should thus be favourable, and adding 0.2 mM of PS-8 as photosensitizer ($E^0(Ir(ppy)_3^+/Ir(ppy)_3^*$ ≈ -1.73 V versus the saturated calomel electrode (SCE) and $E^0(Ir(ppy)_3/Ir(ppy)_3^-$ ≈ -2.19 V *vs.* SCE)[133] to the solution indeed enhanced the photocatalytic CO_2 reduction so that 47 h of irradiation gave a TON in CO of 198 relative to Fe-*p*-TMA (Figure 3.4, red), which was much more efficient than the previous systems. More interestingly, besides CO and H_2, a third product in the gas phase was found through gas chromatography. This peak was preliminarily proved to be methane by injection of standard CH_4 samples (Figure 3.5). The system achieved a TON of CH_4 of 31 with a selectivity of *ca.* 12% in 47 h. In addition, some hydrogen was formed with a TON of 24 and selectivity of 10%.

To prove that the CO_2 reduction reaction was catalyzed by the CAT, multiple control experiments were conducted. In one control experiment, argon gas was supplied in the solution instead of CO_2, which resulted in the exclusive production of hydrogen with a TON of 43 (Table 3.1). Without CAT, SD or light, no product could be detected. When using an isotopically labelled $^{13}CO_2$ gas feed, mass spectrometry showed signals for $^{13}CH_4$ (m/z = 17), confirming that

this product is derived from $^{13}CO_2$ photochemical reduction. Whereas using general $^{12}CO_2$ (Figure 3.6), mass spectrometry showed signals for $^{12}CH_4$ (m/z = 16).

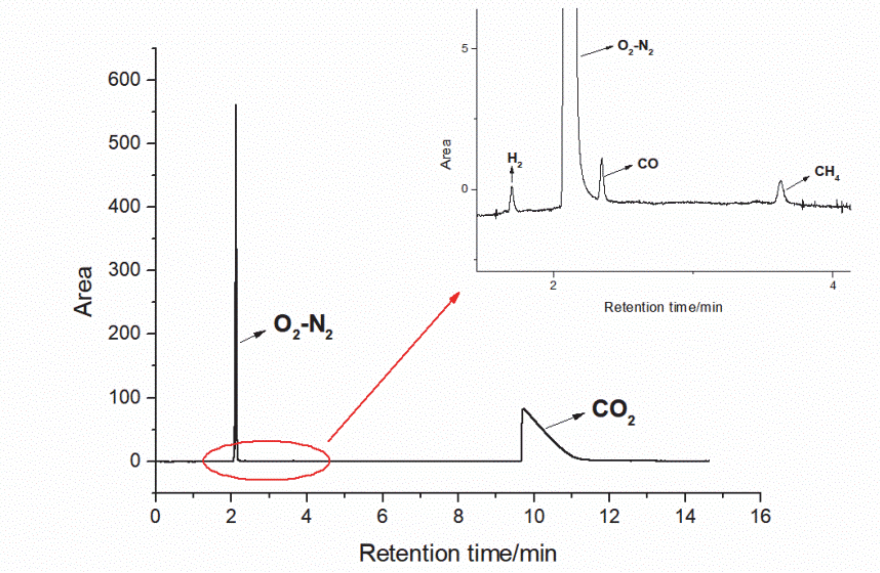

Figure 3.5 Gas chromatogram of the headspace after 47 h irradiation (> 420 nm) of a CO_2-saturated ACN solution containing 2 μM Fe-*p*-TMA, 0.05 M TEA and 0.2 mM PS-8.

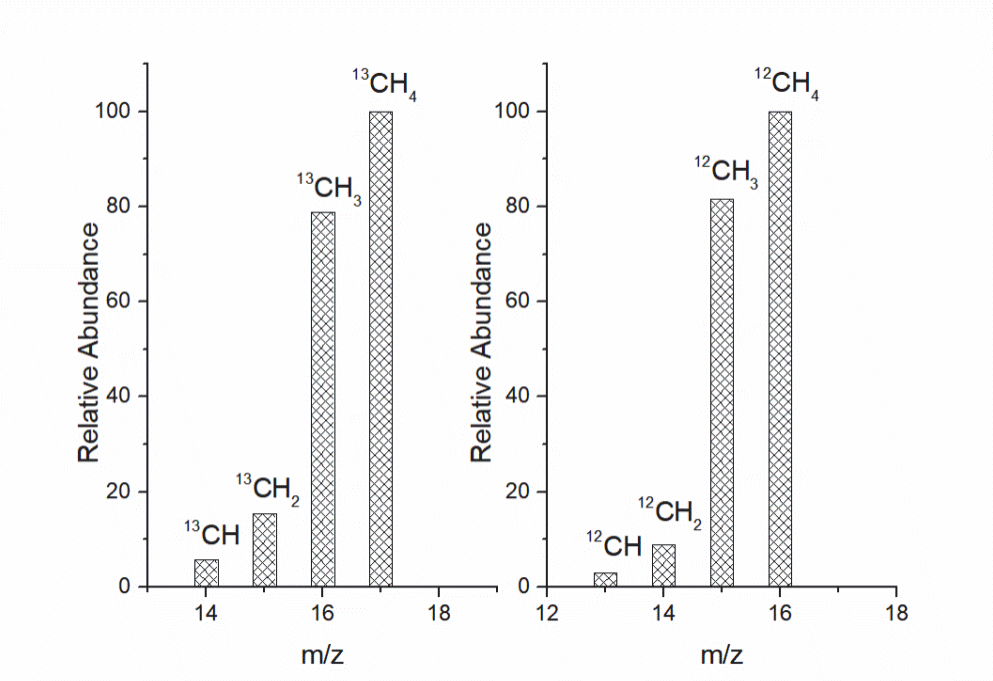

Figure 3.6 Mass spectra of methane obtained after 47 h irradiation of solutions feed with $^{13}CO_2$ (left) and $^{12}CO_2$ (right).

3.2.3 Experiments under CO atmosphere

As shown in Figure 3.4, the production rate of CH_4 was quite slow at the first few hours and then increased rapidly. Evolution of the different products shows that methane production starts only after a large amount of CO has built up, suggesting that CO is an intermediate in the methane formation process. On the other hand, we have also previously shown by ultraviolet-visible spectroscopy (Figure 2.5) that irradiation of a CO_2 saturated solution of CAT without a sensitizer (in that case, only CO is obtained) led to the formation of detectable amounts of $Fe^{II}CO$ species. We may thus hypothesize that this iron-carbonyl adduct is an intermediate for further reduction towards methane in the presence of a strong reducing agent. To explore the influence of CO on methane formation more directly, experiments were then conducted in a 1 atm CO-saturated acetonitrile solution under visible light irradiation ($\lambda > 420$ nm), with PS-8 as PS and TEA as SD. After 47 h of illumination, CH_4 was found to be the main products through gas chromatograph (Figure 3.7) and this system achieved a turnover number of CH_4 of 89 (Figure 3.8). The slightly lowered H_2 production and increased CH_4 production by almost was a factor of three compared to the experiment using a CO_2-saturated solution: 83% of product was CH_4 and 17% of product was H_2, with the CH_4 formation rate of 1, 865 μmol h^{-1} g^{-1}.

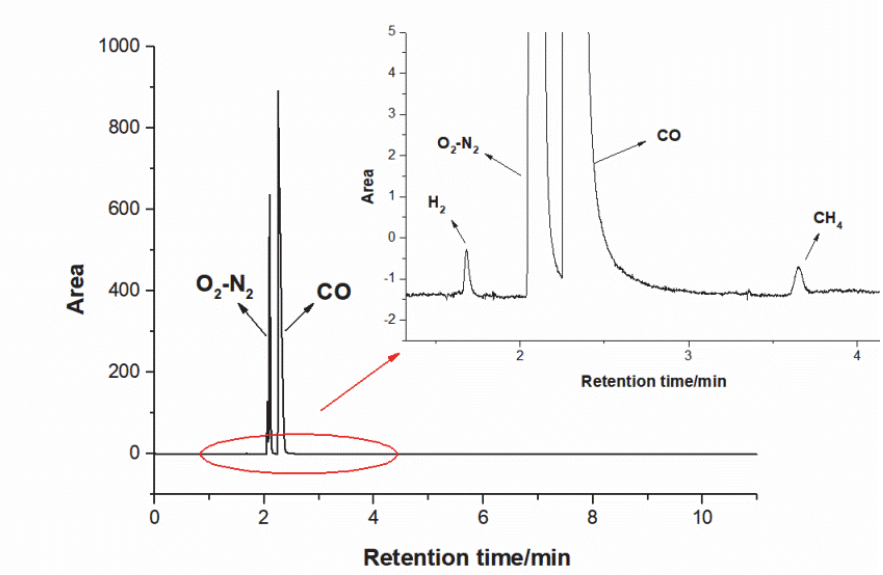

Figure 3.7 Gas chromatogram measured after 47 irradiation (> 420 nm) of a CO-saturated ACN solution containing 2 μM Fe-*p*-TMA, 0.05 M TEA and 0.2 mM PS-8.

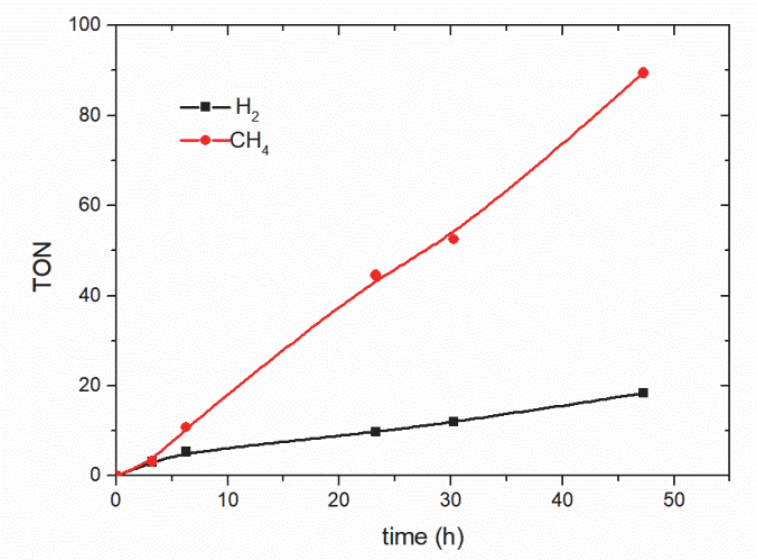

Figure 3.8 H_2 (black) and CH_4 (red) formation with time during irradiation (λ > 420 nm) of a CO-saturated ACN solution containing 2 μM Fe-*p*-TMA, 0.05 M TEA and 0.2 mM PS-8.

3.2.4 Optimization of the system

Under CO_2 atmosphere, blank experiments in the absence of CAT, SD or light achieved nothing or trace of H_2 (entry 6, 7, and 8 in Table 3.1), while a longer irradiation time of 102 h gave TON_{CO} of 367, TON_{CH4} of 79 and TON_{H2} of 26, respectively. With the addition of a weak acid (0.1 M TFE), the efficiency of the system somewhat increased, *i.e.* TON_{CO} of 198 to 240, TON_{CH4} of 31 to 66 and TON_{H2} of 24 to 73 in 47 h irradiation (entry 2 and 3 in Table 3.1 and Figure 3.9 b and c). Under CO atmosphere, blank experiments in the absence of CAT or in the absence of light did not give any reduction product (entries 13 and 14 in Table 3.1), while a longer irradiation time of 102 h enhanced the selectivity for methane further to 87% (entry 11 in Table 3.1 and Figure 3.9d). Addition of a weak acid in moderate concentration (trifluoroethanol 0.1 M) slightly increased the methane formation rate (from a TON of 140 to 159) with some loss of selectivity (from 87% to 82%; entry 12 in Table 3.1). The successful methane evolution under these conditions over 102 h with an average rate of 1,467 μmol h^{-1} g^{-1} illustrates the robustness, activity and selectivity of the catalytic system. Taking 159 as the highest turnover number for CH_4, we obtain a quantum yield Φ of about 0.18% after 102 h of irradiation (see experimental section for details of the calculation).

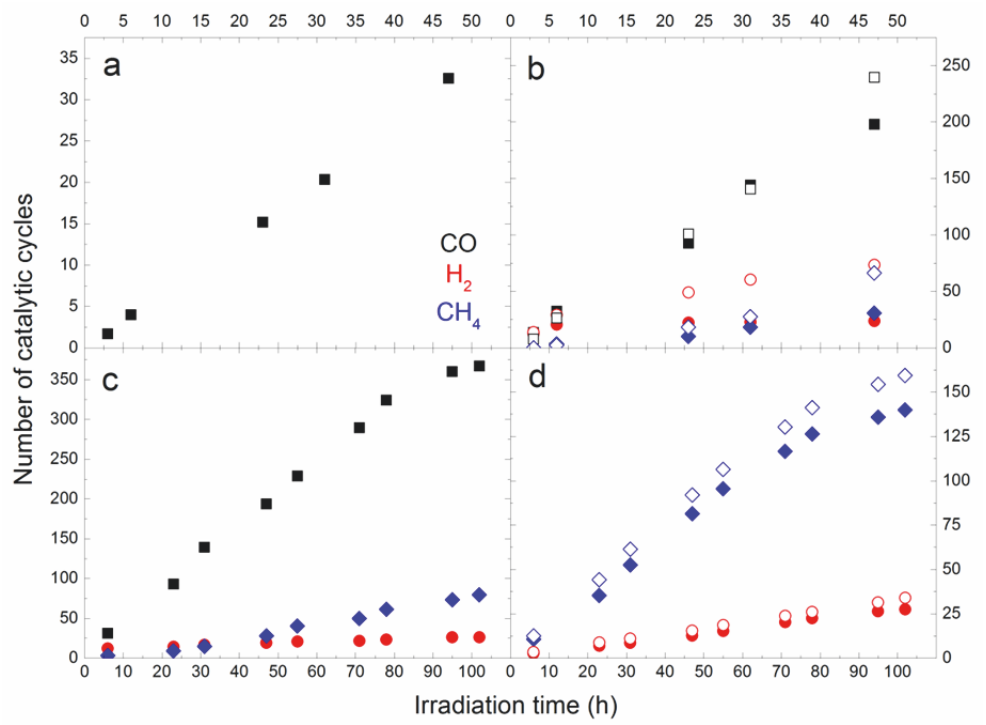

Figure 3.9 Photochemical reduction of CO_2 upon visible light irradiation. Gaseous reduction products obtained in a 1 atm CO_2 (a, b, c) or CO-saturated (d) 2 µM Fe-*p*-TMA and 50 mM TEA acetonitrile solution. a, CO generation with no sensitizer. b, Gas products in the presence of 0.2 mM of PS-8 (filled symbols; + 0.1 M TFE, open symbols). c, Extended irradiation in the presence of 0.2 mM of PS-8. d, Gas products under CO atmosphere, in the presence of 0.2 mM of PS-8 (filled symbols; + 0.1 M TFE, open symbols).[116]

When replacing Fe-*p*-TMA by Fe-*o*-OH (Table 1), which carries -OH groups at all ortho, ortho' positions of the four phenyl rings[96] instead of trimethylammonio groups at the para positions, methane was also evolved although in slightly smaller amounts (turnover number 26 after 47 h irradiation and 14% selectivity, Table 3.1, entry 9). The standard redox potential $E^0(Fe^I/Fe^0) = -1.575$ V *vs.* SCE[134] in DMF for Fe-*o*-OH is only 75 mV more negative than for Fe-*p*-TMA, and as in the latter case, the substituents on the phenyls may help stabilizing reaction intermediates (through internal H bonds involving the -OH groups). In contrast, the non-substituted tetraphenyl Fe porphyrin (FeTPP, Table 1) only gives CO and H_2 (with turnover numbers/selectivities of 84/79% and 22/21%, respectively) under the same irradiation conditions[89], probably owing to its much more negative standard redox potentials (for example, $E^0(Fe^I/Fe^0) = -1.67$ V *vs.* SCE in DMF)[135] and the absence of phenyl ring substituents for stabilizing intermediate species involved in hydrocarbon production. The ability to produce methane is thus not restricted to Fe-*p*-TMA, and it is probably a more general property of Fe porphyrins that have a sufficiently positive

standard redox potential and are functionalized with substituents that can stabilize intermediates involved in the catalytic cycle.

Table 3.1 Catalytic performance and structures of catalysts and sensitizer.[116]

Entry	[Fe-*p*-TMA] μM	Gas	[PS-8] mM	[TEA] mM	λ nm	Time h	TONs CO	CH_4	H_2
1	2	CO_2	-	50	> 420	47	33	-	-
2	2	CO_2	0.2	50	> 420	47	198	31	24
3*	2	CO_2	0.2	50	> 420	47	240	66	73
4	2	CO_2	0.2	50	> 420	102	367	79	26
5	2	Ar	0.2	50	> 420	47	-	-	43
6	-	CO_2	0.2	50	> 420	47	3	-	1
7	2	CO_2	0.2	-	> 420	23	5	-	-
8	2	CO_2	0.2	50	dark	23	-	-	-
9†	2	CO_2	0.2	50	> 420	47	139	26	15
10	2	CO	0.2	50	> 420	47	-	89	18
11	2	CO	0.2	50	> 420	102	-	140	28
12*	2	CO	0.2	50	> 420	102	-	159	34
13	-	CO	0.2	50	> 420	47	-	-	-
14	2	CO	0.2	50	dark	23	-	-	-

* in the presence of 0.1 M TFE, † with Fe-o-OH as catalyst.

As we have shown that increasing the irradiation time increased the amount of CO_2 reduction products generated, a longest irradiation time of 102 h in these series experiments was conducted. The final TON_{CH4} reached 79, corresponding to a production rate of 763 μmol per hour per gram of catalyst (μmol $h^{-1}g^{-1}$), which exceeds the rate of many other catalysts[129, 131a, 131b, 131e, 136] that generate methane from CO_2. The linear evolution of both CO and CH_4 over more than 80 h and the stable absorption spectrum of the system under irradiation (Figure 3.10), with no evidence for degradation of the sensitizer PS-8 or Fe-*p*-TMA, illustrate the stability of the catalytic system.

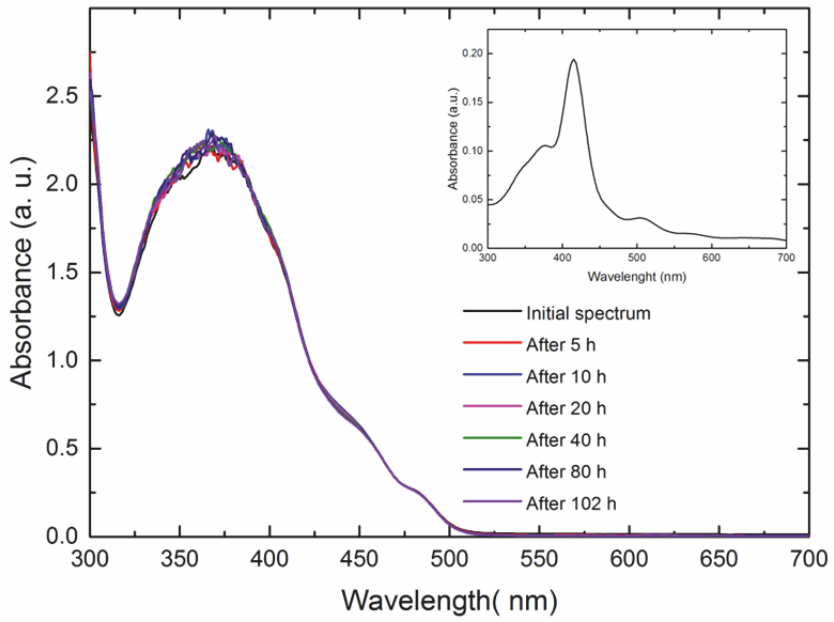

Figure 3.10 Evolution of the absorption spectrum with time. The absorption spectrum of a CO_2-saturated acetonitrile solution containing 2 µM of Fe-*p*-TMA, 0.2 mM of PS-8, 0.05 M of TEA upon visible (> 420 nm) light irradiation remains stable over the course of experiments, highlighting the stability of the system. The inset shows the absorption spectrum of 2 µM Fe-*p*-TMA in acetonitrile (no PS), revealing that in the photocatalytic mix, >90% of photons above 420 nm are absorbed by PS-8.[116]

3.2.5 A possible mechanism for CH_4 formation

One of the key parameters for CO_2 reduction beyond the two-electron production of CO is the driving force for charge transfer from the excited state of the sensitizer. When replacing PS-8 by the less-reducing ruthenium complex $Ru(bpy)_3^{2+}$ (where bpy is 2,2'-bipyridine; $E^0(Ru(bpy)_3^{2+}/Ru(bpy)_3^{+}) \approx$ -1.33 V versus SCE and $E^0(Ru(bpy)_3^{3+}/Ru(bpy)_3^{2+*}) =$ -0.81 V *vs.* SCE)[133], only CO and H_2 and no CH_4 were obtained, possibly because the Ru excited state or its reduced form are not able to trigger the carbonyl reduction from the $Fe^{II}CO$ adduct. The values for the reduction/oxidation potentials for the investigated species found in literature and the measured values are summarized Figure 3.11.[133] All values are converted with respect to SCE. Both the reduction potential (-2.19 V) and the determined excited state reduction potential (-1.73 V) of PS-8 are more negative than all three redox couples related to the Fe porphyrin (Fe^{III}/Fe^{II}, Fe^{II}/Fe^{I} and Fe^{I}/Fe^{0}), which means that the electron transfer from PS-8 to Fe-*p*-TMA is thermodynamically feasible. The redox potentials of TEA (Et_3N/Et_3N^{+}) given in references range from +0.69 V up to 0.73 V,[137] which are more positive than excited state oxidation potential and less positive than oxidation potential of PS-8. Therefore, the electron transfer from TEA to

*$Ir^{III}(ppy)_3$ is thermodynamically infeasible while the electron transfer from TEA to $Ir^{IV}(ppy)_3$ is thermodynamically feasible. The following emission quenching experiments further confirm the results.

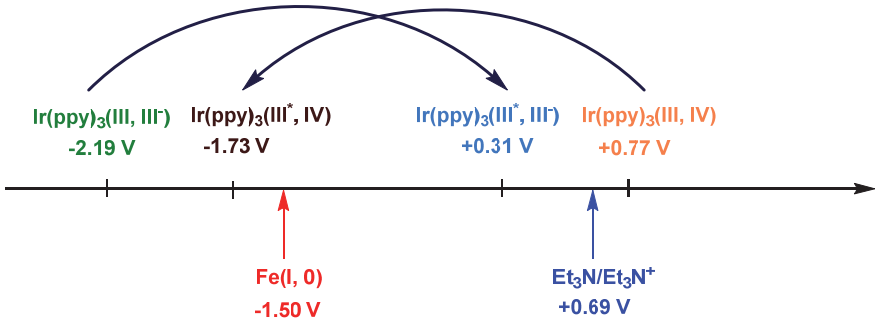

Figure 3.11 Reduction/oxidation potentials for the investigated system in V *vs.* SCE.

Emissions quenching experiments between the excited state of the PS-8 and Fe-*p*-TMA or TEA were shown in Figure 3.12. PS-8 and TEA revealed very weak quenching with TEA, while it is very efficient and diffusion-controlled with Fe-*p*-TMA ($k_q \approx 1.7 \times 10^{10}$ M^{-1} s^{-1}), suggesting that direct electron transfer occurs from the excited PS-8 to the Fe-porphyrin through an oxidative quenching process, which is in line with the above redox potential analysis.

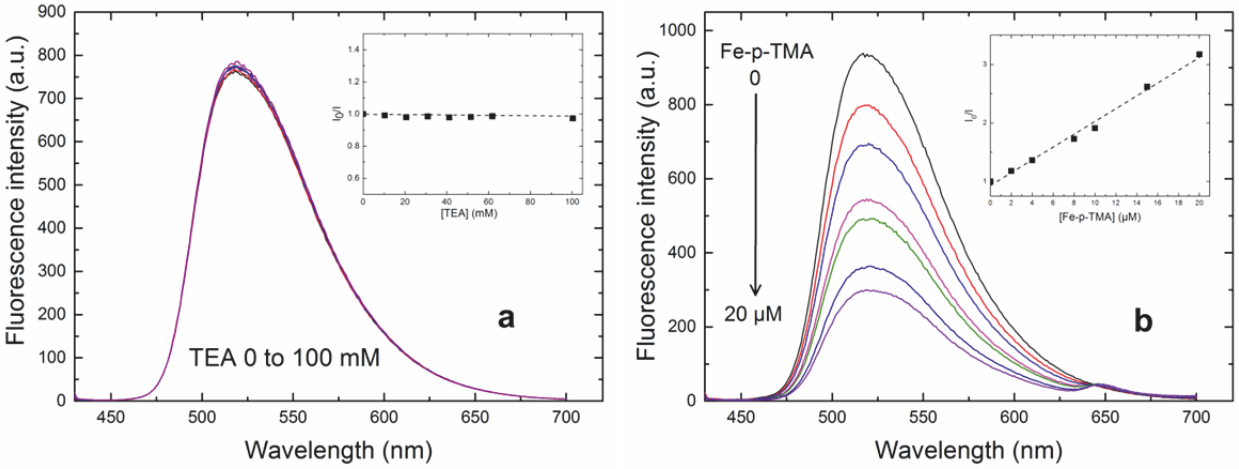

Figure 3.12 PS-8 emission quenching after excitation at 420 nm. a, Upon increasing concentration of TEA in a 0.1 mM ACN solution of $Ir(ppy)_3$, no emission quenching is observed, as confirmed by the Stern-Volmer analysis (inset). b, Upon increasing concentration of Fe-*p*-TMA in a 0.2 mM ACN solution of $Ir(ppy)_3$, emission quenching is observed corresponding to a diffusion-controlled quenching rate of $(1.7 \pm 0.1)\times10^{10}$ M^{-1} s^{-1} as determined by Stern-Volmer analysis (inset). a.u., arbitrary units. I_0/I is the emission intensity without quencher divided by the emission intensity with a known concentration of quencher.[116]

After electron transfer, the oxidized PS-8 is reduced by TEA upon irradiation, thereby closing the catalytic cycle and generating the protonated triethylamine $TEAH^+$ that could then act as proton donor, as seen before.[89] Figure 3.13 sketches a plausible mechanism based on these considerations, which involves a postulated formyl intermediate[138] that may be stabilized by through-space interactions between the positive charges of the trimethylammonio groups and the partial negative charge on the CHO species bound to the metal. CO_2 was reduced into CO with two electrons and then followed with complete reduction of the $Fe^{II}CO$ adduct necessitating six electrons. Overall, the starting Fe^{III} porphyrin (top left) is reduced with three electrons to the catalytically active Fe^0 species. The Fe^0 species reduces CO_2, with the resultant Fe^I regenerated through electron transfer from the excited photosensitizer (right-hand side cycle). The CO produced binds to Fe^{II} and is further reduced with a total of six electrons (transferred from the excited sensitizer) and six protons to generate methane, via a postulated Fe^I-formyl (Fe^ICHO) intermediate (left-hand side cycle).

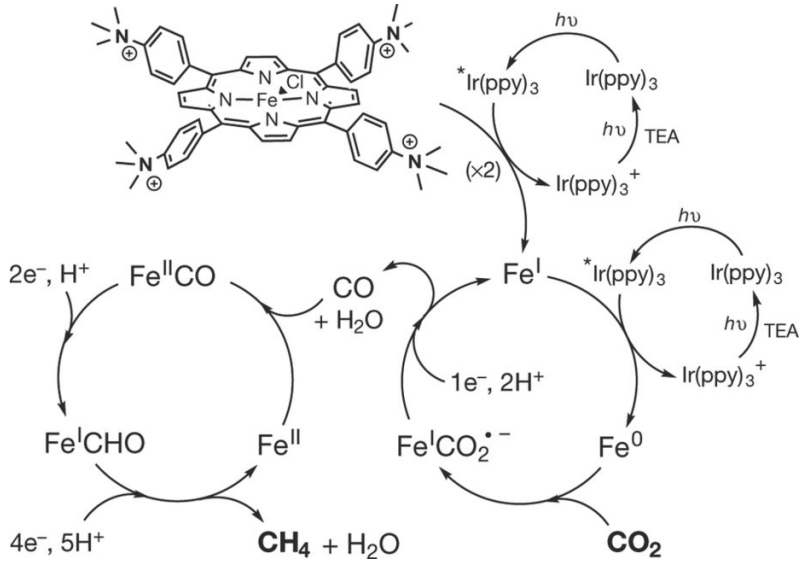

Figure 3.13 Proposed mechanism for CO_2 reduction to CH_4 by Fe-*p*-TMA.[116]

To summarize, Fe-*p*-TMA is able to reduce CO_2 into CO and then to CH_4 under visible light irradiation with PS-8 as sensitizer. In the absence of added sensitizer, the catalyst reduces selectively CO_2 to CO. The pure CO could be catalytically transformed by the same catalyst into CH_4 with 82% catalytic selectivity and 159 TON over several days, under the same mild conditions (ambient temperature and pressure, visible light). New roads towards solar fuels using earth abundant Fe-based molecular complex are thus opened.

3.3 $Ir(ppy)_2(bpy)PF_6$ sensitized system for photocatalytic CO_2 reduction in aqueous conditions

3.3.1 Building of an aqueous photochemical system

In Nature, green plants convert CO_2 into carbohydrates a complex biochemical process occurring in water environment. However, most of the reported photochemical CO_2 reduction systems are in organic solvent, mainly ACN and DMF. In contrast, the photochemical CO_2-to-CO conversion in water has only been achieved in few cases, with modest turnover number and limited stability over time.[139] The easy occurrence of the photocatalytic proton reduction is competitive with the CO_2 reduction reaction, which may inevitably results in a decrease of the efficiency and selectivity for the latter. Therefore, to develop a highly active and selective water-containing photochemical CO_2 reduction system is very necessary for constructing an artificial photosynthesis cycle. In addition, water is used not only as the reaction solvent but also both as the proton and electron sources, which is noticeably environmental friendly.

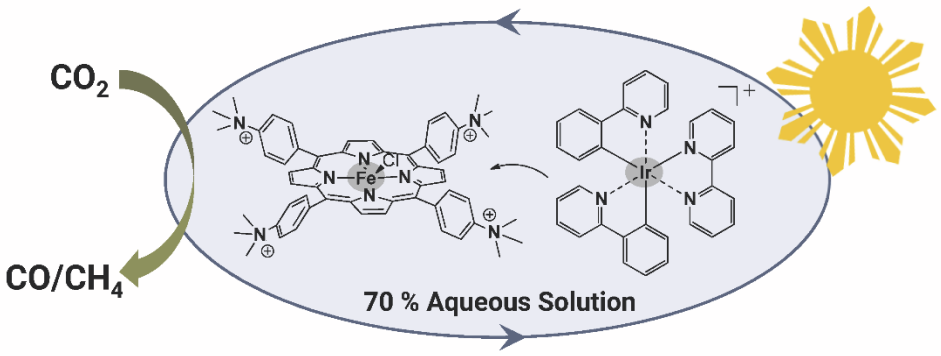

Figure 3.14 $Ir(ppy)_2(bpy)PF_6$ sensitized Fe-*p*-TMA system for photocatalytic CO_2 reduction in aqueous conditions.

We have previously demonstrated the remarkable performance of Fe-*p*-TMA catalyst (Figure 3.14) under visible light irradiation to both achieve the two electrons CO_2-to-CO catalytic reduction in aqueous solutions (acetonitrile/water 1:9 v/v)[112] and the eight electron CO_2-to-CH_4 conversion in ACN when combined with an iridium-based photosensitizer,[116] belonging to a well-known class of compounds for photoredox catalysis.[140] We now investigate the possible CH_4 generation can be realized in aqueous solutions (ACN/water 3:7 v:v, ACN being required to allow a decent solubility of the PS) when a water-compatible analog of the iridium complex

sensitizer, $[Ir(ppy)_2(bpy)]^+$ (PS-9) is used (Figure 3.14). This sensitizer presents relevant photophysical properties such as a long excited-state lifetime (several hundreds of nanoseconds)[105b, 141] and a highly negative redox potential (*ca.* -1.45 V *vs.* SCE)[142] in its reduced form. The thermal population of the dissociative ^{3}d–d state from the ^{3}MLCT excited state can be suppressed in the case of PS-9 because of the high ligand-field stabilization of the strong σ-donor character of the ppy ligand.[143] This results in both high photochemical stability of the Ir(III) complexes and a long lifetime of the excited state of the Ir(III) complexes, which promotes efficient electron transfer from an electron donor.

Herein we show the use of PS-9 for photochemical CO_2 reduction with Fe-porphyrin catalyst. Ir-9 has a relatively intense absorption band even at wavelengths longer than 450 nm, and its excited state has a longer lifetime than that of typical sensitizer $[Ru(bpy)_3]^{2+}$. Although the performances remain limited by the instability of the sensitizer upon prolonged irradiation, we have found it opens the door for the use of water as solvent in the generation of solar fuels from CO_2 catalysis in homogeneous systems.

3.3.2 Preliminary experiments in ACN solutions

As both the structure and properties of PS-8 and PS-9 are quite similar, we conducted a series of experiments in ACN with PS-9 to make a straight comparison with previous results. As shown in Figure 3.15, three kinds of tertiary amine (TEA, TEOA and DIPEA) were used as SD. Similarly to what has been observed with PS-8 sensitizer, CO, H_2, and CH_4 were produced with CO being the major product (ca. 60% catalytic selectivity with a maximum TON of 178, Table 3.2), while methane was produced with ca. 10% selectivity (TON of 32 with TEA as a sacrificial donor).

Using TEA as SD led to the highest TON for the reduction products (CO, CH_4) among the three amines tested (TEA, TEOA and DIPEA), but no major difference could be observed in terms of both efficiency and catalytic selectivity (Table 3.2).

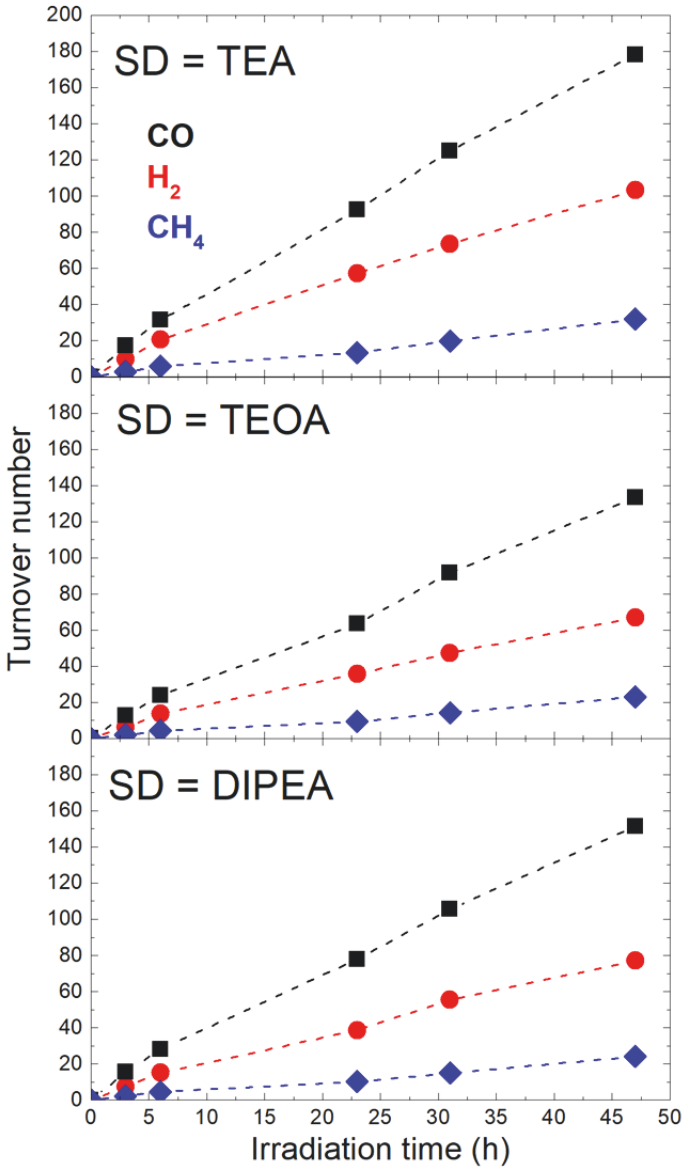

Figure 3.15 CO (black squares), H_2 (red circles), and CH_4 (blue diamonds) formation (turnover numbers) upon visible-light irradiation ($\lambda > 420$ nm) of a CO_2-saturated ACN solution containing 2 μM Fe-*p*-TMA catalyst, 0.2 mM $[Ir(ppy)_2(bpy)]^+$ sensitizer, and 0.05 M TEA (top), TEOA (middle), or DIPEA (bottom) as sacrificial electron donor.

We then conducted a series of experiments using a mix of 30% ACN and 70% water (v/v) as the reaction solvent, chosen to maximize the water proportion while allowing a suitable solubility for $[Ir(ppy)_2(bpy)]^+$ to ensure an efficient light absorption. Keeping all other parameters (including concentration) identical, we observed (Figure 3.16) a lower amount of all reduction products, which may be ascribed to a significantly lower solubility of the reactant (CO_2) in the reaction mixture. The sacrificial electron donor giving the best efficiency is TEA, once again

with no major difference in terms of efficiency and catalytic selectivity for the three SDs that have been employed (Table 3.2).

Table 3.2 Turnover number (TON, ± 5%) and catalytic selectivity (CS) of a 2 μM Fe-*p*-TMA CO_2-saturated solution in the presence of 0.2 mM PS and 0.05 M SD after 47 h of visible (> 420 nm) light irradiation.

PS	Solvent	SD	TON			CS (%)		
			H_2	CO	CH_4	H_2	CO	CH_4
$Ir(ppy)_2(bpy)^+$	ACN	TEA	103	178	32	33	57	10
		TEOA	67	134	23	30	60	10
		DIPEA	77	151	24	31	60	9
$Ir(ppy)_2(bpy)^+$	ACN/H_2O	TEA	5	24	3	16	75	9
		TEOA	4	19	3	15	73	12
		DIPEA	4	20	3	15	74	11
$Ir(ppy)_3$	ACN[a]	TEA	24	198	31	10	78	12
	ACN[b]	TEA	18	-	89	17	-	83
	ACN[c]	TEA	19	-	100	16	-	84
	ACN[d]	TEA	45	-	195	19	-	81

a Under CO_2 atmosphere[116], Table 3.1, entry 2. b Under CO atmosphere[116], Table 3.1, entry 10. c Under CO atmosphere + 0.5 M TFE, this study. d Under CO atmosphere + 0.5 M TFE, this study (102 h irradiation).

Regarding methane formation, catalytic selectivity was close to 10%, with a maximum TON of 3 obtained with all SDs. Overall, a ca. 75% catalytic selectivity for CO was measured, corresponding to a TON in the range of 20 to 25. At first look, these results are not surprising since all SDs have relatively close oxidation potentials (0.5-0.8 V *vs.* SCE range);[114, 144] however, TEOA has a lower pK_a (7.9)[114] than TEA (10.7) and DIPEA (10.5)[145] so one could have expected a higher generation of H_2 in the former case, which was not observed.

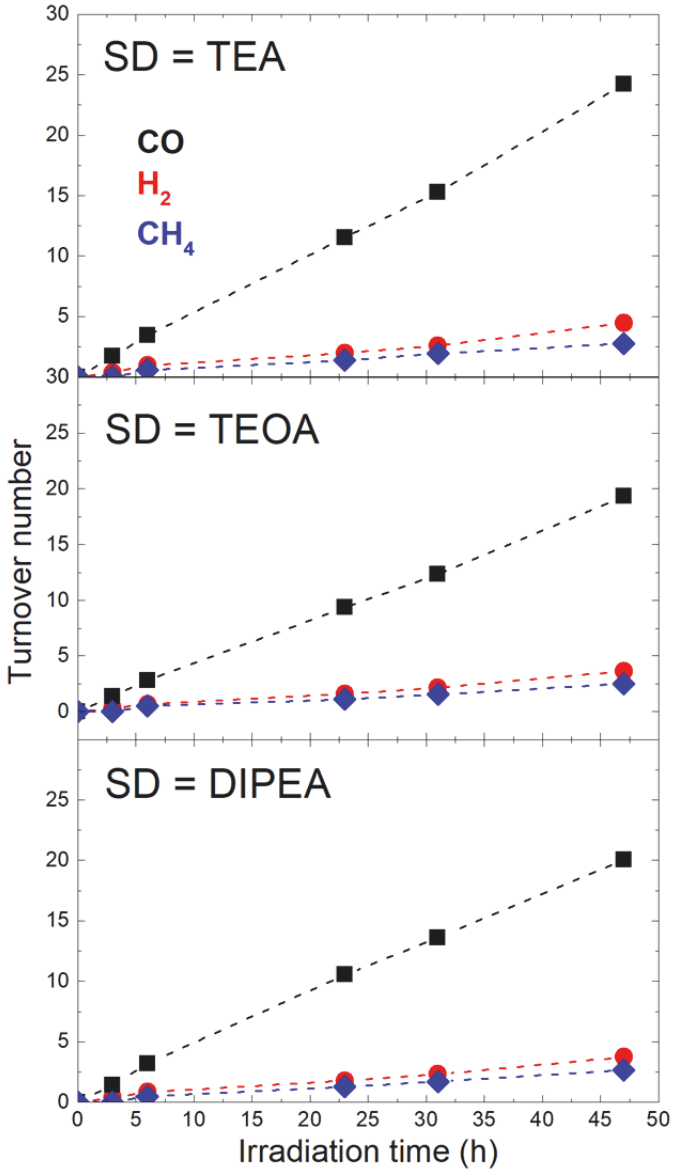

Figure 3.16. CO (black squares), H_2 (red circles), and CH_4 (blue diamonds) formation (turnover numbers) upon visible-light irradiation ($\lambda > 420$ nm) of a CO_2-saturated ACN/H_2O (3:7 v/v) solution containing 2 μM Fe-*p*-TMA catalyst, 0.2 mM $[Ir(ppy)_2(bpy)]^+$ sensitizer, and 0.05 M TEA (top), TEOA (middle), or DIPEA (bottom) sacrificial electron donor.

3.3.3 Electron transfer mechanism in this system

To help understanding the reaction mechanism in aqueous solutions, we conducted emission quenching experiments upon exciting the $[Ir(ppy)_2(bpy)]^+$ sensitizer at 420 nm in the presence of increasing concentration of TEA, TEOA or DIPEA (Figure 3.17-3.19). Analysis of emission quenching using the Stern-Volmer analysis and the excited-state lifetime measured by time-

resolved laser kinetics (145 ns, Figure 3.20) gives quenching rate constants of 5.8×10^6, 4.6×10^6, and 1.4×10^8 M^{-1} s^{-1} for TEA, TEOA, and DIPEA, respectively.

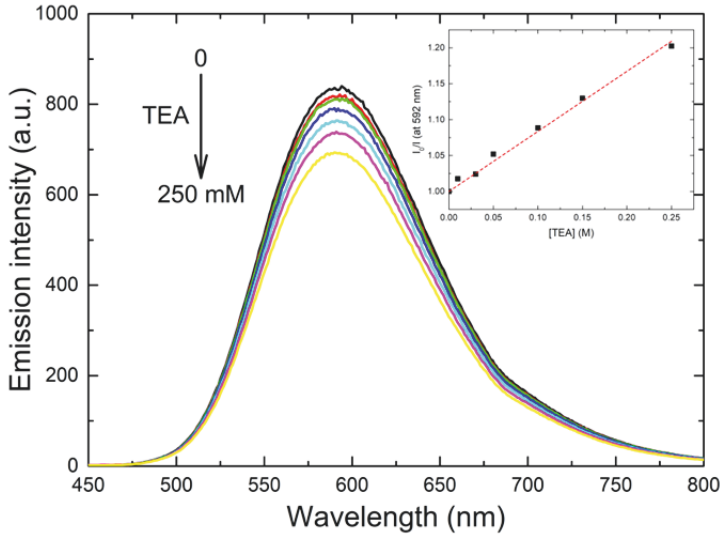

Figure 3.17 Emission spectra of a 0.2 mM $[Ir(ppy)_2(bpy)]^+$ solution in ACN/H_2O (3:7 v/v) containing 0 (black), 10 (red), 30 (green), 50 (blue), 100 (cyan), 150 (magenta), and 250 mM (yellow) TEA. The inset shows the linear plot ($R^2 = 0.994$) of the normalized emission at 592 nm versus TEA concentration according to the Stern-Volmer equation.

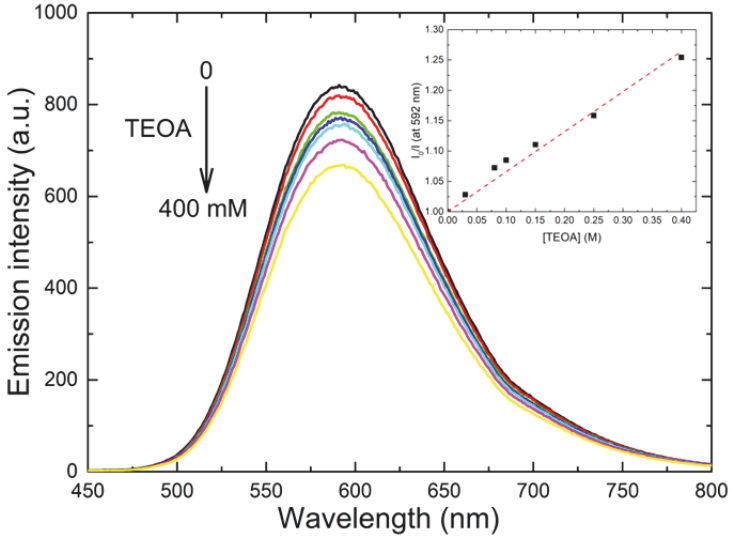

Figure 3.18 Emission spectra of a 0.2 mM $[Ir(ppy)_2(bpy)]^+$ solution in ACN/H_2O (3:7 v/v) containing 0 (black), 30 (red), 80 (green), 100 (blue), 150 (cyan), 250 (magenta), and 400 mM (yellow) TEOA. The inset shows the linear plot ($R^2 = 0.999$) of the normalized emission at 592 nm versus TEOA concentration according to the Stern-Volmer equation.

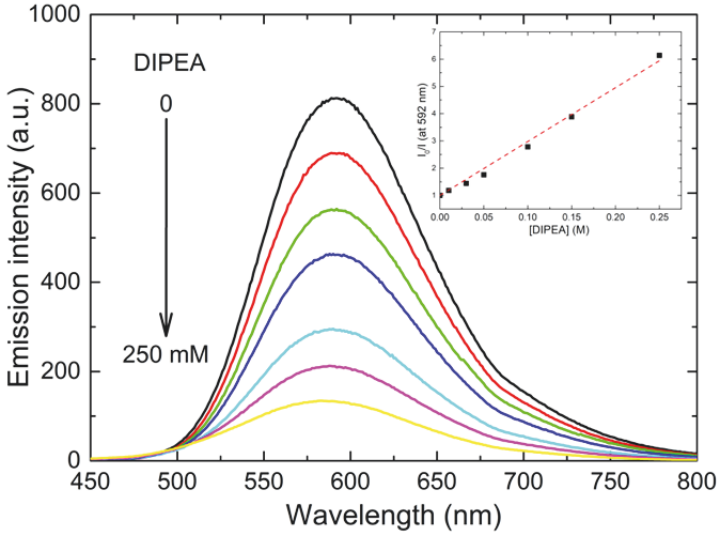

Figure 3.19 Emission spectra of a 0.2 mM $[Ir(ppy)_2(bpy)]^+$ solution in ACN/H_2O (3:7 v/v) containing 0 (black), 10 (red), 30 (green), 50 (blue), 100 (cyan), 150 (magenta), and 250 mM (yellow) DIPEA. The inset shows the linear plot (R^2 = 0.997) of the normalized emission at 592 nm versus DIPEA concentration according to the Stern-Volmer equation.

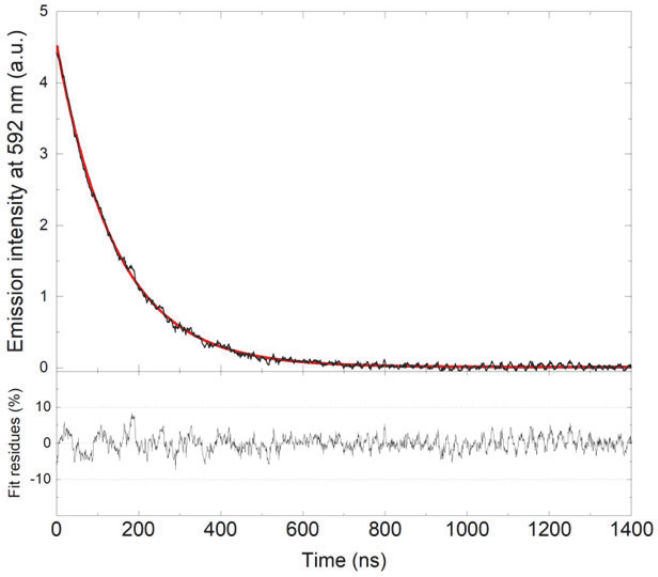

Figure 3.20 Time-resolved kinetic trace at 592 nm (black, top), monoexponential fit (red, top) and fit residues (bottom) of the $[Ir(ppy)_2(bpy)]^+$ emission after excitation at 420 nm of a 0.2 mM solution in ACN/H_2O (3:7 v/v) degassed with argon. The excited state lifetime is *ca.* 145 ns.

However, no quenching was detected with Fe-*p*-TMA (Table 3.3). As we demonstrated before,[112] Fe-*p*-TMA has a non-negligible absorbance at λ_{ex} = 420 nm (Figure 3.21) so that introducing an attenuation factor for emission quenching measurements (Figure 3.20) is necessary. The excitation attenuation due to the absorption of Fe-*p*-TMA at the irradiation wavelength then leads to a lower excitation of $[Ir(ppy)_2(bpy)]^+$: the measured intensity is thus

lower than the real emission. Considering a mean solution thickness of 5 mm and taking into account absorbance values at each Fe-*p*-TMA concentration, the predicted emission intensity as a function of [Fe-*p*-TMA] (Inset, Figure 3.21) perfectly matches the experimentally measured emission intensity. One can thus conclude that the emission decrease is not due to a quenching reaction between $^{*}[Ir(ppy)_2(bpy)]^{+}$ and Fe-*p*-TMA but is in fact due to optical attenuation.

Table 3.3 Rate constant of the emission quenching of $^{*}[Ir(ppy)_2(bpy)]^{+}$ (0.2 mM in ACN/H_2O (3:7 v/v)) by TEA, TEOA and DIPEA sacrificial electron donors and by Fe-*p*-TMA catalyst.

	TEA	TEOA	DIPEA	Fe-*p*-TMA
K_q ($M^{-1}s^{-1}$)	$(5.78 \pm 0.14) \times 10^6$	$(4.55 \pm 0.18) \times 10^6$	$(1.36 \pm 0.04) \times 10^8$	0

These results first revealed that the excited sensitizer is quenched via a reductive pathway from the sacrificial amine and is thus reduced into the anionic form $[Ir(ppy)_2(bpy)]^{\bullet -}$ (see below), as reported before.[146] Second, the quenching rate constants are well below the diffusion limit, also as already reported[147] so that the initial electron transfer steps leading to the catalytic active species (Fe^0) are of low efficiency. It is important to note that these characteristics are in contrast with what we observed before with $Ir(ppy)_3$ in organic solvent. In that latter case, the quenching process goes through an oxidative electron transfer with the catalyst at a rate constant close to the diffusion limit.[116]

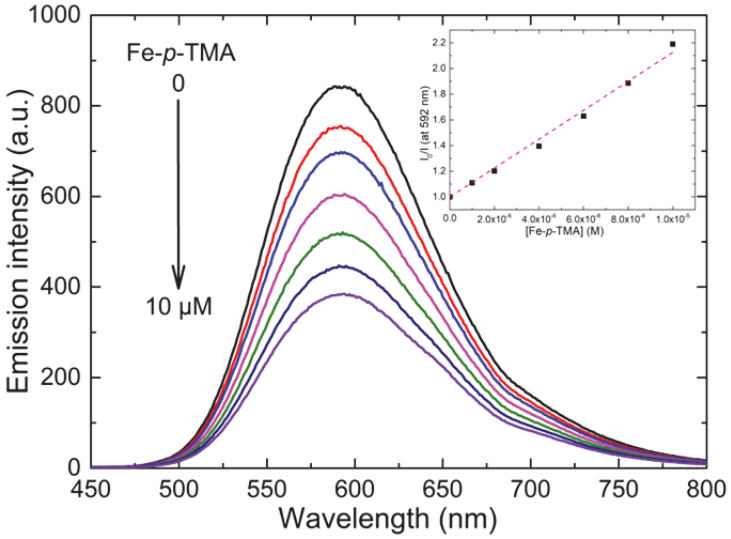

Figure 3.20 Emission spectra of a 0.2 mM $[Ir(ppy)_2(bpy)]^{+}$ solution in ACN/H_2O (3:7 v/v) containing 0 (black), 1 (red), 2 (blue), 4 (magenta), 6 (olive), 8 (navy), and 10 mM (violet) Fe-*p*-TMA. The inset shows the linear plot ($R^2 = 0.980$) of the normalized emission at 592 nm versus Fe-*p*-TMA concentration according to the Stern-Volmer equation.

On the other hand, the values for the reduction/oxidation potentials for the investigated species of $[Ir(ppy)_2(bpy)]^+$ found in literature and the measured values are summarized Figure 3.22.[147c] As we can see, the oxidation potential for the process of $^*[Ir(ppy)_2(bpy)]^+$ to $[Ir(ppy)_2(bpy)]^{2+}$ is -0.85 V *vs.* SCE and the Fe-*p*-TMA displays the third reduction event at *ca.* -1.50 V *vs.* SCE. Evidently, the oxidative quenching by direct electron transfer from the excited state of PS to CAT is highly thermodynamically unfavorable, which is also in line with the emission quenching experiments. Therefore in the initial stage, the excited state of the iridium PS should be reductively quenched by SD to give a reduced species $[Ir(ppy)_2(bpy)]$ (E^0 = -1.42 V *vs.* SCE for $[Ir(ppy)_2(bpy)]^+$/ $[Ir(ppy)_2(bpy)]$), which is much more capable to reduce Fe^{III} into Fe^0 active site. Besides, the concentration of SD is always much higher than that of CAT, which is also in favor of a reductive quenching pathway.

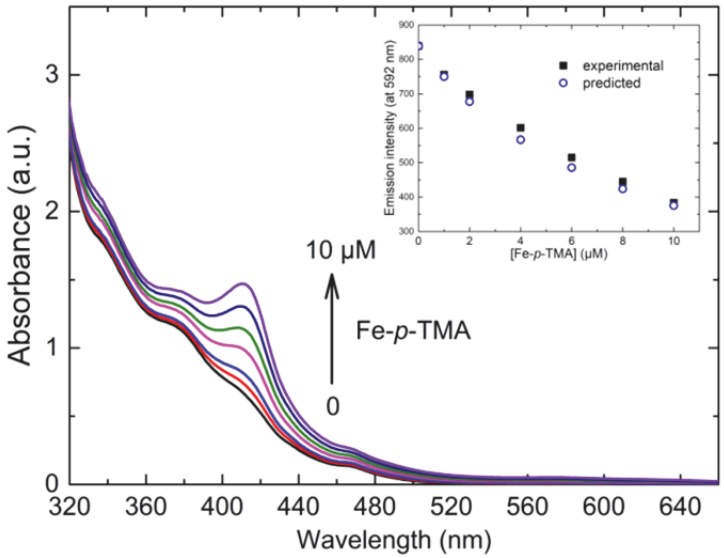

Figure 3.21 Absorption of a 0.2 mM $[Ir(ppy)_2(bpy)]^+$ solution in ACN/H_2O (3:7 v/v) containing 0(black), 1 (red), 2 (blue), 4 (magenta), 6 (olive), 8 (navy), and 10 µM (violet) Fe-*p*-TMA showing the typical Soret band of the porphyrin growing around 415 nm. Inset: measured (black squares) and predicted (blue circles) emission intensity at 592 nm of an ACN/H_2O (3:7 v/v) solution containing 0.2 mM $Ir(ppy)_2(bpy)^+$ as a function of the concentration of Fe-*p*-TMA.

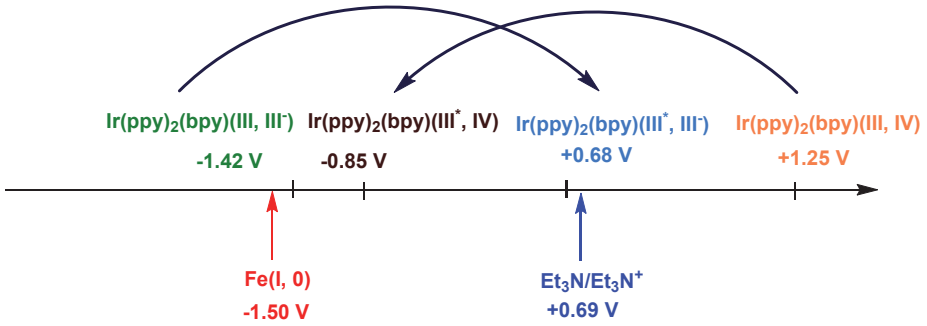

Figure 3.22 Reduction/oxidation potentials for the investigated system in V *vs.* SCE.

Interestingly, even if the quenching rate constant is ca. 25 times faster for DIPEA than for TEA, TON with DIPEA remains lower than for TEA, thus highlighting, as already noticed, the absence of simple rationalization in the choice of a particular amine as SD.[114] The choice of a suitable SD is difficult to rationalize. For instance, Bernhard *et al.* described the superiority of TEA over TEOA for their photocatalytic system for stability reasons.[148] Chang *et al.* observed an improved efficiency with TEA rather than TEOA,[149] whereas Zou *et al.* reported the improved reductive quenching rates with TEOA *vs.* TEA.[150] The conditions are nevertheless rather different from one experiment to another, depending on the requisites of each property (solubility, activity of the catalysts…) in the considered catalytic systems. There is therefore no clear-cut consensus, TEA and TEOA having very similar properties. Conclusively, picking an organic amine SD over another depends on many parameters, including the property of the reaction components and the overall reaction medium.

3.3.4 Stability of the photochemical system

When employing the neutral $Ir(ppy)_3$ as sensitizer in organic media, we previously determined that CO was a key intermediate product in the CO_2 reduction process, and that the $Fe^{II}CO$ adduct species was further reduced in a multi-electron multi-proton process to afford CH_4.[116] Without any addition of acid, residual water and/or SD protonated form could act as the proton source. Addition of a weak acid such as trifluoroethanol (TFE) accelerates the reaction and as shown in Figure 3.23, optimized conditions consisting of the addition of 0.5 M TFE allow the system to reach, after 102 h irradiation, 195 TON in CH_4, with a selectivity of 81% (also see in Table 3.3). Using larger acid concentration or a stronger acid may lead to selectivity decrease and larger amount of hydrogen.

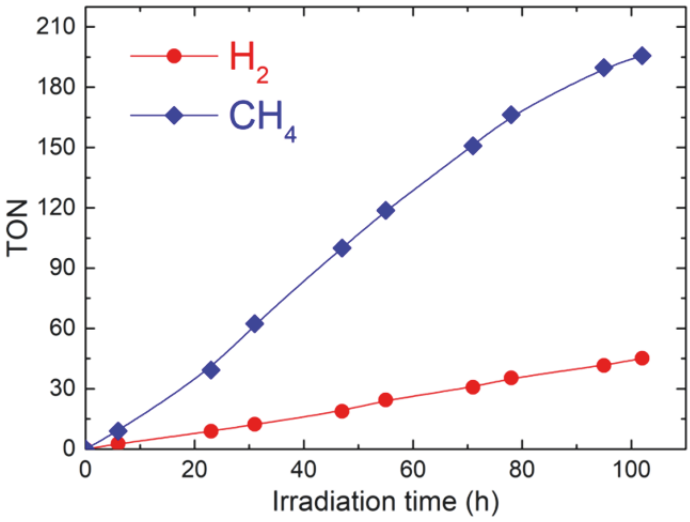

Figure 3.23 Gaseous products formation (turnover numbers) upon visible-light irradiation (> 420 nm) of a CO-saturated ACN solution containing 2 μM Fe-*p*-TMA catalyst, 0.2 mM $Ir(ppy)_3$ sensitizer, 0.05 M TEA as sacrificial electron donor, and 0.5 M TFE as proton source.

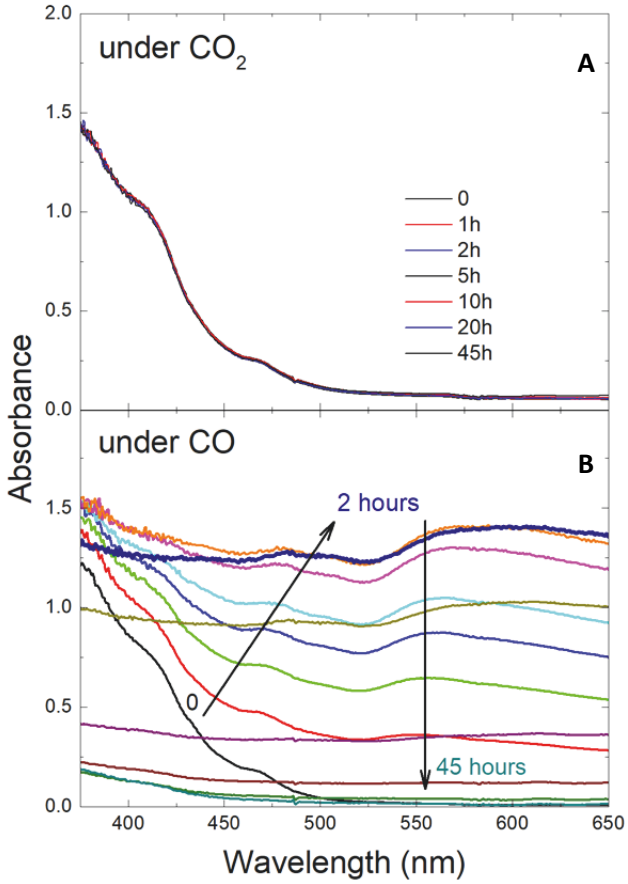

Figure 3.24 Spectral evolution upon visible-light irradiation (> 420 nm) for a CO_2-saturated (A) and CO-saturated (B) ACN/H_2O (3:7 v/v) solution containing 2 μM Fe-*p*-TMA as catalyst, 0.2 mM $[Ir(ppy)_2(bpy)]^+$ as sensitizer, and 0.05 M TEA as electron donor.

We further transposed this approach to the aqueous system containing $[Ir(ppy)_2(bpy)]^+$ as photosensitizer and performed irradiation in CO saturated solutions. We observed in this case a different behavior. After a few tens of minutes of visible-light irradiation, the color of the solution drastically faded and a precipitate finally appeared, as showed in Figure 3.24, whereas no change at all was observed during a similar experiment conducted under CO_2 atmosphere. The observed precipitation could be ascribed to a structural modification of the iridium sensitizer giving an insoluble form. Otherwise, it has been reported[151] that cationic $[Ir(ppy)_2L_2]^+$ complexes (L being ancillary ligand such as pyridine, acetonitrile) can bind to CO and/or to acetonitrile and optical signatures of these complexes give peaks close to 450 and 485 nm, respectively, the latter being observable in our experiment (Figure 3.24).

We thus hypothesize that electron transfer from the sacrificial electron donor to the excited sensitizer induces the loss of the bpy ligand[148a] and its replacement by CO and/or ACN ligands, as illustrated in Scheme 3.1. To confirm this hypothesis, we conducted infrared spectroscopy measurement (Figure 3.25), which revealed two vibrations at ca. 2255 and 2295 cm^{-1}, which closely match with CO vibration in $Ir(CO)_x$ complexes.[151-152]

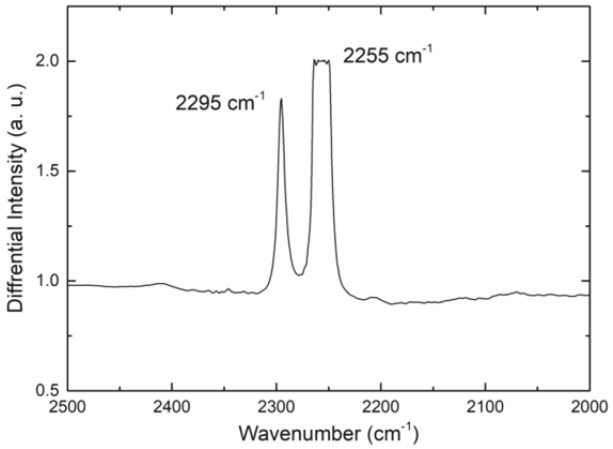

Figure 3.25 Differential infrared spectrum of 1mM $[Ir(ppy)_2(bpy)]^+$ and 0.05 M TEA in ACN/H_2O (3:7 v/v) under CO atmosphere after 60 min irradiation (> 420 nm).

At the same time, cyclic voltammetry (Figure 3.26) also revealed the apparition of an irreversible reduction wave at ca. -2 V *vs.* SCE under CO, as previously observed.[151] All these evidences showed the instability of bpy ligand binding to Ir center under irradiation.

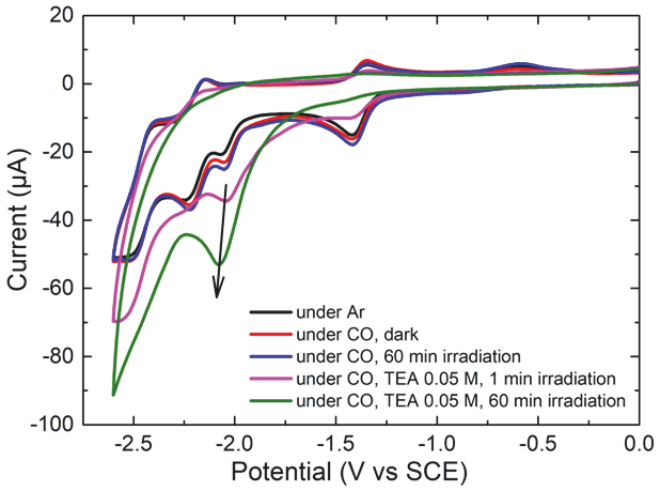

Figure 3.26 Cyclic voltammetry (ν = 0.1 Vs^{-1} in ACN, 0.5 mM $[Ir(ppy)_2(bpy)]^+$, 0.1 M $TBAPF_6$) at a 3 mm glassy carbon electrode under Ar (black), under CO in dark (red), under CO after 60 min $\lambda > 420$ nm irradiation (blue), under CO + 0.05 M TEA after 1 min (pink) and under CO + 0.05 M TEA after 60 min irradiation (green).

Finally, upon electron transfer to the $^*[Ir(ppy)_2(bpy)]^+$ sensitizer from a sacrificial reductant such as TEA, the spin density in the reduced sensitizer is predominantly located on the bpy ligand, generating a $bpy^{\bullet-}$ radical anion.[153] Such electron localization in the antibonding LUMO contributes to the poor observed photostability and favors the bpy ligand loss. Such lower stability of cationic Ir^{III} complexes compared to that of neutral cyclometalated Ir^{III} complexes (such as $Ir(ppy)_3$) could be assigned to the stronger ligand field of the C^N ligands compared to that of the N^N coordinating ligand.[146c]

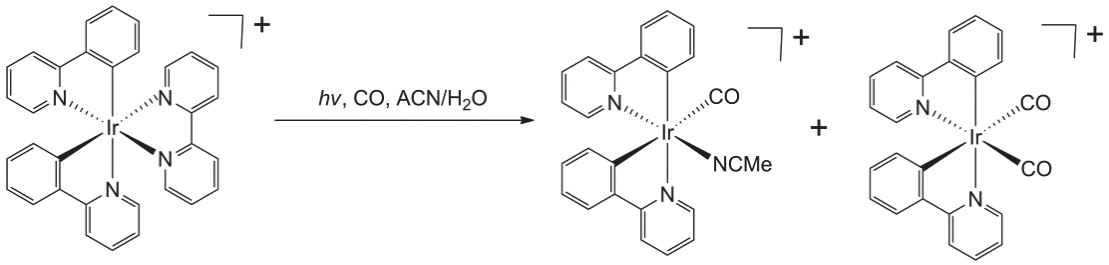

Scheme 3.1 Possible reactions leading to the decomposition of $[Ir(ppy)_2(bpy)]^+$ in the presence of CO as substrate.

3.3.5 Conclusions

Photochemical reduction of CO_2 has been achieved using an iron porphyrin as catalyst, an iridium complex $[Ir(ppy)_2bpy]^+$ as sensitizer and various amines as sacrificial electron donor. Upon visible light irradiation, CO was the main product (178 TON in optimized conditions) and a

substantial amount of CH_4 was also produced (32 TON, 10% catalytic selectivity) while H_2 was formed as a minor byproduct when acetonitrile was used as a solvent. Among the various amines employed, TEA appeared as the best choice to maximize CO_2 product formation. Remarkably, the CO_2 catalytic reduction could also be realized in aqueous conditions (acetonitrile/water 3:7 v:v). In that case, the main product was again carbon monoxide while methane was produced with selectivity up to 10% (3 TON). Efficiency of the catalytic system is hampered by the limited CO_2 solubility and most importantly by instability of the sensitizer that leads to CO ligandation and further loss of activity. Despite these limitations, this work opens the door to further studies in pure water once more stable sensitizers have been designed.

3.4 Organic dyes sensitized visible-light-driven CO_2-to-CH_4 reaction

3.4.1 Building organic dyes-based photochemical systems

As we have already shown above and also according to literatures, the popular molecular photochemical CO_2 reduction is mostly studied via a multi-component catalytic system. A typical manmade system always contains a photosensitizer and a heterogeneous or homogeneous catalyst.[154] A large majority of these studies has employed precious-metal polypyridyl ruthenium and iridium photosensitizers. These metal complexes exhibit essential characteristics, including strong absorption of visible light by means of spin-allowed metal-to-ligand charge transfer (MLCT), efficient conversion to long lifetime triplet MLCT excited (^{3}MLCT) state because of heavy atom effect, and excellent redox reversibility.[155] Their redox properties of the ground and excited states are easily tailored through ligand and metal modifications. However, both ruthenium and iridium are precious metals and amongst the rarest elements on the earth, escalating their costs and presenting concerns related to sustainability and scalability, driving the need to realize new photosensitizers incorporating non-precious metals[74, 156] or develop entirely organic succedaneums.[157] Some of these compounds (PS-1, PS-2, PS-3 and PS-4) have been discussed in the previous chapter. Other common organic sensitizers used for solar fuel conversion are Eosin Y,[158] rhodamine dyes,[159] perylene diimides[160] and carbazolyls,[161] which are excited state oxidants and operate through a reductive quenching cycle. Although a few strong

reducing organic photosensitizers exist, many do not efficiently absorb visible light.[162] Photosensitizers obviously have to exhibit both wide and strong visible light absorption ranges and appropriate redox properties. As part of efforts to design and examine new systems based solely on earth-abundant elements, we have tried to design such a new homogenous system for the photocatalytic reduction of CO_2 using highly absorbing organic dyes and an iron-porphyrin molecular catalyst.

We have already shown in Chapter 2 that Fe-*p*-TMA could convert CO_2 into CO with PP as the sensitizer. However, in this system, no CH_4 could be detected by the GC. The possible reason could be that the reduction potential of PP was too low to further reduce the Fe-CO intermediate into CH_4. As a consequence, the great challenge is to develop a new sensitizer possessing a stronger reducing power. In general, photosensitizers that possess such strong excited state reducing power are rare, in particular for pure organic systems.

To address this challenge, we have brought our interest to the work of Miyake and co-workers who developed a series of visible-light organic photosensitizers, including perylene,[163] N, N-diaryl dihydropenazines,[164] and N-aryl phenoxazines[165] that mediate electron through an oxidative quenching pathway in photoredox applications.[166] Dihydrophenazine and phenoxazine contain electro-rich chromophore motifs that form stable radical cations upon oxidation and enable them to be strong excited state reductant.[167] In the following part, we will discuss organic PSs based on the dihydrophenazine (Phen1, 5, 10-di(2-naphthyl)-5, 10-dihydrophenazine) and phenoxazine (Phen2, 3,7-di(4-biphenyl)-1-naphthalene-10-phenoxazine) motifs (Scheme 3.2) combined with Fe-*p*-TMA catalyst for CO_2 reduction.

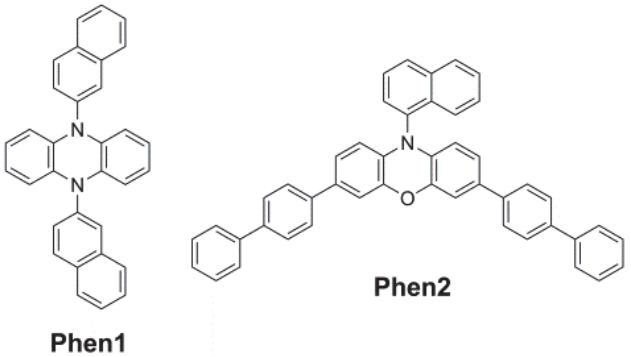

Scheme 3.2 Molecular structures of the investigated phenoxazine-based organic photosensitizers (Phen1, Phen2).

These organic chromophores exhibit photon absorption in the visible region, redox reversibility, good triplet quantum yields [*e.g.* 2% (Phen1) and 90% (Phen2)], and long triplet lifetimes [*ca.* 4.3 ± 0.5 μs (Phen1) and 480 ± 50 μs (Phen2)].[165d] In particular, Phen1 and Phen2 were specifically engineered as strong excited-state electron donors with highly negative excited state reduction potentials for oxidative quenching applications. The triplet excited state reduction potential values of Phen1 and Phen2 are $E^0(^2Phen1^{\bullet+}/^3Phen1^*)$ = -1.69 V *vs.* SCE and $E^0(^2Phen2^{\bullet+}/^3Phen2^*)$ = -1.80 V *vs.* SCE, respectively. Notably, these values closely match the $E^0(Ir(IV)/^3Ir(III)^*)$ = -1.73 V *vs.* SCE for $Ir(ppy)_3$, which was successfully employed for the photochemical reduction of CO_2 to CH_4. Given these properties, we hypothesized that Phen1 or Phen2 could directly replace $Ir(ppy)_3$ in the light-driven tandem catalysis with Fe-*p*-TMA for CO_2 reduction.

3.4.2 Photochemical CO_2 reduction experiments

As shown in Figure 3.27 (open symbols), in our typical photochemical assembly, now containing 10 μM Fe-*p*-TMA, 1 mM Phen2, and 0.1 M TEA of CO_2-saturated DMF solution under visible irradiation (> 435 nm), we found H_2, CO and CH_4 in the gas phase. DMF was used as the solvent instead of ACN because of a higher solubility of Phen2 in the former one. Wavelength higher than 435 nm of light source instead of higher than 420 nm was chosen because we hoped to make full use of Phen2 to absorb visible light and avoid the catalyst itself absorbing light energy. After 47 h reaction, CH_4 production with a TON of 8 was observed, alongside with the formation of H_2 and CO (TON of 8 and 50, respectively).

Furthermore, we found that with the addition of 0.1 M TFE as an external acid, the production of CO and CH_4 was noticeably improved (TON of 71 and 14, respectively, see in Figure 3.27, solid symbols), whereas the formation of H_2 remained almost unchanged. The presence of TFE could play a role through hydrogen bonding as shown in Figure 3.28, in lowering the activation energy of CO_2 reduction and in enabling the direct proton transfer from acid to the activated CO_2 substrate. Similar effects were reported in the literature that the introducing of TFE will greatly enhance the catalysis of CO_2 reduction.[168] They use both experimental and calculated methods to show that a proton involving step is rat-limiting for the overall catalytic cycle. The second protonation is always less favorable than the first one. The intermolecular proton transfer *via* non-

cooperative hydrogen bonds to acid in solution provides a relevant model for biological systems and homogeneous catalysts for small molecule activation.

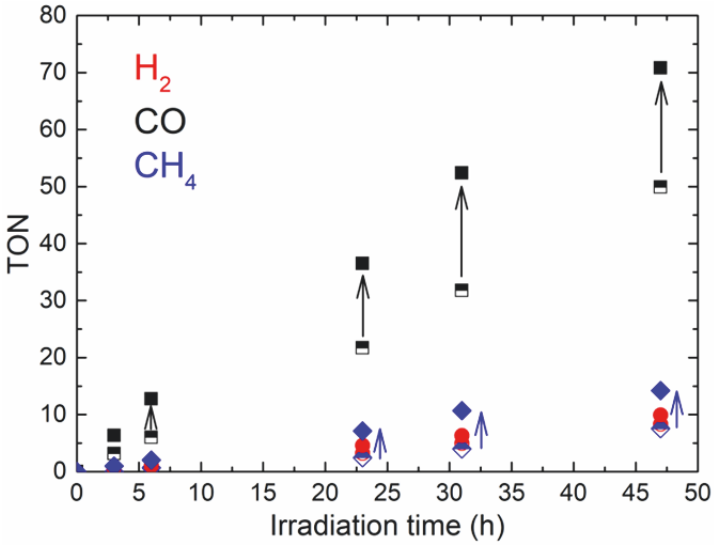

Figure 3.27 Generation of CO (black squares), H_2 (red circles) and CH_4 (blue diamonds) with time upon visible irradiation (> 435 nm) of a CO_2-saturated DMF solution containing 10 μM Fe-*p*-TMA, 1 mM Phen2 and 0.1 M TEA (open symbols); addition of 0.1 M TFE as an external acid is indicated by "filled symbols". Arrows indicate increase in product formation upon addition of an external acid.

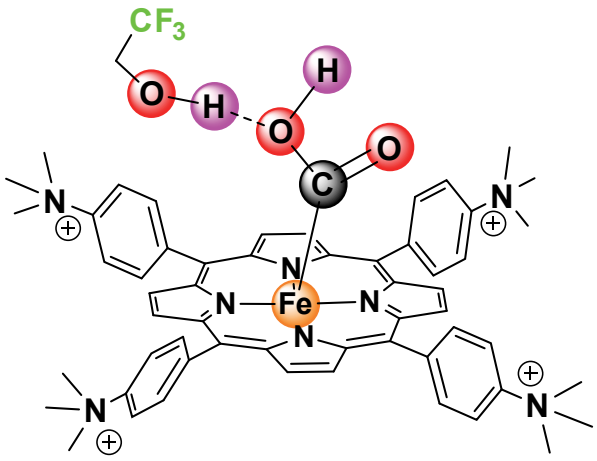

Figure 3.28 Structure of possible weak acid adduct through hydrogen bonding.

Blank experiments showed that the omission of any single reactive component (Fe-catalyst, organic sensitizer, SD, CO_2 or light) produced no CH_4. GC-MS experiments performed under a $^{13}CO_2$ atmosphere confirmed that the produced CH_4 originated from CO_2 as shown in Figure 3.29.

Moreover, long term irradiation (over 100 h) led to a TON in CH_4 of 29 and CO of 140 (Figure 3.30). The stability of the system was followed by UV-Vis absorption spectroscopy over the

entire irradiation course (Figure 3.31) and it showed no significant Fe-*p*-TMA or Phen2 degradation. It indicates that Phen2 as a PS, which is an organic analogue of $Ir(ppy)_3$ can be a good candidate in solar fuel conversion.

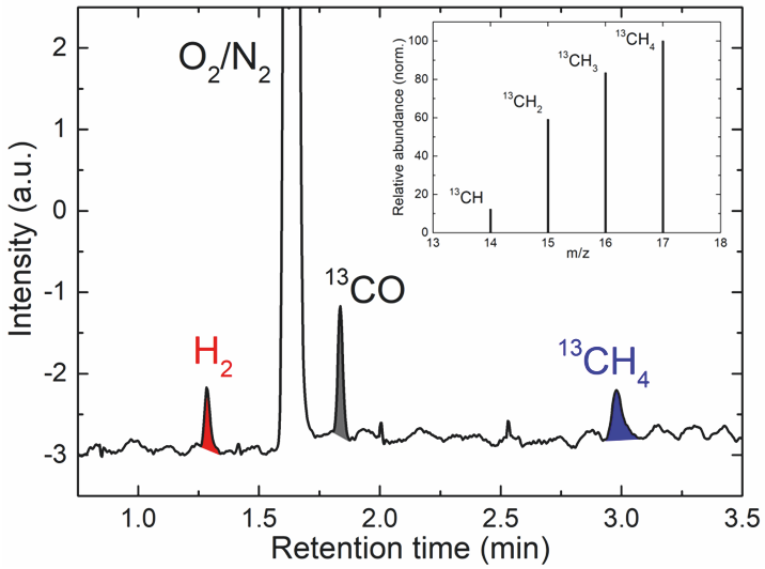

Figure 3.29 Typical gas chromatogram of the sample headspace after several hours of visible light irradiation of a solution containing 10 µM Fe-*p*-TMA, 1 mM Phen2, 0.1 M TEA and 0.1 M TFE in DMF and saturated $^{13}CO_2$. The inset shows the corresponding mass spectra of methane.

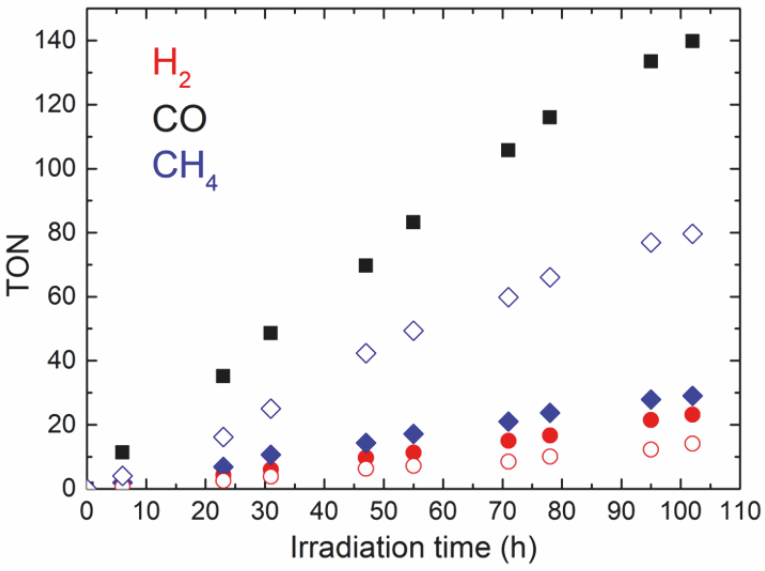

Figure 3.30 CO (black squares), H_2 (red circles) and CH_4 (blue diamonds) generation with time upon visible light irradiation (> 435 nm) of a CO_2- (filled symbols) or CO-saturated (open symbols) DMF solution containing 10 µM Fe-*p*-TMA, 1 mM Phen2, 0.1 M TEA and 0.1 M TFE.

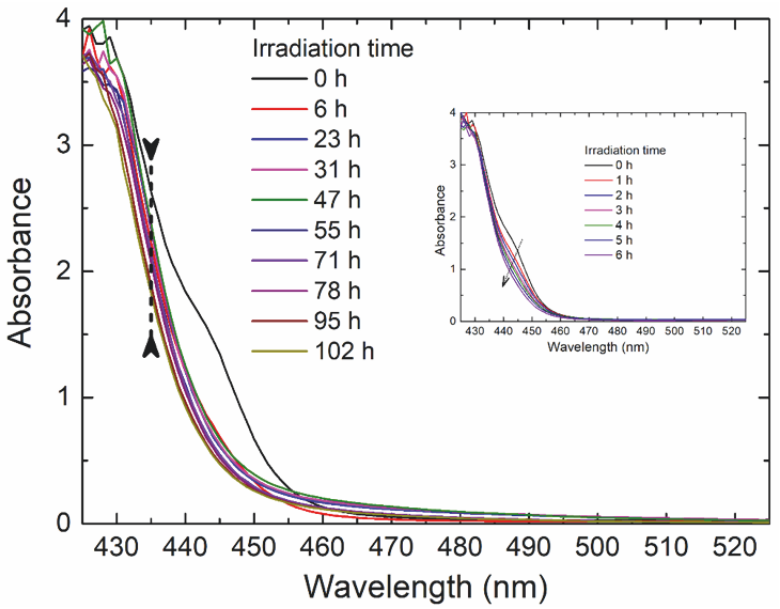

Figure 3.31 Evolution of the absorption spectrum upon visible light (> 435 nm) irradiation with time of a CO_2-saturated DMF solution containing 10 μM Fe-*p*-TMA, 1 mM Phen2, 0.1 M TEA and 0.1 M TFE. The double arrow shows the irradiation threshold (435 nm). Inset: evolution of the absorption spectrum in the first six hours of irradiation.

3.4.3 Photochemical CO reduction experiments

According to our previously demonstrated dual catalysis employing Fe-*p*-TMA and $Ir(ppy)_3$, CO could also be used as the starting substrate for CH_4 production.[116] The rationale was that CO is an intermediary species toward the highly reduced CH_4 product. In Figure 3.32, using Phen2 as a photosensitizer in a CO-saturated solution, we observed the formation of CH_4 with a TON of 9 and a selectivity of 30%, while H_2 was formed as the major product. The addition of 0.1 M TFE, however, significantly boosted CH_4 formation with a TON of 45 and 87% selectivity upon 24 h of irradiation. The nature of the SD had only minor effects on CH_4 production, *e.g.* similar results were obtained with TEA, DIPEA and BIH, while TEOA gave lower CH_4 production. GC/MS experiments performed under a ^{13}CO atmosphere again confirmed that the produced CH_4 was originated from CO (Figure 3.33).

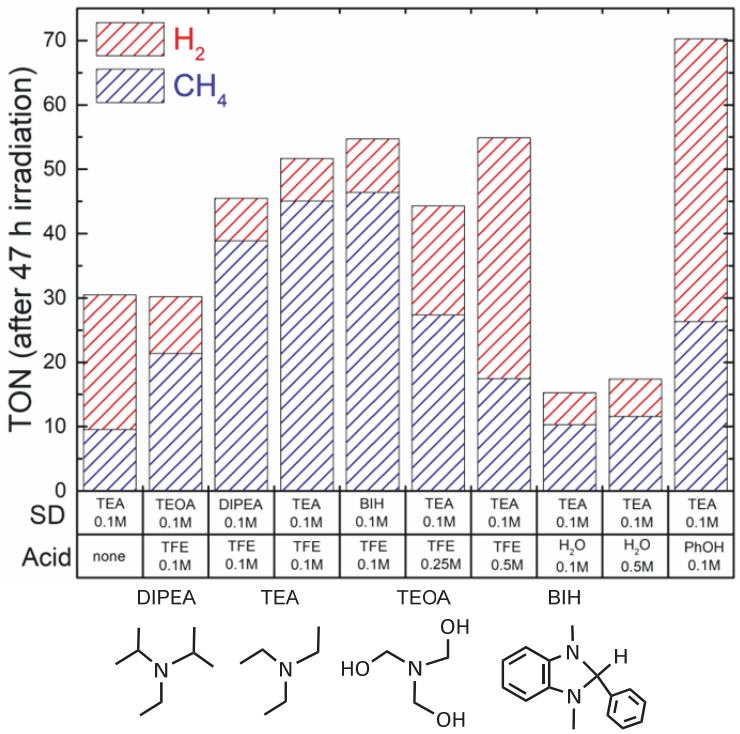

Figure 3.32 TON in H_2 (red) and CH_4 (blue) measured after 47 h of visible light irradiation (> 435 nm) of a CO-saturated DMF solution containing 10 µM Fe-*p*-TMA, 1 mM Phen2, in the presence of various SDs and added acids.

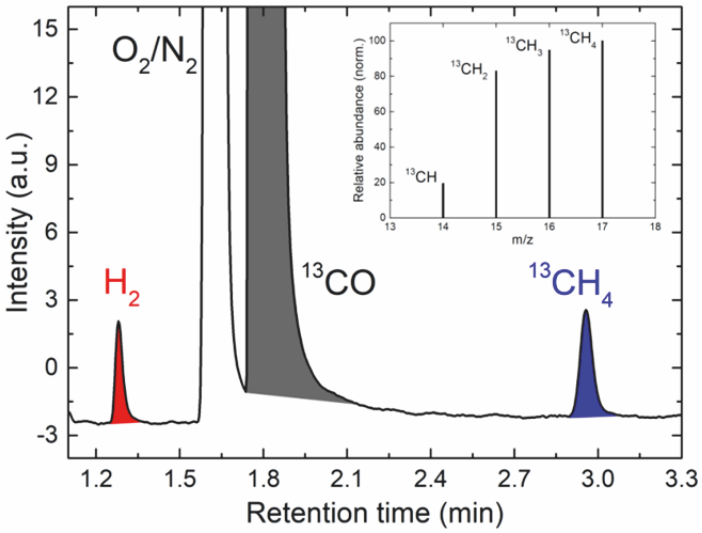

Figure 3.33 Typical gas chromatogram of the sample headspace after several hours of visible-light irradiation of a solution containing 10 µM Fe-*p*-TMA, 1 mM Phen2, 0.1 M TEA and 0.1 M TFE in DMF and saturated labelled ^{13}CO. The inset shows the corresponding mass spectra of methane.

Table 3.4 TON of gaseous products measured after 47 h of visible light (> 435 nm) irradiation of DMF solution containing 10 μM Fe-*p*-TMA, 1 mM Phen2 and various components (SD, CO_2/CO, acid).

				TON		
entry	Gas	SD (M)	Acid (M)	H_2	CO	CH_4
1	CO_2	TEA (0.1)	none	8	50	8
2	CO_2	TEA (0.1)	TFE (0.1)	10	71	14
3	**CO_2**	**TEA (0.1)**	**TFE (0.1)**	**23[a]**	**140[a]**	**29[a]**
4	CO	TEA (0.1)	none	21	-	10
5	CO	TEA (0.1)	TFE (0.1)	7	-	45
6	CO	TEOA (0.1)	TFE (0.1)	9	-	21
7	CO	DIPEA (0.1)	TFE (0.1)	7	-	39
8	CO	BIH (0.1)	TFE (0.1)	8	-	46
9	**CO**	**TEA (0.1)**	**TFE (0.1)**	**14[a]**	-	**80[a]**
10	CO	TEA (0.1)	TFE (0.25)	17	-	27
11	CO	TEA (0.1)	TFE (0.5)	37	-	17
12	CO	TEA (0.1)	H_2O (0.1)	5	-	10
13	CO	TEA (0.1)	H_2O (0.5)	6	-	12
14	CO	TEA (0.1)	PhOH (0.1)	44	-	26

a. after 102 h of light irradiation.

On contrary, the nature of the acid had a marked influence on the CH_4 yield (Figure 3.32). Water, being a weaker acid than TFE, resulted in a much lower amount of CH_4 even with concentration up to 0.5 M. Conversely, the addition of 0.1 M phenol, which is a stronger proton donor than TFE, resulted in forming H_2 as a major product and a decrease in CH_4 production. Further, the use of higher concentrations of TFE (greater than 0.1 M) reversed the catalytic selectivity toward H_2 formation. Thus, it showed that 0.1 M TFE provided proper acidity and concentration to maximize CH_4 production and suppress H_2 evolution. By employing 0.1 M TFE

in a CO-saturated DMF solution irradiated for 102 h, we were able to produce CH_4 in 80 TON and 85% selectivity. As a comparison, the noble metal $Ir(ppy)_3$ catalyzed CH_4 production in 195 TON and 81 % selectivity under similar reaction conditions (with 0.5 M TFE at optimized conditions). It is important to note that the Fe catalyst concentration in the $Ir(ppy)_3$ case was 5 times less as compared to this study, and thus the absolute mol number of methane produced by the catalytic system comprising Fe-*p*-TMA + Phen2 is in fact 2 times larger. Table 3.4 below summarizes key results from Figures 3.27, 3.30 and 3.32.

Notably, replacing Phen2 by the less reducing Phen1 led to the exclusive formation of CO (TON 60, selectivity 90%) and H_2 (TON 6) upon irradiation of a CO_2-saturated solution. The lower energy conversion efficiency may be due to the much lower visible light extinction coefficient and faster triplet life time of Phen1 compared with Phen2. On the other hand, irradiation of a CO-saturated solution with Phen1 only furnished H_2 as detectable product. These results indicate that the slightly lower reducing ability of Phen1 led to the inability to further reduce CO.

3.4.4 Electron transfer mechanism in this system

To investigate the electron transfer mechanism in this system, emission quenching experiments were conducted upon exciting the Phen2 sensitizer at 435 nm in the presence of increasing concentration of TEA or Fe-*p*-TMA. As shown in Figure 3.34, there is no noticeable quenching when adding TEA with the concentration ranging from 0 to 200 mM. While with increasing concentration of Fe-*p*-TMA from 0 to 10 μM, it shows very efficient quenching (Figure 3.35). Analysis of emission quenching using the Stern-Volmer analysis and the excited-state lifetime that was measured by time-resolved laser kinetics (443 ± 18 μs, Figure 3.36) lead to a quenching rate constant of $(1.60 \pm 0.07) \times 10^8\ M^{-1}s^{-1}$, which is a second order rate constant. There results indicated that electron transfer in this system occurs through an oxidative quenching pathway, which is also very similar to what has been obtained when $Ir(ppy)_3$ was used as the SD.

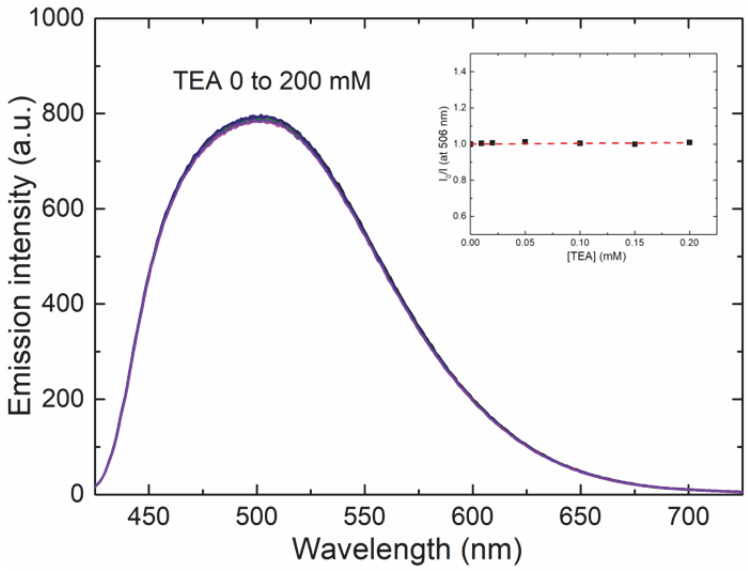

Figure 3.34 Emission spectra of a 0.2 mM Phen2 DMF solution containing 0 (black), 10 (red), 20 (blue), 50 (magenta), 100 (olive), 150 (navy) and 200 (violet) mM TEA. Inset: linear plot of the normalized emission at 506 nm versus TEA concentration according to the Stern-Volmer equation.

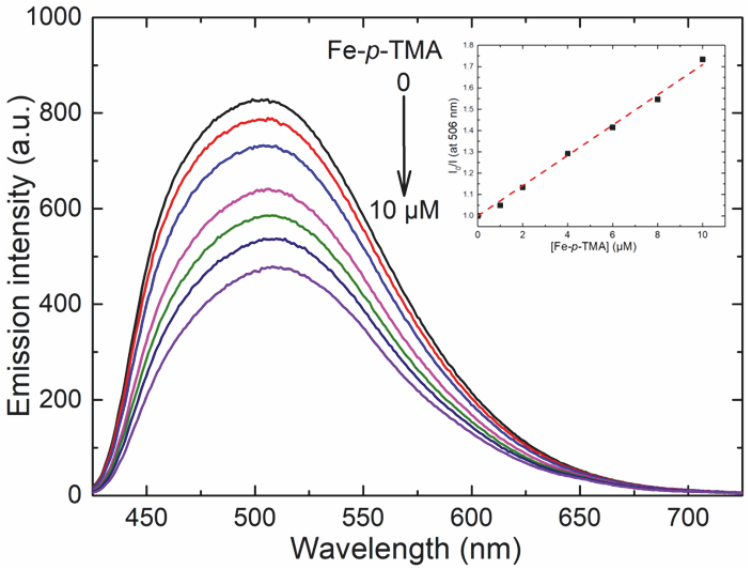

Figure 3.35 Emission spectra of a 0.2 mM Phen2 DMF solution containing 0 (black), 1 (red), 2 (blue), 4 (magenta), 6 (olive), 8 (navy) and 10 (violet) µM Fe-*p*-TMA. Inset: linear plot (R^2 = 0.994) of the normalized emission at 506 nm versus Fe-*p*-TMA concentration according to the Stern-Volmer equation.

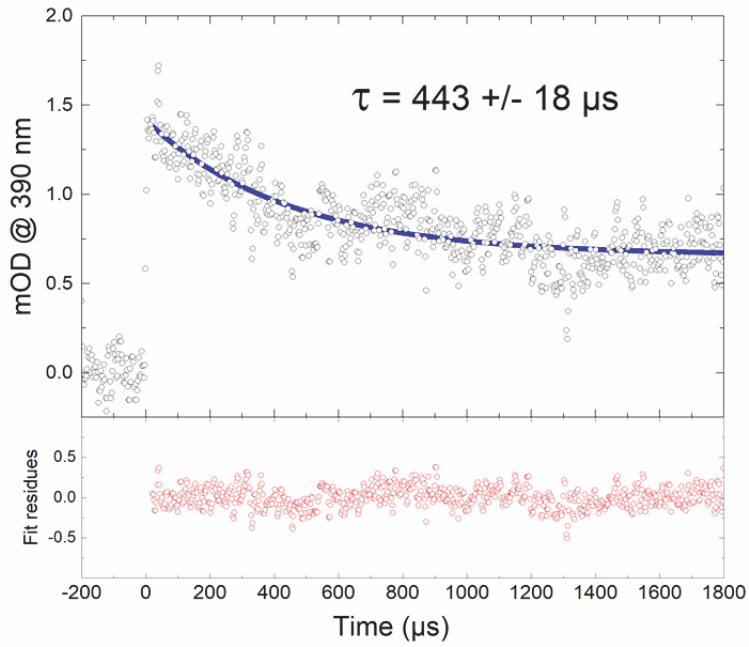

Figure 3.36 Time-resolved kinetic trace at 390 nm (black open circles, top), monoexponential fit (blue line, top) and fit residues (red open circles, bottom) of the Phen2 excited state after excitation at 420 nm of a 5 µM solution in DMF degassed with argon. The corresponding excited state lifetime is ca. 443 ± 18 µs, in accordance with previously reported value.[155] Low concentration and low excitation energy were used to limit triplet-triplet annihilation (TTA).

Formation of the key Fe^0 intermediate is considered to be one of the essential processes in the mechanism for the electro- and photochemical CO_2 reduction catalyzed by Fe porphyrin.[96, 134, 169] It is already known that the oxidation potential for the oxidation of $^3Phen2^*$ to $^2Phen2^{\bullet+}$ is -1.80 V *vs.* SCE,[165d] which is more negative than all the redox couples related to the Fe porphyrin (Fe^{III}/Fe^{II}, Fe^{II}/Fe^{I} and Fe^{I}/Fe^{0}).[100c] The oxidative quenching by direct electron transfer from the excited state of the Phen2 photosensitizer to the Fe catalyst is thermodynamically favorable, thus allowing the generation of potential catalytically active Fe^{II}, Fe^{I}, and Fe^0 species upon light irradiation. Interestingly, this experiment probes the singlet excited-state of Phen2 (which has a 90% triplet quantum yield), and some reactivity likely occurs from the triplet excited-state.

Considering that the formation of a CH_4 molecule requires the transfer of 8 protons, we conducted GC-MS experiments with the addition of labeled CF_3CD_2OD or D_2O. As shown in Figure 3.37 and 3.38, MS results in these two parallel experiments are very similar. CD_4 is not the main component and products are made up of CD_4, CD_3H, CD_2H_2, CDH_3 and CH_4, which indicates that the proton source is probably not unique and that proton exchange occurs in the system between TEA, TFE and even traces of water in the solvent. It is also in line with the fact

that even without the presence of TFE, CH_4 can also be observed. However, it is still difficult to identify the proton source. More studies are needed to figure out the mechanism of this iron-catalyzed photochemical reaction.

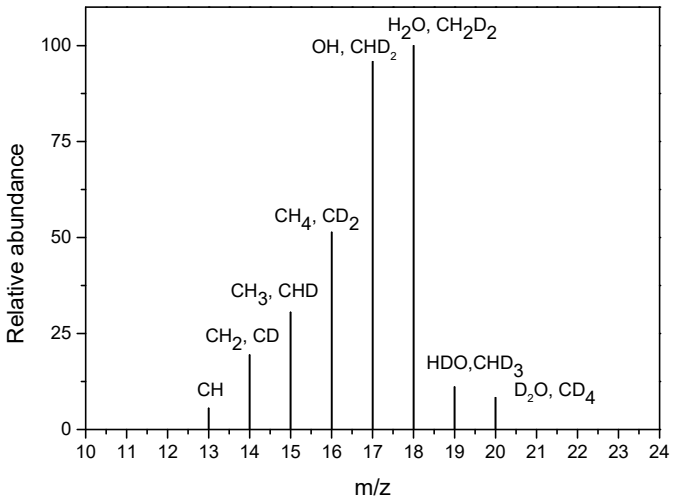

Figure 3.37 Typical GC-MS experiment of the sample headspace after several hours of visible light irradiation of a solution containing 10 μM Fe-*p*-TMA, 1 mM Phen2, 0.1 M TEA and 0.1 M CF_3CD_2OD in DMF and saturated CO_2 solution.

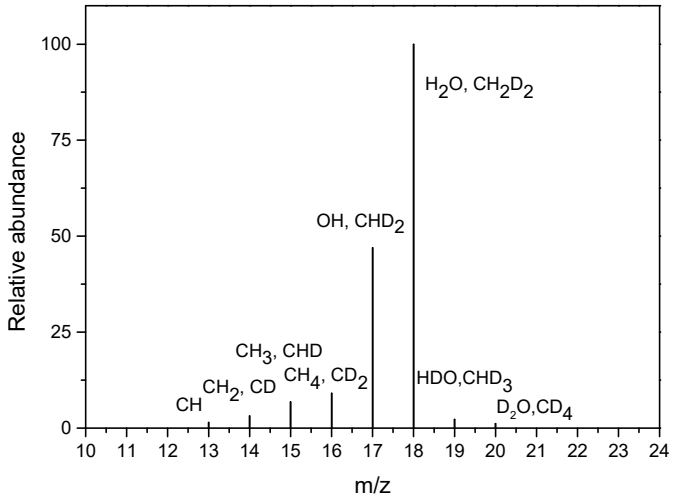

Figure 3.38 Typical GC-MS experiment of the sample headspace after several hours of visible light irradiation of a solution containing 10 μM Fe-*p*-TMA, 1 mM Phen2, 0.1 M TEA and 0.1 M D_2O in DMF and saturated CO_2 solution.

Based on the above analysis, Scheme 3.3 highlights our proposed mechanism. We suggest that CO_2 first complexes to the triply-reduced Fe^0 species (in the form of $Fe^{I}CO_2^{\bullet-}$), which upon protonation[104] and elimination of water, generates a $Fe^{II}CO$ intermediate. We note that the electron-rich Fe^0 species can react with $2H^+$ to form Fe^{II} and the undesired H_2 as byproduct. The

$Fe^{II}CO$ intermediate can eliminate the CO product upon proposed $1e^-$ reduction and alternatively participate in further $6H^+/6e^-$ reduction to produce the ultimate CH_4. Notably, the $^2Phen2^{\bullet+}/^3Phen2^*$ redox couple fulfills the crucial role of providing highly reducing electrons to enable subsequent multi-electron and-proton transfer processes that convert CO to CH_4. After transferring an electron, the oxidized $Phen2^{\bullet+}$ species is reduced by the SD (*e.g.* TEA) to regenerate a neutral Phen2 molecule.

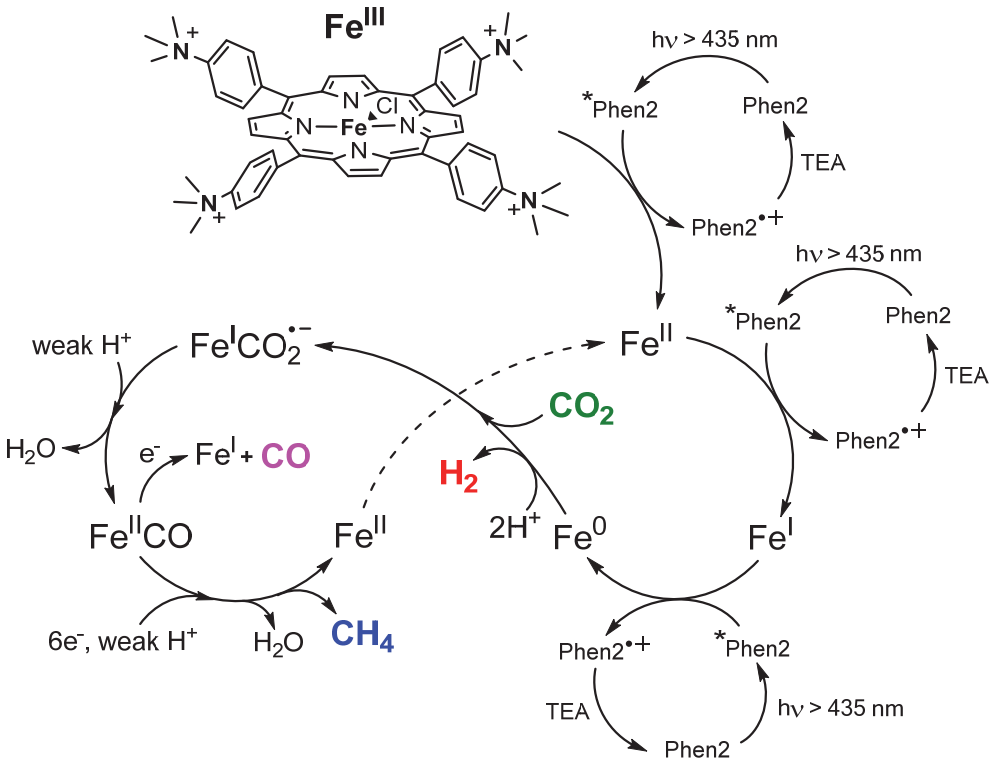

Scheme 3.3 Proposed mechanism for the $8e^-/8H^+$ reduction of CO_2 to CH_4 by tandem catalysis of Phen2 and Fe-*p*-TMA.

3.4.5 Conclusions

In conclusion, we have shown that the visible-light-driven $8e^-/8H^+$ reduction of CO_2 to CH_4 using an organic phenoxazine-based photosensitizer (Phen2) and an earth-abundant iron porphyrin catalyst (Fe-*p*-TMA) at ambient conditions is possible. In a CO_2-saturated DMF solution, CO (TON of 140) and CH_4 (TON of 29) were produced after 102 h of light irradiation; whereas in a CO-saturated solution, CH_4 was produced with TON up to 80 and a selectivity of

85%. This work is expected to advance the field of photochemical CO_2 reduction and contribute to the mechanistic understanding of multi-electron and -proton transfer processes in CO_2 reduction. Future development will include in-depth mechanistic studies and achieve similar catalysis in aqueous conditions.[112]

3.5 Sub-conclusion and sub-perspectives for photocatalytic CO_2-to-CH_4 conversion

In this chapter, we discussed the photochemical reduction of CO_2 into both CO and CH_4 using an iron porphyrin complex combined with noble metal complexes or organic dye as photosensitizer, and different kinds of organic amines as sacrificial electron donor. These catalytic systems are not only efficient, but also can keep stable for nearly one week in the present conditions. Our study demonstrates the possibility of designing and tailoring molecular metal porphyrin complex to promote homogeneous photochemical catalysis of CO_2 reduction. According to the literature, besides Fe-porphyrin, Cr-, Mn-, Co-, Ni-, Pd-, Cu-, Zn- and Ga-porphyrin complexes were also reported for molecular catalysis of CO_2 reduction.[126, 170] We have done preliminary experiments (not described in this manuscript) where Fe was replaced by Co or Cu as the porphyrin metal center, and the photochemical CO_2 reduction could still process. Both CO and CH_4 have been detected as products with these alternative catalysts. However, catalytic efficiency and selectivity were poorer than Fe-porphyrin. It thus seems that both metal center and porphyrin ligand indeed strongly affect the process. For a detailed investigation of the mechanism, more work needs to be conducted and the support of theoretical calculations is also desirable.

Chapter 4 Conclusions and Perspectives

4.1 General conclusions

In this thesis, the main objective was to design a highly efficient, selective and stable molecular photochemical CO_2 reduction process using visible light as the only energy input. The catalytic system is made up of multi-components, *i.e.* an iron porphyrin complex as the catalytic molecular center, an organic amine as the sacrificial electron donor and a photosensitizer for absorbing visible light energy and transferring it to the catalytic center. The presented results describe the molecular photocatalytic reduction of CO_2 in several different systems, including non-sensitized CO_2-to-CO conversion, purpurin sensitized CO_2-to-CO conversion in water solution, iridium complex sensitized CO_2-to-CH_4 conversion, iridium complex sensitized CO_2-to-CH_4 conversion in aqueous solution and organic dye sensitized CO_2-to-CH_4 conversion. The results could be summarized as follows.

1. Photochemical catalytic CO_2 reduction was studied by choosing Fe-porphyrin complexes as catalysts due to their unique physicochemical properties but also because they were proved, in our team, to be highly efficient molecular catalysts for the electrochemical CO_2 reduction. With the introduction of four trimethylammonio groups on the para positon of their phenyl rings, the photochemical reduction of CO_2 to CO, even without any additional photosensitizer, has been achieved under visible light. In this configuration, the porphyrin catalyst both acts as a visible light harvester and as the catalytic active center. Irradiation does not lead to catalyst photodegradation and the competitive hydride formation pathway previously observed with other porphyrin derivatives is avoided. Thanks to the stabilizing role of the four positively charged groups, the catalyst is highly selective and robust, generating pure CO from CO_2 with a 100% selectivity, a total TON of 101 and no loss of activity over 2.5 days, but at a moderate rate.

2. As natural photosynthesis approached by plants and other organisms is realized in aqueous conditions, it is of great significance to conduct the “artificial” photochemical CO_2 reduction in similar media, making the process even much cheaper and more environmentally friendly. For this purpose, we used the same earth abundant metal based molecular catalyst and choose a water soluble organic and very common dye, *i.e.* purpurin, as the photosensitizer. The photochemical reaction were

conducted in aqueous solutions (acetonitrile:water 1:9 v:v) under visible light irradiation. CO was produced with a catalytic selectivity of 95% and turnover number up to 120 after two days. Catalysis is ultimately limited by progressive sensitizer photodegradation, but it could be restarted by adding fresh sensitizer. Photochemical CO_2 reduction in water-containing system still remains rare in literatures. This work is a good example of developing meaningful efficient CO_2 photocatalysis in water.

3. Photochemical CO_2 reduction process was also studied using a noble metal photosensitizer, *i.e.* $Ir(ppy)_3$. As the excited state of $Ir(ppy)_3$ is a strong reductant, which may further reduce the Fe-CO intermediate, CO was found to be the main products while a certain amount of CH_4 was also produced. Interestingly, CO could also be the substrate for photochemical CH_4 production, which indicates that CO is an intermediate in the full CO_2-to-CH_4 cycle. Under optimized conditions, the TON of the system for CO_2-to-CH_4 conversion reaches 367 for CO, 79 for CH_4 and 26 for H_2 in 102 h, with the corresponding catalytic selectivity of 78%, 17% and 5%, respectively. The TON for CO-to-CH_4 conversion is 159 for CH_4 and 34 for H_2, with the corresponding catalytic selectivity of 82% and 18%. Unfortunately, we still failed to detect possible intermediates, such as HCHO or CH_3OH, most probably due to their very low instantaneous concentrations and their short lifetimes during the process. An intense work is necessary to better understand the mechanism. This example was the first reported molecular photocatalyst for $8e^-/8H^+$ reduction of CO_2 into methane. It could be beneficial to develop CO_2-to-CH_4 conversion at the surface of semiconductors since it may also open new research strategies for molecular catalysis of multi-electron/proton reduction of CO_2.

4. CO_2 reduction in pure water solution is always much more attractive than in organic solvent. $Ir(ppy)_2(bpy)PF_6$ was introduced instead of $Ir(ppy)_3$ as the photosensitizer in an analogous system for CO_2 reduction in aqueous solution as solvent. To make a comparison with the former system, experiments were conducted in acetonitrile first. Upon visible light irradiation, CO was the main reduction product (TON of 178 in optimized conditions) and a substantial amount of CH_4 was also produced (TON of 32, 10% catalytic selectivity) while H_2 was formed as a minor byproduct when acetonitrile was used as a solvent. Among the various amines employed, TEA appeared as the best choice to maximize CO_2 reduction products. Remarkably, the process could also be realized in aqueous conditions (acetonitrile/water 3:7 v:v). In this case, the main product was still carbon monoxide while methane was produced with selectivity up to 10% (TON of 3). Efficiency of the catalytic system is hampered by the limited CO_2 solubility and most importantly by instability of the

sensitizer that leads to CO ligandation and further loss of activity. Despite these limitations, this work opens a door to further studies in (ultimately pure) water once more stable sensitizers will be designed.

5. It is also of great significance too is to find cheaper organic dyes instead of the noble iridium complexes used as sensitizer. In this purpose, a phenoxazine-based organic photosensitizer, *i.e.* Phen2, was demonstrated to help catalyzing the $8e^-/8H^+$ visible-light-driven reduction of CO_2 to CH_4. It was the first noble metal free molecular photochemical system for CO_2-to-CH_4 conversion in ambient conditions. In a CO_2-saturated DMF solution, CO (TON of 140) and CH_4 (TON of 29) were produced after 102 h of light irradiation, whereas in a CO-saturated solution, CH_4 was produced with TON up to 80 and a selectivity of 85% and a quantum yield of *ca.* 0.4%. This work is expected to advance the field of photochemical CO_2 reduction and contribute to the mechanistic understanding of multi-electron and multi-proton transfer processes in CO_2 reduction.

Generally, this thesis confirmed the great specificity of the modified iron porphyrin with four strong electron withdrawing substituent groups to catalyze CO_2 conversion under ambient conditions. Integrating different catalytic components, the active porphyrin catalyst can not only convert CO_2 into CO, but also convert CO_2 directly into CH_4, which is a milestone in the field of molecular photochemical CO_2 reduction. Moreover, these reactions could be conducted not only in organic solutions, but also in aqueous conditions. Both CO_2 and CO could be used as the substrates for CH_4 generation. In addition, not only noble metal sensitizers, but also cheap commercial organic sensitizer could drive these reactions. This study opened up a perspective strategy towards obtaining efficient, selective, inexpensive and stable molecular photochemical CO_2 reduction in the future research.

4.2 Future perspectives

The year 2016 was the first in History reaching carbon dioxide concentration in the atmosphere above 400 ppm, and it is not expected to drop any time soon. Since the increasing content of this greenhouse gas in the atmosphere has been recognized, the development of efficient chemical routes for the conversion of waste CO_2 has attracted much attention. The viability of large-scale CO_2 conversion to value-added products, and especially energy carriers, is still a matter of debate. The most desired solution to utilize CO_2 emitted from the exhaust gases is to use it as the

feedstock for the production of synthetic fuels by energy storage in chemical bonds. In association with renewable energy sources, the production of energy carrier molecules could not only have the advantage of replacing at least in part fossil fuel-based energy sources, but also of reducing CO_2 emissions into the atmosphere. In this thesis, we have used an organic amine as the electron and proton donor, which is unsustainable, non-green and contaminative. Future work will also have to look at photocatalysis without using a sacrificial electron donor. The required electrons and protons could come from the splitting of H_2O, taking full advantage of the oxidation reaction occurring along with CO_2 reduction, thus mimicking natural photosynthesis.

According to IUPAC, the definition of photocatalysis is as follows: *change in the rate of a chemical reaction or its initiation under the action of ultraviolet, visible or infrared radiation in the presence of a substance-the photocatalyst-that absorbs light and is involved in the chemical transformation of the reaction partners*. Fe-porphyrin itself could absorb light and then use it directly for CO_2 reduction. However, this process is of quite low efficiency and thus an extra component-the photosensitizer-is always needed to increase the efficiency of solar energy utilization. Future work should thus focus on developing more efficient, stable, cheaper and possibly water-compatible photosensitizer. For example, several reports highlighted semiconductor quantum dots as photosensitizer in photocatalysis. Besides, we can introduce a chromophoric moity directly into a photocatalytic center through chemical bonding to form a binary or tandem assembly, where one part is dedicated to light harvesting and the other to the catalysis. In this case, the electron transfer between chromophore and catalytic center may be fast and efficient so as to increase the global energy conversion efficiency.

Despite the impressive progress, the efficiency of most reported systems is far from being acceptable for industrial applications. Hence, the core issue is still to develop an ideal catalyst, which is active enough, stable enough and cheap enough to be scalable. In addition, reaction conditions are also very important issues, for example, increasing the reaction temperature and pressure. Moreover, as the concentration of CO_2 in the atmosphere is quite low and since its capture and reconcentration require a large energy input, it is also very attractive to develop catalysis under low concentration of CO_2, ultimately using air as the direct substrate.

Photosynthesis basically supplies the carbon source for all organic compounds on Earth. It is an ideal green process for the conversion of light energy into chemical energy, which makes use

of CO_2 (equation 31). Inspired by the Nature's strategy, the development of sustainable and straightforward catalytic process not only to C_1 products but also to C-C bond-forming reactions in industrially relevant target molecules will be the 'crown jewel' of organic synthesis and catalysis research in the future. For example, sodium acrylate is an industrially important compound, with a global market volume of about 4 million tons and is commonly used as a monomer in the production of superabsorber polymers. Thus, the direct synthesis of acrylic acid from CO_2 and ethylene represents an economically attractive but also most challenging dream reaction (equation 32). Ethylene glycol is another important raw material in the manufacture of polyester fibers and polyethylene terephthalate resins used in bottling. The direct hydrogenation of CO_2 to produce this chemical in bulk scale might be a prime example for selective reductive coupling using carbon dioxide and could substitute its traditional synthesis from ethylene oxide (equation 33). In addition, the reductive methylation of much more widely available arenes, for example, benzene (from biogas), to generate toluene and xylenes is also highly interesting (equation 34).

$$6\ CO_2 + 6\ H_2O \xrightarrow{Cat./h\nu} C_6H_{12}O_6 + 6\ O_2 \quad (31)$$

$$CO_2 + CH_2{=}CH_2 \xrightarrow{Cat.} CH_2{=}CHCOOH \quad (32)$$

$$2\ CO_2 + H_2 \xrightarrow{Cat.} HOOC\text{-}COOH \xrightarrow{Cat.,H_2} HOCH_2\text{-}CH_2OH + 2\ H_2O \quad (33)$$

$$CO_2 + 3\ H_2 + C_6H_6\ (\text{benzene}) \xrightarrow{Cat.} C_7H_8\ (\text{toluene}) + 2H_2O \quad (34)$$

"Dream" reactions driven by artificial photosynthesis. (31) Natural photosynthesis; (32) Direct synthesis of acrylic acid from ethylene and CO_2; (33) Ethylene glycol synthesis via reductive coupling of CO_2; (34) Reductive methylation of benzene using H_2 and CO_2.

It is also my hope that future efforts toward more efficient photochemical conversion of CO_2 and other small molecules (such as H_2O, N_2…) will, as a welcome byproduct, also lead to an improved understanding of the fundamental processes involved in photocatalysis. This knowledge should prove widely useful in a large amount of fields relevant to humanity.

Chapter 5 Experiments and methods

5.1 Materials

5.1.1 Commercial reagents

Solids NaOH (99.5%), KOH (99.5%), $NaHCO_3$ (99%), KCl (99.5%), $KHCO_3$ (99.5%) $K_2C_2O_4$ (99.5%) and $FeCl_3 \cdot 6H_2O$ (99.5%) were purchased from Merck; KH_2PO_4 (97%) was purchased from Prolabo; K_2HPO_4 (99.5%) was purchased from Labosi; *fac*-(Tris(2-phenylpyridine))iridium(III) (99%) was purchased from Sigma-Aldrich. $FeCl_3 \cdot 6H_2O$ (99%), $FeBr_2$ (99%) and phenol (99.5%) were purchased from Alfa Aesar; (2, 2'-bipyridine)bis(2-phenylpyridinato)iridium(III) hexafluorophosphate ($Ir(ppy)_2(bpy)PF_6$, 90%) was purchased from TCI. $(NH_4)_2$-$Fe(SO_4)_2 \cdot 6H_2O$ (99%), purpurin (90%), benzaldehyde (99%), N, N'-dimethyl-1, 2-phenylenediamine (99%) and 2-phenylbenzimidazole (99.5%) were purchased from Sigma Aldrich; NH_4PF_6 (99.5%) was purchased from Acros Organics; NBu_4PF_6 (99%) and Ethylenediaminetetraacetic acid disodium salt (EDTA, 99%) were purchased from Fluka; free base 5,10,15,20-tetra(N,N,N-trimethyl-4-anilinium)porphyrin tetrachloride was purchased from Frontier Scientific, Phen1 and Phen2 were obtained from Miyake lab.

All chemicals were used as received without further purification.

Liquids and solvents Acetone (99.8%), methanol (99.8%), ethanol (99.9%), ethyl acetate (99.5%), dichloromethane (99%), 2-propanol (99.0%), and hydrochloric acid (37%) were purchased from VWR. Methyliodide (99%) and acetic acid (99.5%) were purchased from Alfa Aesar. Electrolyte solutions were prepared with ultra-pure water (TKA MicroPure, 0.055 $\mu S \cdot cm^{-1}$) or electrochemical grade acetonitrile, dimethyl sulfoxide, N, N-dimethylformamide (Acros, > 99.8%, over molecular sieves and stored under Argon atmosphere). Triethylamine (TEA, Acros Organics, 99%), triethanolamine (TEOA, Sigma, >99%), N, N-diisopropylethylamine (DIPEA, Fisher Scientific, >99%) and 2, 2, 2-trifluoroethanol (TFE, Romil Ltd., >99.5%) were used without further purification. Methanol and dichloromethane were distilled over calcium hydride; THF was dried over sodium then distilled after addition of benzophenone. Such solvents were freshly distilled or stored overnight under an argon atmosphere.

Gases Argon (> 99.998%), ^{12}CO (> 99.7%), and $^{12}CO_2$ (> 99.7%) gases were purchased from Air Liquide. CH_4 (> 99%) was from Fluka. ^{13}CO (99% content in atom ^{13}C) and $^{13}CO_2$ (99% content in atom ^{13}C) were purchased from Sigma Aldrich. High purity hydrogen was generated from an F-DBS Hydrogen Generator (WM-H2 500).

5.1.2 Synthesis and purifications

Iron(III) 5, 10, 15, 20-Tetra(4'-N, N, N-trimethylanilinium) Porphyrin Pentachloride (Fe-*p*-TMA) A solution of commercial 5, 10, 15, 20-tetra(4'-N, N, N-trimethylanilinium) porphyrin tetrachloride (51 mg, 5.2×10^{-5} mol),[171] anhydrous iron (II) bromide (201 mg, 9.3×10^{-4} mol), and 2,6-lutidine (60 μL, 5.2×10^{-4} mol) in dry methanol was degassed by argon for 15 min; the mixture was stirred at reflux under inert atmosphere for 7 d. After methanol was removed, the resulting solid was sonicated in THF and filtered. The brown solid on the glass frit was washed with dichloromethane and dissolved in methanol; after the mixture was concentrated under reduced pressure, a small amount of concentrated HCl was added with a large quantity of THF to give crude product as a dark red powder.

To purify the sample, the crude samples are dissolved in ultra-pure water. The porphyrin is precipitated by adding 10 equivalents NH_4PF_6 (155 mg, 9.5×10^{-4} mol). The resulting suspension is centrifuged for 10 minutes at 1.0×10^5 rpm to allow for better separation of the liquid and solid phases. The solid is collected and washed with 25 mL ultra-pure water and 10 equivalents NH_4PF_6 (155 mg, 9.5×10^{-4} mol). Traces of initial free-base porphyrin are removed by washing the solid with 15 mL acetone/CH_2Cl_2 (1:1), then 5 mL CH_3OH, and eventually five times 5 mL acetone/CH_2Cl_2 (1:1). Then, the residue is treated by 22.5 mL acetone and 2.5 mL concentrated HCl (37%) is added dropwise to exchange both iron ligand and anilinium counter-ions. The resulting suspension is sonicated for 10 minutes then centrifuged for 10 minutes at 1.0×10^5 rpm. After the supernatant is removed, the solid phase is collected and washed with 25 mL acetone. The residue is then dissolved in a minimum of methanol and precipitated with ethyl acetate. The solvent is eventually removed in vacuo to obtain Fe-*p*-TMA as a dark red powder (49.9 mg, 44%). HRMS (ESI): calculated for m/z ($C_{56}H_{60}ClFeN_8^{4+}$) 233.8501, found 233.8490. UV-vis (methanol) λ_{max} = 414 nm (Soret band).

(1, 3-dimethyl-2-phenyl-2, 3-dihydro-1H-benzo[d]imidazole) (BIH) A solution of N, N'-dimethyl-1, 2-phenylenediamine (1.5 g, 7.7 mmol) was treated with 4 g of methyl iodide in 10 mL of methanol containing 0.32 g of NaOH.[172] The reaction mixture was heated at 110 °C overnight in a Pyrex bottle. The longer the reaction period, the higher was the yield of the salt, especially for the substances having the electron-withdrawing substituents. The brown crude product was decolorized by the activated carbon in hot aqueous ethanol (ethanol:H_2O, 5:1 v/v). After removal of the solvent, the product was recrystallized from absolute ethanol. The yield was over 80%. Without further purification, to a solution of 1.7 g this product in 60 mL of CH_3OH was slowly added with 459 mg $NaBH_4$ in ice-bath. The reaction took place instantaneously to give a cloudy, white suspension. The reaction mixture was stirred vigorously for 1 h under Ar. After removal of the solvent under reduced pressure, the white solid was recrystallized from ethanol:H_2O (2:1 v/v) to give a colorless crystalline product. The yield was over 80% (0.87 g). IR (KBr) 3038 (w), 2953 (w), 2861 (w), 2801 (w), 1601 (m), 1495 (s), 1456 (m), 1368 (s), 1295 (m), 1234 (m), 1157 (m), 1121 (m), 1061 (m), 777 (m), 741 (m), 700 (m) cm^{-1}; ^{1}H-NMR (DMSO-d_6) δ 2.52 (s, 6 H, NCH_3), 4.88 (s, 1 H, 2-H), 6.46 (m, 2 H, 5-H), 6.64 (m, 2 H, 4-H), 7.44-7.59 (m, 5 H, phenyl); UV-vis (2-propanol-H_2O, 4:1 v/v) λ_{max} nm (log ϵ) 312 (3.82), 260 (3.70).

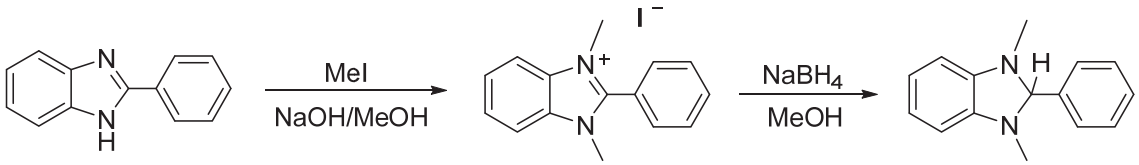

Scheme 5.1 Synthesis routes of BIH

$K_3[Fe(C_2O_4)_3]\cdot 3H_2O$ Weigh approximately 9.0 g of hydrated potassium oxalate, $K_2C_2O_4\cdot H_2O$ into a 250 mL beaker. Add 30 mL of distilled water and heat to dissolve the solids (do not boil). In a second small beaker dissolve 4.4 g of $FeCl_3\cdot 6H_2O$ in a minimum amount of cold water (10-15 mL). Add the $FeCl_3\cdot 6H_2O$ solution to the warm oxalate solution and stir with a glass rod. Allow the product to crystallize (away from strong sunlight) by cooling the solution in an ice-water mixture. Collect the green crystalline product, $K_3[Fe(C_2O_4)_3]\cdot 3H_2O$, by filtration and dry it under vacuum.

$$3\ K_2C_2O_4\cdot H_2O\ (aq) + FeCl_3\cdot 6H_2O\ (aq) \rightarrow K_3[Fe(C_2O_4)_3]\cdot 3H_2O\ (aq) + 3KCl\ (aq)$$

The complex anion is photo-sensitive. This means that upon exposure to light of an appropriate wavelength (< 450 nm in this case) the $[Fe(C_2O_4)_3]^{3-}$ undergoes an intramolecular redox reaction in which the Fe(III) anion is reduced to Fe(II) while one of the oxalate groups is oxidized to CO_2.

$$[Fe(C_2O_4)_3]^{3-} \rightarrow Fe^{2+} + 5/2C_2O_4^{2-} + CO_2\,(g)$$

The generated Fe^{2+} then can readily be detected by adding a buffered solution of phenanthroline. The absorbance of the solution at 510 nm was recorded and the value was used to calculate the number of Fe^{2+} ions generated during the irradiation process.

5.2 Methods

5.2.1 Simulated solar light

The main figure-of-merit for a solar CO_2 reduction device is its performance under real sunlight. However, even real sunlight does not have the same intensity and spectral distribution everywhere on earth. To facilitate meaningful comparisons of device performances, the performance characteristics are usually quoted for the so-called AM 1.5G conditions. This stands for "air mass 1.5 global", and refers to the spectral distribution and intensity of sunlight on a 37° south-facing tilted surface after it has traveled through 1.5 times the thickness of the earth's atmosphere. The latter corresponds to a solar zenith angle of 48.19°. The AM 1.5G spectrum includes both the direct and the diffuse contributions of the incident sunlight, and has a total integrated intensity of 1000 W/m^2. The most recent and widely used AM 1.5G reference spectrum is published by the American Society for Testing and Materials as the ASTM-G173-03 standard, and represents a reasonable average for the 48 contiguous states of the USA over a period of 1 year [ASTM G173-03(2012), Standard Tables for Reference Solar Spectral Irradiances: Direct Normal and Hemispherical on 37° Tilted Surface, ASTM International, West Conshohocken, PA, 2012, https://www.astm.org/Standards/G173.htm]. The corresponding international standard is IEC 60904-3 (3nd edition, 2016).

Since real AM 1.5G sunlight is not readily available at all times and at all locations, solar simulators are used. Making a reasonably good solar simulator is far from trivial. One cannot use halogen lamps since their maximum color temperature is limited to ~3200 K, which is much lower than the color temperature of the sun (5800 K). Xenon lamps are widely accepted to give

the best match to the solar spectrum. Newport LCS-100 solar simulator (see Figure 5.1) is usually used in photovoltaic cell research requiring a certified system for small illumination areas. The 38 × 38 mm simulators meet Class ABB as defined by ASTM, IEC and JIS standards. All electronics are built into the lamp housing and are factory preset to run the 100 W xenon bulb with integrated reflector at the proper current and voltage. For replacement assemblies, a “drop in” design eliminates the need for lamp alignment. An integrated attenuator allows partial sun irradiance.

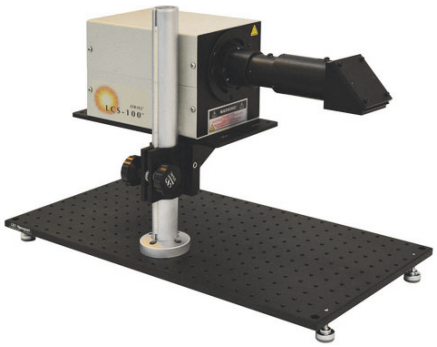

Figure 5.1 Photo of Newport LCS-100 solar simulator.

In addition, optical filters are used to optimize the overall spectral shape and to remove (to some extent) the sharp lines in the emission spectrum of xenon. Schott long-pass filters (also known as edge filters) possess a steep absorption range. This property allows for a sharp separation between the blocking and transmission range. Moreover, the filters are practically insensitive to the angle of installation. In this thesis, both Schott GG420 and GG435 long pass filters are used and their transmittance spectroscopies are illustrated in Figure 5.2.

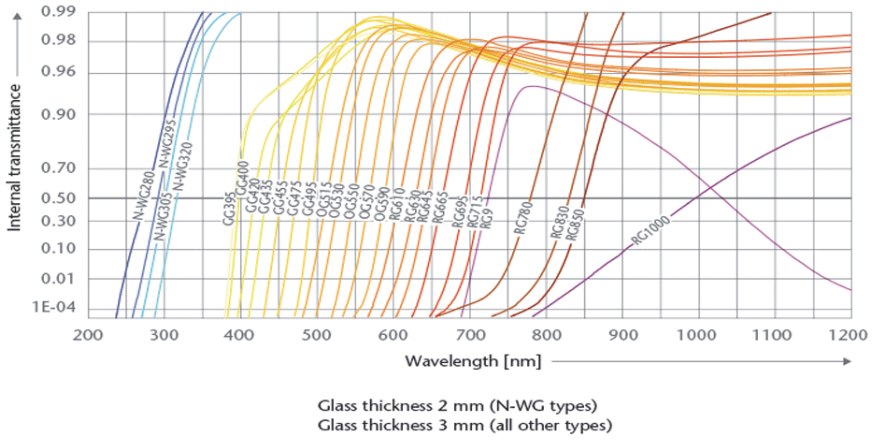

Figure 5.2 Transmittance spectroscopies of Schott GG420 and GG435 long pass filters. (https://www.itos.de/en/schott-optical-filters/long-pass/gg395-gg400-gg420/)

5.2.2 UV-Visible spectroscopy

UV-visible absorption measurements were done with an Agilent Technologies Cary 60 or an Analytic Jena Specord 600 UV/VIS spectrophotometer. Aliquots of the solution were poured into a quartz cell (1 cm in length). Typical spectral region ranged from 200-800 nm and it was swept at a rate of 720 $nm \cdot s^{-1}$.

5.2.3 Fluorescence spectra

Emission quenching measurements were conducted with a Cary Eclipse fluorescence spectrophotometer (Agilent Technologies), with the excitation wavelength set at 420 nm (PS-8 PS-9, and PP) or 435 nm (Phen2) and the emission spectrum measured between 430 nm and 700 nm (PS-8), 450 nm and 800 nm (PS-9), 500 nm and 800 nm (PP) or 440 nm and 750 nm . Emission intensities used for the Stern-Volmer analysis were taken at 517 nm (PS-8), 592 nm (PS-9), 605 nm (PP) or 506 nm (Phen2), that is, the emission maximum of PS.

5.2.4 Transient absorption spectroscopy

Transient absorption kinetic was measured with an Edinburgh Instruments LP920-KS laser flash photolysis spectrometer. The solutions were excited at 420 nm (5 ns pulse, 2 to 4 mW per pulse) via a Continuum SLOPO Plus OPO pumped by a frequency-tripled Continuum Surelite II-10 Nd:YAG laser. Right-angle probe light was provided by an Osram XBO 450 W ozone free pulsed xenon lamp and then collected into a spectrograph. Excited state lifetime of Phen2 was determined by measuring kinetics of the ground state recovery at 390 nm, *i.e.* the absorption maximum of Phen2, thanks to a Hamamatsu R928 photomultiplier tube linked to a Tektronix TDS 3012C 100 MHz oscilloscope. Temperature of the sample port was set at 20°C by a Quantum Northwest TC125 Peltier effect controller. The Edinburgh Instruments L900 software ensured the control and the synchronization of the whole setup.

5.2.4 Infrared spectroscopy

Infrared spectra were recorded on a PerkinElmer Spectrum BX FTIR spectrometer equipped with a Specac Omni Cell P/N 800 measurement cell. The Omni-Cell™ is a multidisciplinary

support allowing the simple analysis in static mode and at ambient temperature of sample in transmission mode (Figure 5.3). This support accepts both rectangular windows for the analysis of liquids and round windows for analysis according to the technique "Mull", the windows for the analysis of liquid being available in removable or seals.

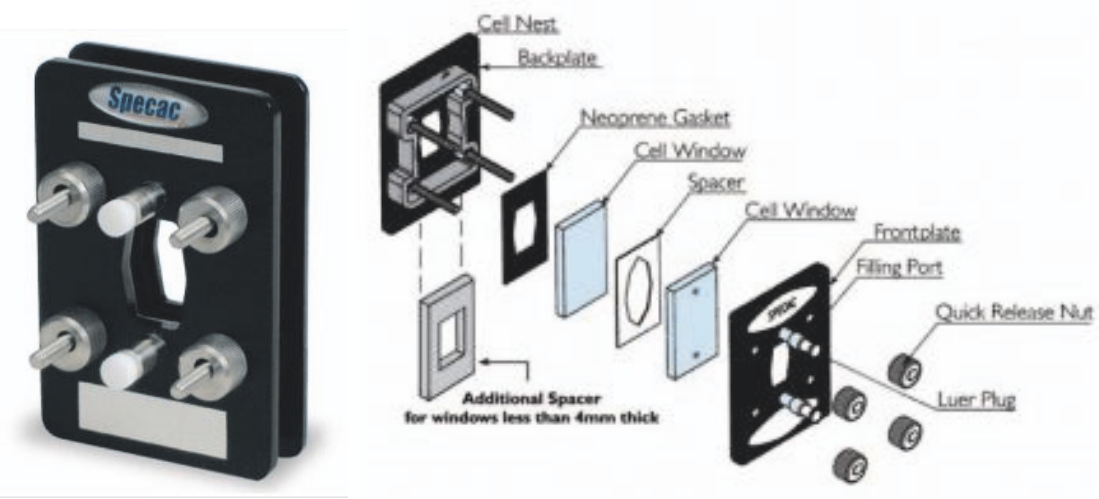

Figure 5.3 Specac Omni Cell® P/N 800 measurement cell for liquid IR spectroscopy.

5.2.5 Nuclear magnetic resonance (NMR) spectroscopy

The ^{1}H NMR and ^{13}C NMR spectra were recorded on a Bruker Avance III 400-MHz spectrometer and were referenced to the resonances of the solvent used.

Notably, the metalation of the free base porphyrin is performed with iron(II) species. Even though the reaction occurs under inert argon atmosphere, oxygen traces from ambient air readily oxidizes the metal center to the oxidation state +3. Unfortunately, iron(III) is paramagnetic and prevents the acquisition of clean NMR spectra of such highly conjugated compounds. Some experiments have been attempted to reduce in-situ the porphyrin center to Fe^{II} by adding a reducing metal (zinc) or compounds such as $NOBF_4$ that bind to the metal and yield Fe^{II} species. None of these attempts were successful in delivering neat NMR spectra.

5.2.6 Gas chromatography and GC-MS

Gas chromatography analyses of gas evolved in the headspace during the electrolysis were performed with an Agilent Technologies 7820A GC system equipped with a thermal conductivity

detector. H_2, CO and CH_4 production was quantitatively detected using a CP-CarboPlot P7 capillary column (25 m in length and 25 µm internal diameter). Temperature was held at 150 °C for the detector and 35 °C for the oven. The carrier gas was argon flowing at 7.95 mL/min at constant pressure of 0.6 bars. Injection was performed via a 250 µL gas-tight (Hamilton) syringe previously degassed with CO_2. The GC analysis was shown in Figure 5.4. Conditions allowed detection of H_2, O_2, N_2, CO, and CO_2. Calibration curves for H_2, CO and CH_4 were determined separately by injecting known quantities of pure gas (see Figure 5.5).

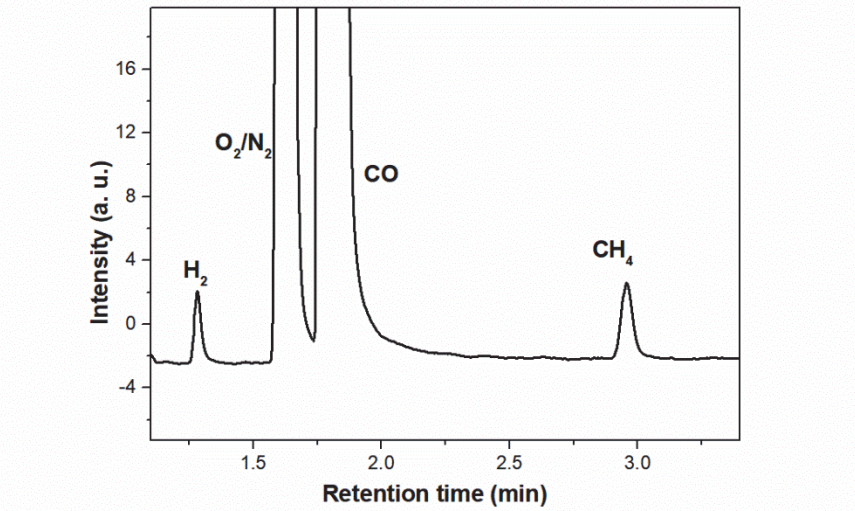

Figure 5.4 Gas chromatography analyses. Products concentration in the electrolysis cell is derived from the area of each peak.

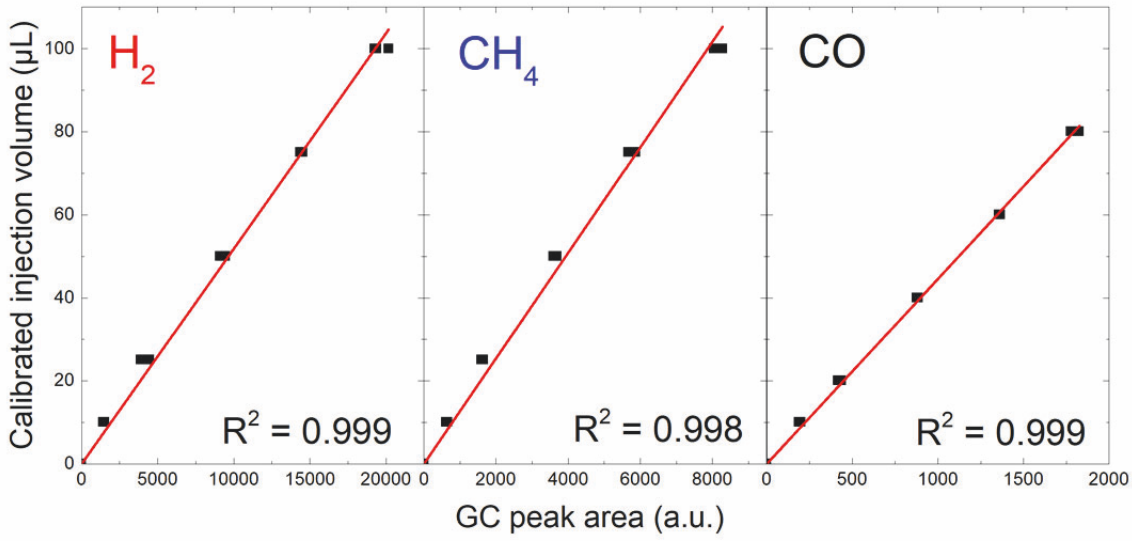

Figure 5.5 Calibration curves for gas chromatography quantification for H_2 (left panel), CH_4 (middle panel) and CO (right panel) and corresponding coefficients of linear correlation (R^2).

GC-MS for detecting the labeled gas products were obtained by a ThermoFisher Scientific TRACE Ultra gas chromatograph equipped with a CP 7514 column (Agilent Technologies) and coupled to a DSQ II mass spectrometer in positive ionization mode, using a TriPlus headspace autosampler.

The mass spectra for detecting the organic compounds were recorded on a Microtof-Q of Bruker Daltonics. Injection method was high resolution electrospray (ESI).

5.2.7 Ionic chromatography

Ionic chromatography (IC) was used for the detection and quantification of formate in aqueous and organic samples recovered from the reactor after decompression. The presence of other anions, such as acetate, fluoride, chloride, oxalate, etc. can also be determined using this technique. Ionic chromatography measurements were performed with a Thermo Scientific Dionex ICS-1100 system equipped with a Dionex ERS 500 electrolytically regenerated suppressor. All the samples were diluted 50 folds with ultra-pure water before analyzed through IC. Calibration curve for formate was determined separately by injecting known quantities of pure sample.

5.2.8 pH measurements

pH measurements were performed with Hanna pH210 and HI221 instruments and 6 mm microelectrodes (Fisher).

5.2.9 Cyclic voltammetry

Cyclic voltammograms were obtained in a three-electrode cell by use of a Metrohm Autolab potentiostats/galvanostat interfaced with Nova software. The working electrode was a 3 mm diameter glassy carbon disk carefully polished with 1 μm diamond paste (DP-PasteM) then thoroughly rinsed in acetone then absolute ethanol before use. The counterelectrode was a platinum wire and the reference electrode was an aqueous SCE electrode. All experiments were carried out either under argon or carbon dioxide atmosphere at 21 °C, the double-wall jacketed cell being thermostated by circulation of water. The cell was sealed during measurements and the

solution was saturated with argon or carbon dioxide between measurements. Ohmic drop was compensated through the positive feedback compensation method implemented in the instrument.

5.2.10 Photochemical experiments setup

Each solution was prepared just before the experiment. The solvent was degassed with Ar for approximately 10 min, and then TEA and/or TFE was added. After keeping the solution approximately 5 more minutes under Ar atmosphere, it was poured with a syringe onto the solid porphyrin and photosensitizer previously placed under inert atmosphere. Then, the solution (3.5 mL) was transferred to a sealable fluorescence 1 × 1 cm quartz Suprasil cuvette (Hellma 117.100F-QS) equipped with a home-made glassware, leaving a headspace of approximately 23 mL (see Scheme 5.1). The cuvette was degassed previously through a vial filled with the solvent, TFE, and Et_3N (if present) for approximately 20 min with Ar, CO_2 or CO to prevent any evaporation. The typical composition of the sample was 2-10 μM porphyrin, 0.05-0.1 M sacrificial electron donor, 0.2-0.1 mM photosensitizer and 0-1 M TFE (see figures for details of each experiment). Then, the solution in the cuvette was irradiated perpendicularly with a Xenon lamp through an irradiation window of 5 cm × 5 cm by using a Schott GG optical filter and a 2 cm long glass OS cell filled with water to cut off IR. Gas products were analyzed via GC and liquid products were analyzed via ^{1}H NMR, ^{13}C NMR and IC. UV-vis analysis was made directly via the home-made glassware.

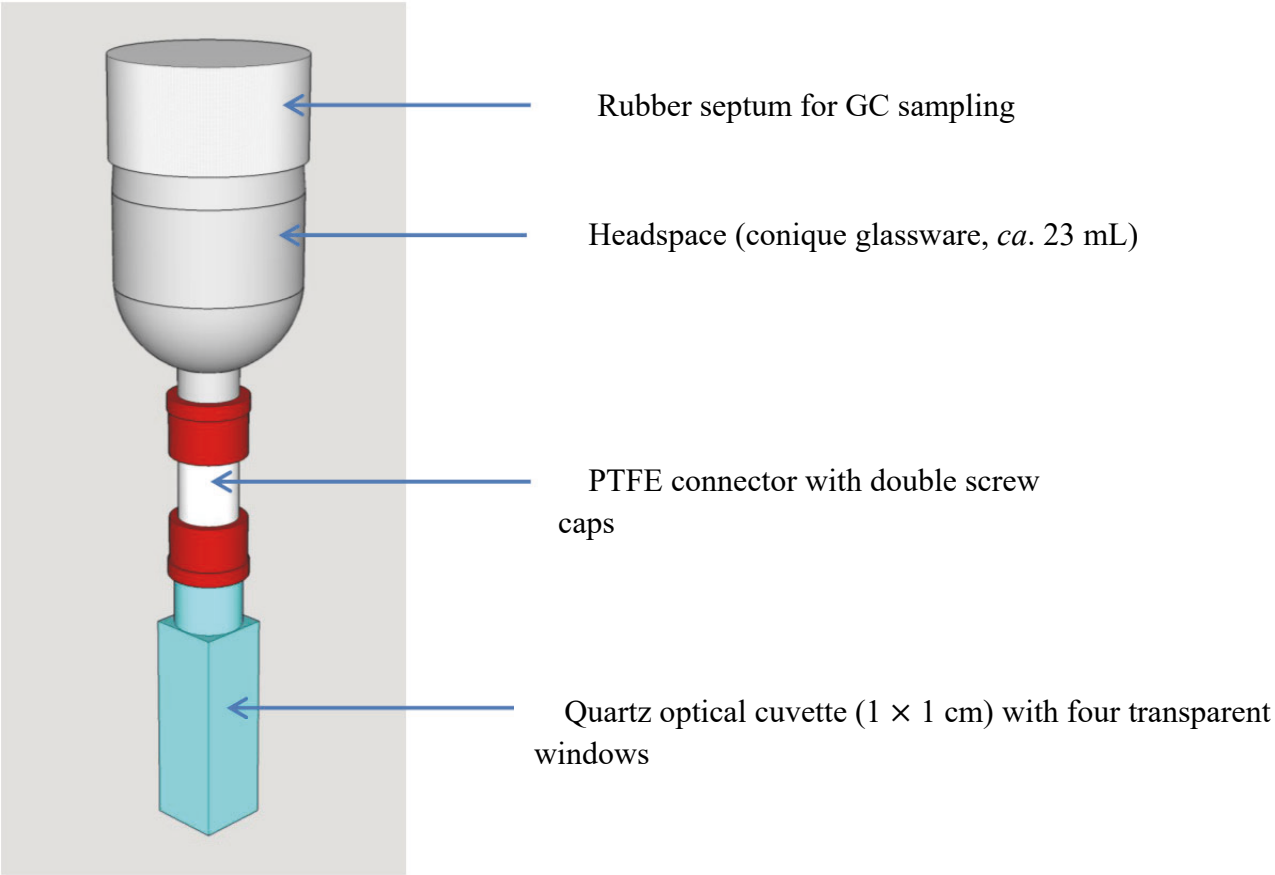

Scheme 5.1 Home-designed photochemical cell.

5.2.11 Details on the quantum yield calculations

The number of incident photons was measured using the classical iron ferrioxalate ($K_3Fe(C_2O_4)_3$) chemical actinometer.[173] Thus, 3mL (V_1) of an aqueous solution containing the iron actinometer (0.15 M) and H_2SO_4 (0.05 M) was irradiated with a solar simulator (Newport LCS-100) equipped with band pass filters, and using the same experimental setup as in the case of the photocatalytic reactions. The time of the irradiation was kept as short as possible to avoid more than 10% decomposition of the actinometer. Before each measurement, the power output of the lamp was measured using a laser & power energy meter (Gentec Solo 2). After irradiation, an aliquot of 0.180 mL (V_2) was taken and 2 mL of a buffered solution of phenanthroline (0.015 M / 0.5 M H_2SO_4) were added together with distilled H_2O to give a final volume of 25 mL (V_3). The absorbance of the solution at 510 nm was recorded and the value was used to calculate the number of Fe^{2+} ions ($n[Fe^{2+}]$) generated during the irradiation process through the following equation:

$$n[Fe^{2+}] = \frac{V_1 \cdot V_3 \cdot (A - A_0)}{1000 \cdot V_2 \cdot \varepsilon_0}$$

where V_1 = volume of actinometer solution irradiated (mL)

V_2 = volume of aliquot taken for analysis (mL)

V_3 = final volume to which the aliquot V_2 is diluted (mL)

A = measured optical density at 510 nm

A_0 = measured optical density at 510 nm of a non-irradiated sample

ε_0 = experimental value of the molar extinction coefficient of the Fe^{2+} complex (11100 L $mol^{-1}cm^{-1}$)

Finally, the number of incident photons per second (# photons) is calculated using the following equation:

$$\#\ \text{photons}\ (s^{-1}) = \frac{6.022 \times 10^{23} \cdot n[Fe^{2+}]}{\Phi_\lambda \cdot t}$$

where Φ_λ = quantum yield of Fe^{2+} formation, 1.07 was taken from the literature[174]

t = time of irradiation (s)

Using three independent measurements, we determined that the number of incident photons to the sample was (2.18 ± 0.17) × 10^{19} photons per hour. The CO-to-CH_4 reduction being a six-electron process, the overall quantum yield Φ of the process was determined using the following equation:

$$\Phi_{CH_4}(\%) = \frac{Number\ of\ CH_4\ molecules\ formed\ \times 6}{Number\ of\ incident\ photons} \times 100\%$$

For example, taking 159 as the highest turnover number for CH_4 (Table 3.1, entry 12), we obtain a quantum yield Φ of about 0.18% after 102 h of irradiation.

Notations

[Q]	quencher concentration
c	speed of light
C	total passed charge
E	potential
E^0	redox potential
E_{CB}	conduction band potential
E_g	bandgap energy
E_p	energy of photon
E_{VB}	valence band potencial
F	Faraday constant
h	Planck's constant
I	emission intensity with a quencher
I_0	emission intensity
k_q	apparent quenching rate constant
n	number of needed electrons for product evolution
t	reaction time
T	temperature
v	scan rate
w_P	work terms required to bring the product
w_R	work terms required to bring the reactant
γ	γ-Radiation
ΔG^0	Gibbs free energy
ΔH^0	Standard enthalpy
ε_S	solvent dielectric constant
λ	photon wavelength
λ_{ex}	excited wavelength
ν	photon frequency
τ_0	exited-state lifetime
Φ	quantum yield

Terms and Abbreviations

IEO2017	International Energy Outlook 2017
9CNA	9-cyanoanthracene
AA	ascorbic acid
ACN	acetonitrile
ASA	amino salicylic acid
ATP	adenosine triphosphate
BIH	1,3-dimethyl-2-phenyl-2,3-dihydro-1H-benzo[d]imidazole
BNAH	1-benzyl-1,4-dihydronicotinamide
bpy	2, 2'-bipyridine
C_2H_4	ethylene
C_2H_5OH	ethanol
C_2H_6	ethane
C_3H_7OH	n-propanol
CAT	catalyst
CB	conduction band
CH_3OH	methanol
CH_4	methane
CO	carbon monoxide
CO_2	carbon dioxide
Co-POM	Co-porphyrin-oligomers
CS	catalytic selectivity
CV	cyclic voltammetry
cyclam	1, 4, 8, 11-tetraazacyclotetradecane
DFT	density functional theory
DIPEA	N, N-diisopropylethylamine
dmb	4, 4'-dimethyl-2, 2'-bipyridine
DMF	N, N'-dimethylformamide
DRIFTS	diffuse reflectance infrared Fourier transform spectroscopy
EA	electron acceptor
ECCE	electrochemical chemical chemical electrochemical
ECEC	electrochemical chemical electrochemical chemical
ED	electron donor
EDTA	ethylenediamine tetraacetic acid
FE	faradaic efficiency
Fe-*p*-TMA	5, 10, 15, 20-tetra(4'-N, N, N-trimethylanilinium) porphyrin iron(III) pentachloride
FeTCPP	meso-tetraphenylporphine- 4,4',4",4'"-tetracarboxylic acid, iron (III) chloride
FeTPP	5, 10, 15, 20-Tetraphenyl-21H,23H-porphine iron(III) chloride
GC	gas chromatograph
g-C_3N_4	graphitic carbon nitride

$H_2C_2O_4$	oxalic acid
HCHO	formaldehyde
$HCOO^-$	formate
HCOOH	formic acid
HOMO	highest occupied molecular orbital
IPCC	Intergovernmental Panel on Climate Change
IR	infrared
LMCT	ligand to metal charge transfer
LUMO	lowest unoccupied molecular orbital
MC	metallocorrole
MEDA	2-(dimethylamino)ethanethiol
MLCT	metal to ligand charge transfer
MN	metallocorrin
MP	metalloporphyrin
MPc	metallophthalocyanine
MS	mass spectrum
N719	Di-tetrabutylammonium cis-bis(isothiocyanato)bis(2,2′-bipyridyl-4,4′-dicarboxylato)ruthenium(II)
NHC	N-heterocyclic carbene
NHE	normal hydrogen electrode
NP	nanoparticle
NREL	National Renewable Energy Laboratory
PCAT	photocatalyst
PCET	proton-coupled electron transfer
Phen1	5,10-di(2-naphthyl)-5,10-dihydrophenazine
Phen2	3,7-di(4-biphenyl)-1-naphthalene-10-phenoxazine
PhOH	phenol
PP	purpurin
ppy	2-phenylpyridine
PS	photosensitizer
QD	quantum dot
qpy	2, 2′: 6′, 2″: 6″, 2‴-quaterpyridine
QY	quantum yield
RDS	rate determining step
SC	semiconductor
SCE	saturated calomel electrode
SD	sacrificial electron donor
TEA	triethylamine
TEOA	triethanolamine
TFE	2, 2, 2-trifluoroethanol
THF	tetrahydrofuran
TOF	turnover frequency
TON	turnover number

TTA	triplet-triplet annihilation
UV	ultra violet
UV-Vis	ultraviolet-visible
VB	valence band
WE	work electrode

Acknowledgements

I would like to express my appreciation to all the people who have appeared in my life, for their love and harassment, to make me happy and strong.

First of all, I would like to thank Prof. Alain Deronzier. Actually I had never seen him, nor known his features. Maybe we will miss each other if we meet in the street someday. It was three years ago that he fortuitously recommended me to LEM for a Ph.D. under the supervision of Prof. M. Robert. Life is really like a box of chocolate and you never know what you are going to get. I was born in a small, poor and unenlightened village in the center of China, where most of the young even have no chance to go to college. Before that, I had never thought I could have the chance to study in Paris. I guess Alain must be a very gracious and warmhearted man. It was him that changed my life path. I will remember him and be grateful to him forever in my deep heart.

I really hope to express my heartfelt thanks to my supervisors, Prof. Julien Bonin and Prof. Marc Robert for their entire academic and personal supports during the past three years. They taught me how to think creatively and approach scientific explorations in the right way, which will benefit the rest of my life. I would also like to acknowledge the contributions of Prof. Jean-Michel Savéant, Prof. Cyrille Costentin, Prof. Miyake, Dr. Elodie Anxolabéhère, Dr. Benoit Limoges, Dr. Cédric Tard, etc. Together, they have brought significant advice and promoted diverse, profitable discussions all along these three years.

Many of my colleagues who were present in the beginning of my Ph.D. are now gone and others have arrived since then. To all of them, Iban, Antoine, Arnaud, Hachem, Charlie, Niklas, Cheng as well as Claudio, Min, Etienne, Alexis, Kristian Yee-Seul, Khalil, Martin, Célia, Hussein, Jérémy, Bing, Lydia, Benjamin, Justine, Telmo, Rabia, Fumiaki, etc. I wish to express my appreciation. All the daily empowering interactions contributed all long these three years. I'm also grateful for the experimental assistance and data analysis I received from various people working within the Lavoisier building. Thank you for providing me a challenging environment for my studies.

My parents' kindness is higher than the mountain, and longer than the river. In my late twenties, I felt ashamed that I did not support them. I appreciate their love, support and encouragement whenever needed. Without them it would not be possible for me to complete this work.

This work is supported under LEM at Université Paris Diderot and China Scholarship Council. I express my gratitude to my financial sponsors.

Lastly, I would like to thank this enlightened time of progress that we live in, giving us the opportunities to realize our dreams and find our self-worth.

Bibliography

1. Administration, U. S. E. I. International Energy Outlook Executive Summary. https://www.eia.gov/outlooks/ieo/exec_summ.php.
2. Ciais, P.; Sabine, C.; Bala, G.; Bopp, L.; Brovkin, V.; Canadell, J.; Chhabra, A.; DeFries, R.; Galloway, J.; Heimann, M., Carbon and other biogeochemical cycles. In *Climate change 2013: the physical science basis. Contribution of Working Group I to the Fifth Assessment Report of the Intergovernmental Panel on Climate Change*, Cambridge University Press: 2014; pp 465-570.
3. Solar, S.; Getoff, N.; Surdhar, P. S.; Armstrong, D. A.; Singh, A., Oxidation of Tryptophan and N-Methylindole by N_3^-, $Br_2^{\cdot-}$, and $(SCN)_2^{\cdot-}$ Radicals In Light and Heavy-Water Solutions: A Pulse Radiolysis Study. *J. Phys. Chem.* **1991,** *95* (9), 3639-3643.
4. Hartmann, D. L.; Tank, A. M. K.; Rusticucci, M.; Alexander, L. V.; Brönnimann, S.; Charabi, Y. A. R.; Dentener, F. J.; Dlugokencky, E. J.; Easterling, D. R.; Kaplan, A., Observations: atmosphere and surface. In *Climate Change 2013 the Physical Science Basis: Working Group I Contribution to the Fifth Assessment Report of the Intergovernmental Panel on Climate Change*, Cambridge University Press: 2013.
5. Amenda, J. P.; Helgeson, H. C., Solubilities of the common L-alpha-amino acids as a function of temperature and solution pH. *Pure Appl. Chem.* **1997,** *69*, 935.
6. Collins, M.; Knutti, R., Chapter 12: Long-term Climate Change: Projections, Commitments and Irreversibility–Final Draft, Underlying Scientific–Technical Assessment. *Working Group 1 contribution to the IPCC fifth assessment report: Climate Change 2013: The physical science basis* **2013**.
7. Oppenheim, J.; Beinhocker, E., Climate change and the economy: myths versus realities. *McKinsey & Company, available at http://www. euractiv. com/25/images/Climate_change_myths. pdf (accessed on 15 July 2009)* **2009**.
8. Lewis, N. S.; Nocera, D. G., Powering the planet: Chemical challenges in solar energy utilization. *Proc. Natl. Acad. Sci. U.S.A.* **2006,** *103* (43), 15729-15735.
9. Bartocci, C.; Maldotti, A.; Varani, G.; Carassiti, V.; Battioni, P.; Mansuy, D., Iron meso-tetra(2,6-dichlorophenyl)porphyrin as a very efficient catalyst for the photoreduction of carbon tetrachloride by alcohols. *J. Chem. Soc., Chem. Commun.* **1989,** (14), 964-965.
10. Planck, M., On the law of distribution of energy in the normal spectrum. *Annalen der physik* **1901,** *4* (553), 1.
11. Faunce, T. A.; Lubitz, W.; Rutherford, A. W.; MacFarlane, D. R.; Moore, G. F.; Yang, P.; Nocera, D. G.; Moore, T. A.; Gregory, D. H.; Fukuzumi, S.; Yoon, K. B.; Armstrong, F. A.; Wasielewski, M. R.; Styring, S., Energy and environment policy case for a global project on artificial photosynthesis. *Energy Environ. Sci.* **2013,** *6* (3), 695-698.
12. (a) Steinberg-Yfrach, G.; Rigaud, J.-L.; Durantini, E. N.; Moore, A. L.; Gust, D.; Moore, T. A., Light-driven production of ATP catalysed by F 0 F 1-ATP synthase in an artificial photosynthetic membrane. *Nature* **1998,** *392* (6675), 479; (b) Steinberg-Yfrach, G.; Liddell, P. A.; Hung, S.-C.; Moore, A. L.; Gust, D.; Moore, T. A., Conversion of light energy to proton potential in liposomes by artificial photosynthetic reaction centres. *Nature* **1997,** *385* (6613), 239.
13. Quinn, E. L.; Jones, C. L., *Carbon dioxide*. Reinhold Publishing Corporation; New York.: 1936.
14. Bamberger, C.; Robinson, P. R., Thermochemical splitting of water and carbon dioxide with cerium compounds. *Inorg. Chim. Acta* **1980,** *42*, 133-137.

15. (a) Getoff, N.; Scholes, G.; Weiss, J., Reduction of carbon dioxide in aqueous solutions under the influence of radiation. *Tetrahedron Lett.* **1960,** *1* (39), 17-23; (b) Willis, C.; Boyd, A., Excitation in the radiation chemistry of inorganic gases. *International Journal for Radiation Physics and Chemistry* **1976,** *8* (1-2), 71-111.
16. Jee, H. S.; Nishio, N.; Nagai, S., Continuous CH4 Production from H2 and CO2 by Methanobacterium thermoautotrophicum in a fixed-bed reactor. *Journal of Fermentation Technology* **1988,** *66* (2), 235-238.
17. Amatore, C.; Saveant, J. M., Mechanism and kinetic characteristics of the electrochemical reduction of carbon dioxide in media of low proton availability. *J. Am. Chem. Soc.* **1981,** *103* (17), 5021-5023.
18. Lehn, J.-M.; Ziessel, R., Photochemical Generation of Carbon Monoxide and Hydrogen by Reduction of Carbon Dioxide and Water under Visible Light Irradiation. *Proc. Natl. Acad. Sci. U.S.A.* **1982,** *79* (2), 701-704.
19. Chang, X.; Wang, T.; Gong, J., CO_2 photo-reduction: insights into CO_2 activation and reaction on surfaces of photocatalysts. *Energy Environ. Sci.* **2016,** *9* (7), 2177-2196.
20. Bolton, J. R., Solar fuels. *Science* **1978,** *202* (4369), 705-711.
21. (a) Hong, J.; Zhang, W.; Ren, J.; Xu, R., Photocatalytic reduction of CO_2: a brief review on product analysis and systematic methods. *Analytical methods* **2013,** *5* (5), 1086-1097; (b) Qiao, J.; Liu, Y.; Hong, F.; Zhang, J., A review of catalysts for the electroreduction of carbon dioxide to produce low-carbon fuels. *Chem. Soc. Rev.* **2014,** *43* (2), 631-675.
22. Huynh, M. H. V.; Meyer, T. J., Proton-coupled electron transfer. *Chem. Rev.* **2007,** *107* (11), 5004-5064.
23. Costentin, C.; Robert, M.; Savéant, J.-M., Catalysis of the Electrochemical Reduction of Carbon Dioxide. *Chem. Soc. Rev.* **2013,** *42* (6), 2423-2436.
24. Habisreutinger, S. N.; Schmidt-Mende, L.; Stolarczyk, J. K., Photocatalytic reduction of CO2 on TiO2 and other semiconductors. *Angew. Chem., Int. Ed.* **2013,** *52* (29), 7372-7408.
25. Ji, Y.; Luo, Y., Theoretical study on the mechanism of photoreduction of CO2 to CH4 on the anatase TiO2 (101) surface. *ACS Catal.* **2016,** *6* (3), 2018-2025.
26. Neaţu, S. t.; Maciá-Agulló, J. A.; Concepción, P.; Garcia, H., Gold–copper nanoalloys supported on TiO_2 as photocatalysts for CO_2 reduction by water. *J. Am. Chem. Soc.* **2014,** *136* (45), 15969-15976.
27. Kang, Q.; Wang, T.; Li, P.; Liu, L.; Chang, K.; Li, M.; Ye, J., Photocatalytic reduction of carbon dioxide by hydrous hydrazine over Au–Cu alloy nanoparticles supported on $SrTiO_3/TiO_2$ coaxial nanotube arrays. *Angewandte Chemie* **2015,** *127* (3), 855-859.
28. Mistry, H.; Varela, A. S.; Bonifacio, C. S.; Zegkinoglou, I.; Sinev, I.; Choi, Y.-W.; Kisslinger, K.; Stach, E. A.; Yang, J. C.; Strasser, P., Highly selective plasma-activated copper catalysts for carbon dioxide reduction to ethylene. *Nat. Commun.* **2016,** *7*, 12123.
29. (a) Lee, S.; Kim, D.; Lee, J., Electrocatalytic production of C_3-C_4 Compounds by conversion of CO_2 on a chloride-induced bi-phasic Cu_2O-Cu catalyst. *Angew. Chem., Int. Ed.* **2015,** *54* (49), 14701-14705; (b) Geioushy, R.; Khaled, M. M.; Alhooshani, K.; Hakeem, A. S.; Rinaldi, A., Graphene/ZnO/Cu_2O electrocatalyst for selective conversion of CO_2 into n-propanol. *Electrochim. Acta* **2017,** *245*, 456-462.
30. (a) Kozuch, S.; Martin, J. M., "Turning over" definitions in catalytic cycles. ACS Publications: 2012; (b) Lente, G., Comment on "'Turning Over'Definitions in Catalytic Cycles". *ACS Catal.* **2013,** *3* (3), 381-382.
31. Zhang, N.; Long, R.; Gao, C.; Xiong, Y., Recent progress on advanced design for photoelectrochemical reduction of CO_2 to fuels. *Science China Materials* **2018**, 1-35.

32. Sun, Z.; Ma, T.; Tao, H.; Fan, Q.; Han, B., Fundamentals and Challenges of Electrochemical CO_2 Reduction Using Two-Dimensional Materials. *Chem* **2017,** *3* (4), 560-587.
33. Yang, C.; Yu, X.; Heißler, S.; Nefedov, A.; Colussi, S.; Llorca, J.; Trovarelli, A.; Wang, Y.; Wöll, C., Surface faceting and reconstruction of ceria nanoparticles. *Angew. Chem., Int. Ed.* **2017,** *56* (1), 375-379.
34. Chen, X.; Shen, S.; Guo, L.; Mao, S. S., Semiconductor-based photocatalytic hydrogen generation. *Chem. Rev.* **2010,** *110* (11), 6503-6570.
35. (a) Concepcion, J. J.; House, R. L.; Papanikolas, J. M.; Meyer, T. J., Chemical approaches to artificial photosynthesis. National Acad Sciences: 2012; (b) Liu, C.; Colón, B. C.; Ziesack, M.; Silver, P. A.; Nocera, D. G., Water splitting–biosynthetic system with CO_2 reduction efficiencies exceeding photosynthesis. *Science* **2016,** *352* (6290), 1210-1213; (c) Sakimoto, K. K.; Wong, A. B.; Yang, P., Self-photosensitization of nonphotosynthetic bacteria for solar-to-chemical production. *Science* **2016,** *351* (6268), 74-77.
36. Brudvig, G. W.; Campagna, S., Introduction to a themed issue of Chemical Society Reviews on artificial photosynthesis. *Chem. Soc. Rev.* **2017,** *46* (20), 6085-6087.
37. (a) Halmann, M., Photoelectrochemical reduction of aqueous carbon dioxide on p-type gallium phosphide in liquid junction solar cells. *Nature* **1978,** *275* (5676), 115; (b) Kumar, B.; Llorente, M.; Froehlich, J.; Dang, T.; Sathrum, A.; Kubiak, C. P., Photochemical and photoelectrochemical reduction of CO_2. *Annu. Rev. Phys. Chem.* **2012,** *63*, 541-569; (c) Das, S.; Daud, W. W., RETRACTED: Photocatalytic CO2 transformation into fuel: A review on advances in photocatalyst and photoreactor. Elsevier: 2014; (d) Das, S.; Daud, W. W., A review on advances in photocatalysts towards CO_2 conversion. *RSC Adv.* **2014,** *4* (40), 20856-20893; (e) Xie, S.; Zhang, Q.; Liu, G.; Wang, Y., Photocatalytic and photoelectrocatalytic reduction of CO_2 using heterogeneous catalysts with controlled nanostructures. *Chem. Commun.* **2016,** *52* (1), 35-59.
38. Harriman, A.; Gratzel, M., Energy Resources through Photochemistry and Catalysis. *Academic Press, New York* **1983**, 163.
39. (a) Kanemoto, M.; Hosokawa, H.; Wada, Y.; Murakoshi, K.; Yanagida, S.; Sakata, T.; Mori, H.; Ishikawa, M.; Kobayashi, H., Semiconductor photocatalysis. Part 20.—Role of surface in the photoreduction of carbon dioxide catalysed by colloidal ZnS nanocrystallites in organic solvent. *J. Chem. Soc., Faraday Trans.* **1996,** *92* (13), 2401-2411; (b) Zhou, R.; Guzman, M. I., CO2 reduction under periodic illumination of ZnS. *J.Phys.Chem. C* **2014,** *118* (22), 11649-11656.
40. Chen, J.; Xin, F.; Qin, S.; Yin, X., Photocatalytically reducing CO_2 to methyl formate in methanol over ZnS and Ni-doped ZnS photocatalysts. *Chem. Eng. J.* **2013,** *230*, 506-512.
41. Kočí, K.; Reli, M.; Kozák, O.; Lacný, Z.; Plachá, D.; Praus, P.; Obalová, L., Influence of reactor geometry on the yield of CO_2 photocatalytic reduction. *Catal. Today* **2011,** *176* (1), 212-214.
42. Chaudhary, Y. S.; Woolerton, T. W.; Allen, C. S.; Warner, J. H.; Pierce, E.; Ragsdale, S. W.; Armstrong, F. A., Visible light-driven CO_2 reduction by enzyme coupled CdS nanocrystals. *Chem. Commun.* **2012,** *48* (1), 58-60.
43. Fujiwara, H.; Hosokawa, H.; Murakoshi, K.; Wada, Y.; Yanagida, S.; Okada, T.; Kobayashi, H., Effect of surface structures on photocatalytic CO_2 reduction using quantized CdS nanocrystallites. *The Journal of Physical Chemistry B* **1997,** *101* (41), 8270-8278.
44. Sasan, K.; Lin, Q.; Mao, C.; Feng, P., Open framework metal chalcogenides as efficient photocatalysts for reduction of CO_2 into renewable hydrocarbon fuel. *Nanoscale* **2016,** *8* (21), 10913-10916.

45. Liu, L.; Zhao, H.; Andino, J. M.; Li, Y., Photocatalytic CO2 reduction with H_2O on TiO_2 nanocrystals: Comparison of anatase, rutile, and brookite polymorphs and exploration of surface chemistry. *ACS Catal.* **2012,** *2* (8), 1817-1828.
46. Xie, S.; Wang, Y.; Zhang, Q.; Deng, W.; Wang, Y., MgO-and Pt-promoted TiO_2 as an efficient photocatalyst for the preferential reduction of carbon dioxide in the presence of water. *ACS Catal.* **2014,** *4* (10), 3644-3653.
47. Yan, Y.; Yu, Y.; Huang, S.; Yang, Y.; Yang, X.; Yin, S.; Cao, Y., Adjustment and matching of energy band of TiO2-based photocatalysts by metal Ions (Pd, Cu, Mn) for photoreduction of CO_2 into CH_4. *J.Phys.Chem. C* **2017,** *121* (2), 1089-1098.
48. Tahir, M.; Amin, N. S., Photocatalytic CO2 reduction and kinetic study over In/TiO_2 nanoparticles supported microchannel monolith photoreactor. *Applied Cat. A* **2013,** *467*, 483-496.
49. Tahir, M.; Amin, N. S., Indium-doped TiO_2 nanoparticles for photocatalytic CO_2 reduction with H_2O vapors to CH4. *Applied Cat. B* **2015,** *162*, 98-109.
50. Qin, G.; Zhang, Y.; Ke, X.; Tong, X.; Sun, Z.; Liang, M.; Xue, S., Photocatalytic reduction of carbon dioxide to formic acid, formaldehyde, and methanol using dye-sensitized TiO_2 film. *Applied Cat. B* **2013,** *129*, 599-605.
51. Finkelstein-Shapiro, D.; Petrosko, S. H.; Dimitrijevic, N. M.; Gosztola, D.; Gray, K. A.; Rajh, T.; Tarakeshwar, P.; Mujica, V., CO_2 preactivation in photoinduced reduction via surface functionalization of TiO_2 nanoparticles. *J. Phys. Chem. Lett.* **2013,** *4* (3), 475-479.
52. Sahara, G.; Kumagai, H.; Maeda, K.; Kaeffer, N.; Artero, V.; Higashi, M.; Abe, R.; Ishitani, O., Photoelectrochemical Reduction of CO_2 Coupled to Water Oxidation Using a Photocathode with a Ru (II)–Re (I) Complex Photocatalyst and a CoO x/TaON Photoanode. *J. Am. Chem. Soc.* **2016,** *138* (42), 14152-14158.
53. Kumagai, H.; Sahara, G.; Maeda, K.; Higashi, M.; Abe, R.; Ishitani, O., Hybrid photocathode consisting of a CuGaO 2 p-type semiconductor and a Ru (ii)–Re (i) supramolecular photocatalyst: non-biased visible-light-driven CO_2 reduction with water oxidation. *Chem. Sci.* **2017,** *8* (6), 4242-4249.
54. Kuriki, R.; Ishitani, O.; Maeda, K., Unique solvent effects on visible-light CO_2 reduction over ruthenium (II)-complex/carbon nitride hybrid photocatalysts. *ACS Appl. Mater. Inter.* **2016,** *8* (9), 6011-6018.
55. Sato, S.; Arai, T.; Morikawa, T.; Uemura, K.; Suzuki, T. M.; Tanaka, H.; Kajino, T., Selective CO_2 conversion to formate conjugated with H2O oxidation utilizing semiconductor/complex hybrid photocatalysts. *J. Am. Chem. Soc.* **2011,** *133* (39), 15240-15243.
56. Qin, S.; Xin, F.; Liu, Y.; Yin, X.; Ma, W., Photocatalytic reduction of CO_2 in methanol to methyl formate over CuO–TiO_2 composite catalysts. *J. Colloid Interf. Sci.* **2011,** *356* (1), 257-261.
57. Xiong, Z.; Lei, Z.; Kuang, C.-C.; Chen, X.; Gong, B.; Zhao, Y.; Zhang, J.; Zheng, C.; Wu, J. C., Selective photocatalytic reduction of CO_2 into CH4 over Pt-Cu_2O TiO_2 nanocrystals: the interaction between Pt and Cu_2O cocatalysts. *Applied Cat. B* **2017,** *202*, 695-703.
58. Chang, X.; Wang, T.; Zhang, P.; Wei, Y.; Zhao, J.; Gong, J., Stable Aqueous Photoelectrochemical CO_2 Reduction by a Cu_2O Dark Cathode with Improved Selectivity for Carbonaceous Products. *Angew. Chem., Int. Ed.* **2016,** *55* (31), 8840-8845.
59. Reli, M.; Huo, P.; Šihor, M.; Ambrožová, N.; Troppová, I.; Matějová, L.; Lang, J.; Svoboda, L.; Kuśtrowski, P.; Ritz, M., Novel TiO_2/C_3N_4 photocatalysts for photocatalytic reduction of CO_2 and for photocatalytic decomposition of N_2O. *J. Phys. Chem. A* **2016,** *120* (43), 8564-8573.
60. Shi, H.; Zhang, C.; Zhou, C.; Chen, G., Conversion of CO_2 into renewable fuel over Pt–gC_3N_4/$KNbO_3$ composite photocatalyst. *RSC Adv.* **2015,** *5* (113), 93615-93622.

61. Shi, H.; Chen, G.; Zhang, C.; Zou, Z., Polymeric g-C3N4 coupled with $NaNbO_3$ nanowires toward enhanced photocatalytic reduction of CO_2 into renewable fuel. *ACS Catal.* **2014,** *4* (10), 3637-3643.
62. Sakimoto, K. K.; Zhang, S. J.; Yang, P., Cysteine–Cystine Photoregeneration for Oxygenic Photosynthesis of Acetic Acid from CO_2 by a Tandem Inorganic–Biological Hybrid System. *Nano Lett.* **2016,** *16* (9), 5883-5887.
63. Wang, C.; Thompson, R. L.; Baltrus, J.; Matranga, C., Visible light photoreduction of CO2 using CdSe/Pt/TiO_2 heterostructured catalysts. *J. Phys. Chem. Lett.* **2009,** *1* (1), 48-53.
64. (a) Chen, Y.; Li, C. W.; Kanan, M. W., Aqueous CO_2 reduction at very low overpotential on oxide-derived Au nanoparticles. *J. Am. Chem. Soc.* **2012,** *134* (49), 19969-19972; (b) Kim, D.; Resasco, J.; Yu, Y.; Asiri, A. M.; Yang, P., Synergistic geometric and electronic effects for electrochemical reduction of carbon dioxide using gold–copper bimetallic nanoparticles. *Nat. Commun.* **2014,** *5*, 4948.
65. Koike, T.; Akita, M., Visible-light radical reaction designed by Ru- and Ir-based photoredox catalysis. *Inorg. Chem. Front.* **2014,** *1* (8), 562-576.
66. Whitten, D. G., Photoinduced electron transfer reactions of metal complexes in solution. *Acc. Chem. Res.* **1980,** *13* (3), 83-90.
67. Tinnemans, A.; Koster, T.; Thewissen, D.; Mackor, A., Tetraaza-macrocyclic cobalt (II) and nickel (II) complexes as electron-transfer agents in the photo (electro) chemical and electrochemical reduction of carbon dioxide. *Recueil des Travaux Chimiques des Pays-Bas* **1984,** *103* (10), 288-295.
68. Morris, A. J.; Meyer, G. J.; Fujita, E., Molecular approaches to the photocatalytic reduction of carbon dioxide for solar fuels. *Acc. Chem. Res.* **2009,** *42* (12), 1983-1994.
69. (a) Matsuoka, S.; Yamamoto, K.; Pac, C.; Yanagida, S., Enhanced p-Terphenyl-Catalyzed Photoreduction of CO_2 to CO through the Mediation of Co (III)–Cyclam Complex. *Chem. Lett.* **1991,** *20* (12), 2099-2100; (b) Matsuoka, S.; Yamamoto, K.; Ogata, T.; Kusaba, M.; Nakashima, N.; Fujita, E.; Yanagida, S., Efficient and selective electron mediation of cobalt complexes with cyclam and related macrocycles in the p-terphenyl-catalyzed photoreduction of carbon dioxide. *J. Am. Chem. Soc.* **1993,** *115* (2), 601-609.
70. Fujita, E., Photochemical Carbon Dioxide Reduction with Metal Complexes. *Coord. Chem. Rev.* **1999,** *185-186*, 373-384.
71. Guo, Z.; Cheng, S.; Cometto, C.; Anxolabéhère-Mallart, E.; Ng, S.-M.; Ko, C.-C.; Liu, G.; Chen, L.; Robert, M.; Lau, T.-C., Highly efficient and selective photocatalytic CO_2 reduction by iron and cobalt quaterpyridine complexes. *J. Am. Chem. Soc.* **2016,** *138* (30), 9413-9416.
72. Chan, S. L.-F.; Lam, T. L.; Yang, C.; Yan, S.-C.; Cheng, N. M., A robust and efficient cobalt molecular catalyst for CO_2 reduction. *Chem. Commun.* **2015,** *51* (37), 7799-7801.
73. Yang, C.; Mehmood, F.; Lam, T. L.; Chan, S. L.-F.; Wu, Y.; Yeung, C.-S.; Guan, X.; Li, K.; Chung, C. Y.-S.; Zhou, C.-Y., Stable luminescent iridium (iii) complexes with bis (N-heterocyclic carbene) ligands: photo-stability, excited state properties, visible-light-driven radical cyclization and CO_2 reduction, and cellular imaging. *Chem. Sci.* **2016,** *7* (5), 3123-3136.
74. Takeda, H.; Ohashi, K.; Sekine, A.; Ishitani, O., Photocatalytic CO_2 reduction using Cu (I) photosensitizers with a Fe (II) catalyst. *J. Am. Chem. Soc.* **2016,** *138* (13), 4354-4357.
75. Hawecker, J.; Lehn, J.-M.; Ziessel, R., Efficient photochemical reduction of CO 2 to CO by visible light irradiation of systems containing Re (bipy)$(CO)_3X$ or Ru $(bipy)_3^{2+}$–Co^{2+} combinations as homogeneous catalysts. *J. Chem. Soc., Chem. Commun.* **1983,** (9), 536-538.
76. Hayashi, Y.; Kita, S.; Brunschwig, B. S.; Fujita, E., Involvement of a Binuclear Species with the Re− C (O) O− Re Moiety in CO_2 Reduction Catalyzed by Tricarbonyl Rhenium (I)

Complexes with Diimine Ligands: Strikingly Slow Formation of the Re− Re and Re− C (O) O− Re Species from Re (dmb)(CO) 3S (dmb= 4, 4 '-Dimethyl-2, 2 '-bipyridine, S= Solvent). *J. Am. Chem. Soc.* **2003,** *125* (39), 11976-11987.
77. Sullivan, B. P.; Meyer, T. J., Kinetics and mechanism of CO_2 insertion into a metal-hydride bond. A large solvent effect and an inverse kinetic isotope effect. *Organometallics* **1986,** *5* (7), 1500-1502.
78. Creutz, C.; Chou, M. H., Rapid transfer of hydride ion from a ruthenium complex to C_1 species in water. *J. Am. Chem. Soc.* **2007,** *129* (33), 10108-10109.
79. (a) Gibson, D. H.; Yin, X., Synthesis and Reactions of fac-Re (dmbpy)$(CO)_3$X (dmbpy= 4, 4 '-dimethyl-2, 2 '-bipyridyl; X= COOH, COOMe, H, OH, and OCHO). *J. Am. Chem. Soc.* **1998,** *120* (43), 11200-11201; (b) Gibson, D. H.; Yin, X.; He, H.; Mashuta, M. S., Synthesis and Reactions of fac-[Re (dmbpy)(CO) 3X](dmbpy= 4, 4 '-Dimethyl-2, 2 '-bipyridine; X= COOH, CHO) and Their Derivatives. *Organometallics* **2003,** *22* (2), 337-346.
80. Schreier, M.; Gao, P.; Mayer, M. T.; Luo, J.; Moehl, T.; Nazeeruddin, M. K.; Tilley, S. D.; Grätzel, M., Efficient and selective carbon dioxide reduction on low cost protected Cu 2 O photocathodes using a molecular catalyst. *Energy Environ. Sci.* **2015,** *8* (3), 855-861.
81. Schreier, M.; Luo, J.; Gao, P.; Moehl, T.; Mayer, M. T.; Grätzel, M., Covalent immobilization of a molecular catalyst on Cu2O photocathodes for CO_2 reduction. *J. Am. Chem. Soc.* **2016,** *138* (6), 1938-1946.
82. Gholamkhass, B.; Mametsuka, H.; Koike, K.; Tanabe, T.; Furue, M.; Ishitani, O., Architecture of Supramolecular Metal Complexes for Photocatalytic CO_2 Reduction: Ruthenium− Rhenium Bi-and Tetranuclear Complexes. *Inorg. Chem.* **2005,** *44* (7), 2326-2336.
83. (a) Bourrez, M.; Orio, M.; Molton, F.; Vezin, H.; Duboc, C.; Deronzier, A.; Chardon-Noblat, S., Pulsed-EPR Evidence of a Manganese (II) Hydroxycarbonyl Intermediate in the Electrocatalytic Reduction of Carbon Dioxide by a Manganese Bipyridyl Derivative. *Angew. Chem., Int. Ed.* **2014,** *53* (1), 240-243; (b) Sampson, M. D.; Nguyen, A. D.; Grice, K. A.; Moore, C. E.; Rheingold, A. L.; Kubiak, C. P., Manganese catalysts with bulky bipyridine ligands for the electrocatalytic reduction of carbon dioxide: Eliminating dimerization and altering catalysis. *J. Am. Chem. Soc.* **2014,** *136* (14), 5460-5471.
84. (a) Grodkowski, J.; Behar, D.; Neta, P.; Hambright, P., Iron porphyrin-catalyzed reduction of CO_2. Photochemical and radiation chemical studies. *J. Phys. Chem. A* **1997,** *101* (3), 248-254; (b) Behar, D.; Dhanasekaran, T.; Neta, P.; Hosten, C.; Ejeh, D.; Hambright, P.; Fujita, E., Cobalt porphyrin catalyzed reduction of CO_2. Radiation chemical, photochemical, and electrochemical studies. *J. Phys. Chem. A* **1998,** *102* (17), 2870-2877; (c) Grodkowski, J.; Dhanasekaran, T.; Neta, P.; Hambright, P.; Brunschwig, B. S.; Shinozaki, K.; Fujita, E., Reduction of cobalt and iron phthalocyanines and the role of the reduced species in catalyzed photoreduction of CO_2. *J. Phys. Chem. A* **2000,** *104* (48), 11332-11339; (d) Grodkowski, J.; Neta, P., Cobalt corrin catalyzed photoreduction of CO_2. *J. Phys. Chem. A* **2000,** *104* (9), 1848-1853; (e) Grodkowski, J.; Neta, P.; Fujita, E.; Mahammed, A.; Simkhovich, L.; Gross, Z., Reduction of cobalt and iron corroles and catalyzed reduction of CO2. *J. Phys. Chem. A* **2002,** *106* (18), 4772-4778.
85. Dhanasekaran, T.; Grodkowski, J.; Neta, P.; Hambright, P.; Fujita, E., P-terphenyl-sensitized photoreduction of CO_2 with cobalt and iron porphyrins. Interaction between CO and reduced metalloporphyrins. *J. Phys. Chem. A* **1999,** *103* (38), 7742-7748.
86. Fujita, E.; Creutz, C.; Sutin, N.; Szalda, D. J., Carbon dioxide activation by cobalt (I) macrocycles: factors affecting carbon dioxide and carbon monoxide binding. *J. Am. Chem. Soc.* **1991,** *113* (1), 343-353.

87. Hammouche, M.; Lexa, D.; Momenteau, M.; Saveant, J. M., Chemical catalysis of electrochemical reactions. Homogeneous catalysis of the electrochemical reduction of carbon dioxide by iron ("0") porphyrins. Role of the addition of magnesium cations. *J. Am. Chem. Soc.* **1991,** *113* (22), 8455-8466.
88. Lian, S.; Kodaimati, M. S.; Dolzhnikov, D. S.; Calzada, R.; Weiss, E. A., Powering a CO_2 Reduction Catalyst with Visible Light through Multiple Sub-picosecond Electron Transfers from a Quantum Dot. *J. Am. Chem. Soc.* **2017,** *139* (26), 8931-8938.
89. Bonin, J.; Chaussemier, M.; Robert, M.; Routier, M., Homogeneous photocatalytic reduction of CO_2 to CO using iron (0) porphyrin catalysts: mechanism and intrinsic limitations. *ChemCatChem* **2014,** *6* (11), 3200-3207.
90. Bonin, J.; Robert, M.; Routier, M., Selective and Efficient Photocatalytic CO_2 Reduction to CO Using Visible Light and an Iron-Based Homogeneous Catalyst. *J. Am. Chem. Soc.* **2014,** *136* (48), 16768-16771.
91. Lin, L.; Hou, C.; Zhang, X.; Wang, Y.; Chen, Y.; He, T., Highly efficient visible-light driven photocatalytic reduction of CO_2 over g-C3N4 nanosheets/tetra (4-carboxyphenyl) porphyrin iron (III) chloride heterogeneous catalysts. *Applied Cat. B* **2018,** *221*, 312-319.
92. Zhao, G.; Pang, H.; Liu, G.; Li, P.; Liu, H.; Zhang, H.; Shi, L.; Ye, J., Co-porphyrin/carbon nitride hybrids for improved photocatalytic CO_2 reduction under visible light. *Applied Cat. B* **2017,** *200*, 141-149.
93. Trickett, C. A.; Helal, A.; Al-Maythalony, B. A.; Yamani, Z. H.; Cordova, K. E.; Yaghi, O. M., The chemistry of metal–organic frameworks for CO_2 capture, regeneration and conversion. *Nature Reviews Materials* **2017,** *2* (8), 17045.
94. Tripkovic, V.; Vanin, M.; Karamad, M.; Björketun, M. r. E.; Jacobsen, K. W.; Thygesen, K. S.; Rossmeisl, J., Electrochemical CO_2 and CO reduction on metal-functionalized porphyrin-like graphene. *J.Phys.Chem. C* **2013,** *117* (18), 9187-9195.
95. Shen, J.; Kolb, M. J.; Gottle, A. J.; Koper, M. T., DFT study on the mechanism of the electrochemical reduction of CO_2 catalyzed by cobalt porphyrins. *J.Phys.Chem. C* **2016,** *120* (29), 15714-15721.
96. Costentin, C.; Drouet, S.; Robert, M.; Savéant, J.-M., A Local Proton Source Enhances CO_2 Electroreduction to CO by a Molecular Fe Catalyst. *Science* **2012,** *338* (6103), 90-94.
97. (a) Kapusta, S.; Hackerman, N., Carbon dioxide reduction at a metal phthalocyanine catalyzed carbon electrode. *J. Electrochem. Soc.* **1984,** *131* (7), 1511-1514; (b) Sonoyama, N.; Kirii, M.; Sakata, T., Electrochemical reduction of CO_2 at metal-porphyrin supported gas diffusion electrodes under high pressure CO_2. *Electrochem. Commun.* **1999,** *1* (6), 213-216.
98. Huckaba, A. J.; Sharpe, E. A.; Delcamp, J. H., Photocatalytic Reduction of CO_2 with Re-Pyridyl-NHCs. *Inorg. Chem.* **2015,** *55* (2), 682-690.
99. (a) Bediako, D. K.; Costentin, C.; Jones, E. C.; Nocera, D. G.; Saveant, J.-M., Proton-Electron Transport and Transfer in Electrocatalytic Films. Application to a Cobalt-Based O_2-Evolution Catalyst. *J. Am. Chem. Soc.* **2013,** *135* (28), 10492–10502; (b) Rakowski Dubois, M.; Dubois, D. L., Development of molecular electrocatalysts for CO_2 reduction and H2 production/oxidation. *Acc. Chem. Res.* **2009,** *42* (12), 1974-1982.
100. (a) Chen, L.; Guo, Z.; Wei, X.-G.; Gallenkamp, C.; Bonin, J.; Anxolabéhère-Mallart, E.; Lau, K.-C.; Lau, T.-C.; Robert, M., Molecular catalysis of the electrochemical and photochemical reduction of CO_2 with Earth-abundant metal complexes. Selective production of CO vs HCOOH by switching of the metal center. *J. Am. Chem. Soc.* **2015,** *137* (34), 10918-10921; (b) Costentin, C.; Robert, M.; Savéant, J.-M., Current issues in molecular catalysis illustrated by iron porphyrins as catalysts of the CO_2-to-CO electrochemical conversion. *Acc. Chem. Res.* **2015,** *48*

(12), 2996-3006; (c) Bonin, J.; Maurin, A.; Robert, M., Molecular catalysis of the electrochemical and photochemical reduction of CO_2 with Fe and Co metal based complexes. Recent advances. *Coord. Chem. Rev.* **2017,** *334*, 184-198; (d) Takeda, H.; Cometto, C.; Ishitani, O.; Robert, M., Electrons, photons, protons and earth-abundant metal complexes for molecular catalysis of CO_2 reduction. *ACS Catal.* **2016,** *7* (1), 70-88.
101. (a) Kalyanasundaram, K., Luminescence and redox reactions of the metal-to-ligand charge-transfer excited state of tricarbonylchloro-(polypyridyl) rhenium (I) complexes. *J. Chem. Soc., Faraday Trans. 2* **1986,** *82* (12), 2401-2415; (b) Lees, A. J., Luminescence properties of organometallic complexes. *Chem. Rev.* **1987,** *87* (4), 711-743; (c) Meyer, T. J., Chemical approaches to artificial photosynthesis. *Acc. Chem. Res.* **1989,** *22* (5), 163-170; (d) Kirgan, R. A.; Sullivan, B. P.; Rillema, D. P., Photochemistry and photophysics of coordination compounds: rhenium. In *Photochemistry and Photophysics of Coordination Compounds II*, Springer: 2007; pp 45-100.
102. Maurin, A.; Ng, C.-O.; Chen, L.; Lau, T.-C.; Robert, M.; Ko, C.-C., Photochemical and electrochemical catalytic reduction of CO_2 with NHC-containing dicarbonyl rhenium (I) bipyridine complexes. *Dalton Trans.* **2016,** *45* (37), 14524-14529.
103. (a) Yuan, Y. J.; Yu, Z. T.; Chen, X. Y.; Zhang, J. Y.; Zou, Z. G., Visible-Light-Driven H_2 Generation from Water and CO_2 Conversion by Using a Zwitterionic Cyclometalated Iridium (III) Complex. *Chemistry–A European Journal* **2011,** *17* (46), 12891-12895; (b) Sato, S.; Morikawa, T.; Kajino, T.; Ishitani, O., A highly efficient mononuclear iridium complex photocatalyst for CO_2 reduction under visible light. *Angewandte Chemie* **2013,** *125* (3), 1022-1026; (c) Genoni, A.; Chirdon, D. N.; Boniolo, M.; Sartorel, A.; Bernhard, S.; Bonchio, M., Tuning iridium photocatalysts and light irradiation for enhanced CO_2 reduction. *ACS Catal.* **2016,** *7* (1), 154-160.
104. Rao, H.; Bonin, J.; Robert, M., Non-sensitized selective photochemical reduction of CO_2 to CO under visible light with an iron molecular catalyst. *Chem. Commun.* **2017,** *53* (19), 2830-2833.
105. (a) Tamaki, Y.; Koike, K.; Morimoto, T.; Ishitani, O., Substantial Improvement in the Efficiency and Durability of a Photocatalyst for Carbon Dioxide Reduction using a Benzoimidazole Derivative as an Electron Donor. *J. Catal.* **2013,** *304*, 22-28; (b) Kuramochi, Y.; Ishitani, O., Iridium (III) 1-phenylisoquinoline complexes as a photosensitizer for photocatalytic CO_2 reduction: a mixed system with a Re (I) catalyst and a supramolecular photocatalyst. *Inorg. Chem.* **2016,** *55* (11), 5702-5709.
106. Hasegawa, E.; Takizawa, S.; Seida, T.; Yamaguchi, A.; Yamaguchi, N.; Chiba, N.; Takahashi, T.; Ikeda, H.; Akiyama, K., Photoinduced electron-transfer systems consisting of electron-donating pyrenes or anthracenes and benzimidazolines for reductive transformation of carbonyl compounds. *Tetrahedron* **2006,** *62* (27), 6581-6588.
107. Costentin, C.; Drouet, S.; Passard, G.; Robert, M.; Savéant, J.-M., Proton-coupled electron transfer cleavage of heavy-atom bonds in electrocatalytic processes. Cleavage of a C–O bond in the catalyzed electrochemical reduction of CO_2. *J. Am. Chem. Soc.* **2013,** *135* (24), 9023-9031.
108. (a) Costentin, C.; Dridi, H.; Savéant, J.-M., Molecular catalysis of H_2 evolution: Diagnosing heterolytic versus homolytic pathways. *J. Am. Chem. Soc.* **2014,** *136* (39), 13727-13734; (b) Costentin, C.; Passard, G.; Robert, M.; Savéant, J.-M., Ultraefficient Homogeneous Catalyst for the CO_2-to-CO Electrochemical Conversion. *Proc. Natl. Acad. Sci. U.S.A.* **2014,** *111* (42), 14990-14994.

109. Costentin, C.; Robert, M.; Savéant, J.-M.; Tatin, A., Efficient and Selective Molecular Catalyst for the CO_2-to-CO Electrochemical Conversion in Water. *Proc. Natl. Acad. Sci. U.S.A.* **2015,** *112* (22), 6882-6886.
110. Azcarate, I.; Costentin, C.; Robert, M.; Savéant, J.-M., Through-space charge interaction substituent effects in molecular catalysis leading to the design of the most efficient catalyst of CO_2-to-CO electrochemical conversion. *J. Am. Chem. Soc.* **2016,** *138* (51), 16639-16644.
111. Bara, J. E.; Carlisle, T. K.; Gabriel, C. J.; Camper, D.; Finotello, A.; Gin, D. L.; Noble, R. D., Guide to CO_2 separations in imidazolium-based room-temperature ionic liquids. *Ind. Eng. Chem. Res.* **2009,** *48* (6), 2739-2751.
112. Rao, H.; Bonin, J.; Robert, M., Visible-light Homogeneous Photocatalytic Conversion of CO_2 into CO in Aqueous Solutions with an Iron Catalyst. *ChemSusChem* **2017,** *10* (22), 4447-4450.
113. Miliani, C.; Romani, A.; Favaro, G., Acidichromic effects in 1, 2-di-and 1, 2, 4-tri-hydroxyanthraquinones. A spectrophotometric and fluorimetric study. *J. Phys. Org. Chem.* **2000,** *13* (3), 141-150.
114. Pellegrin, Y.; Odobel, F., Sacrificial Electron Donor Reagents for Solar Fuel Production. *C. R. Chim.* **2017,** *20* (3), 283-295.
115. Tan, J. A.; Garakyaraghi, S.; Tagami, K. A.; Frano, K. A.; Crockett, H. M.; Ogata, A. F.; Patterson, J. D.; Wustholz, K. L., Contributions from excited-state proton and electron transfer to the blinking and photobleaching dynamics of alizarin and purpurin. *J.Phys.Chem. C* **2016,** *121* (1), 97-106.
116. Rao, H.; Schmidt, L. C.; Bonin, J.; Robert, M., Visible-light-driven methane formation from CO_2 with a molecular iron catalyst. *Nature* **2017,** *548* (7665), 74.
117. Cohen, S. G.; Parola, A.; Parsons Jr, G. H., Photoreduction by amines. *Chem. Rev.* **1973,** *73* (2), 141-161.
118. Donaldson, T. L.; Nguyen, Y. N., Carbon dioxide reaction kinetics and transport in aqueous amine membranes. *Industrial & Engineering Chemistry Fundamentals* **1980,** *19* (3), 260-266.
119. Vaidya, P. D.; Kenig, E. Y., CO_2-alkanolamine reaction kinetics: a review of recent studies. *Chemical Engineering & Technology* **2007,** *30* (11), 1467-1474.
120. Liu, Q.; Yang, X.; Li, L.; Miao, S.; Li, Y.; Li, Y.; Wang, X.; Huang, Y.; Zhang, T., Direct catalytic hydrogenation of CO_2 to formate over a Schiff-base-mediated gold nanocatalyst. *Nat. Commun.* **2017,** *8* (1), 1407.
121. Sutin, N.; Brunschwig, B. S. *Electron transfer in weakly interacting systems*; Brookhaven National Lab.: 1981.
122. (a) Ma, S.; Kenis, P. J., Electrochemical conversion of CO2 to useful chemicals: current status, remaining challenges, and future opportunities. *Curr. Opin. Chem. Eng.* **2013,** *2* (2), 191-199; (b) Aresta, M.; Dibenedetto, A.; Angelini, A., Catalysis for the valorization of exhaust carbon: from CO_2 to chemicals, materials, and fuels. Technological use of CO_2. *Chem. Rev.* **2013,** *114* (3), 1709-1742.
123. (a) Parajuli, R.; Gerken, J. B.; Keyshar, K.; Sullivan, I.; Sivasankar, N.; Teamey, K.; Stahl, S. S.; Cole, E. B., Integration of anodic and cathodic catalysts of Earth-abundant materials for efficient, scalable CO_2 reduction. *Top. Catal.* **2015,** *58* (1), 57-66; (b) Tatin, A.; Comminges, C.; Kokoh, B.; Costentin, C.; Robert, M.; Savéant, J.-M., Efficient electrolyzer for CO_2 splitting in neutral water using earth-abundant materials. *Proc. Natl. Acad. Sci. U.S.A.* **2016,** *113* (20), 5526-5529.

124. Sahara, G.; Ishitani, O., Efficient Photocatalysts for CO_2 Reduction. *Inorg. Chem.* **2015,** *54* (11), 5096-5104.
125. Shen, J.; Kortlever, R.; Kas, R.; Birdja, Y. Y.; Diaz-Morales, O.; Kwon, Y.; Ledezma-Yanez, I.; Schouten, K. J. P.; Mul, G.; Koper, M. T., Electrocatalytic reduction of carbon dioxide to carbon monoxide and methane at an immobilized cobalt protoporphyrin. *Nat. Commun.* **2015,** *6*, 8177.
126. Weng, Z.; Jiang, J.; Wu, Y.; Wu, Z.; Guo, X.; Materna, K. L.; Liu, W.; Batista, V. S.; Brudvig, G. W.; Wang, H., Electrochemical CO_2 reduction to hydrocarbons on a heterogeneous molecular Cu catalyst in aqueous solution. *J. Am. Chem. Soc.* **2016,** *138* (26), 8076-8079.
127. (a) Manthiram, K.; Beberwyck, B. J.; Alivisatos, A. P., Enhanced electrochemical methanation of carbon dioxide with a dispersible nanoscale copper catalyst. *J. Am. Chem. Soc.* **2014,** *136* (38), 13319-13325; (b) Xie, M. S.; Xia, B. Y.; Li, Y.; Yan, Y.; Yang, Y.; Sun, Q.; Chan, S. H.; Fisher, A.; Wang, X., Amino acid modified copper electrodes for the enhanced selective electroreduction of carbon dioxide towards hydrocarbons. *Energy Environ. Sci.* **2016,** *9* (5), 1687-1695.
128. Weng, Z.; Wu, Y.; Wang, M.; Jiang, J.; Yang, K.; Huo, S.; Wang, X.-F.; Ma, Q.; Brudvig, G. W.; Batista, V. S., Active sites of copper-complex catalytic materials for electrochemical carbon dioxide reduction. *Nat. Commun.* **2018,** *9* (1), 415.
129. Wu, T.; Zou, L.; Han, D.; Li, F.; Zhang, Q.; Niu, L., A carbon-based photocatalyst efficiently converts CO_2 to CH_4 and C_2H_2 under visible light. *Green Chem.* **2014,** *16* (4), 2142-2146.
130. Chen, J.; Falivene, L.; Caporaso, L.; Cavallo, L.; Chen, E. Y.-X., Selective Reduction of CO_2 to CH_4 by Tandem Hydrosilylation with Mixed Al/B Catalysts. *J. Am. Chem. Soc.* **2016,** *138* (16), 5321-5333.
131. (a) AlOtaibi, B.; Fan, S.; Wang, D.; Ye, J.; Mi, Z., Wafer-Level Artificial Photosynthesis for CO_2 Reduction into CH_4 and CO Using GaN Nanowires. *ACS Catal.* **2015,** *5* (9), 5342-5348; (b) Liu, X.; Inagaki, S.; Gong, J., Heterogeneous Molecular Systems for Photocatalytic CO_2 Reduction with Water Oxidation. *Angew. Chem., Int. Ed.* **2016,** *55* (48), 14924-14950; (c) Wang, H.; Chen, Y.; Hou, X.; Ma, C.; Tan, T., Nitrogen-doped graphenes as efficient electrocatalysts for the selective reduction of carbon dioxide to formate in aqueous solution. *Green Chem.* **2016,** *18* (11), 3250-3256; (d) Ong, W.-J.; Putri, L. K.; Tan, Y.-C.; Tan, L.-L.; Li, N.; Ng, Y. H.; Wen, X.; Chai, S.-P., Unravelling charge carrier dynamics in protonated gC_3N_4 interfaced with carbon nanodots as co-catalysts toward enhanced photocatalytic CO_2 reduction: A combined experimental and first-principles DFT study. *Nano Research* **2017,** *10* (5), 1673-1696; (e) Yu, L.; Li, G.; Zhang, X.; Ba, X.; Shi, G.; Li, Y.; Wong, P. K.; Yu, J. C.; Yu, Y., Enhanced activity and stability of carbon-decorated cuprous oxide mesoporous nanorods for CO_2 reduction in artificial photosynthesis. *ACS Catal.* **2016,** *6* (10), 6444-6454.
132. Primer, D. N.; Karakaya, I.; Tellis, J. C.; Molander, G. A., Single-electron transmetalation: an enabling technology for secondary alkylboron cross-coupling. *J. Am. Chem. Soc.* **2015,** *137* (6), 2195-2198.
133. Prier, C. K.; Rankic, D. A.; MacMillan, D. W., Visible light photoredox catalysis with transition metal complexes: applications in organic synthesis. *Chem. Rev.* **2013,** *113* (7), 5322-5363.
134. Costentin, C.; Passard, G.; Robert, M.; Savéant, J.-M., Pendant acid–base groups in molecular catalysts: H-bond promoters or proton relays? Mechanisms of the conversion of CO_2 to CO by electrogenerated iron (0) porphyrins bearing prepositioned phenol functionalities. *J. Am. Chem. Soc.* **2014,** *136* (33), 11821-11829.

135. Bhugun, I.; Lexa, D.; Savéant, J.-M., Homogeneous catalysis of electrochemical hydrogen evolution by iron (0) porphyrins. *J. Am. Chem. Soc.* **1996,** *118* (16), 3982-3983.
136. Wang, Y.; Bai, X.; Qin, H.; Wang, F.; Li, Y.; Li, X.; Kang, S.; Zuo, Y.; Cui, L., Facile One-Step Synthesis of Hybrid Graphitic Carbon Nitride and Carbon Composites as High-Performance Catalysts for CO_2 Photocatalytic Conversion. *ACS Appl. Mater. Inter.* **2016,** *8* (27), 17212-17219.
137. (a) Chow, Y. L.; Danen, W. C.; Nelsen, S. F.; Rosenblatt, D. H., Nonaromatic aminium radicals. *Chem. Rev.* **1978,** *78* (3), 243-274; (b) Miller, L. L.; Nordblom, G.; Mayeda, E. A., Simple, comprehensive correlation of organic oxidation and ionization potentials. *The Journal of Organic Chemistry* **1972,** *37* (6), 916-918; (c) Smith, J. R. L.; Masheder, D., Amine oxidation. Part IX. The electrochemical oxidation of some tertiary amines: the effect of structure on reactivity. *J. Chem. Soc., Perkin Trans. 2* **1976,** (1), 47-51.
138. (a) Appel, A. M.; Bercaw, J. E.; Bocarsly, A. B.; Dobbek, H.; DuBois, D. L.; Dupuis, M.; Ferry, J. G.; Fujita, E.; Hille, R.; Kenis, P. J., Frontiers, opportunities, and challenges in biochemical and chemical catalysis of CO_2 fixation. *Chem. Rev.* **2013,** *113* (8), 6621-6658; (b) Hsieh, E. T.; Randall, J. C., Monomer sequence distributions in ethylene-1-hexene copolymers. *Macromolecules* **1982,** *15* (5), 1402-1406.
139. (a) Mochizuki, K.; Manaka, S.; Takeda, I.; Kondo, T., Synthesis and Structure of [6, 6 '-Bi (5, 7-dimethyl-1, 4, 8, 11-tetraazacyclotetradecane)] dinickel (II) Triflate and Its Catalytic Activity for Photochemical CO_2 Reduction. *Inorg. Chem.* **1996,** *35* (18), 5132-5136; (b) Neri, G.; Forster, M.; Walsh, J. J.; Robertson, C.; Whittles, T.; Farràs, P.; Cowan, A. J., Photochemical CO_2 reduction in water using a co-immobilised nickel catalyst and a visible light sensitiser. *Chem. Commun.* **2016,** *52* (99), 14200-14203; (c) Kuehnel, M. F.; Orchard, K. L.; Dalle, K. E.; Reisner, E., Selective photocatalytic CO_2 reduction in water through anchoring of a molecular Ni catalyst on CdS nanocrystals. *J. Am. Chem. Soc.* **2017,** *139* (21), 7217-7223.
140. Koike, T.; Akita, M., Visible-light radical reaction designed by Ru-and Ir-based photoredox catalysis. *Inorg. Chem. Front.* **2014,** *1* (8), 562-576.
141. (a) Garces, F.; King, K.; Watts, R., Synthesis, structure, electrochemistry, and photophysics of methyl-substituted phenylpyridine ortho-metalated iridium (III) complexes. *Inorg. Chem.* **1988,** *27* (20), 3464-3471; (b) Hallett, A. J.; White, N.; Wu, W.; Cui, X.; Horton, P. N.; Coles, S. J.; Zhao, J.; Pope, S. J., Enhanced photooxidation sensitizers: the first examples of cyclometalated pyrene complexes of iridium (III). *Chem. Commun.* **2012,** *48* (88), 10838-10840; (c) Sun, J.; Zhong, F.; Yi, X.; Zhao, J., Efficient Enhancement of the Visible-Light Absorption of Cyclometalated Ir (III) Complexes Triplet Photosensitizers with Bodipy and Applications in Photooxidation and Triplet–Triplet Annihilation Upconversion. *Inorg. Chem.* **2013,** *52* (11), 6299-6310.
142. (a) Ohsawa, Y.; Sprouse, S.; King, K.; DeArmond, M.; Hanck, K.; Watts, R., Electrochemistry and spectroscopy of ortho-metalated complexes of iridium (III) and rhodium (III). *J. Phys. Chem.* **1987,** *91* (5), 1047-1054; (b) Call, A.; Codolà, Z.; Acuña-Parés, F.; Lloret-Fillol, J., Photo-and Electrocatalytic H2 Production by New First-Row Transition-Metal Complexes Based on an Aminopyridine Pentadentate Ligand. *Chemistry–A European Journal* **2014,** *20* (20), 6171-6183; (c) Song, X.; Wen, H.; Ma, C.; Chen, H.; Chen, C., Hydrogen Photogeneration Catalyzed by a Cobalt Complex of a Pentadentate Aminopyridine-based Ligand. *New J. Chem.* **2015,** *39* (3), 1734-1741.
143. Sajoto, T.; Djurovich, P. I.; Tamayo, A. B.; Oxgaard, J.; Goddard III, W. A.; Thompson, M. E., Temperature dependence of blue phosphorescent cyclometalated Ir (III) complexes. *J. Am. Chem. Soc.* **2009,** *131* (28), 9813-9822.

144. McTiernan, C.; Morin, M.; McCallum, T.; Scaiano, J.; Barriault, L., Polynuclear gold (I) complexes in photoredox catalysis: understanding their reactivity through characterization and kinetic analysis. *Catal. Sci. Technol.* **2016,** *6* (1), 201-207.
145. Kuboki, A.; Sekiguchi, T.; Sugai, T.; Ohta, H., A Facile Access to Aryl α-Sialosides: the Combination of a Volatile Amine Base and Acetonitrile in Glycosidation of Sialosyl Chlorides. *Synlett* **1998,** *1998* (05), 479-482.
146. (a) Gärtner, F.; Sundararaju, B.; Surkus, A. E.; Boddien, A.; Loges, B.; Junge, H.; Dixneuf, P. H.; Beller, M., Light-Driven Hydrogen Generation: Efficient Iron-Based Water Reduction Catalysts. *Angew. Chem., Int. Ed.* **2009,** *48* (52), 9962-9965; (b) Zhang, P.; Jacques, P.-A.; Chavarot-Kerlidou, M.; Wang, M.; Sun, L.; Fontecave, M.; Artero, V., Phosphine coordination to a cobalt diimine–dioxime catalyst increases stability during light-driven H2 production. *Inorg. Chem.* **2012,** *51* (4), 2115-2120; (c) Yuan, Y.-J.; Yu, Z.-T.; Chen, D.-Q.; Zou, Z.-G., Metal-complex Chromophores for Solar Hydrogen Generation. *Chem. Soc. Rev.* **2017,** *46* (3), 603-631.
147. (a) Goldsmith, J. I.; Hudson, W. R.; Lowry, M. S.; Anderson, T. H.; Bernhard, S., Discovery and high-throughput screening of heteroleptic iridium complexes for photoinduced hydrogen production. *J. Am. Chem. Soc.* **2005,** *127* (20), 7502-7510; (b) Cline, E. D.; Adamson, S. E.; Bernhard, S., Homogeneous catalytic system for photoinduced hydrogen production utilizing iridium and rhodium complexes. *Inorg. Chem.* **2008,** *47* (22), 10378-10388; (c) Zhang, P.; Wang, M.; Na, Y.; Li, X.; Jiang, Y.; Sun, L., Homogeneous photocatalytic production of hydrogen from water by a bioinspired $[Fe_2S_2]$ catalyst with high turnover numbers. *Dalton Trans.* **2010,** *39* (5), 1204-1206.
148. (a) Tinker, L. L.; Bernhard, S., Photon-Driven Catalytic Proton Reduction with a Robust Homoleptic Iridium (III) 6-Phenyl-2, 2′-bipyridine Complex (Ir $(C^{\wedge}N^{\wedge}N)^{2+}$). *Inorg. Chem.* **2009,** *48* (22), 10507-10511; (b) Curtin, P. N.; Tinker, L. L.; Burgess, C. M.; Cline, E. D.; Bernhard, S., Structure− activity correlations among iridium (III) photosensitizers in a robust water-reducing system. *Inorg. Chem.* **2009,** *48* (22), 10498-10506.
149. Thoi, V. S.; Kornienko, N.; Margarit, C. G.; Yang, P.; Chang, C. J., Visible-light photoredox catalysis: selective reduction of carbon dioxide to carbon monoxide by a nickel N-heterocyclic carbene–isoquinoline complex. *J. Am. Chem. Soc.* **2013,** *135* (38), 14413-14424.
150. Yuan, Y.-J.; Zhang, J.-Y.; Yu, Z.-T.; Feng, J.-Y.; Luo, W.-J.; Ye, J.-H.; Zou, Z.-G., Impact of ligand modification on hydrogen photogeneration and light-harvesting applications using cyclometalated iridium complexes. *Inorg. Chem.* **2012,** *51* (7), 4123-4133.
151. Shik Chin, C.; Eum, M. S.; yi Kim, S.; Kim, C.; Kwon Kang, S., Blue-Light-Emitting Complexes: Cationic (2-Phenylpyridinato) iridium (III) Complexes with Strong-Field Ancillary Ligands. *Eur. J. Inorg. Chem.* **2007,** *2007* (3), 372-375.
152. Wang, C.; Lewis, A. R.; Batchelor, R. J.; Einstein, F. W.; Willner, H.; Aubke, F., Synthesis, molecular structure, and vibrational spectra of mer-tris (carbonyl) iridium (III) fluorosulfate, mer-$Ir(CO)_3(SO_3F)_3$. *Inorg. Chem.* **1996,** *35* (5), 1279-1285.
153. Bokarev, S. I.; Hollmann, D.; Pazidis, A.; Neubauer, A.; Radnik, J.; Kühn, O.; Lochbrunner, S.; Junge, H.; Beller, M.; Brückner, A., Spin density distribution after electron transfer from triethylamine to an $[Ir(ppy)_2(bpy)]^+$ photosensitizer during photocatalytic water reduction. *Phys. Chem. Chem. Phys.* **2014,** *16* (10), 4789-4796.
154. (a) Rosas-Hernández, A.; Steinlechner, C.; Junge, H.; Beller, M., Photo-and Electrochemical Valorization of Carbon Dioxide Using Earth-Abundant Molecular Catalysts. *Top. Curr. Chem.* **2018,** *376* (1), 1; (b) Francke, R.; Schille, B.; Roemelt, M., Homogeneously

Catalyzed Electroreduction of Carbon Dioxide—Methods, Mechanisms, and Catalysts. *Chem. Rev.* **2018,** *118* (9), 4631-4701.
155. Arias-Rotondo, D. M.; McCusker, J. K., The photophysics of photoredox catalysis: a roadmap for catalyst design. *Chem. Soc. Rev.* **2016,** *45* (21), 5803-5820.
156. (a) Luo, S. P.; Mejía, E.; Friedrich, A.; Pazidis, A.; Junge, H.; Surkus, A. E.; Jackstell, R.; Denurra, S.; Gladiali, S.; Lochbrunner, S., Photocatalytic Water Reduction with Copper-Based Photosensitizers: A Noble-Metal-Free System. *Angewandte Chemie* **2013,** *125* (1), 437-441; (b) Rosas-Hernández, A.; Steinlechner, C.; Junge, H.; Beller, M., Earth-abundant photocatalytic systems for the visible-light-driven reduction of CO_2 to CO. *Green Chem.* **2017,** *19* (10), 2356-2360.
157. Romero, N. A.; Nicewicz, D. A., Organic photoredox catalysis. *Chem. Rev.* **2016,** *116* (17), 10075-10166.
158. Lazarides, T.; McCormick, T.; Du, P.; Luo, G.; Lindley, B.; Eisenberg, R., Making hydrogen from water using a homogeneous system without noble metals. *J. Am. Chem. Soc.* **2009,** *131* (26), 9192-9194.
159. Yoshioka, E.; Kohtani, S.; Jichu, T.; Fukazawa, T.; Nagai, T.; Kawashima, A.; Takemoto, Y.; Miyabe, H., Aqueous-medium carbon–carbon bond-forming radical reactions catalyzed by excited rhodamine B as a metal-free organic dye under visible light irradiation. *The Journal of organic chemistry* **2016,** *81* (16), 7217-7229.
160. Ghosh, I.; Ghosh, T.; Bardagi, J. I.; König, B., Reduction of aryl halides by consecutive visible light-induced electron transfer processes. *Science* **2014,** *346* (6210), 725-728.
161. Uoyama, H.; Goushi, K.; Shizu, K.; Nomura, H.; Adachi, C., Highly efficient organic light-emitting diodes from delayed fluorescence. *Nature* **2012,** *492* (7428), 234.
162. (a) Poelma, S. O.; Burnett, G. L.; Discekici, E. H.; Mattson, K. M.; Treat, N. J.; Luo, Y.; Hudson, Z. M.; Shankel, S. L.; Clark, P. G.; Kramer, J. W., Chemoselective Radical Dehalogenation and C–C Bond Formation on Aryl Halide Substrates Using Organic Photoredox Catalysts. *The Journal of organic chemistry* **2016,** *81* (16), 7155-7160; (b) Treat, N. J.; Sprafke, H.; Kramer, J. W.; Clark, P. G.; Barton, B. E.; Read de Alaniz, J.; Fors, B. P.; Hawker, C. J., Metal-free atom transfer radical polymerization. *J. Am. Chem. Soc.* **2014,** *136* (45), 16096-16101; (c) Discekici, E. H.; Treat, N. J.; Poelma, S. O.; Mattson, K. M.; Hudson, Z. M.; Luo, Y.; Hawker, C. J.; de Alaniz, J. R., A highly reducing metal-free photoredox catalyst: design and application in radical dehalogenations. *Chem. Commun.* **2015,** *51* (58), 11705-11708.
163. Miyake, G. M.; Theriot, J. C., Perylene as an organic photocatalyst for the radical polymerization of functionalized vinyl monomers through oxidative quenching with alkyl bromides and visible light. *Macromolecules* **2014,** *47* (23), 8255-8261.
164. (a) Theriot, J. C.; Lim, C.-H.; Yang, H.; Ryan, M. D.; Musgrave, C. B.; Miyake, G. M., Organocatalyzed atom transfer radical polymerization driven by visible light. *Science* **2016,** *352* (6289), 1082-1086; (b) Lim, C.-H.; Ryan, M. D.; McCarthy, B. G.; Theriot, J. C.; Sartor, S. M.; Damrauer, N. H.; Musgrave, C. B.; Miyake, G. M., Intramolecular charge transfer and ion pairing in N, N-diaryl dihydrophenazine photoredox catalysts for efficient organocatalyzed atom transfer radical polymerization. *J. Am. Chem. Soc.* **2016,** *139* (1), 348-355.
165. (a) Pearson, R. M.; Lim, C.-H.; McCarthy, B. G.; Musgrave, C. B.; Miyake, G. M., Organocatalyzed atom transfer radical polymerization using N-Aryl phenoxazines as photoredox catalysts. *J. Am. Chem. Soc.* **2016,** *138* (35), 11399-11407; (b) Ramsey, B. L.; Pearson, R. M.; Beck, L. R.; Miyake, G. M., Photoinduced organocatalyzed atom transfer radical polymerization using continuous flow. *Macromolecules* **2017,** *50* (7), 2668-2674; (c) Ryan, M. D.; Pearson, R. M.; French, T. A.; Miyake, G. M., Impact of light intensity on control in photoinduced

organocatalyzed atom transfer radical polymerization. *Macromolecules* **2017,** *50* (12), 4616-4622; (d) Du, Y.; Pearson, R. M.; Lim, C. H.; Sartor, S. M.; Ryan, M. D.; Yang, H.; Damrauer, N. H.; Miyake, G. M., Strongly Reducing, Visible-Light Organic Photoredox Catalysts as Sustainable Alternatives to Precious Metals. *Chemistry–A European Journal* **2017,** *23* (46), 10962-10968.
166. Theriot, J. C.; McCarthy, B. G.; Lim, C. H.; Miyake, G. M., Organocatalyzed atom transfer radical polymerization: perspectives on catalyst design and performance. *Macromolecular rapid communications* **2017,** *38* (13), 1700040.
167. Hiraoka, S.; Okamoto, T.; Kozaki, M.; Shiomi, D.; Sato, K.; Takui, T.; Okada, K., A stable radical-substituted radical cation with strongly ferromagnetic interaction: Nitronyl nitroxide-substituted 5, 10-diphenyl-5, 10-dihydrophenazine radical cation. *J. Am. Chem. Soc.* **2004,** *126* (1), 58-59.
168. Chapovetsky, A.; Welborn, M.; Luna, J. M.; Haiges, R.; Miller III, T. F.; Marinescu, S. C., Pendant hydrogen-bond donors in cobalt catalysts independently enhance CO_2 reduction. *ACS central science* **2018,** *4* (3), 397-404.
169. Costentin, C.; Savéant, J.-M., Multielectron, Multistep Molecular Catalysis of Electrochemical Reactions: Benchmarking of Homogeneous Catalysts. *ChemElectroChem* **2014,** *1* (7), 1226-36.
170. Birdja, Y. Y.; Shen, J.; Koper, M. T., Influence of the metal center of metalloprotoporphyrins on the electrocatalytic CO_2 reduction to formic acid. *Catal. Today* **2017,** *288*, 37-47.
171. Rahiman, A. K.; Bharathi, K. S.; Sreedaran, S.; Narayanan, V., Epoxidation of styrene by Fe, Mn, and V metalloporphyrins encapsulated Si, Al, Ti and V-MCM-41. *Catal. Lett.* **2009,** *127* (1-2), 175-182.
172. (a) Craig, J. C.; Ekwurire, N. N.; Fu, C. C.; Walker, K. A., Conversion of carboxylic acids into aldehydes and their c-1 or c-2 deuteriated derivatives. *Synthesis* **1981,** *1981* (04), 303-305; (b) Hasegawa, E.; Seida, T.; Chiba, N.; Takahashi, T.; Ikeda, H., Contrastive photoreduction pathways of benzophenones governed by regiospecific deprotonation of imidazoline radical cations and additive effects. *The Journal of organic chemistry* **2005,** *70* (23), 9632-9635.
173. Alsabeh, P. G.; Rosas-Hernández, A.; Barsch, E.; Junge, H.; Ludwig, R.; Beller, M., Iron-catalyzed photoreduction of carbon dioxide to synthesis gas. *Catal. Sci. Technol.* **2016,** *6* (10), 3623-3630.
174. Montalti, M.; Credi, A.; Prodi, L.; Gandolfi, M. T., *Handbook of photochemistry*. CRC press: 2006.